FUNDAMENTAL STUDIES OF ELECTRONIC ACTIVATION METHODS FOR SULFATED GLYCOSAMINOGLYCAN CHARACTERIZATION

by

LAUREN E. PEPI

(Under the Direction of I. Jonathan Amster)

ABSTRACT

Glycosaminoglycans (GAGs) are complex linear carbohydrates that participate in a broad range of biological processes. Their structural analysis is challenging, and there has been considerable research into tandem mass spectrometry (MS/MS) approaches. Electron activation methods such as electron detachment dissociation (EDD) produce glycosidic fragments and an abundance of cross-ring fragmentation, but this approach is confined to FTICR mass spectrometers. EDD has been shown to accurately identify sulfate position of GAG oligosaccharides and can distinguish C-5 uronic acid stereochemistry in some cases. We have investigated other electronic excitation methods that can produce EDD-like fragmentation behavior. Charge transfer dissociation (CTD), and ultraviolet photodissociation (UVPD) and negative electron transfer dissociation (NETD) have great potential for the analysis of sulfated GAGs. For each method, the location of sulfate modifications can be assigned. Additionally, C-5 uronic acid stereochemistry could be determined when epimer pairs were tested. The advancement of electron-based activation methods allows for full GAG sequencing in a variety of instrumentation.

INDEX WORDS: Carbohydrate, sulfated glycosaminoglycan, Fourier transform ion cyclotron resonance mass spectrometry, electron detachment dissociation, negative electron transfer dissociation, charge transfer dissociation, ultraviolet photodissociation, mass spectrometry, tandem mass spectrometry

FUNDAMENTAL STUDIES OF ELECTRONIC ACTIVATION METHODS FOR SULFATED GLYCOSAMINOGLYCAN CHARACTERIZATION

by

LAUREN E. PEPI

B.A., Assumption College, 2015

A Dissertation Submitted to the Graduate Faculty of The University of Georgia in Partial Fulfillment of the Requirements for the Degree

DOCTOR OF PHILOSOPHY

ATHENS, GEORGIA

2020

FUNDAMENTAL STUDIES OF ELECTRONIC ACTIVATION METHODS FOR SULFATED GLYCOSAMINOGLYCAN CHARACTERIZATION

by

LAUREN E. PEPI

Major Professor:	I. Jonathan Amster
Committee:	Jeffery Urbauer
	Ron Orlando

Electronic Version Approved:

Ron Walcott
Dean of the Graduate School
The University of Georgia
December 2020

DEDICATION

To mom

ACKNOWLEDGEMENTS

None of the work presented here would have been possible without help from group members and collaborators. First, I would like to thank my advisor, Jon Amster, for giving me the opportunity to work in his lab and learn so much over the past 5+ years even after I failed his midterm my first semester. Dr. Amster has pushed me to strive and become the independent problem solver I am today. My committee members, Dr. Urbauer and Dr. Orlando, thank you for all of your support and advice over the years. I would also like to thank past Amster group members, especially Franklin E. Leach III and Isaac Agyekum. All the carbohydrates analyzed for this work were available thanks to the labs of Robert J. Linhardt at Rensselaer Polytechnic Institute (Fuming Zhang) and Geert-Jan Boons at the Complex Carbohydrate Research Center at the University of Georgia (Pradeep Chopra). The charge transfer dissociation work was done in collaboration with the lab of Glen P. Jackson at West Virginia University (Zachary J. Sasiene, Praneeth M. Mendis) who hosted me on two separate occasions to perform these experiments. The ultraviolet photodissociation work was done in collaboration with the lab of Jennifer S. Brodbelt at the University of Texas at Austin (Dustin Klein). I would also like to thank the undergraduate researchers who have worked under me during these 5+ years (Megan Wigginton and Marshall Liss). I would like to thank my friends and family who have provided infinite moral support over these 5+ years and who were quick to learn to stop asking me when I am graduating. And finally, I would like to thank James for not only pretending to understand me when I go off on rants about my research, but for never stopping to remind me that I could do this.

TABLE OF CONTENTS

Page

LIST OF TABLES

Page

LIST OF FIGURES

Page

CHAPTER 1

Introduction and Literature Review

Pepi, L. E.; Sanderson, P.; Stickney, M.; & Amster, I. J., *Mol. Cell. Proteomics*. (2020) In press.

Glycosaminoglycan Overview

The structural diversity of GAGs makes them challenging targets for analysis. Mass spectrometry (MS) has played an important role in this endeavor, due to its high sensitivity, specificity for discerning subtle differences in structure, and its capability to examine complex mixtures. Proteoglycans (PGs) consist of a core protein along with one or more covalently bound GAG chains.[1] The biological function of the PG is typically determined by the GAG component. GAGs are primarily found on the surface of cells or in the extracellular matrix [2]. GAGs are classified into four main groups: heparin/heparan sulfate (Hp/HS), chondroitin sulfate/dermatan sulfate (CS/DS), keratan sulfate (KS), and hyaluronic acid (HA).[2] Hp/HS and CS/DS participate in a number of biological processes, and their analysis is the focus of this review. GAGs are long, linear polysaccharides with repeating disaccharide units. Hp/HS and CS/DS are composed of a N-acetyl amino sugar and an uronic acid. The first biosynthesis step, chain elongation, produces a uniform repeating polymer of a N-acetyl amino sugar (GlcNAc for Hp/HS, and GalNAc for CS/DS) and glucuronic acid. The chains are subsequently modified by deacetylases, sulfotransferases, and epimerases to produce highly complex and heterogeneous structures. Sulfo-modified GAGs are negatively charged and highly polar molecules. Due to the complex nature and the biological relevance of Hp/HS and CS/DS, these GAG families have been the focus of considerable research into the development of new MS approaches to analysis.

HA is an unsulfated GAG composed of repeating disaccharide units of N-acetylgalactosamine (GalNAc) and glucuronic acid (GlcA) joined by alternating β(1,4) and β(1,3) linkage.[2] In addition to being unmodified by sulfotransferases, HA is also unmodified by epimerases. HA is distributed in the neural, connective, and epithelial tissues, and there is an estimated 15 g of HA in an adult human body. HA can weigh as much as 100-10,000 kDa,

making it quite large.[3] Recently, HA has been a component used in dermal fillers and has been a desired ingredient in many face creams and treatments due to its chemical-physical properties, biodegradability, biocompatibility, and versatility.[4-5] However, due to the consistent, unmodified structure, there has not been a need to continuously characterize HA using mass spectrometry. KS is made of repeating disaccharide units of galactose (Gal) and GlcNAc joined by alternating β(1,4) and β(1,3) linkage.[2] The disaccharide building blocks of KS can be unsulfated, monosulfated or disulfated. KS is primarily found in the cartilage, cornea, and bone. It has been shown to participate in development and healing of the central nervous system. [6] Though KS is sulfated, it can only be sulfated at the 6-*O* position on either the Gal or GlcNAc residue, making its structure predictable. For this reason, KS characterization by MS does not require much additionally development.[7-8]

CS occurs in a variety of locations within mammals, including extracellular matrix such as connective tissue and cartilage, tethered to proteins on the cell surface, and also as secreted proteoglycans. It is widely used as a treatment for osteoarthritis and cataracts, as it has anti-inflammatory and pain reducing properties.[9-10] CS is up-regulated in the extracellular matrix of scar tissue and perineuronal nets, making it a useful treatment following neural injury.[10] CS can be as large as 100,000 kDa.[11] CS has a disaccharide backbone composed of GalNAc and GlcA joined by an alternating β(1,4) and β(1,3) linkage, respectively.[2, 12] Chondroitin sulfate is polymerized into chains that can be hundreds of residues long and is usually composed of hybrid structures containing more than one type of chondroitin disaccharide unit. There are three principal types of chondroitin sulfate, CS-A, CS-B (also known as dermatan sulfate) and CS-C. CS-A and CS-B are predominantly sulfated at the 4-*O* position of the GalNAc, whereas CS-C has 6-*O* sulfated GalNAc subunits.[2] An example of CS and DS is shown in Figures 1.1A and

1.1B. Dermatan sulfate (CS-B/DS) is composed of repeating disaccharide units containing GalNAc and iduronic acid (IdoA), which differs from GlcA only in C-5 stereochemistry.[2] Dermatan sulfates are the primary GAG in the dermis and are responsible for binding proteins involved in modulation of a broad range of physiological processes. Other patterns of modification, including those with two sulfo-groups per disaccharide, have been reported; CS-D has 2-*O* sulfation on the uronic acid and 6-*O* sulfation on the GalNAc, and CS-E has 4-*O* and 6-*O* sulfation on the GalNAc.[13]

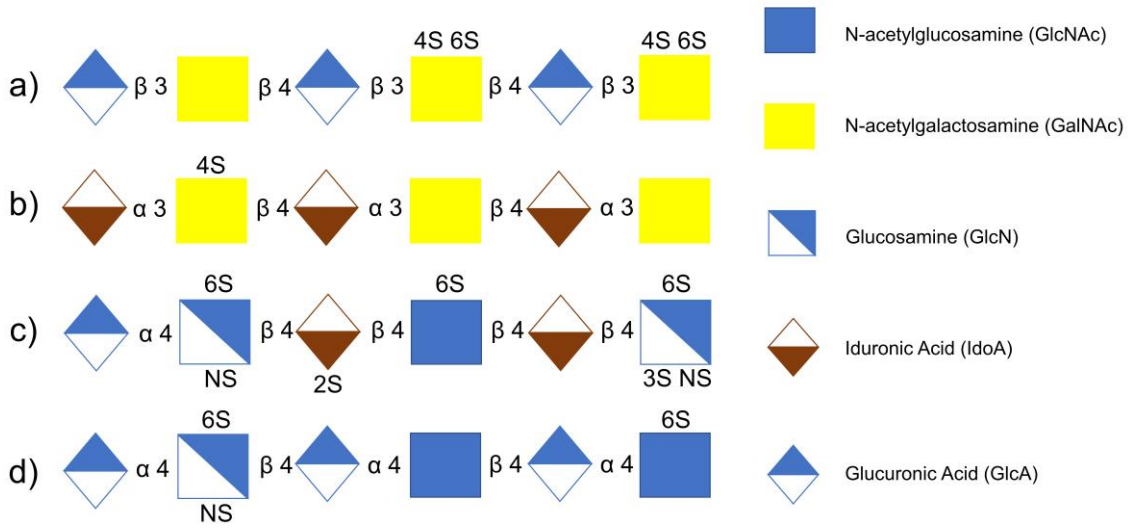

Figure 1.1. Example Hp/HS and CS/DS chains. a) chondroitin sulfate chain, b) dermatan sulfate chain, c) heparan sulfate chain with both IdoA and GlcA and 2-*O* sulfation, d) heparan sulfate chain with GlcA.

Hp and HS are structurally the most complex members of the GAG polysaccharides.[14] One of the main functions of Hp is anticoagulation and prevention of vein thrombosis and pulmonary embolism. Hp is produced in mast cells and has more sulfates per hexosamine than HS.[15] HS is produced by most mammalian cells, and located on cell surfaces and in the extracellular matrix.[16] Hp can weigh up to ~14 kDa whereas HS can weigh up to ~75 kDa.[17] Hp/HS are composed of uronic acid and N-acetyl glucosamine repeating disaccharide subunits[16], and joined by alternating α(1,4) and β(1,4) linkage.[2] Example heparan sulfate structures are illustrated in Figures 1.1C and 1.1D. The uronic acid of the repeating disaccharide unit can be either L-IdoA or D-GlcA, both of which can be 2-*O* sulfated, however this sulfation pattern is predominantly seen on IdoA (IdoA2S).[15, 18] The D-(GlcN) can be N-sulfated (GlcNS) or N-acetylated (GlcNAc), both of which could have 6-*O* sulfation, and the GlcNS can also be 3-*O* sulfated.[12, 15-16, 19-20] Despite an understanding of some of the biological roles GAGs possess, there is still room for development in understanding their structure-function relationship. The complexity of the biosynthesis of GAGs creates complex mixtures and heterogeneous structures, creating a need for the structural characterization of GAGs.

There is considerable interest in determining the structures of GAGs and relating these to their biological activity. Past research has shown the importance of GAG structure in relation to function, specifically when related to protein binding.[19, 21-22] However, GAG structural analysis remains a significant analytical challenge.[23-24] The biosynthesis of GAGs is a non-template driven, enzymatic process. GAG biosynthesis starts with a heterogenous copolymer that undergoes extensive modification by sulfotransferases and epimerase. This process results in non-uniform GAG chains with varying degrees of acetylation and sulfation and produces complex mixtures of biological GAGs.[2] Additionally, GAGs are generally available only in

small quantities and cannot be overexpressed or amplified like other biopolymers, specifically proteins and nucleic acids.[25] This combined with their high molecular weight limits the applicability of tools such as nuclear magnetic resonance (NMR) or X-Ray diffraction.[26-28] For these reasons, the development of mass spectrometry methods for GAG analysis has attracted significant research effort. GAGs have two features that impact the MS methodologies that are applied, specifically their anionic nature and the fragility of their sulfo-modifications. MS methodology developments have greatly improved in the last decade as a result of advances in on-line separations, ion activation techniques, and software for automated analysis of complex MS and MS/MS data. The research discussed herein focus on advancements in ion activation techniques for GAG structural analysis.

Mass Spectrometry of Glycosaminoglycans

ESI is the standard approach for analyzing GAG samples via mass spectrometry. Negative ion mode is typically employed, as the carboxyl groups and sulfate modifications present in GAGs make them highly anionic. GAGs have high ionization efficiency in negative ion mode and the process can be tuned to be soft enough to avoid loss of labile sulfate modifications.[29] ESI of GAGs typically produces multiple charge states and alkali ion heterogeneity (Na^+/H^+ exchange) which can either be exploited for controlling ion activation or suppressed by addition of formic acid or diethylamine to produce a clearer spectrum.[30-31]

Composition Analysis

Composition analysis is typically the first step in GAG analysis and can be useful for some basic and general information. Accurate mass measurement by MS provides the means to assign chain length (dp), and the type and number of modifications present in a GAG oligomer.

Composition analysis can be paired with disaccharide analysis to assign general modification motifs for GAG species.[32-33] General changes in GAG composition have been linked to many medical conditions and developmental biology.[34-37] One challenge in assigning composition based on accurate mass measurement is heterogeneity from sodium/hydrogen exchange. Molecules with a number of ionizable sites, such as GAGs or nucleic acids, are susceptible to replacement of acidic protons by alkali cations. This can produce a broad distribution of molecular species. When convoluted with a distribution of compositions and charge states, this can give rise to complex mass spectra, as seen in Figure 1.2 for a mixture of full length CS glycans from bikunin.[23] Spreading the molecular ion over a number of alkali exchange states reduces the intensity of the peaks and makes the assignment of composition more difficult. Desalting the sample with a spin filter, and adding dilute formic acid or diethylamine to the electrospray solvent can significantly decrease the degree of cation exchange, making the signals stronger by reducing the heterogeneity of the molecular ion.[38-39] High degrees of alkali exchange can result in an added degree of difficulty for analyzing GAGs chromatographically. Ion suppression is often utilized for on-line chromatographic analysis of GAGs. The ion suppressor removes alkali and ammonium ions from the mobile phase, improving the signal strength.[40]

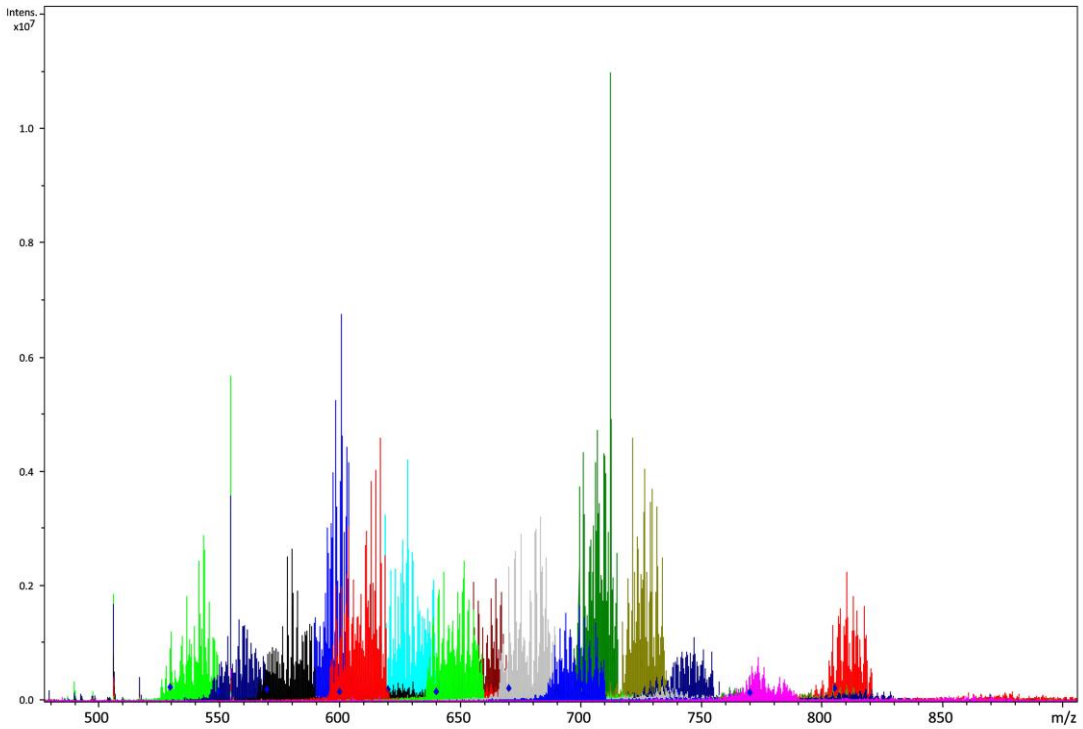

Figure 1.2. Improvement in S/N in the FTICR mass spectrum of the bikunin CS mixture achieved by combining mass spectra acquires over narrow overlapping *m/z* regions. Reprinted with permission from reference 15. Copyright 2008 American Chemical Society.

GAG Sequencing

Tandem mass spectrometry (MS/MS) is a powerful tool for identifying the location of modifications within a GAG oligomer. Mass-selected precursor ions are activated, and undergo fragmentation processes to yield a tandem mass spectrum. The fragment ions provide information that can be used to assign the structure of the precursor ion. The principal means of fragmenting a precursor ion are collisional activation, electron-based activation, ion-ion reactions and photodissociation.[41-55] The wide variety of available activation methods provide the means to

fragment via many different reaction channels, and can provide a range of structural details. In general, there are two broad categories of fragmentation types, glycosidic bond cleavage, and cross-ring cleavage, as shown in Figure 1.3. A series of ions from glycosidic cleavage between all residues provides composition information for each residue in a GAG chain, for example, the number of sulfo-modifications or the presence of N-acetyl in an amino sugar. Glycosidic cleavages give rise to fragments labeled B and C for fragment ions containing the non-reducing end of an oligomer or Y and Z for reducing end fragment ions.[56] A pair of glycosidic product ions, e.g. B and C, arise from fragmentation on either side of the oxygen atom that forms the glycosidic bond. The cleavage is accompanied with a hydrogen migration between the two fragments, ending on the oxygen of the cleaved glycosidic bond. For this reason, these complementary glycosidic cleavage products (B/C or Y/Z) differ in composition by H_2O, and in mass by 18 Da. This fixed mass difference facilitates the identification of such pairs of glycosidic cleavage products. One consequence of the hydrogen migration that accompanies glycosidic bond cleavage is the formation of a double bond on the residue that loses the hydrogen. Z-ions will have a double bond on their non-reducing end residue, and if this residue is a uronic acid, it will have the same composition as a D-uronic acid. For oligomers that have a D-uronic acid at their non-reducing end, it can be difficult to distinguish some Z-ions from C-ions because their composition and mass can be identical.

The other category of fragmentation process, cross-ring cleavage, results from breaking two bonds within a monomer residue. The bonds are numbered as shown in Figure 1.3, and are denoted as $^{n,m}A$ or $^{n,m}X$ for non-reducing end and reducing end fragment ions, respectively.[56] The superscripts n and m denote the specific bonds within a monomer ring that have been cleaved. Cross-ring fragment ions are useful for assigning the location of a modification within a sugar

residue. The energy required to produce a cross-ring fragment is higher than that for glycosidic cleavage, because more bonds are broken in the former case. The choice of activation method influences the abundance of cross-ring versus glycosidic cleavage products, and is an important consideration in selecting the method of analysis.

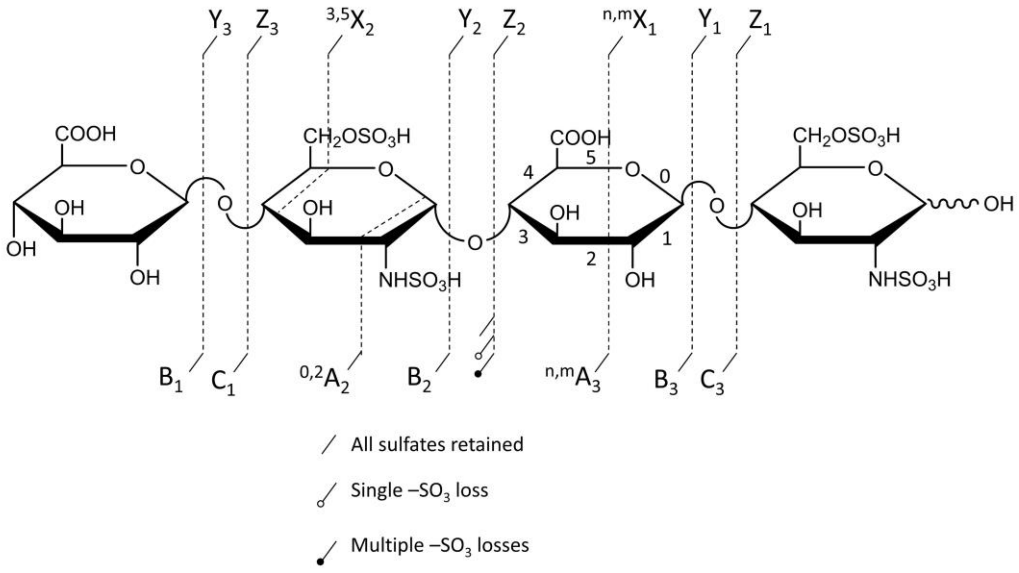

Figure 1.3. Domon and Costello nomenclature for glycosaminoglycan fragmentation. Key denotes symbols used for sulfate decomposition.

Collision induced dissociation (CID) was one of the first fragmentation techniques to be applied to GAG sequencing.[24, 54, 57] A collision with a neutral gas atom causes an increase in the internal energy of the precursor ion. The excess energy drives unimolecular dissociation by cleaving the most labile bonds, specifically the glycosidic linkages. In addition, sulfo-modifications undergo a facile rearrangement to release SO_3. CID leads to fragmentation by the

lowest energy reaction pathway, which often is uninformative sulfate decomposition. The sulfate modification is most labile in its protonated form, and is stabilized by deprotonation or metal cation-hydrogen exchange resulting in more informative cleavages.[30, 55, 58-59] However, adding a metal cation into the sample increases the complexity of the mass spectrum by introducing heterogeneity to the molecular ion region. Although cross-ring cleavages are not prevalent in CID spectra, highly ionized precursors can generate them as demonstrated for highly-sulfated HS/Hp oligomers by Kailemia *et al*.[58] In this work, sodium-hydrogen (Na-H) exchange was utilized to fully ionize the pentasaccharide Arixtra™ for sequencing studies.

CID is accessible on a wide variety of commercially available mass spectrometers. Reinhold *et al.* used CID on an ion trap instrument in a multistep MS^n experiment to determine sequence information of highly sulfated GAGs.[60] Chemical derivatization, specifically permethylation with stable isotope analogs, allowed the authors to determine site specific sulfate location upon sequential MS/MS experiments performed in positive ion mode. Higher-energy collisional dissociation (HCD) is a similar type of collisional fragmentation found specifically on Thermo Fisher Scientific Orbitrap instruments. HCD, while still a low energy collision process, differs from CID in that it occurs in a collision cell located after the C-trap in a Thermo Orbitrap instrument rather than within the linear ion trap as for conventional CID, and allows observation of small product ions that fall below one-third of the *m/z* of the precursor, a limit of CID within the ion trap itself. CID and HCD fragmentation occur on the order of milliseconds making them suitable to combine with different separation techniques. Recently, Sharp *et al.* sequenced mixtures of chemically derivatized HS oligosaccharides using on-line LC and CID MS/MS.[61-62] Derivatization prevented loss of sulfate modifications and resulted in informative fragmentation upon collisional dissociation. Although CID does not produce a significant amount of cross-ring

cleavages without additional modification in the form of metal cation-hydrogen exchange or derivatization, it can be a vital tool for analyzing modestly sulfated GAGs (1 or fewer sulfo-modifications per disaccharide) and combined with high throughput separation experiments. Additionally, it has been shown that when analyzing oligosaccharides with Δ-unsaturated uronic acid at the non-reducing end, facile retro-Diels alder rearrangement occurs.[63] This results in the formation of more cross-ring cleavages than when a saturated uronic acid is present at the non-reducing end.[64]

Photodissociation is another ion activation approach for assigning the structure of GAGs. Infrared multiphoton dissociation (IRMPD) produces ample glycosidic cleavages in GAGs as well as other types of glycans.[31, 51, 65-66] IRMPD typically uses an infrared laser such as the 10.6 mm output of a CO_2 laser, to raise the internal energy of trapped ions through the serial absorption of infrared photons.[67] Absorption of a single IR photon merely raises the vibrational energy of the precursor. In order to access a dissociative excited state, many IR photons must be absorbed, as implied by the name infrared *multiphoton* dissociation. Activation by IRMPD is a threshold process that accesses the lowest energy fragmentation pathways. As with CID, IRMPD yields minimal cross-ring cleavages and a high degree of SO_3 loss for protonated sulfate modifications. Wolff *et al.* showed that IRMPD produces similar fragmentation to CID in GAG standards, illustrated in Figures 1.4B and 1.4C.[68] IRMPD requires a fully ionized precursor to produce informative fragmentation. This can be achieved by choosing a high charge precursor or by exchanging a metal cation such as Na^+ for protons in ionizable functional groups (sulfate and carboxylate). McClellan *et al.* demonstrated the importance of precursor selection when using IRMPD.[69] Different charge state precursors were shown to produce different fragment ions, with higher charge states being preferred. This phenomenon has been shown when using collisional

methods as well. IRMPD is most frequently implemented on a Fourier Transform ion cyclotron resonance mass spectrometer (FTICR MS), as it requires a high vacuum environment during the multiple steps of photon absorption, to avoid collisional relaxation of the intermediate photoexcited states. More recently, ultraviolet photodissociation (UVPD) has been used for the analysis of GAG standards.[41] UVPD uses an ultraviolet laser to raise the internal energy of trapped ions, resulting in fragmentation.[70] Unlike IRMPD, a single UV photon is adequate to raise the precursor ion into a dissociative state. Racaud *et al.* used UVPD in the 220-290 nm range to dissociate heparin-derived disaccharide dianions.[71] This favored informative cross-ring fragments and yielded electron-photodetachment ions as well as the corresponding charge-reduced neutral loss products. This study also demonstrated the importance of deprotonated sulfo-modifications for informative fragmentation.[71] Klein *et al.* showed that UVPD at either 193 nm or 213 nm produced both glycosidic and cross-ring fragmentation in GAG standards ionized in negative mode, while maintaining sulfate modifications.[41] As demonstrated by Klein *et al.*, UVPD does not require a fully ionized precursor to produce informative fragmentation. A HS tetramer with deprotonation of only two of its four ionizable sites yields cross-ring and glycosidic cleavage with minimal sulfo-decomposition, as shown in Figure 1.5.[41] UVPD works well with ion trap instruments as there is no requirement for high vacuum, in contrast to IRMPD.[70]

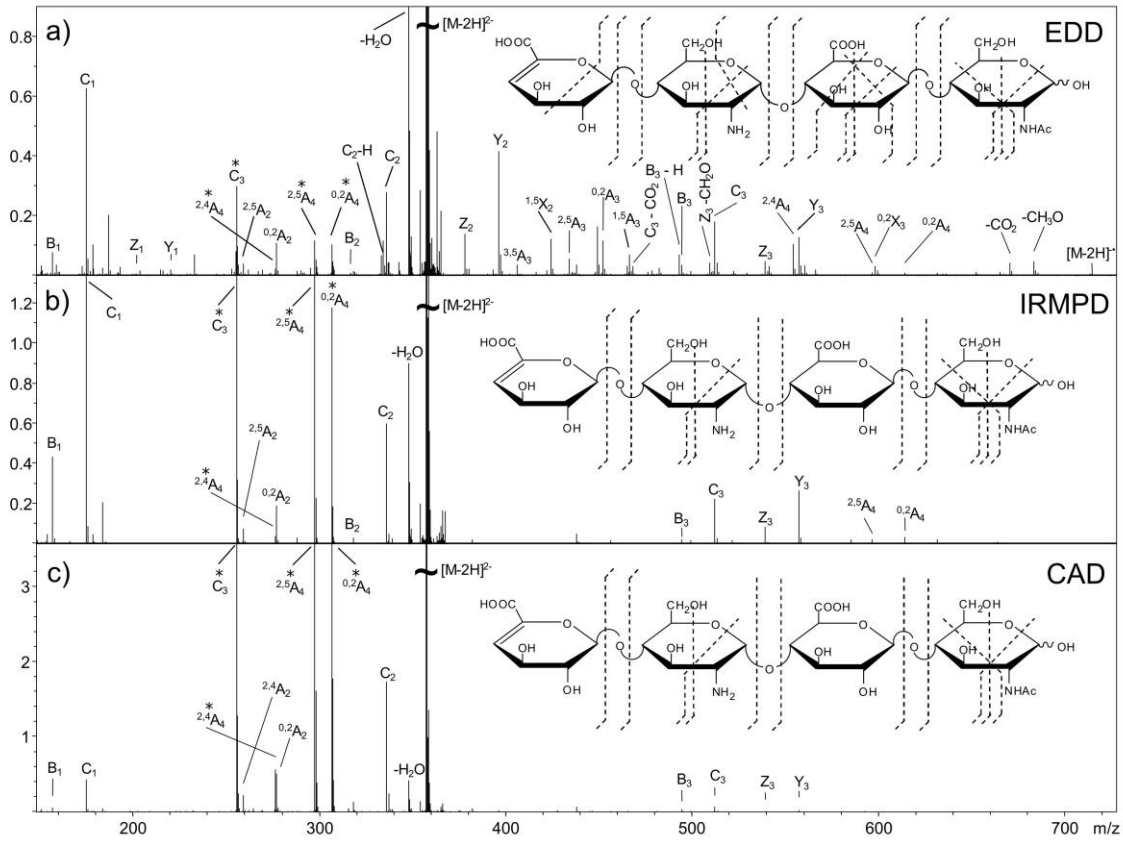

Figure 1.4. Tandem MS spectra of $[M-2H]^{2-}$ of tetrasaccharide ΔUA-GlcN-GlcA-GlcNAc a) EDD spectrum and cleavage map b) IRMPD spectrum and cleavage map and c) CAD spectrum and cleavage map. Reprinted with permission from reference 84. Copyright 2007 American Chemical Society.

Electron-based activation methods play a significant role in contemporary biological mass spectrometry. Electron detachment dissociation (EDD) has been widely used for the analysis of GAG chains.[31, 41, 47-49, 51-53, 65, 68, 72] EDD operates by irradiating multiply charged negative ions with 15-20 eV electrons. This causes ion activation via electronic excitation, and

promotes electron detachment and radical formation, with the production of both even- and odd-electron fragment ions.[68] Unlike vibrational-activation methods such as CID and IRMPD, EDD yields a large quantity of cross-ring cleavages. In the past, EDD was restricted primarily to FTICR MS due to the need to trap ions in a static electric field during electron bombardment. EDD of GAGs was first applied to HS tetrasaccharide standards with a modest degree of sulfation, and was found to produce far more fragmentation products than IRMPD or CID, as shown in Figure 1.4.[68] This technique has since been expanded and used for longer, more highly sulfated GAGs.[28, 49, 51-53, 65] Wolff *et al.* showed the capability of EDD to distinguish epimeric HS tetrasaccharides that differ only by C-5 stereochemistry in the uronic acid closest to the reducing end.[44] Agyekum *et al.* developed a diagnostic ratio for assigning C-5 stereochemistry in a diverse pool of HS tetramers.[49] Leach *et al.* investigated the importance of precursor selection using synthetic Hp/HS tetramers with 1-2 sulfates per disaccharide unit.[47] EDD produced the best results when the degree of ionization equaled one more than the number of sulfate-modifications. The addition of sodium counter ions was used to create ionized carboxyl groups to increase the likelihood of electron detachment from the carboxylate for highly sulfated GAGs.[47] Electron-induced dissociation (EID), which irradiates singly charged anions with 6-20 eV electrons, activates ions by electronic excitation.[46] EID produces similar fragmentation to EDD, but without going through the process of electron detachment. Wolff *et al.* showed that EID produces an abundance of cross-ring fragmentation, resulting in EDD-like fragmentation.[46] The presence of cross-ring fragmentation primarily within hexuronic acid residues in both EID and EDD suggest these residues are more labile when activated via electronic excitation.[46]

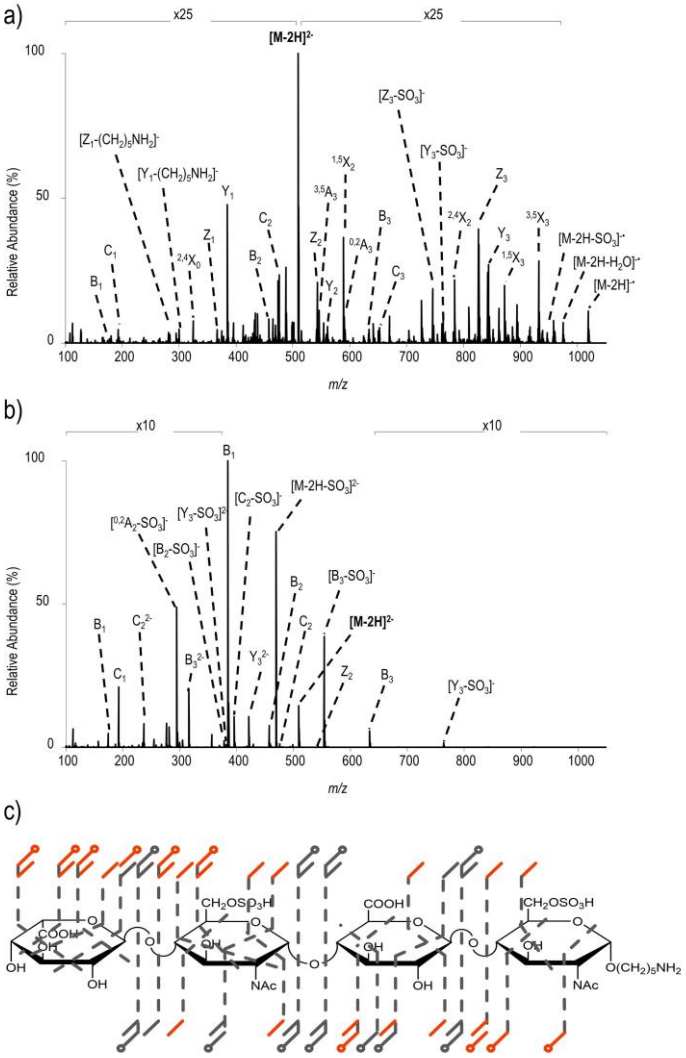

Figure 1.5. a) UVPD spectrum and b) HCD spectrum of $[M\text{-}2H]^{2-}$ (*m/z* 509) of disulfated tetrasaccharide IdoA-GlcNAc6S-GlcA-GlcNAc6S-$(CH_2)_5NH_2$. c) Annotated structure showing fragment ions for both UVPD and HCD, with fragments only seen in UVPD outlined in red. Reprinted with permission from reference 59. Copyright 2019 American Chemical Society.

Negative electron transfer dissociation (NETD) is another useful ion activation technique for GAGs.[73-74] NETD is the negative complement to electron transfer dissociation (ETD). This ion-ion reaction involves gas phase electron transfer from a multiply charged anion precursor to a reagent cation.[75] Commonly, this reagent species is fluoranthene radical cation, however Xe^+ or SF_5^+ can also be used.[74, 76] Like EDD, NETD produces a radical intermediate that fragments to both even- and odd-electron products. NETD of GAGs was originally demonstrated with ion trap MS but can also be implemented with FTICR MS and Orbitrap MS.[74, 77-79] The electron transfer process in NETD occurs rapidly, on the order of 10-100 ms. This compares quite favorably to EDD, which generally uses activation times of 1 s. The short reaction time for NETD allows it to be paired with on-line separation techniques such as high-performance liquid chromatography (HPLC) and capillary zone electrophoresis (CZE). Leach *et al.* showed the ability to produce informative fragmentation of GAGs on a 10 ms time scale using NETD.[79] Wu *et al.* used NETD to distinguish 3-*O* versus 6-*O* sulfation in the amino sugar residues of HS oligomers up to dp6 in length.[80] Figure 1.6 illustrates the capability of NETD to produce cross-ring fragment ions that identify the location of all sulfation modifications in a HS tetramer, with a precursor that is deprotonated at only 4 of its 6 ionizable sites. The ability to distinguish 3-*O* from 6-*O* sulfation with a less than fully ionized precursor is promising for incorporation with on-line separations, where one has less control over the charge-state of the precursor ion than with infusion of a sample. Table 1.1 compares the activation methods discussed.

Table 1.1. List of activation methods commonly used for GAG characterization.

MS/MS Method	Pros	Cons
Collision Induced Dissociation (CID)	• Easily accessible • Available on wide variety of spectrometers • Produces abundance of glycosidic cleavages	• Requires highly ionized precursor ion • Does not produce high abundance of cross-ring cleavages • High degree of SO_3 loss
Infrared Multiphoton Dissociation (IRMPD)	• Ample glycosidic cleavages	• Requires highly ionized precursor ion • Requires Infrared laser • Multiple IR photons needed • Minimal cross-ring cleavages • Requires high vacuum environment
Ultraviolet Photodissociation (UVPD)	• Does not require highly ionized precursor • Single UV photon needed • High abundance of both glycosidic and cross-ring cleavages • Can be implemented on variety of spectrometers	• Requires UV laser
Electron Detachment Dissociation (EDD)	• Does not require fully ionized precursor ion • High abundance of both glycosidic and cross-ring cleavages	• Long experiment time • Requires source of electrons • Typically implemented on FTICR MS • Requires multiply charged precursor ion
Electron Induced Dissociation (EID)	• High abundance of cross-ring and glycosidic cleavages • Works on singly charged precursor ion	• Requires source of electrons • Requires singly charged precursor ion
Negative Electron Transfer Dissociation (NETD)	• Can be implemented on variety of spectrometers • Does not require fully ionized precursor ion • High abundance of cross-ring and glycosidic cleavages	• Shorter experiment times, can be implemented with separation techniques • Requires electron acceptor and carrier gas

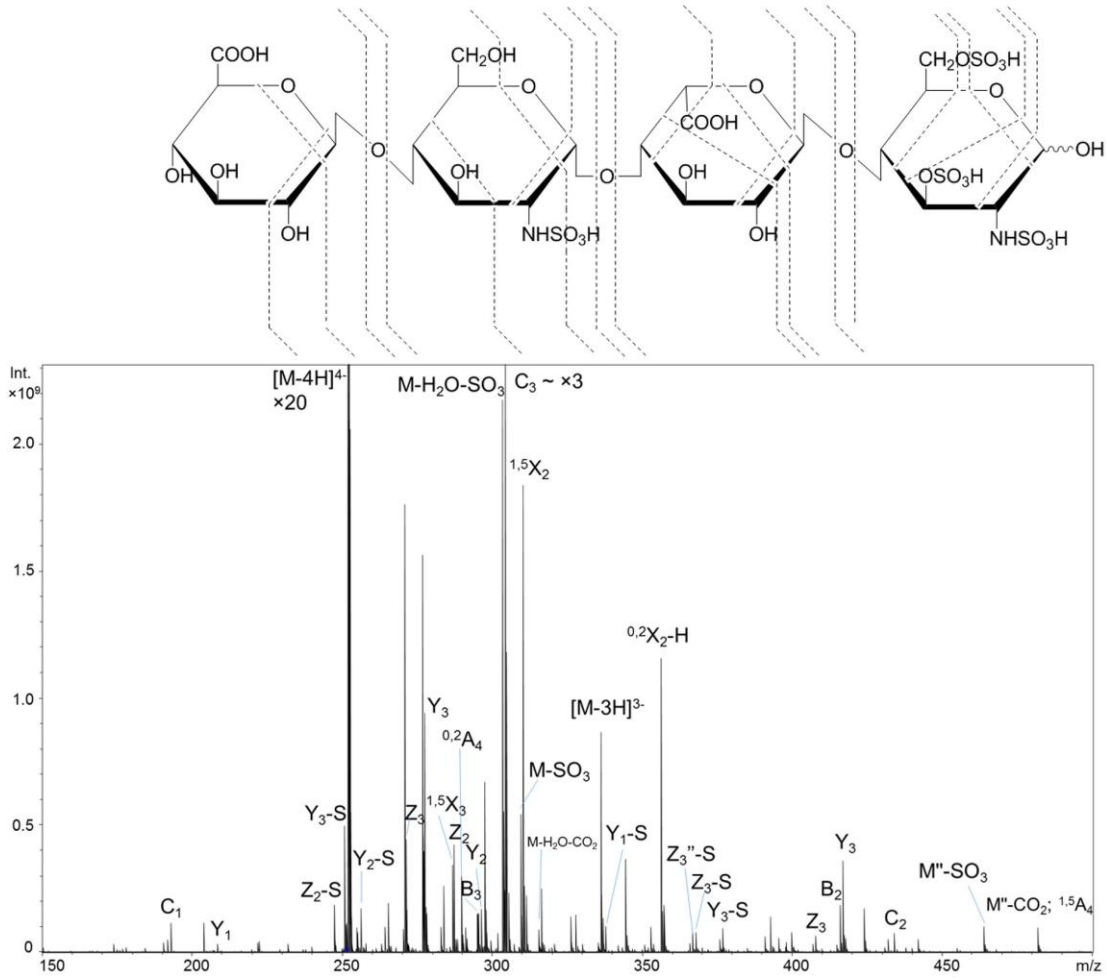

Figure 1.6. NETD spectrum of $[M-4H]^{4-}$ of tetrasulfated tetrasaccharide GlcA-GlcNS-IdoA-GlcNS3S6S and cleavage map illustrating the ability for NETD to distinguish 3-*O* sulfation from 6-*O* sulfation with the presence of $^{0,3}A_4$. Reprinted with permission with reference 96. Copyright 2018 American Chemical Society.

Applications

Mass spectrometry has been utilized for decades to tackle GAGs. Most of the initial work used a bottom-up approach in which enzymatic digestion of the GAG is performed prior to MS analysis to reduce the complexity of the sugars.[57, 81-82] Disaccharide analysis is still performed routinely to statistically determine the components and disaccharide backbone motifs of longer chains, but it results in a loss of structural information such as linkage, order, and sulfation patterns.[82-83] However, the location and organization of modification patterns on GAGs dictate their biological activity. Thus, the most recent endeavors have focused on partially digested sugars that retain biological function, and even full-length glycan chains.

Capillary zone electrophoresis (CZE) paired with NETD MS/MS has recently been used to determine the composition of GAGs found in human urine.[84] This work looked at urine from both males and females, separated into two age groups (young adults aged 23-25 and adults aged 35-45). These groups only represent a small number of nondiverse individuals and were not controlled for diet, hydration level or evaluated for health. It was found that female urine for both age groups had higher levels of HS than males (75.7% and 68.1%, respectively), and males had higher levels of CS than females (31% and 24%, respectively).[84] For both males and females, it was found that young adults had a higher level of HS whereas older adults had higher levels of CS. Disaccharide analysis based on LC-MS multiple reaction monitoring (MRM) identified unsulfated (0S) as the predominant HS disaccharide and 4-*O* sulfated (4S) as the predominant CS disaccharide.[82, 84] Though these were the most predominate sulfation patterns found, a wide range of sulfation patterns for both HS and CS was seen. Further analysis by molecular weight analysis and CZE-MS/MS found oligosaccharides ranging from dp2-20.[84]

Expanding upon past work which digested HS from bovine brain tissues, Zaia and coworkers demonstrated the ability to detect and analyze GAGs, N-glycans, and proteins from histological tissues.[85-86] By profiling different glycan classes as well as proteins, more detailed information can be obtained regarding temporally and spatially regulated tissue phenotypes.[86] A workflow was developed in which fixed or fresh tissue can be digested to yield GAGs, N-glycans, and proteins at once. This involved sequential enzymatic digestion by hyaluronidase, chondroitinase ABC, heparin lysases, trypsin, and PNGase F to the same area of interest.[86] Products were then analyzed using LC-MS. For GAGs, it was found that digestion time can be reduced by more than half (200 min to 50 min) when using microwave-assisted tissue digestion compared to incubator digestion. When investigating fresh and fixed mouse brain and liver samples, HA, CS and HS were in the mouse brain samples, whereas only HS was in the liver samples. It is known that HA and CS liver expression in rats is only 5-10% of that expressed in brains, which could explain why only HS was in the liver.[87] It was also determined that a tissue spot size as small as 0.5 μL (1 mm) could be used for GAG digestion.[86] Therefore, a specific area of tissue can be analyzed as opposed to bulk tissue analysis, allowing for analysis of both pathological and nonpathological sample regions.[86]

Recent studies of a CS binding protein have displayed a potential for this recombinant protein to facilitate the delivery of anti-cancer compounds into the tumor environment.[88] The malarial protein VAR2CSA binds to distinct types of CS that were until recently thought to be exclusively found in the placenta. However, this same CS is found in malignant cells and can be targeted by recombinant VAR2CSA (rVAR2).[88] To determine the structure of the CS found in both placenta and malignant tumors, disaccharide analysis was done using chondroitinase ABC and SEC-MS.[89] Collisional energy was applied for MS/MS to determine sulfation position of

disaccharides.[90] SEC-MS results showed that for bovine trachea CS, 90% of the compounds identified were mono-sulfated and 10% were un-sulfated. In contrast, cancer-associated CS was 98% mono-sulfated.[88] MS/MS results showed that of the 90% mono-sulfated CS, 79.6% was 4-*O* sulfated and 20.4% was 6-*O* sulfated (for lymphoma cells 4-*O* and 6-*O* sulfation was found to be 69.8% and 30.2%, respectively).[88] Further studies determined that 17 proteins, including syndecan 1, carbonic anhydrase IX, CD44 and CS-A modified proteoglycan CSPG4 can carry placental CS when overexpressed. Primary human tumor specimens representing 17 major human cancer types were tested to determine the inter-tumor diversity in expression of PGs able to display placenta CS. This placental CS was differentially, yet complementarily expressed in each of the 17 cancer groups tested.[88] The interaction of rVAR2 with the CS-modified form of CD44 in melanoma cells was validated. rVAR2 pulled down glycosylated CD44 from melanoma protein lysates. These data suggest that rVAR2 can be used to broadly target placental CS chains in human malignancies with differing PG expressions.[88] Further studies on the ability for rVAR2 to target tumor cells are ongoing.[91-92]

As an alternative to the bottom-up approaches to GAG characterization described above, there is a small body of work on the top-down analysis of intact glycan chains isolated from PGs. The simplest PGs, bikunin and decorin, have been the subject of this approach, with the GAG chains being analyzed using high resolution mass spectrometry.[23, 93-95] Though it is easier to analyze digested GAG chains, intact decorin and bikunin GAG chains have been analyzed.[93-95] For bikunin, the PG fraction was proteolyzed by actinase E digestion to yield a serine terminated glycan that was isolated by strong anion exchange spin columns.[93-95] For decorin, the GAG component was released by base-catalyzed β-elimination under reducing conditions.[95] The resulting heterogeneous mixture of GAGs released was separated into fractions of different chain

lengths by a series of steps including size exclusion chromatography, strong anion exchange, and polyacrylamide gel electrophoresis (PAGE).[93-95] Chains up to dp45 have been purified and analyzed using these techniques. Bikunin and decorin both have a single GAG chain attached to a core protein, making them the simplest proteoglycans. Bikunin has a CS chain, whereas decorin has a longer DS chain. The sequencing of the GAG chains of bikunin and decorin were accomplished by the Linhardt and Amster groups in collaboration. These studies used several stages of purification to fractionate the full-length glycans prior to MS analysis, as well as high resolution MS to examine the unfractionated mixture of intact glycans. The fractions were then analyzed using FTMS instruments (both Orbitrap MS and FTICR MS instruments) using MS1 for compositional assignment and CID/HCD MS/MS for sequencing. These analyses found the complexity of these mixtures to be far lower than anticipated for a random distribution of modifications.[23, 94-95] For bikunin, a conserved pattern of modification was observed for all the glycans that were analyzed (dp27-dp43). Decorin glycans were found to be more complicated, but also had a relatively small number of modification patterns. An example is presented in Figure 1.7 which shows the GAG chain of decorin connected to the protein core, a representative CID spectrum of a dp20 GAG, and the overall sequence motif for the GAG chain. Although top-down analysis of the full-length glycans from two PGs have been reported, it is unlikely that the top-down strategy will be useful for other PGs. Biologically relevant PGs are likely to rely on bottom-up methods.

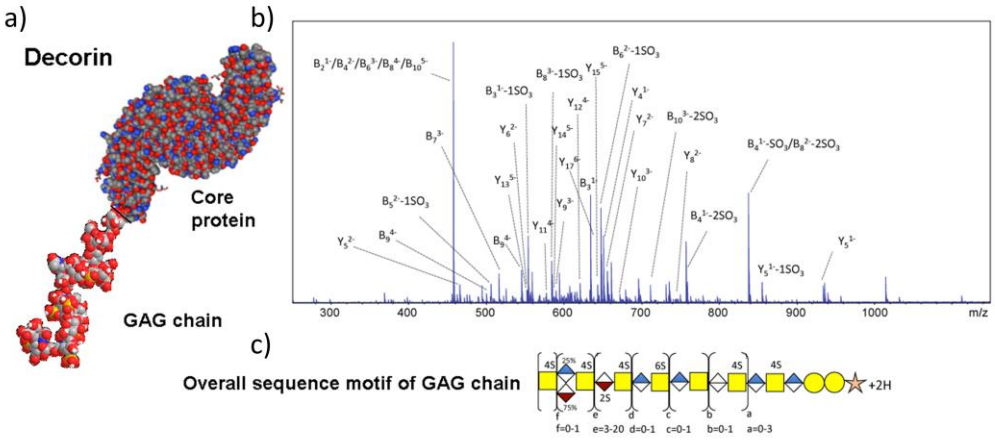

Figure 1.7. Modeled structure and motif of decorin glycosaminoglycan. a) Space-filled structure of decorin PG, with the core protein from PDB (1XCD). Carbons (gray), hydrogens (white), oxygens (red), nitrogens (blue), and sulfurs (yellow) are shown. The O-linked GAG chain (dp20–8S) is shown with the reducing end (RE) and nonreducing end (NRE). b) CID tandem mass spectrum of decorin GAG chain dp20 with 7 sulfo-modifications. c) Structural motif for decorin GAG chains determined by MS. Reprinted with permission from reference 23. Copyright 2017 American Chemical Society.

Conclusions

While challenges remain for the analysis of GAGs, recent advances, and research in MS of complex GAGs has paved the way for faster and more complete analysis. The evolution of MS/MS methods has led to more detailed structural characterization for this class of carbohydrates. Structures of GAG chains of different lengths and modifications can be

determined by MS/MS, especially when using electron-based methods. Recent advances in GAG analysis software have led to a faster analysis process, and a simplified way to identify unknown sample structures. With the wide variety of separation techniques that can be coupled to MS, more complex samples can be explored on a reasonable timescale to determine composition and sequence information. GAG analysis has mostly focused on shorter chains, but the sequencing of intact GAG chains such as bikunin and decorin demonstrate the capabilities of MS analysis. Future developments will integrate the isolation of biologically relevant regions of GAG chains with MS analysis, to address significant problems in biology and medicine.

Chapter 2 outlines the experimental procedures for the analysis and preparation of GAG standards utilized in this dissertation. GAG standards are prepared by chemical synthesis using a modular approach and by enzymatic digestion from naturally-derived polysaccharides. Mass spectrometry approaches for the characterization of these standards using charge transfer dissociation, ultraviolet photodissociation, electron detachment dissociation, negative electron transfer dissociation and collision induced dissociation are presented.

Implementation of charge transfer dissociation for the analysis of GAG standards is detailed in **Chapter 3**. Charge transfer dissociation can be implemented on a variety of mass spectrometers, including Thermo Fisher and Bruker ion trap instruments. Due to the high energy collisions of the highly energized He^+ with the analyte anions, extensive fragmentation is seen. Both heparan sulfate and chondroitin sulfate standards were analyzed to assess the fragmentation capabilities of CTD for GAG standards. Sulfate modification identification was comparable to EDD, and hexuronic acid stereochemistry was distinguishable for CS-A and DS.

The ability to distinguish hexuronic acid stereochemistry of CS-A and DS tetrasaccharides using UVPD is outlined in **Chapter 4**. Additionally, the optimization of

parameters previously shown to be imperative for protein fragmentation was investigated for the fragmentation of GAGs. This includes ionization state, wavelength, location of photodissociation, and number of laser shots. The effect these parameters have on fragmentation efficiency as well as on the ability to distinguish epimers differing only in hexuronic acid stereochemistry is shown.

The experimental parameters for NETD FTICR MS/MS of GAGs are examined in **Chapter 5**. NETD of GAGs using an FTICR MS has previously been demonstrated, however the amount of time analyte anions are accumulated with reagent cations has not been tested. The fragmentation efficiency as well as a comparison of assigned and unassigned fragment ions is detailed. Previous work has been done using EDD and CID to determine the ideal ionization state for optimal fragmentation. Here we also examine different ionization states of the heparin-like pharmaceutical, Fondaparinux Sodium, and the effect this has on fragmentation efficiency.

Acknowledgements

The authors are grateful for generous financial support from the National Institutes of Health, T32GM107004, P41GM103390 and U01CA231074.

References

(1) Ly, M.; Laremore, T. N.; Linhardt, R. J., Proteoglycomics: Recent Progress and Future Challenges. *Omics: A Journal of Integrative Biology* **2010,** *14*, 389-399.

(2) Varki, A.; Cummings, R. D.; Esko, J. D.; Freeze, H. H.; Stanley, P.; Bertozzi, C. R.; Hart, G. W.; Etzler, M. E., *Essentials of Glycobiology*. NY, 2009; Vol. 2.

(3) Fraser, J. R. E.; Laurent, T. C.; Laurent, U., Hyaluronan: its nature, distribution, functions and turnover. *Journal of internal medicine* **1997,** *242*, 27-33.

(4) Fallacara, A.; Manfredini, S.; Durini, E.; Vertuani, S., Hyaluronic acid fillers in soft tissue regeneration. *Facial Plastic Surgery* **2017,** *33*, 087-096.

(5) Raia, N. R.; Partlow, B. P.; McGill, M.; Kimmerling, E. P.; Ghezzi, C. E.; Kaplan, D. L., Enzymatically crosslinked silk-hyaluronic acid hydrogels. *Biomaterials* **2017,** *131*, 58-67.

(6) Heinegård, D.; Axelsson, I., Distribution of keratan sulfate in cartilage proteoglycans. *Journal of Biological Chemistry* **1977,** *252*, 1971-1979.

(7) Auray-Blais, C.; Collerette-Tremblay, J.; Lavoie, P., UPLC–MS/MS analysis of keratan sulfate from urine samples collected on filter paper for monitoring & follow-up of Morquio A patients. *Bioanalysis* **2018,** *10*, 1181-1192.

(8) Li, Q.; Li, G.; Zhao, X.; Shan, X.; Cai, C.; Zhao, J.; Zhang, F.; Linhardt, R. J.; Yu, G., Structural characterization and interaction with RCA120 of a highly sulfated keratan sulfate from blue shark (Prionace glauca) cartilage. *Marine drugs* **2018,** *16*, 128.

(9) Clegg, D. O.; Reda, D. J.; Harris, C. L.; Klein, M. A.; O'Dell, J. R.; Hooper, M. M.; Bradley, J. D.; Bingham, C. O.; Weisman, M. H.; Jackson, C. G.; Lane, N. E.; Cush, J. J.; Moreland, L. W.; Schumacher, H. R.; Oddis, C. V.; Wolfe, F.; Molitor, J. A.; Yocum, D. E.; Schnitzer, T. J.; Furst, D. E.; Sawitzke, A. D.; Shi, H.; Brandt, K. D.; Moskowitz, R. W.; Williams, H. J.,

Glucosamine, Chondroitin Sulfate, and the Two in Combination for Painful Knee Osteoarthritis. *New England Journal of Medicine* **2006,** *354,* 795-808.

(10) Shen, Y.; Tenney, A. P.; Busch, S. A.; Horn, K. P.; Cuascut, F. X.; Liu, K.; He, Z.; Silver, J.; Flanagan, J. G., PTPσ Is a Receptor for Chondroitin Sulfate Proteoglycan, an Inhibitor of Neural Regeneration. *Science* **2009,** *326,* 592-596.

(11) Igarashi, N.; Takeguchi, A.; Sakai, S.; Akiyama, H.; Higashi, K.; Toida, T., Effect of Molecular Sizes of Chondroitin Sulfate on Interaction with L-Selectin. *International Journal of Carbohydrate Chemistry* **2013,** *2013,* 856142.

(12) Sugahara, K.; Kitagawa, H., Recent advances in the study of the biosynthesis and functions of sulfated glycosaminoglycans. *Current Opinion in Structural Biology* **2000,** *10,* 518-527.

(13) Watanabe, H.; Yamada, Y.; Kimata, K., Roles of Aggrecan, a Large Chondroitin Sulfate Proteoglycan, in Cartilage Structure and Function. *The Journal of Biochemistry* **1998,** *124,* 687-693.

(14) Zhang, Q.; Du, Y.; Chen, J.; Xu, G.; Yu, T.; Hua, X.; Zhang, J., Investigation of chondroitin sulfate D and chondroitin sulfate E as novel chiral selectors in capillary electrophoresis. *Analytical and Bioanalytical Chemistry* **2014,** *406,* 1557-1566.

(15) Esko, J. D.; Lindahl, U., Molecular diversity of heparan sulfate. *The Journal of Clinical Investigation* **2001,** *108,* 169-173.

(16) Rabenstein, D. L., Heparin and heparan sulfate: structure and function. *Natural Product Reports* **2002,** *19,* 312-331.

(17) Uyama, T.; Kitagawa, H.; Sugahara, K., 3.05 - Biosynthesis of Glycosaminoglycans and Proteoglycans. In *Comprehensive Glycoscience*, Kamerling, H., Ed. Elsevier: Oxford, 2007; pp 79-104.

(18) Sasisekharan, R.; Raman, R.; Prabhakar, V., Glycomics approach to structure-function relationships of glycosaminoglycans. *Annual Review of Biomedical Engineering* **2006,** *8*, 181-231.

(19) Thacker, B. E.; Xu, D.; Lawrence, R.; Esko, J. D., Heparan sulfate 3-O-sulfation: a rare modification in search of a function. *Matrix Biology* **2014,** *35*, 60-72.

(20) Xu, D.; Esko, J. D., Demystifying Heparan Sulfate–Protein Interactions. *Annual Review of Biochemistry* **2014,** *83*, 129-157.

(21) Zhao, Y.; Singh, A.; Li, L.; Linhardt, R. J.; Xu, Y.; Liu, J.; Woods, R. J.; Amster, I. J., Investigating changes in the gas-phase conformation of Antithrombin III upon binding of Arixtra using traveling wave ion mobility spectrometry (TWIMS). *Analyst* **2015,** *140*, 6980-6989.

(22) Moure, M. J.; Eletsky, A.; Gao, Q.; Morris, L. C.; Yang, J. Y.; Chapla, D.; Zhao, Y.; Zong, C.; Amster, I. J.; Moremen, K. W.; Boons, G. J.; Prestegard, J. H., Paramagnetic Tag for Glycosylation Sites in Glycoproteins: Structural Constraints on Heparan Sulfate Binding to Robo1. *ACS Chemical Biology* **2018,** *13*, 2560-2567.

(23) Chi, L.; Wolff, J. J.; Laremore, T. N.; Restaino, O. F.; Xie, J.; Schiraldi, C.; Toida, T.; Amster, I. J.; Linhardt, R. J., Structural Analysis of Bikunin Glycosaminoglycan. *Journal of the American Chemical Society* **2008,** *130*, 2617-2625.

(24) Zamfir, A.; Seidler, D. G.; Kresse, H.; Peter-Katalinić, J., Structural characterization of chondroitin/dermatan sulfate oligosaccharides from bovine aorta by capillary electrophoresis and electrospray ionization quadrupole time-of-flight tandem mass spectrometry. *Rapid Communications in Mass Spectrometry* **2002,** *16*, 2015-2024.

(25) Kailemia, M. J.; Ruhaak, L. R.; Lebrilla, C. B.; Amster, I. J., Oligosaccharide Analysis by Mass Spectrometry: A Review of Recent Developments. *Analytical Chemistry* **2014,** *86*, 196-212.

(26) Staples, G. O.; Zaia, J., Analysis of Glycosaminoglycans Using Mass Spectrometry. *Current Proteomics* **2011,** *8*, 325-336.

(27) Zaia, J., Glycosaminoglycan glycomics using mass spectrometry. *Molecular & Cellular Proteomics* **2013,** *12*, 885-92.

(28) Zhou, W.; Håkansson, K., Structural Characterization of Carbohydrates by Fourier Transform Tandem Mass Spectrometry. *Current Proteomics* **2011,** *8*, 297-308.

(29) Zaia, J., Mass spectrometry and the emerging field of glycomics. *Chemical Biology* **2008,** *15*, 881-92.

(30) Zaia, J., Principles of mass spectrometry of glycosaminoglycans. *Journal of Biomacromolecular Mass Spectrometry* **2005,** *1*, 3-36.

(31) Wolff, J. J.; Laremore, T. N.; Busch, A. M.; Linhardt, R. J.; Amster, I. J., Influence of charge state and sodium cationization on the electron detachment dissociation and infrared multiphoton dissociation of glycosaminoglycan oligosaccharides. *Journal of the American Society for Mass Spectrometry* **2008,** *19*, 790-798.

(32) Gill, V. L.; Aich, U.; Rao, S.; Pohl, C.; Zaia, J., Disaccharide Analysis of Glycosaminoglycans Using Hydrophilic Interaction Chromatography and Mass Spectrometry. *Analytical Chemistry* **2013,** *85*, 1138-1145.

(33) Hitchcock, A. M.; Bowman, M. J.; Staples, G. O.; Zaia, J., Improved Workup for Glycosaminoglycan Disaccharide Analysis using Capillary Electrophoresis with Laser-Induced Fluorescence Detection. *Electrophoresis* **2008,** *29*, 4538-4548.

(34) Margolis, R. U.; Margolis, R. K.; Chang, L. B.; Preti, C., Glycosaminoglycans of brain during development. *Biochemistry* **1975,** *14*, 85-88.

(35) Kovalszky, I.; Pogany, G.; Molnar, G.; Jeney, A.; Lapis, K.; Karacsonyi, S.; Szecseny, A.; Iozzo, R. V., Altered glycosaminoglycan composition in reactive and neoplastic human liver. *Biochemical and Biophysical Research Communications* **1990,** *167*, 883-890.

(36) Zhang, Z.; Ohtake-Niimi, S.; Kadomatsu, K.; Uchimura, K., Reduced molecular size and altered disaccharide composition of cerebral chondroitin sulfate upon Alzheimer's pathogenesis in mice. *Nagoya Journal of Medical Science* **2016,** *78*, 293-301.

(37) Pudelko, A.; Wisowski, G.; Olczyk, K.; Kozma, E. M., The dual role of the glycosaminoglycan chondroitin-6-sulfate in the development, progression and metastasis of cancer. *FEBS Journal* **2019,** *286*, 1815-1837.

(38) Sanderson, P.; Stickney, M.; Leach, F. E.; Xia, Q.; Yu, Y.; Zhang, F.; Linhardt, R. J.; Amster, I. J., Heparin/heparan sulfate analysis by covalently modified reverse polarity capillary zone electrophoresis-mass spectrometry. *Journal of Chromatography A* **2018,** *1545*, 75-83.

(39) Yu, Y.; Zhang, F.; Renois-Predelus, G.; Amster, I. J.; Linhardt, R. J., Filter-entrapment enrichment pull-down assay for glycosaminoglycan structural characterization and protein interaction. *Carbohydrate Polymers* **2020**, 116623.

(40) Zaia, J., On-line separations combined with MS for analysis of glycosaminoglycans. *Mass Spectrometry Reviews* **2009,** *28*, 254-272.

(41) Klein, D. R.; Leach, F. E.; Amster, I. J.; Brodbelt, J. S., Structural Characterization of Glycosaminoglycan Carbohydrates Using Ultraviolet Photodissociation. *Analytical Chemistry* **2019,** *91*, 6019-6026.

(42) Wolff, J. J.; Amster, I. J.; Chi, L. L.; Linhardt, R. J., Electron detachment dissociation of glycosaminoglycan tetrasaccharides. *Journal of the American Society for Mass Spectrometry* **2007,** *18*, 234-244.

(43) Wolff, J. J.; Laremore, T. N.; Busch, A. M.; Linhardt, R. J.; Amster, I. J., Electron detachment dissociation of dermatan sulfate oligosaccharides. *J Am Soc Mass Spectrom* **2008,** *19*, 294-304.

(44) Wolff, J. J.; Chi, L. L.; Linhardt, R. J.; Amster, I. J., Distinguishing glucuronic from iduronic acid in glycosaminoglycan tetrasaccharides by using electron detachment dissociation. *Analytical Chemistry* **2007,** *79*, 2015-2022.

(45) Leach, F. E.; Wolff, J. J.; Laremore, T. N.; Linhardt, R. J.; Amster, I. J., Evaluation of the experimental parameters which control electron detachment dissociation, and their effect on the fragmentation efficiency of glycosaminoglycan carbohydrates. *Int J Mass Spectrom* **2008,** *276*, 110-115.

(46) Wolff, J. J.; Laremore, T. N.; Aslam, H.; Linhardt, R. J.; Amster, I. J., Electron-Induced Dissociation of Glycosaminoglycan Tetrasaccharides. *J Am Soc Mass Spectrom* **2008,** *19*, 1449-1458.

(47) Leach, F. E.; Arungundram, S.; Al-Mafraji, K.; Venot, A.; Boons, G.-J.; Amster, I. J., Electron detachment dissociation of synthetic heparan sulfate glycosaminoglycan tetrasaccharides varying in degree of sulfation and hexuronic acid stereochemistry. *International Journal of Mass Spectrometry* **2012,** *330-332*, 152-159.

(48) Huang, Y.; Yu, X.; Mao, Y.; Costello, C. E.; Zaia, J.; Lin, C., De Novo Sequencing of Heparan Sulfate Oligosaccharides by Electron-Activated Dissociation. *Anal Chem* **2013,** *85*, 11979-11986.

(49) Agyekum, I.; Zong, C.; Boons, G. J.; Amster, I. J., Single Stage Tandem Mass Spectrometry Assignment of the C-5 Uronic Acid Stereochemistry in Heparan Sulfate Tetrasaccharides using Electron Detachment Dissociation. *Journal of the American Society for Mass Spectrometry* **2017,** *28*, 1741-1750.

(50) Prabhakar, V.; Capila, I.; Sasisekharan, R., The Structural Elucidation of Glycosaminoglycans. In *Glycomics: Methods and Protocols*, Packer, N. H.; Karlsson, N. G., Eds. Humana Press: Totowa, NJ, 2009; pp 147-156.

(51) Oh, H. B.; Leach, F. E.; Arungundram, S.; Al-Mafraji, K.; Venot, A.; Boons, G.-J.; Amster, I. J., Multivariate Analysis of Electron Detachment Dissociation and Infrared Multiphoton Dissociation Mass Spectra of Heparan Sulfate Tetrasaccharides Differing Only in Hexuronic acid Stereochemistry. *Journal of The American Society for Mass Spectrometry* **2011,** *22*, 582-590.

(52) Leach, F. E.; Ly, M.; Laremore, T. N.; Wolff, J. J.; Perlow, J.; Linhardt, R. J.; Amster, I. J., Hexuronic Acid Stereochemistry Determination in Chondroitin Sulfate Glycosaminoglycan Oligosaccharides by Electron Detachment Dissociation. *J Am Soc Mass Spectrom* **2012,** *23*, 1488-1497.

(53) Agyekum, I.; Patel, A. B.; Zong, C.; Boons, G.-J.; Amster, I. J., Assignment of hexuronic acid stereochemistry in synthetic heparan sulfate tetrasaccharides with 2-O-sulfo uronic acids using electron detachment dissociation. *Int J Mass Spectrom* **2015,** *390*, 163-169.

(54) Zaia, J.; McClellan, J. E.; Costello, C. E., Tandem Mass Spectrometric Determination of the 4S/6S Sulfation Sequence in Chondroitin Sulfate Oligosaccharides. *Analytical Chemistry* **2001,** *73*, 6030-6039.

(55) Zaia, J.; Costello, C. E., Tandem Mass Spectrometry of Sulfated Heparin-Like Glycosaminoglycan Oligosaccharides. *Analytical Chemistry* **2003,** *75*, 2445-2455.

(56) Domon, B.; Costello, C. E., A systematic nomenclature for carbohydrate fragmentations in FAB-MS/MS spectra of glycoconjugates. *Glycoconjugate journal* **1988,** *5*, 397-409.

(57) Desaire, H.; Sirich, T. L.; Leary, J. A., Evidence of Block and Randomly Sequenced Chondroitin Polysaccharides: Sequential Enzymatic Digestion and Quantification Using Ion Trap Tandem Mass Spectrometry. *Analytical Chemistry* **2001,** *73*, 3513-3520.

(58) Kailemia, M. J.; Li, L.; Ly, M.; Linhardt, R. J.; Amster, I. J., Complete Mass Spectral Characterization of a Synthetic Ultralow-Molecular-Weight Heparin Using Collision-Induced Dissociation. *Analytical Chemistry* **2012,** *84*, 5475-5478.

(59) Kailemia, M. J.; Li, L.; Xu, Y.; Liu, J.; Linhardt, R. J.; Amster, I. J., Structurally Informative Tandem Mass Spectrometry of Highly Sulfated Natural and Chemoenzymatically Synthesized Heparin and Heparan Sulfate Glycosaminoglycans. *Molecular & Cellular Proteomics* **2013,** *12*, 979-990.

(60) Guo, Q.; Reinhold, V. N., Advancing MSn spatial resolution and documentation for glycosaminoglycans by sulfate-isotope exchange. *Analytical and Bioanalytical Chemistry* **2019,** *411*, 5033-5045.

(61) Liang, Q.; Chopra, P.; Boons, G.-J.; Sharp, J. S., Improved de novo sequencing of heparin/heparan sulfate oligosaccharides by propionylation of sites of sulfation. *Carbohydrate Research* **2018,** *465*, 16-21.

(62) Huang, R.; Zong, C.; Venot, A.; Chiu, Y.; Zhou, D.; Boons, G.-J.; Sharp, J. S., De Novo Sequencing of Complex Mixtures of Heparan Sulfate Oligosaccharides. *Analytical Chemistry* **2016,** *88*, 5299-5307.

(63) Saad, O. M.; Leary, J. A., Delineating mechanisms of dissociation for isomeric heparin disaccharides using isotope labeling and ion trap tandem mass spectrometry. *Journal of the American Society for Mass Spectrometry* **2004,** *15*, 1274-1286.

(64) Zaia, J.; Miller, M. J. C.; Seymour, J. L.; Costello, C. E., The role of mobile protons in negative ion CID of oligosaccharides. *Journal of the American Society for Mass Spectrometry* **2007,** *18*, 952-960.

(65) Leach, F. E.; Xiao, Z.; Laremore, T. N.; Linhardt, R. J.; Amster, I. J., Electron detachment dissociation and infrared multiphoton dissociation of heparin tetrasaccharides. *Int J Mass Spectrom* **2011,** *308*, 253-259.

(66) Wolff, J. J.; Laremore, T. N.; Leach, F. E.; Linhardt, R. J.; Amster, I. J., Electron Capture Dissociation, Electron Detachment Dissociation and Infrared Multiphoton Dissociation of Sucrose Octasulfate. *European Journal of Mass Spectrometry* **2009,** *15*, 275-281.

(67) Håkansson, K.; Cooper, H. J.; Emmett, M. R.; Costello, C. E.; Marshall, A. G.; Nilsson, C. L., Electron capture dissociation and infrared multiphoton dissociation MS/MS of an N-glycosylated tryptic peptide to yield complementary sequence information. *Analytical Chemistry* **2001,** *73*, 4530-4536.

(68) Wolff, J. J.; Amster, I. J.; Chi, L.; Linhardt, R. J., Electron detachment dissociation of glycosaminoglycan tetrasaccharides. *Journal of the American Society for Mass Spectrometry* **2007,** *18*, 234-44.

(69) McClellan, J. E.; Costello, C. E.; O'Conno, P. B.; Zaia, J., Influence of Charge State on Product Ion Mass Spectra and the Determination of 4S/6S Sulfation Sequence of Chondroitin Sulfate Oligosaccharides. *Analytical Chemistry* **2002,** *74*, 3760-3771.

(70) Ly, T.; Julian, R. R., Ultraviolet photodissociation: developments towards applications for mass-spectrometry-based proteomics. *Angewandte Chemie International Edition* **2009,** *48*, 7130-7137.

(71) Racaud, A.; Antoine, R.; Dugourd, P.; Lemoineb, J., Photoinduced dissociation of heparin-derived oligosaccharides controlled by charge location. *Journal of the American Society for Mass Spectrometry* **2010,** *21*, 2077-2084.

(72) Kailemia, M. J.; Park, M.; Kaplan, D. A.; Venot, A.; Boons, G. J.; Li, L.; Linhardt, R. J.; Amster, I. J., High-field asymmetric-waveform ion mobility spectrometry and electron detachment dissociation of isobaric mixtures of glycosaminoglycans. *Journal of the American Society for Mass Spectrometry* **2014,** *25*, 258-68.

(73) Leach, F. E.; Wolff, J. J.; Xiao, Z.; Ly, M.; Laremore, T. N.; Arungundram, S.; Al-Mafraji, K.; Venot, A.; Boons, G.-J.; Linhardt, R. J.; Amster, I. J., Negative electron transfer dissociation Fourier transform mass spectrometry of glycosaminoglycan carbohydrates. *European Journal of Mass Spectrometry* **2011,** *17*, 167-176.

(74) Wolff, J. J.; Leach, F. E.; Laremore, T. N.; Kaplan, D. A.; Easterling, M. L.; Linhardt, R. J.; Amster, I. J., Negative electron transfer dissociation of glycosaminoglycans. *Analytical Chemistry* **2010,** *82*, 3460-3466.

(75) Coon, J. J.; Shabanowitz, J.; Hunt, D. F.; Syka, J. E. P., Electron transfer dissociation of peptide anions. *J Am Soc Mass Spectrom* **2005,** *16*, 880-882.

(76) Rush, M. J. P.; Riley, N. M.; Westphall, M. S.; Syka, J. E. P.; Coon, J. J., Sulfur Pentafluoride is a Preferred Reagent Cation for Negative Electron Transfer Dissociation. *J Am Soc Mass Spectrom* **2017,** *28*, 1324-1332.

(77) Leach, F. E.; Wolff, J. J.; Xiao, Z. P.; Ly, M.; Laremore, T. N.; Arungundram, S.; Al-Mafraji, K.; Venot, A.; Boons, G. J.; Linhardt, R. J.; Amster, I. J., Negative electron transfer dissociation Fourier transform mass spectrometry of glycosaminoglycan carbohydrates. *Eur J Mass Spectrom* **2011,** *17*, 167-176.

(78) Stickney, M.; Sanderson, P.; Leach, F. E.; Zhang, F.; Linhardt, R. J.; Amster, I. J., Online capillary zone electrophoresis negative electron transfer dissociation tandem mass spectrometry of glycosaminoglycan mixtures. *International Journal of Mass Spectrometry* **2019,** *445*, 116209.

(79) Leach, F. E.; Riley, N. M.; Westphall, M. S.; Coon, J. J.; Amster, I. J., Negative Electron Transfer Dissociation Sequencing of Increasingly Sulfated Glycosaminoglycan Oligosaccharides on an Orbitrap Mass Spectrometer. *Journal of The American Society for Mass Spectrometry* **2017,** *28*, 1844-1854.

(80) Wu, J.; Wei, J.; Hogan, J. D.; Chopra, P.; Joshi, A.; Lu, W.; Klein, J.; Boons, G.-J.; Lin, C.; Zaia, J., Negative Electron Transfer Dissociation Sequencing of 3-O-Sulfation-Containing Heparan Sulfate Oligosaccharides. *Journal of The American Society for Mass Spectrometry* **2018,** *29*, 1262-1272.

(81) Li, G.; Steppich, J.; Wang, Z.; Sun, Y.; Xue, C.; Linhardt, R. J.; Li, L., Bottom-Up Low Molecular Weight Heparin Analysis Using Liquid Chromatography-Fourier Transform Mass Spectrometry for Extensive Characterization. *Analytical Chemistry* **2014,** *86*, 6626-6632.

(82) Sun, X.; Li, L.; Overdier, K. H.; Ammons, L. A.; Douglas, I. S.; Burlew, C. C.; Zhang, F.; Schmidt, E. P.; Chi, L.; Linhardt, R. J., Analysis of Total Human Urinary Glycosaminoglycan Disaccharides by Liquid Chromatography–Tandem Mass Spectrometry. *Analytical Chemistry* **2015,** *87*, 6220-6227.

(83) Turiák, L.; Tóth, G.; Ozohanics, O.; Révész, Á.; Ács, A.; Vékey, K.; Zaia, J.; Drahos, L., Sensitive method for glycosaminoglycan analysis of tissue sections. *Journal of Chromatography A* **2018,** *1544*, 41-48.

(84) Han, X.; Sanderson, P.; Nesheiwat, S.; Lin, L.; Yu, Y.; Zhang, F.; Amster, I. J.; Linhardt, R. J., Structural analysis of urinary glycosaminoglycans from healthy human subjects. *Glycobiology* **2020,** *30*, 143-151.

(85) Shao, C.; Shi, X.; Phillips, J. J.; Zaia, J., Mass Spectral Profiling of Glycosaminoglycans from Histological Tissue Surfaces. *Analytical Chemistry* **2013,** *85*, 10984-10991.

(86) Pantazopoulos, H.; Leon, D. R.; Zaia, J., Workflow for Combined Proteomics and Glycomics Profiling from Histological Tissues. **2014**.

(87) Margolis, R. U.; Margolis, R. K., *Heparin: Structure, Cellular Functions and Clinical Application*. Academic Press: New York: 1979; p 227-241.

(88) Salanti, A.; Clausen, T. M.; Agerbæk, M. Ø.; Al Nakouzi, N.; Dahlbäck, M.; Oo, H. Z.; Lee, S.; Gustavsson, T.; Rich, J. R.; Hedberg, B. J., Targeting human cancer by a glycosaminoglycan binding malaria protein. *Cancer cell* **2015,** *28*, 500-514.

(89) Shi, X.; Zaia, J., Organ-specific heparan sulfate structural phenotypes. *Journal of Biological Chemistry* **2009,** *284*, 11806-11814.

(90) Shao, C.; Shi, X.; White, M.; Huang, Y.; Hartshorn, K.; Zaia, J., Comparative glycomics of leukocyte glycosaminoglycans. *The FEBS journal* **2013,** *280*, 2447-2461.

(91) Clausen, T. M.; Pereira, M. A.; Al Nakouzi, N.; Oo, H. Z.; Agerbæk, M. Ø.; Lee, S.; Ørum-Madsen, M. S.; Kristensen, A. R.; El-Naggar, A.; Grandgenett, P. M., Oncofetal chondroitin sulfate glycosaminoglycans are key players in integrin signaling and tumor cell motility. *Molecular Cancer Research* **2016,** *14*, 1288-1299.

(92) Agerbæk, M. Ø.; Bang-Christensen, S. R.; Yang, M.-H.; Clausen, T. M.; Pereira, M. A.; Sharma, S.; Ditlev, S. B.; Nielsen, M. A.; Choudhary, S.; Gustavsson, T., The VAR2CSA malaria protein efficiently retrieves circulating tumor cells in an EpCAM-independent manner. *Nature communications* **2018,** *9*, 1-13.

(93) Laremore, T. N.; Leach, F. E.; Amster, I. J.; Linhardt, R. J., Electrospray ionization Fourier transform mass spectrometric analysis of intact bikunin glycosaminoglycan from normal human plasma. *International Journal of Mass Spectrometry* **2011,** *305*, 109-115.

(94) Ly, M.; Leach, F. E., 3rd; Laremore, T. N.; Toida, T.; Amster, I. J.; Linhardt, R. J., The proteoglycan bikunin has a defined sequence. *Nature Chemical Biology* **2011,** *7*, 827-33.

(95) Yu, Y.; Duan, J.; Leach, F. E.; Toida, T.; Higashi, K.; Zhang, H.; Zhang, F.; Amster, I. J.; Linhardt, R. J., Sequencing the Dermatan Sulfate Chain of Decorin. *Journal of the American Chemical Society* **2017,** *139*, 16986-16995.

CHAPTER 2

Experimental

Glycosaminoglycan Preparation

Synthetic Heparan Sulfate Oligosaccharide Preparation

Heparan sulfate (HS) tetrasaccharide standards were prepared by chemical synthesis using a modular approach and further purified by silica gel column chromatography.[1] Structures were confirmed by ^{1}H NMR and accurate mass measurement by FTICR-MS.[1]

Chondroitin Sulfate Oligosaccharide Preparation

Chondroitin sulfate A (CS-A) and dermatan sulfate (DS) oligosaccharides were prepared by partial enzymatic depolymerization from bovine trachea chondroitin sulfate A (Celsus laboratories, Cincinnati, OH, USA) and porcine intestinal mucosa dermatan sulfate (Celsus Laboratories) respectively. Full explanations of enzymatic depolymerization and desulfation have been reported previously.[2-3]

Fondaparinux Sodium Preparation

Fondaparinux Sodium was purchased from Fisher Scientific (Hampton, NH, USA). Fondaparinux Sodium was desalted with a 3 kDa Amicon Ultra centrifugal filter (Millipore, Temecula, CA) prior to mass spectrometry analysis. Heparan sulfate chains dp4 and larger do not pass through the 3 kDa membrane.[4] Prior to use filters were conditioned with water, and the

sample was washed with 5-10 filter volumes of water (14,000 x g for 30 min each) depending on the desired sodiated state. 0.1% diethylamine was added to the solvent mixture for additional removal of sodium.

Mass Spectrometry Analysis

0.1 mg/mL of each GAG standard was ionized by nanospray ESI with a spray voltage of 0.8-1.2 kV (pulled glass tip model Econo12-N; New Objective, Woburn, MA). All standards were analyzed in negative ion mode.

Electron Detachment Dissociation

EDD spectra for all samples were collected on a 9.4T Bruker solariX XR Fourier transform ion cyclotron resonance mass spectrometer (Bremen, Germany) with a hollow cathode (HeatWave, Wasonville, CA, USA), which serves as the source of electrons for EDD. Multiply charged precursor ions were isolated in the quadrupole and accumulated for 2-3 s before injection into the dynamically harmonized FTICR cell. Ions were then irradiated for 1 s with 19 eV electrons. The cathode heater was set to 1.5 A and the extraction lens was set to 18.6 ± 0.4 V. 1 M points were acquired for each spectrum and 48 acquisitions were averaged for each stored spectrum. An external calibration was performed using NaTFA clusters, resulting in a mass accuracy of 10 ppm or better. Internal calibration was performed using confidently assigned glycosidic cleavage product ions as internal calibrants. A schematic of EDD is illustrated in Figure B.1.

Negative Electron Transfer Dissociation

NETD experiments were performed using a 9.4 T Bruker solariX XR Fourier transform ion cyclotron resonance mass spectrometer (Berman, Germany. Each experiment was repeated a minimum of three times with similar results for each compound examined. Precursor ions were mass selected in the quadrupole and acquired at a mass resolution of 2 M for 1-3 s. An external calibration was performed using NaTFA clusters, resulting in a mass accuracy of 10 ppm or better. Internal calibration was performed using confidently assigned glycosidic bond cleavages as calibrants.

NETD experiments were performed using a 50-1000 ms reagent accumulation time and a 50 ms reaction time. Fluoranthene cation radicals were generated in the presence of Ar in the chemical ionization (CI) source. Experiments were performed in serial mode, averaging 1 scan, and presented spectra are the result of 3-5 mins of spectral averaging. A schematic of the NETD experiment is illustrated in Figure 2.1.

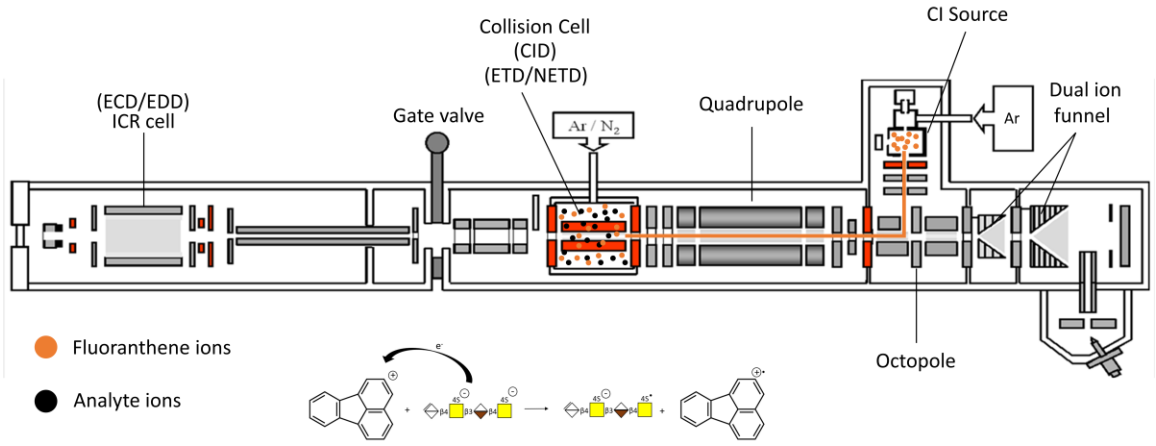

Figure 2.1. NETD schematic on a Bruker solariX XR FTICR MS.

Charge Transfer Dissociation and Collision Induced Dissociation

CTD and CID experiments were performed on a modified Bruker AmaZon 3D ion trap (Bremen, Germany), with a custom vacuum chamber cover. A saddle field fast ion gun (VSW/ Atomtech, Macclesfield, UK) was installed on top of the ring electrode. The saddle field fast ion source was used as the helium cation source, which is described in detail elsewhere.[5] Multiply charged precursor ions were activated with 7.5-8 keV helium cations for 100 ms for CTD. Helium gas flow in the ion gun was controlled via a variable leak valve and measured by the ion trap gauge; the readout was approximately 9.5 $x10^{6}$ mbar. Precursor ions were accumulated for 20-60 ms in the ion trap before isolation. Each stored CTD spectrum was the average of 5 replicate scans, and the presented spectra are typically the result of 1.5-2 mins of spectral averaging. Internal calibration was performed using confidently assigned glycosidic cleavage product ions as internal calibrants. A schematic of the CTD experiment is shown in Figure B.2.

For the experiments involving CTD with resonance ejection, precursor ions were first isolated and irradiated with helium cations to achieve CTD at the MS^2 level. Any unreacted precursor ions were then resonantly ejected at the MS^3 level using on-resonance excitation with an amplitude >3 V. In the absence of CTD at the MS^2 level and the presence of the resonance ejection at the MS^3 level, no fragment ions were observed, thereby verifying the absence of unwanted CID peaks during resonance ejection.

Ultraviolet Photodissociation and Higher-Energy Collisional Dissociation

All experiments were performed on a Thermo Fisher Orbitrap Fusion Lumos mass spectrometer (San Jose, CA, USA). The mass spectrometer was equipped with a Coherent Excistar 193 nm excimer laser (Santa Clara, CA) or a 213 nm CryLas solid state laser (Berlin, Germany) depending on the experiment. Samples were sprayed from a nanoelectrospray static source with a spray voltage of 0.8-1.2 kV. Samples were diluted in 50:50 MeOH:H_2O to a concentration of 50 μg/mL before ionization. Spectra were collected in negative ion mode at a resolving power of 120,000 at *m/z* 200 in full-profile mode. To minimize sulfate decomposition in MS^1 spectra, the ion funnel RF was set to 10%. Precursor ions were isolated in the ion trap using an isolation width of 3 *m/z*. Higher-energy collisional dissociation (HCD) was performed using a normalized collision energy (NCE) of 15-25. 193 nm UVPD was performed in both the low-pressure cell and the high-pressure cell, using 4 or 8 pulses at 4mJ per pulse. 213 nm UVPD experiments were also performed in the low-pressure cell and high-pressure cell, using a variety of pulses at 3 μJ per pulse to result in activation periods ranging from 1 ms- 400 ms. All data presented is an average of 50 transients, resulting in an experimental time of approximately 30-60 s.[6] A schamtic illustrator the UVPD experiment is shown in Figure 2.2.

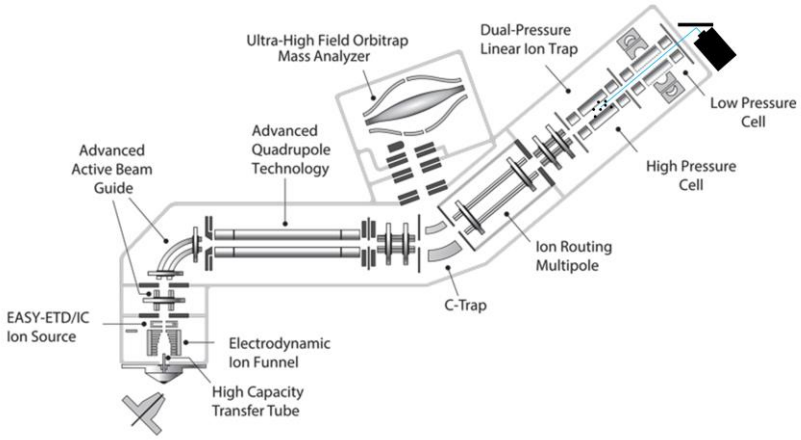

Figure 2.2. UVPD schematic on a Thermo Fisher Orbitrap Fusion Lumos. Analyte ions are depicted as being stored in the High-Pressure Cell.

Data Interpretation and Analysis

Spectra was interpreted using Glycoworkbench 2.0[7] and an in-house GAG analysis software.[8-9] Fragment ions are reported using the Wolff-Amster annotation derived from the Domon and Costello nomenclature.[10-11] Fragment ion maps use dashed lines drawn through the chemical structure to depict fragmentation, and hash marks at the end of the lines indicate the specific fragment ion. Circles at the end of the hash marks represent sulfate decomposition via loss of SO_3 with an open circle representing one SO_3 loss and a filled circle representing multiple SO_3 loss. A tick mark within a hash mark represents loss of hydrogen, and two tick marks

represent the loss of two hydrogen atoms. Donut plots display the percentages of the summed ion abundances for glycosidic fragment ions, cross-ring fragment ions, glycosidic fragment ions with sulfate decomposition and cross-ring fragment ions with sulfate decomposition.

References

(1) Arungundram, S.; Al-Mafraji, K.; Asong, J.; Leach, F. E.; Amster, I. J.; Venot, A.; Turnbull, J. E.; Boons, G.-J., Modular Synthesis of Heparan Sulfate Oligosaccharides for Structure-Activity Relationship Studies. *Journal of the American Chemical Society* **2009,** *131*, 17394-17405.

(2) Leach, F. E.; Ly, M.; Laremore, T. N.; Wolff, J. J.; Perlow, J.; Linhardt, R. J.; Amster, I. J., Hexuronic Acid Stereochemistry Determination in Chondroitin Sulfate Glycosaminoglycan Oligosaccharides by Electron Detachment Dissociation. *Journal of The American Society for Mass Spectrometry* **2012,** *23*, 1488-1497.

(3) Leach, F. E.; Riley, N. M.; Westphall, M. S.; Coon, J. J.; Amster, I. J., Negative Electron Transfer Dissociation Sequencing of Increasingly Sulfated Glycosaminoglycan Oligosaccharides on an Orbitrap Mass Spectrometer. *Journal of The American Society for Mass Spectrometry* **2017,** *28*, 1844-1854.

(4) Sanderson, P.; Stickney, M.; Leach, F. E.; Xia, Q.; Yu, Y.; Zhang, F.; Linhardt, R. J.; Amster, I. J., Heparin/heparan sulfate analysis by covalently modified reverse polarity capillary zone electrophoresis-mass spectrometry. *Journal of Chromatography A* **2018,** *1545*, 75-83.

(5) Hoffmann, W. D.; Jackson, G. P., Charge Transfer Dissociation (CTD) Mass Spectrometry of Peptide Cations Using Kiloelectronvolt Helium Cations. *Journal of The American Society for Mass Spectrometry* **2014,** *25*, 1939-1943.

(6) Klein, D.; Leach, F. I.; Amster, I.; Brodbelt, J., Structural Characterization of Glycosaminoglycan Carbohydrates using Ultraviolet Photodissociation. *Analytical chemistry* **2019**.

(7) Ceroni, A.; Maass, K.; Geyer, H.; Geyer, R.; Dell, A.; Haslam, S. M., GlycoWorkbench: a tool for the computer-assisted annotation of mass spectra of glycans. *Journal of proteome research* **2008,** *7*, 1650-1659.

(8) Duan, J.; Jonathan Amster, I., An Automated, High-Throughput Method for Interpreting the Tandem Mass Spectra of Glycosaminoglycans. *Journal of The American Society for Mass Spectrometry* **2018,** *29*, 1802-1811.

(9) Duan, J.; Pepi, L.; Amster, I. J., A Scoring Algorithm for the Automated Analysis of Glycosaminoglycan MS/MS Data. *Journal of the American Society for Mass Spectrometry* **2019**, 1-12.

(10) Domon, B.; Costello, C. E., A systematic nomenclature for carbohydrate fragmentations in FAB-MS/MS spectra of glycoconjugates. *Glycoconjugate Journal* **1988,** *5*, 397-409.

(11) Wolff, J. J.; Laremore, T. N.; Busch, A. M.; Linhardt, R. J.; Amster, I. J., Influence of charge state and sodium cationization on the electron detachment dissociation and infrared multiphoton dissociation of glycosaminoglycan oligosaccharides. *J Am Soc Mass Spectrom* **2008,** *19*, 790-8.

CHAPTER 3

Structural Characterization of Sulfated Glycosaminoglycans Using Charge Transfer Dissociation

Pepi, L. E., Sasiene, Z. J., Mendis, P. M., Jackson, G. P., & Amster, I. J. *J. Am. Soc. Mass Spectrom.* 2020, 31(10), 2143-2153. Reprinted with permission of publisher

Abstract

Glycosaminoglycans (GAGs) participate in a broad range of physiological processes, and their structures are of interest to researchers in structural biology and medicine. Although they are abundant in tissues and extracellular matrices, their structural heterogeneity makes them challenging analytes. Mass spectrometry, and more specifically, tandem mass spectrometry, is particularly well suited for their analysis. Many tandem mass spectrometry techniques have been examined for their suitability towards the structural characterization of GAGs. Threshold activation methods such as collision induced dissociation (CID) produce mainly glycosidic cleavages and do not yield a broad range of structurally informative cross-ring fragments. Considerable research effort has been directed at finding other means of dissociating gas-phase GAG ions to produce more comprehensive structural information. Here, we compare the structural information of GAGs obtained by charge transfer dissociation (CTD) and electron detachment dissociation (EDD). EDD has previously been applied to GAGs and is known to produce both glycosidic and cross-ring cleavages in similar abundance. CTD has not previously been used to analyze GAGs but has been shown to produce abundant cross-ring cleavages and no sulfate loss when applied to another class of sulfated carbohydrates like algal polysaccharides. In contrast to EDD, which is restricted to FTICR mass spectrometers, CTD can be implemented on other platforms, such as ion trap mass spectrometers (ITMS). Here, we show the capability of CTD-ITMS to produce structurally significant details of the sites of modification in both heparan sulfate (HS) and chondroitin sulfate (CS) standards ranging in length from degree of polymerization (dp) 4 to dp6. EDD and CTD both yield more structural information than CID, and yield similar fractional abundances to one another for glycosidic fragments, cross-ring fragments and neutral losses.

Introduction

Glycosaminoglycans (GAGs) are linear poly-sulfated carbohydrates that exhibit a number of important biological functions, principally through their interactions with proteins.[1-3] Their structural characterization presents a challenge to the analytical community, due to their high variability in the sites of sulfo modification, degree of polymerization, and hexuronic acid stereochemistry, a result of their enzymatic, non-template driven biosynthesis.[4-6] Identifying sites of sulfation is essential to structure-function studies, as it influences the GAG-protein specific binding relationship.[7] Structural changes in GAGs also directly effects the function of the GAG chain. For example, the physiochemical properties of certain GAGs classes are responsible for the viscoelastic properties of cartilage.[8] Of the four established GAG classes, heparin (Hp) and heparan sulfate (HS) are the most diverse.[4] Hp/HS have a high variability in sites of *O*-sulfation, *N*-sulfation, *N*-acetylation and hexuronic acid stereochemistry. Another class of sulfated GAGs, chondroitin sulfate (CS) and dermatan sulfate (DS), also vary in the sites of *O*-sulfation and hexuronic acid stereochemistry. Due to the heterogeneity of GAGs in naturally occurring material, they are difficult to analyze by methods such as nuclear magnetic resonance (NMR) and X-Ray diffraction.[9-11] Disaccharide analysis using LC-MS can be used for analysis from small tissue volumes; however, the extent of enzymolysis in disaccharide analysis limits the structural information available for linkage positions, higher-order patterns and sulfation patterns.[12-13] Advances in mass spectrometry, specifically soft ionization by electrospray (ESI) in combination with advanced methods of ion activation, have led to a more detailed understanding of GAG structure and function.[10-11, 14]

Fourier transform ion cyclotron resonance mass spectrometry (FTICR-MS) is a powerful tool for GAG structural characterization due to its high resolution and mass accuracy.[9, 15] FTICR-MS can

perform collisionally-activated, photo-induced, and electron-based tandem mass spectrometry (MS/MS) methods, which have all been shown to productively dissociate GAGs.[15-30] Due to the acidic nature of the carboxyl groups and sulfo modifications on GAG chains, they are most efficiently analyzed by negative mode ionization using ESI.[25] Mass spectrometry measurement of molecular weight provides details regarding the chain length, number of sulfo modifications, and the number of *N*-acetyl groups present in a GAG chain, however more detailed analysis is needed to assign the location of sulfo- modifications and *N*-acetylated hexosamine residues. MS/MS methods are useful analytical tools for obtaining this information. There are multiple electron-based activation methods for GAG analysis, and some of the more useful ones include electron induced dissociation (EID), electron detachment dissociation (EDD), and negative electron transfer dissociation (NETD).[21, 24-29, 31-36] More recently ultraviolet photodissociation (UVPD) has been shown as a useful MS/MS tool for the analysis of GAGs.[37]

EDD has been extensively studied as a tool for the structural analysis of GAGs.[17-18, 21, 24-29] EDD is accomplished by precursor selection and trapping of multiply-charged negative ions in the analyzer cell of an FTICR mass spectrometer, and bombarding these precursor ions with electrons of a moderate kinetic energy (19 eV). Fragmentation occurs via radical species produced by electron detachment, or from electronically excited even-electron precursor ions. The combination of these two pathways produces rich and complex mass spectra whose analysis provides considerable structural detail.[25-26] A schematic representation of the EDD process is shown in Figure B.1. EDD has been shown to produce both glycosidic and cross-ring fragmentation. Glycosidic cleavage products are used to assign the degree of sulfo modification and acetylation that is present in each monosaccharide, whereas cross-ring fragmentation is used to identify the sites of modification within a sugar residue.[25-26, 29] EDD has also been shown to

minimize sulfate decomposition compared to low-energy or threshold activation methods such as infrared multiphoton dissociation (IRMPD) and collision induced dissociation (CID).[23, 25-27, 31]

In the mid 2000s, Schlathölter's group studied the gas-phase interactions between small biological ions and fast (1-200 keV) reagent ions, including H^+, He^+, He^{2+}, O^{5+} and Xe^{n+}.[38-40] Zubarev's group enabled products of cation-cation reactions to be monitored in a 2D ion trap, [41] and the Jackson group extended the approach to other biological oligomers and negatively charged ions.[42-47] The technique, now termed charge transfer dissociation (CTD), typically uses He^+ cations and has some similarities to helium metastable atom-activated dissociation (MAD).[42, 48-51] CTD exposes gas-phase precursor cations or anions to a beam of helium cations with kinetic energies in the range of 3-10 keV. Helium has a well-defined ionization energy (24.6 eV), which greatly exceeds the electron affinity of any organic molecule. The high kinetic energy provides sufficient energy to overcome any Coulombic barriers between the precursors, such as with cation-cation reactions, and the high electron affinity of helium cations provides excess energy for fragmentation.[38-40, 47] The helium cations abstract electrons (charge transfer) from the precursor ions and cause the oxidized product ions to decompose via high-energy, radical-driven pathways. Recently, CTD was used to analyze sulfated oligosaccharides in both positive and negative ion modes.[44-45] CTD is able to generate *a*- and *x*-ions from singly charged peptide cations, and cross-ring cleavages of oligosaccharides, which are typically not produced by CID.[43-46] A schematic representation of the CTD process is shown in Figure B.2. Here, we report the first application of CTD to the analysis of glycosaminoglycans. This work is motivated by the unique capabilities of CTD for fragmentation via radical pathways, and the potential to yield useful analytical information for the characterization of this challenging class of biomolecules. Moreover, the capability for deployment in ion trap mass spectrometers raises the potential to

analyze GAGs using more widely available instrumentation compared to FTICR mass spectrometers that have been frequently used for GAG analysis to date.

Experimental

Preparation of Synthetic Heparan Sulfate Oligosaccharides

Heparan sulfate (HS) tetrasaccharide standards were prepared by chemical synthesis using a modular approach and further purified by silica gel column chromatography.[18] Structures were confirmed by ^{1}H NMR and accurate mass measurement by FTICR-MS.[18]

Preparation of Chondroitin Sulfate Oligosaccharides

Chondroitin sulfate A (CS-A) and dermatan sulfate (DS) oligosaccharides were prepared by partial enzymatic depolymerization from bovine trachea chondroitin sulfate A (Celsus laboratories, Cincinnati, OH, USA) and porcine intestinal mucosa dermatan sulfate (Celsus Laboratories) respectively. Full explanations of enzymatic depolymerization and desulfation have been reported previously.[32, 36]

Mass Spectrometry

0.1 mg/mL of each GAG standard was ionized by nanospray ESI with a spray voltage of 1.2 kV (pulled glass tip model Econo12-N; New Objective, Woburn, MA). All standards were analyzed in negative ion mode.

EDD spectra for all samples were collected on a 9.4T Bruker solariX XR Fourier transform ion cyclotron resonance mass spectrometer (Bremen, Germany) with a hollow cathode (HeatWave, Wasonville, CA, USA), which serves as the source of electrons for EDD. Multiply

charged precursor ions were isolated in the quadrupole and accumulated for 2-3 s before injection into the dynamically harmonized FTICR cell. Ions were then irradiated for 1 s with 19 eV electrons. The cathode heater was set to 1.5 A and the extraction lens was set to 18.6 ± 0.4 V. 1 M points were acquired for each spectrum and 48 acquisitions were averaged for each stored spectrum. Internal calibration was performed using confidently assigned glycosidic cleavage product ions as internal calibrants.

CTD and CID experiments were performed on a modified Bruker AmaZon 3D ion trap (Bremen, Germany), with a custom vacuum chamber cover. A saddle field fast ion gun (VSW/ Atomtech, Macclesfield, UK) was installed on top of the ring electrode. The saddle field fast ion source was used as the helium cation source, which is described in detail elsewhere.[42] Multiply charged precursor ions were activated with 7.5-8 keV helium cations for 100 ms for CTD. Helium gas flow in the ion gun was controlled via a variable leak valve and measured by the ion trap gauge; the readout was approximately 9.5 $x10^{6}$ mbar. Precursor ions were accumulated for 20-60 ms in the ion trap before isolation. Each stored CTD spectrum was the average of 5 replicate scans, and the presented spectra are typically the result of 1.5-2 mins of spectral averaging. Internal calibration was performed using confidently assigned glycosidic cleavage product ions as internal calibrants.

For the experiments involving CTD with resonance ejection, precursor ions were first isolated and irradiated with helium cations to achieve CTD at the MS^2 level. Any unreacted precursor ions were then resonantly ejected at the MS^3 level using on-resonance excitation with an amplitude >3 V. In the absence of CTD at the MS^2 level and the presence of the resonance

ejection at the MS^3 level, no fragment ions were observed, thereby verifying the absence of unwanted CID peaks during resonance ejection.

Product ions for CID, CTD and EDD were assigned using Glycoworkbench version 2.0, and in-house GAG analysis software.[52-53] All product ions are reported using the annotation scheme proposed by Wolff and Amster, which was derived from the Domon and Costello nomenclature.[26, 54] Fragmentation is illustrated in the molecular structure drawings using dashed lines through the structure and hash marks at the end to indicate the fragment ion. Open circles at the end of hash marks represent SO_3 loss, whereas a closed circle represents multiple SO_3 losses. Donut plots display percentages of the summed ion intensity of fragment ion types (glycosidic fragment, cross-ring fragment, glycosidic fragment with SO_3 loss, cross-ring fragment with SO_3 loss).

Results and Discussion

Well-characterized standards were examined to test the capability of CTD to analyze GAGs. CTD results are compared to that of CID and EDD for a series of heparan sulfate tetrasaccharides, dermatan sulfate tetrasaccharide and hexasaccharide, and chondroitin sulfate A tetrasaccharide. Prior work in our group has demonstrated the capability of EDD on an FTICR to provide a complete set of fragment ions that can be used to assign the structural features of GAG samples. EDD fragmentation was enhanced using highly ionized precursor ions to retain labile sulfate half-ester modifications.[14, 26, 55] For the data presented here, we have selected the optimal precursor charge state (as determined by EDD) to ensure complete deprotonation of sulfate groups, and selected precursors that lie outside the CTD chemical background range (i.e. >*m/z*

350). CTD has previously been shown to produce no sulfate decomposition for sulfo-peptides and sulfo-lipids, and minimal neutral loss for sulfo-oligosaccharides.[43, 45] The previous data therefore suggested that CTD should be an effective ion activation method for GAG samples. The symbol nomenclature used for glycans is displayed in Figure B.3.

Compound 1- HS Tetrasaccharide IdoA-GlcNAc-IdoA-GlcNAc6S-$(CH_2)_5NH_2$

The MS/MS spectrum in Figure 3.1 shows the CTD results for the $[M-2H]^{2-}$ precursor (*m/z* 470.39) of the synthetic HS monosulfated tetrasaccharide IdoA-GlcNAc-IdoA-GlcNAc6S-$(CH_2)_5NH_2$. For comparison, the EDD spectrum of the same precursor is presented in Figure B.4. Both CTD and EDD produce a series of glycosidic fragments ions; however, EDD yields both reducing end and non-reducing end fragments for all the glycosidic cleavages. I.e. all the B, C, Y and Z ions are observed (Figures B.4 and B.5). Both CTD and EDD also produce copious cross-ring cleavages. EDD produced a $^{0,2}A_4$ ion, which confirms the location of *N*-acetylation on the reducing-end glucosamine. Once the *N*-acetylation is confirmed on the reducing terminus, the presence of C_3/Z_1 fragment ions infer that the sulfate is located at the 6-*O* position.[56-57] Though these fragment ions alone do not rule out the possibility of 3-*O* sulfation, the observation of *N*-acetylation rules out 3-*O* sulfation, which occurs only on GlcNS residues.[57] CTD produced $^{2,4}A_4$ and C_3 fragments, which taken together confirm the presence of both *N*-Acetylation and 6-*O* sulfation. EDD produced more fragments than CTD on the uronic acid closest to the reducing end. Both EDD and CTD produced $^{1,5}X_2$ and $^{3,5}X_2$ ions, which together confirm the presence of *N*-acetylation on the glucosamine closest to the non-reducing end. Table B.1 contains a list of identified fragment ions from CTD.

The intensities of glycosidic, cross-ring and sulfate-loss fragment ions are compared for CID, CTD, and EDD in the donut plots shown in Figure B.1B. EDD produced a lower abundance of cross-ring fragments (23.6%) and lower abundance of neutral sulfate losses (8.1%) than CTD (38.7% and 22.2%, respectively). MS/MS spectra of the same precursor using CID is also shown in Figure B.4. The spectrum is dominated by glycosidic cleavages and neutral losses that provide ambiguous information about the locations of the different functional groups.

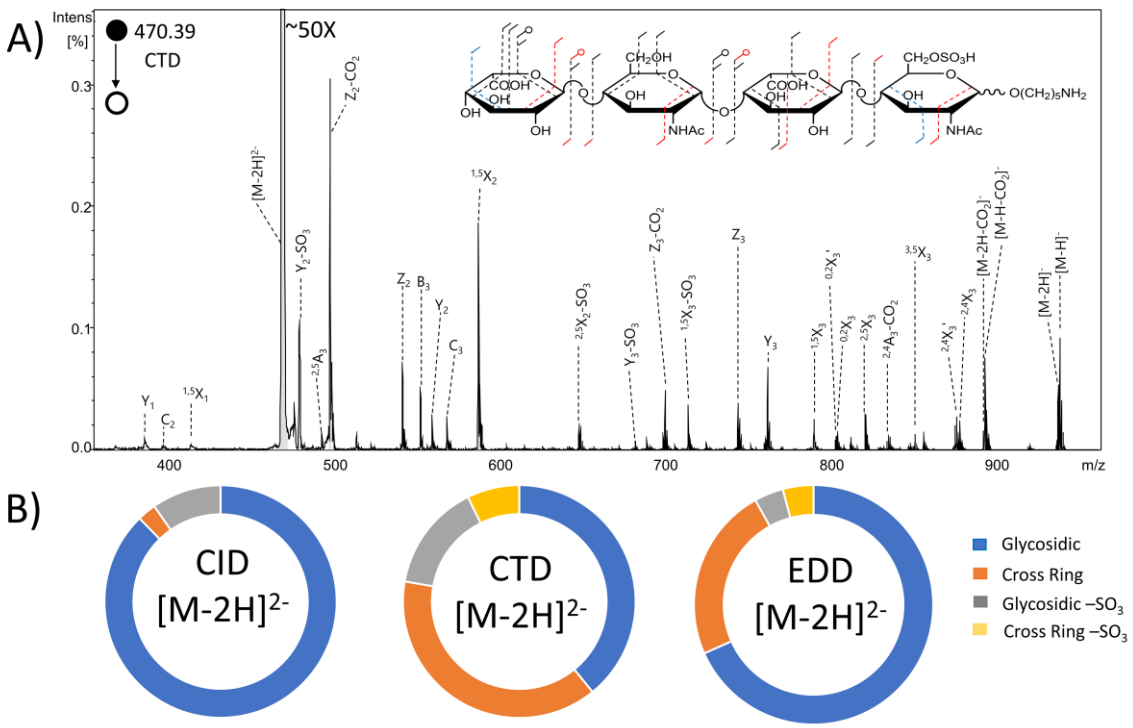

Figure 3.1. (A) CTD spectrum of the $[M-2H]^{2-}$ precursor of synthetic heparan sulfate tetramer standard IdoA-GlcNAc-IdoA-GlcNAc6S-$O(CH_2)_5NH_2$. Molecular structure inset represents fragmentation seen from both CTD and EDD (black), CTD only (blue) and EDD only (red). (B) Fragment type intensity distribution for glycosidic, cross-ring, glycosidic sulfate loss and cross-ring sulfate loss fragments are shown.

Compound 2- HS Tetrasaccharide GlcA-GlcNAc-GlcA2S-GlcNAc-$(CH_2)_5NH_2$

The MS/MS spectrum in Figure 3.2 shows the CTD results for the $[M-2H]^{2-}$ precursor (*m/z* 469.14) of the synthetically produced HS monosulfated tetrasaccharide GlcA-GlcNAc-

GlcA2S-GlcNAc-$(CH_2)_5NH_2$. CID, CTD and EDD each produce fragments at every glycosidic bond (Figures B.6 and B.7). CTD and EDD produced more cross-ring cleavages than CID, as expected for a precursor with a protonated site. Past work investigating the effect of ionization state on CID fragmentation of GAGs showed that few informative fragments are seen with precursors that are not fully ionized.[22] For this sample, CTD produced a greater number of cross-ring cleavages than EDD, specifically on the *N*-acetylglucosamine nearest to the non-reducing end. Neither EDD nor CTD produced cross-ring cleavages on the reducing end *N*-acetylglucosamine. However, both EDD and CTD produced B_3 and C_3 fragments, which confirm the presence of the *N*-acetylation.

On the non-reducing end N-acetylglucosamine, EDD produced a $^{0,2}A_2$ fragment ion, which confirms the presence of the *N*-acetyl group. CTD produced $^{1,5}X_2$ and $^{2,4}X_2$ fragment ions, which confirm the presence of the *N*-acetyl group. For the glucuronic acid closest to the reducing end, EDD produced a $^{0,2}A_3$ fragment, which confirms 2-*O* sulfation, and CTD produced $^{1,5}A_3$ and $^{2,5}A_3$ fragments, which also confirm 2-*O* sulfation for this residue. Incidentally, the biosynthesis of GAGs restricts sulfo-modification in uronic acid to the 2-*O* position, so only glycosidic cleavage is necessary to make this assignment.[57] When comparing the overall intensity of fragment ions (Figure 3.2B), EDD produced a greater abundance of cross-ring fragments than CTD (48.3% and 35.5%); EDD also produced less-abundant sulfate decomposition in both glycosidic and cross-ring fragment ions (4.3% and 2.1% for EDD compared to 5.2% and 5.4% for CTD). Table B.2 contains a list of identified fragment ions from CTD.

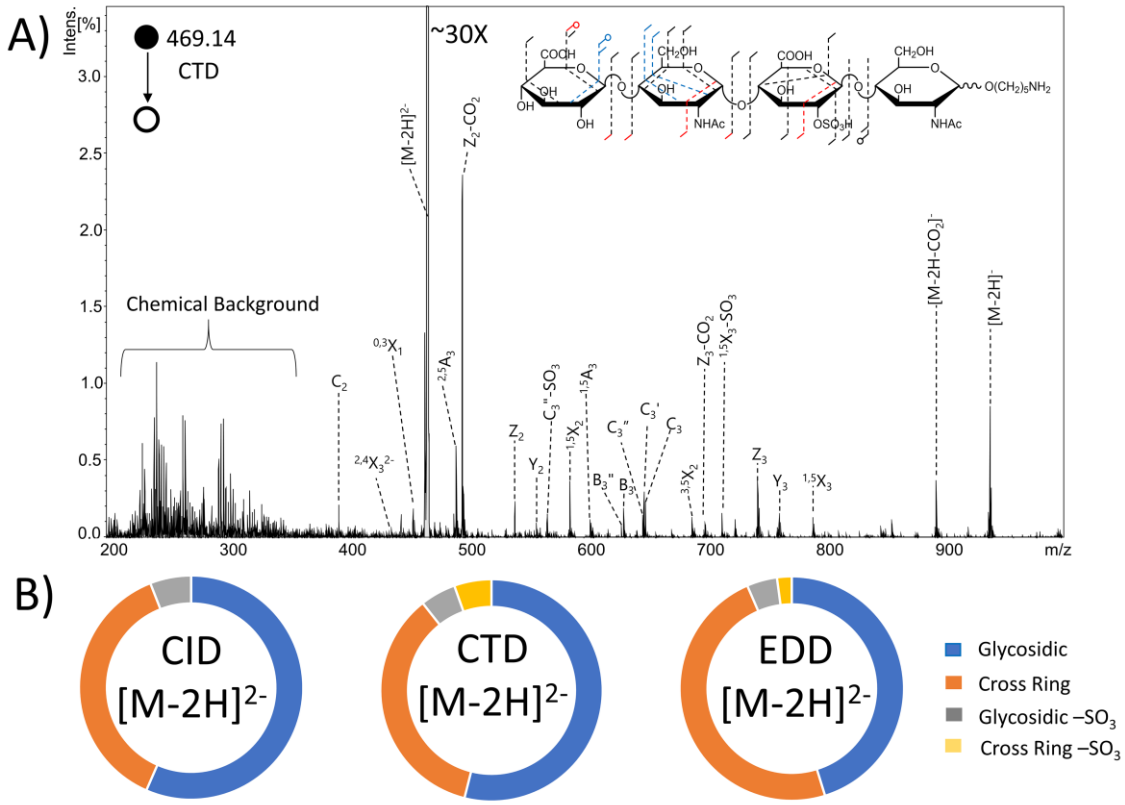

Figure 3.2. (A) CTD spectrum of the $[M-2H]^{2-}$ precursor of synthetic heparan sulfate tetramer standard GlcA-GlcNAc-GlcA2S-GlcNAc-O$(CH_2)_5NH_2$. Molecular structure inset represents fragmentation seen from both CTD and EDD (black), CTD only (blue) and EDD only (red). (B) Fragment type distribution for glycosidic, cross-ring, glycosidic sulfate loss and cross-ring sulfate loss fragments are shown.

Compound 3- HS Tetrasaccharide GlcA-GlcNS6S-GlcA-GlcNS6S-$(CH_2)_5NH_2$

The CID, CTD and EDD results for the $[M-4H+Na]^{3-}$ precursor (*m/z* 372.45) of the synthetic HS tetrasulfated tetrasaccharide GlcA-GlcNS6S-GlcA-GlcNS6S-$(CH_2)_5NH_2$ are shown in Figure B.8. EDD was able to break every glycosidic bond, however CTD was not able to break the central glycosidic bond without sulfate decomposition. Figure 3.3 shows fragment maps with the cleavages produced by CID, CTD and EDD and donut plots showing the intensity distributions of the principal fragment types. CTD produced a $^{0,2}A_2$ cleavage, which confirms the location of the *N*-sulfation on the non-reducing end proximal glucosamine, however CTD did not yield any more cross-ring cleavages in this sugar residue to confirm 6-*O* sulfation. The Y_3 fragment, in combination with the $^{0,2}A_2$ fragment, can be used to determine the presence of a sulfate in this residue on either the 6-*O* or the 3-*O* position; 6-*O* sulfation is more likely, but 3-*O* sulfation cannot be disregarded.[56] EDD also produced a $^{0,2}A_2$ cleavage on the non-reducing end glucosamine, which confirms the presence of the *N*-sulfation, and a $^{1,5}X_2$ fragment, which confirms an additional sulfate modification. However, like for CTD, the location of sulfation cannot be determined. Neither EDD nor CTD produced any informative cross-ring cleavages on the reducing end glucosamine. CTD and EDD yielded glycosidic fragment ions, which confirm the presence of two sulfates on the reducing end amino sugar. EDD produced a greater abundance of cross-ring fragments (26.7%) compared to either CID (2.1%) or CTD (5.7%) (Figure 3.3B). Table A.3 contains a list of identified fragment ions from CTD. Previous work investigating the effect of the ionization state of GAGs on EDD fragmentation efficiency showed superior EDD efficiencies when at least one of the sulfate groups retains a proton or cation and is uncharged.[26] When the GAG is not fully deprotonated, sulfate decomposition is minimized while maintaining informative fragment ions. The precursor ion chosen for these experiments

results in four of the six ionizable sites ionized. A precursor ion with five ionized sites would be ideal for this sample, however the *m/z* value of the $[M-5H]^{5-}$ precursor would have fallen in the region of the CTD spectrum with chemical background (e.g. < *m/z* 350), and so this precursor was not selected. Na-H exchange is a valuable alternative to achieve higher levels of deprotonation. For this work, only Na^+ adducts that were present within the original sample were used, and no additional Na^+ was added. For future work, additional Na-H exchange precursors will be tested. Additionally, the chemical background could be minimized with an oil-free vacuum system and altering the beam conditions. Although the chemical background was minimized in Figure B.5, the low mass cut-off during this experiment was approximately *m/z* 250, so the trapping efficiency for ions near or below this value was negligible. The high degree of sulfo loss and the lower abundance of informative cross-ring fragment ions could be attributable to the dissociation behavior of the less-than optimal precursor ion.

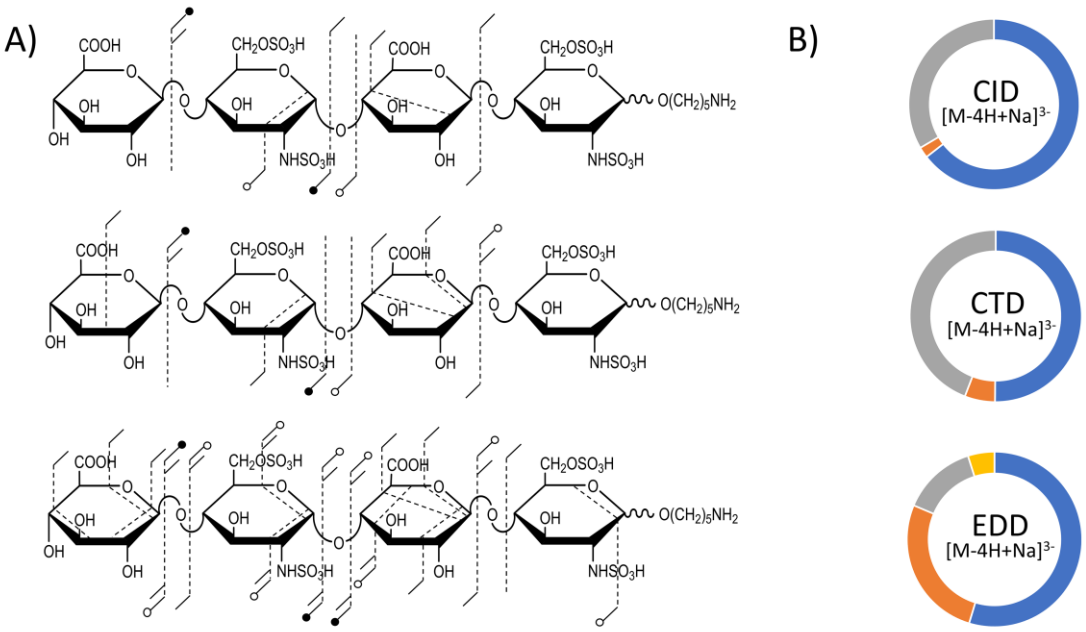

Figure 3.3. (A) Annotated molecular structures of the $[M-4H+Na]^{3-}$ of heparan sulfate tetramer standard GlcA-GlcNS6S-GlcA-GlcNS6S-$O(CH_2)_5NH_2$. Fragment maps with results from CID, CTD and EDD are shown, respectively. (B) Fragment type distribution for glycosidic (blue), cross-ring (orange), glycosidic sulfate loss (gray) and cross-ring sulfate loss (yellow) fragments are shown.

Compound 4- HS Tetrasaccharide IdoA2S-GlcNS6S-IdoA-GlcNAc6S-$(CH_2)_5NH_2$

The MS/MS spectra in Figure 3.4 show the CTD (top) and EDD (bottom) results for the $[M-3H]^{3-}$ precursor (*m/z* 378.47) of the synthetic HS tetrasulfated tetrasaccharide IdoA2S-GlcNS6S-IdoA-GlcNAc6S-$(CH_2)_5NH_2$. Structural annotations for EDD and CTD are presented as well. CTD produced a $^{1,4}A_4$ fragment ion, which confirms 6-*O* sulfation on the reducing end amino sugar. EDD produced a $^{3,5}A_4$ cleavage, which also confirms this sulfation position. Both CTD and EDD produced Z_2/Y_2 and Z_3/Y_3 glycosidic cleavages, which confirm the presence of

two sulfate modifications on the glucosamine residue closest to the non-reducing end. However, EDD produced no informative cross-ring cleavages on this glucosamine to confirm sulfate positions. In contrast, CTD produced a $^{1,4}X_2$ cleavage on the non-reducing end glucosamine, which confirms sulfation at the 6-*O* position. CTD produced no additional cross-ring cleavages to confirm the location of the second sulfate on the glucosamine. However, since CTD confirmed the presence of 6-*O* sulfation on the non-reducing end amino sugar, one can infer that the other sulfate is on the *N* position, especially because 3-*O* sulfation requires *N*-sulfation to be present.[57] The final sulfate modification is located on the non-reducing end uronic acid. The known biosynthetic pathway requires that sulfation on uronic acid is at the 2-*O* position, and only CTD confirmed this location of the sulfate modification by producing a $^{0,3}X_3$ ion. EDD and CTD both produced $^{1,5}X_3$ and $^{2,4}X_3$ fragment ions, which, when combined, confirm the 2-*O* location for the sulfate modification on the uronic acid. CTD produced slightly more abundant cross-ring fragments than EDD (17.9% and 9.8%, respectively); however, both CTD and EDD produced a notable abundance of ions containing sulfate decomposition, specifically from glycosidic cleavages. Sulfate decomposition accounted for 48.1% of assigned fragments for CTD and 40.2% for EDD. Table B.4 contains a list of identified fragment ions from CTD. The abundance of sulfate loss can possibly be attributed to the precursor selection, which has one less ionized site than the number of sulfates on the GAG standard. As stated previously, the ideal precursor for minimizing sulfate decomposition has one more ionized site than the number of sulfate modifications on a GAG.[26] Precursor selection was limited by the chemical background of the CTD experiments, which, when the lower *m/z* limit is set to *m/z* 250, tends to maximize between *m/z* 250-300 and tail off towards *m/z* 350. As mentioned previously, precursors with Na-H exchange can substitute for higher charge states without entering the *m/z* range of the chemical

background. For this preliminary comparison between EDD and CTD, no additional Na^+ was added to the GAG samples, so the presented results might not necessarily reflect the best-case scenarios for structural elucidation using EDD or CTD.

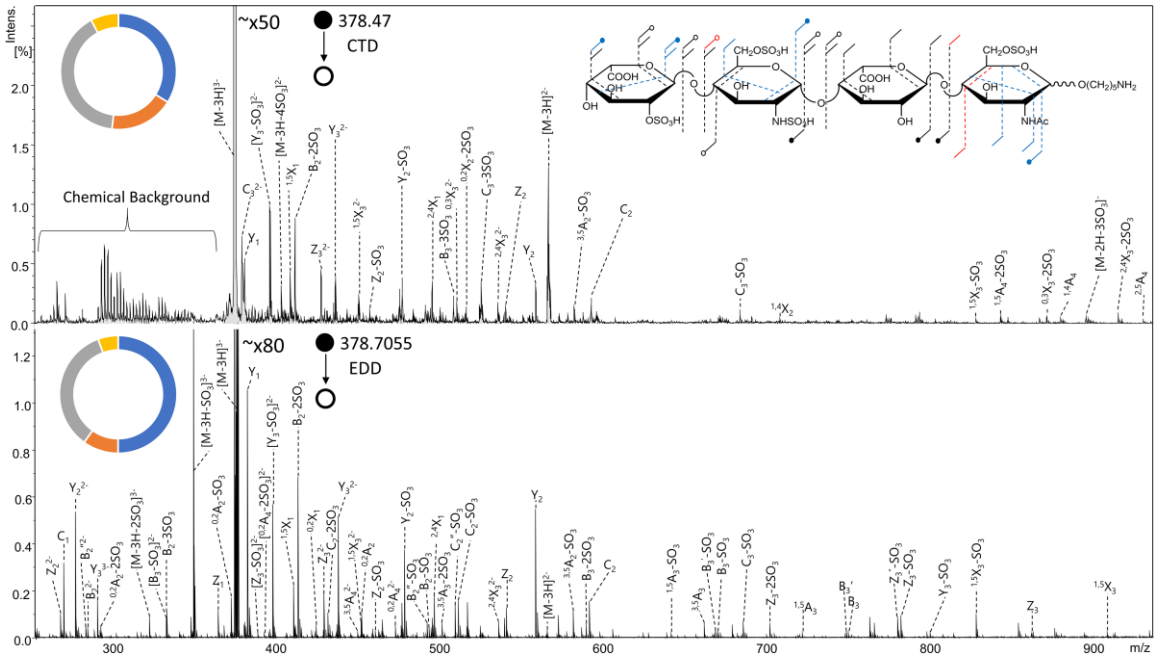

Figure 3.4. MS/MS spectra of the $[M-3H]^{3-}$ precursor of synthetic heparan sulfate tetramer standard IdoA2S-GlcNS6S-IdoA-GlcNAc6S-$O(CH_2)_5NH_2$. (top) CTD MS/MS spectrum (bottom) EDD MS/MS spectrum. Molecular structure inset represents fragmentation seen from both CTD and EDD (black), CTD only (blue) and EDD only (red). Fragment type distribution for glycosidic (blue), cross-ring (orange), glycosidic sulfate loss (gray) and cross-ring sulfate loss (yellow) fragment ions are shown.

Compound 5- DS Tetrasaccharide ΔHexA-GalNAc4S-IdoA-GalNAc4S-OH

Dermatan sulfate (DS) tetrasaccharide is disulfated and is known to have 4-*O* sulfation on both N-acetyl galactosamines. MS/MS spectra from CID, CTD and EDD, as well as annotated molecular structures and donut charts, are shown in Figures B.9 and B.10. Unfortunately, neither EDD nor CTD produce cross-ring fragments that can distinguish 4-*O* from 6-*O* sulfation. However, both CTD and EDD produced B_3 and C_3 fragment ions to confirm the presence of a sulfate modification on the reducing end amino sugar. EDD yielded B_2 and Y_3 fragment ions, which also confirms the presence of a sulfate modification on the non-reducing end amino sugar. CTD produced glycosidic fragment ions breaking the central glycosidic bond (Z_2, Y_2, C_2), but no glycosidic fragments to distinguish the location of the sulfate modification from the non-reducing end amino sugar and uronic acid. Table A.5 contains a list of identified fragment ions from CTD.

The lack of cross-ring fragmentation on the amino sugars has been reported previously when using EDD and other radical-based ion activation techniques.[28, 36-37] The proposed mechanism by Wolff *et al*. suggests that a radical site first forms on the uronic acid carboxylate, either at the initiation of electron detachment or from hydrogen rearrangement. The change in linkage from β-1,4 in HS standards to β-1,3 in CS/DS standards appears to be a major factor in the differences in fragmentation between the two GAG subclasses. Whereas the neutral losses of SO_3 from CTD fragments of highly sulfated algal carrageenans appear to be favored by certain positions,[39] the sulfate losses in HS, CS and DS seem to be less predictable and multiple sulfate losses are observed in both CTD and EDD.

An added benefit to using an ion trap instrument for CTD experiments is the ability to perform resonance ejection to remove unwanted ions from the trap. This can lead to an extension of the dynamic range of the ion trap instrument.[58] In this case, any residual precursor ions remaining after the CTD reaction were resonantly ejected before the mass acquisition scan to prevent space charge effects—such as peak broadening—on fragment ions with lower *m/z* values than the precursor. By ejecting the unreacted precursor ions, the previously suppressed fragment ions became well resolved peaks that could be assigned to specific fragments. A comparison of CTD of the $[M-2H]^{2-}$ precursor (*m/z* 458.46) of DS tetramer with and without resonance ejection is shown in Figure 3.5. There was an overall increase in the abundance and number of fragment ions produced; however, no new cross-ring cleavages on either amino sugar were observed. Resonance ejection CTD produced detectable fragments corresponding to Y_3 and Z_3 fragment ions, possibly because of a trace amount of resonance excitation (CID) during resonance ejection.[59] When combined with the Y_2, Z_2 and C_2 ions from CTD activation, these data confirm a sulfate modification on the non-reducing end amino sugar and not the non-reducing end uronic acid. CTD with resonance ejection yielded a handful of more informative fragmentation, but at a cost of a slightly higher degree of sulfate decomposition (17.8% compared to 16.2% for CTD without resonance ejection) (Figure 3.5C). As mentioned previously, the chemical background of CTD is an ongoing issue requiring improvement in future work.

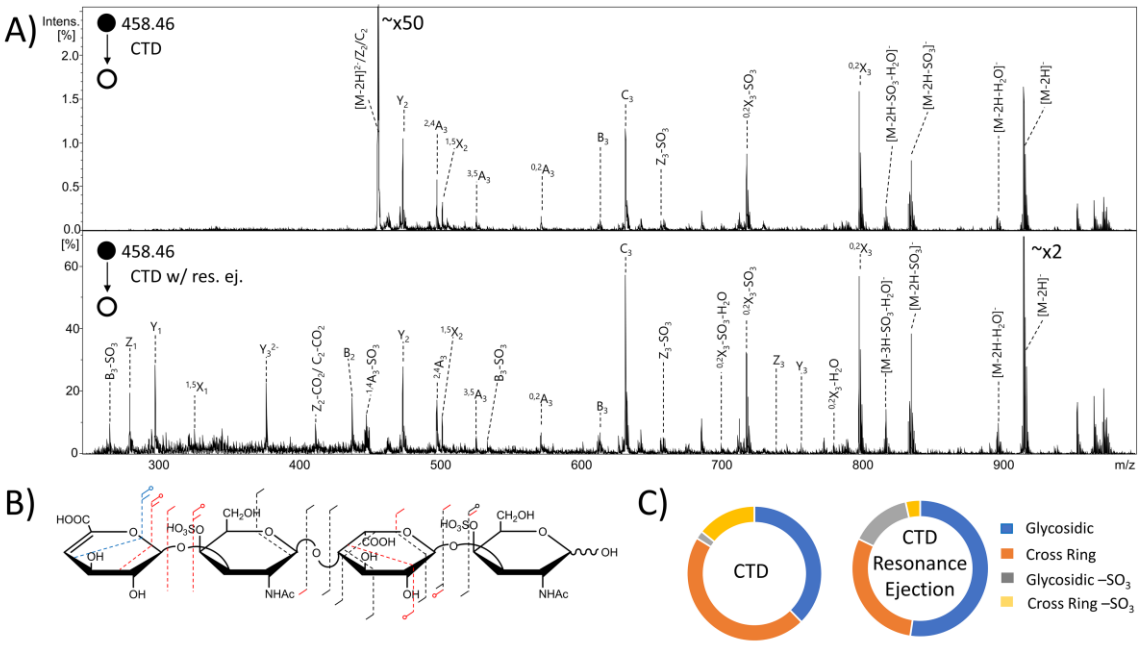

Figure 3.5. MS/MS spectra of the $[M-2H]^{2-}$ precursor of dermatan sulfate tetramer standard ΔHexA-GalNAc4S-IdoA-GalNAc4S-OH. (A) (top) CTD MS/MS spectrum (bottom) CTD MS/MS spectrum with resonance ejection. (B) Molecular structure inset represents fragmentation seen from both CTD and CTD with resonance ejection (black), CTD only (blue) and CTD with resonance ejection only (red). (C) Fragment type distribution for glycosidic, cross-ring, glycosidic sulfate loss and cross-ring sulfate loss fragment ions are shown.

Compound 6- DS Hexasaccharide ΔHexA-GalNAc4S-IdoA-GalNAc4S-IdoA-GalNAc4S-OH

DS hexasaccharide contains three sulfate modifications, all at the 4-*O* position on the three amino sugars. MS/MS results from CID, CTD and EDD experiments of the $[M-3H]^{3-}$ precursor (*m/z* 458.65), as well as annotated molecular structures and donut charts, are shown in Figures B.11 and B.12. Similar to the DS tetramer results, neither EDD nor CTD produced the

necessary cross-ring cleavages to confirm the location of the sulfate modifications at the 4-*O* position on the amino sugars. EDD produced all necessary glycosidic cleavages to confirm that the sulfate modifications are on the amino sugars. CTD produced the necessary glycosidic cleavages to confirm that two of the sulfates are on amino sugars; however, like the DS tetramer, CTD did not produce the necessary glycosidic cleavages to determine if the final sulfate is on the non-reducing end amino sugar or the non-reducing end uronic acid. Table B.6 contains a list of identified fragment ions from CTD. For hexameric oligosaccharides, in comparison to the tetramers examined above, the increase in the number of possible fragmentation peaks leads to spectral congestion in the region above *m/z* 800. As a result of the lower resolving power of the ion trap mass spectrometer, a number of lower abundance ions were unable to be assigned in this region of the mass spectrum. By comparison, the EDD-FTICR measurements on the same sample provide well-resolved peaks that are easily assigned.

CTD with resonance ejection was also performed on this compound. Results comparing CTD with resonance ejection and CTD without resonance ejection are shown in Figure 3.6. Resonance ejection CTD produced a Z_5 fragment ion, which confirms the final sulfate modification is located on the amino sugar. Although resonance ejection hardly changes the relative abundance of fragments with *m/z* values above the precursor *m/z* value, CTD with resonance ejection provides additional peaks below the *m/z* of the precursor and changes the overall distribution of fragment types. For example, CTD with resonance ejection produced a greater percentage of glycosidic cleavage intensity, but less cross-ring cleavage intensity than CTD without resonance ejection, as shown in Figure 3.6C. The overall intensity of sulfo loss peaks increased slightly with resonance ejection CTD (13.4% with resonance ejection versus 11.2% without).

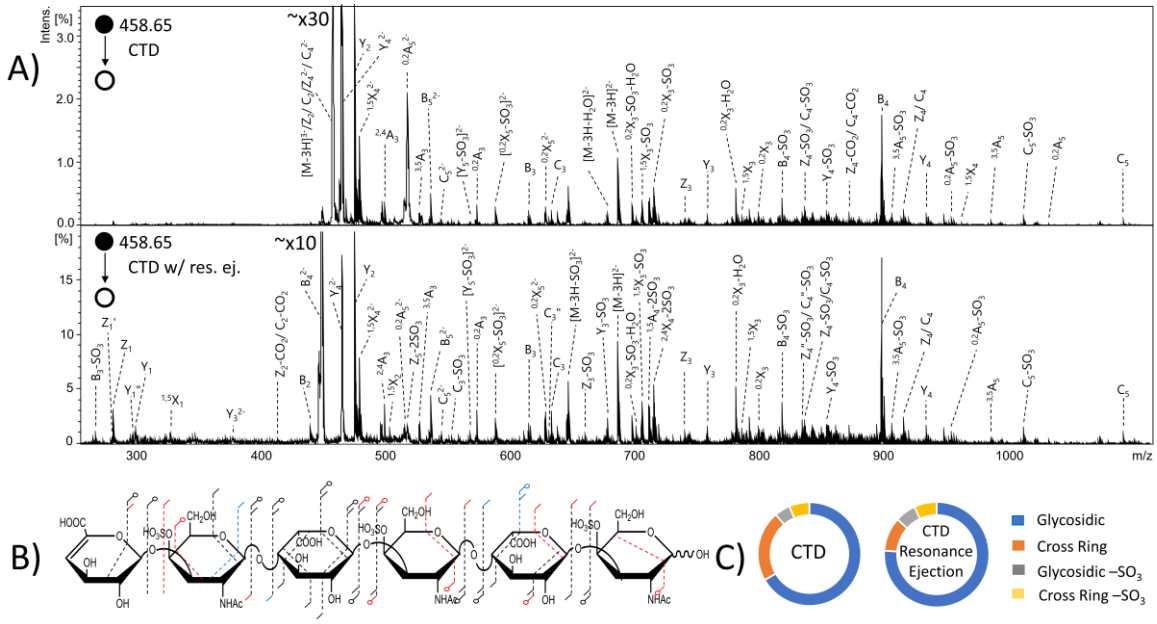

Figure 3.6. MS/MS spectra of the $[M-3H]^{3-}$ precursor of dermatan sulfate hexamer standard ΔHexA-GalNAc4S-IdoA-GalNAc4S-IdoA-GalNAc4S-OH. (A) (top) CTD MS/MS spectrum (bottom) CTD MS/MS spectrum with resonance ejection. (B) Molecular structure inset represents fragmentation seen from both CTD and CTD with resonance ejection (black), CTD only (blue) and CTD with resonance ejection only (red). (C) Fragment type distribution for glycosidic, cross-ring, glycosidic sulfate loss and cross-ring sulfate loss fragment ions are shown.

Compound 7- CS-A Hexasaccaride ΔHexA-GalNAc4S-GlcA-GalNAc4s-GlcA-GalNAc4A-OH

Chondroitin sulfate A (CS-A) hexasaccharide has three sulfate modifications at the 4-*O* position of the amino sugar residues. MS/MS data from CID, CTD and EDD experiments of the $[M-3H]^{3-}$ precursor (*m/z* 458.42) and annotated molecular structures are shown in Figures B.13

and A.14. Similar to the DS samples, the majority of the cross-ring fragmentation of CS-A was on the uronic acid residues, and no cross-ring fragments could distinguish 6-*O* and 4-*O* sulfation by either EDD or CTD. EDD produced all the necessary glycosidic cleavages to confirm sulfate modifications on the amino sugar residues and eliminated the possibility of sulfation on the uronic acid residues. CTD produced the necessary glycosidic cleavages to confirm sulfate modifications on the reducing end amino sugar and central amino sugar. CTD did not produce any glycosidic fragments to distinguish the location of the remaining sulfate modification which could be on either the non-reducing end uronic acid or the adjacent amino sugar. Table B.7 contains a list of identified fragment ions from CTD.

CTD with resonance ejection was performed on this compound (Figure B.15). CTD with resonance ejection yielded the glycosidic cleavages necessary (Y_5 and Z_5) to determine that the final sulfate is located on the non-reducing end amino sugar. When comparing the overall fragment ion intensity between CTD, CID, EDD and CTD with resonance ejection for this compound (Figure 3.7), CTD and EDD produced a similar intensity of cross-ring fragment ions, whereas CID and resonance ejection CTD both produced a significantly lower intensity of the cross-ring fragment ions but a much higher intensity of glycosidic cleavages. CTD with resonance ejection produced a much lower intensity of sulfate decomposition than CTD without resonance ejection.

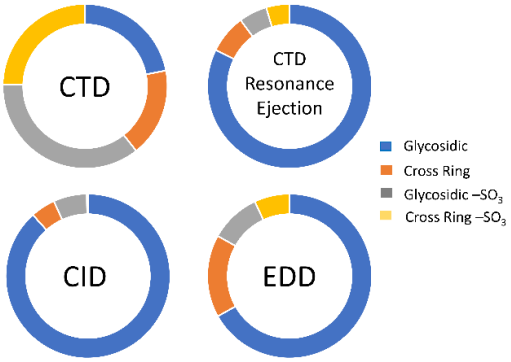

Figure 3.7. MS/MS results of the $[M-3H]^{3-}$ precursor of chondroitin sulfate hexamer standard ΔHexA-GalNAc4S-GlcA-GalNAc4S-GlcA-GalNAc4S-OH. Fragment type distribution for glycosidic, cross-ring, glycosidic sulfate loss and cross-ring sulfate loss fragment ions are shown.

CS-A and DS are isomers, differing in stereochemistry at the C5 position of the uronic acid. CS-A contains glucuronic acid whereas DS contains iduronic acid. Extensive work has been done to investigate the differences produced from MS/MS of these isomers.[32, 60-61] In general, several selected fragment ions exhibit intensity differences that correlate with glucuronic acid versus iduronic acid. The selected precursor ion was significant in yielding these diagnostic differences. Although CTD did not provide differences in intensity of the fragment ions previously shown to be diagnostic in EDD,[32, 60-61] CTD of CS-A had a significantly lower intensity for B_4 fragment ions than DS, as shown in Figure 3.8 for the $[M-3H]^{3-}$ precursor (*m/z* 458). Therefore, the stereochemical differences between CS-A and DS provide readily distinguishable spectral differences. Significantly more work would be necessary to elucidate whether or not CTD provides any general trends between spectral and stereochemical differences.

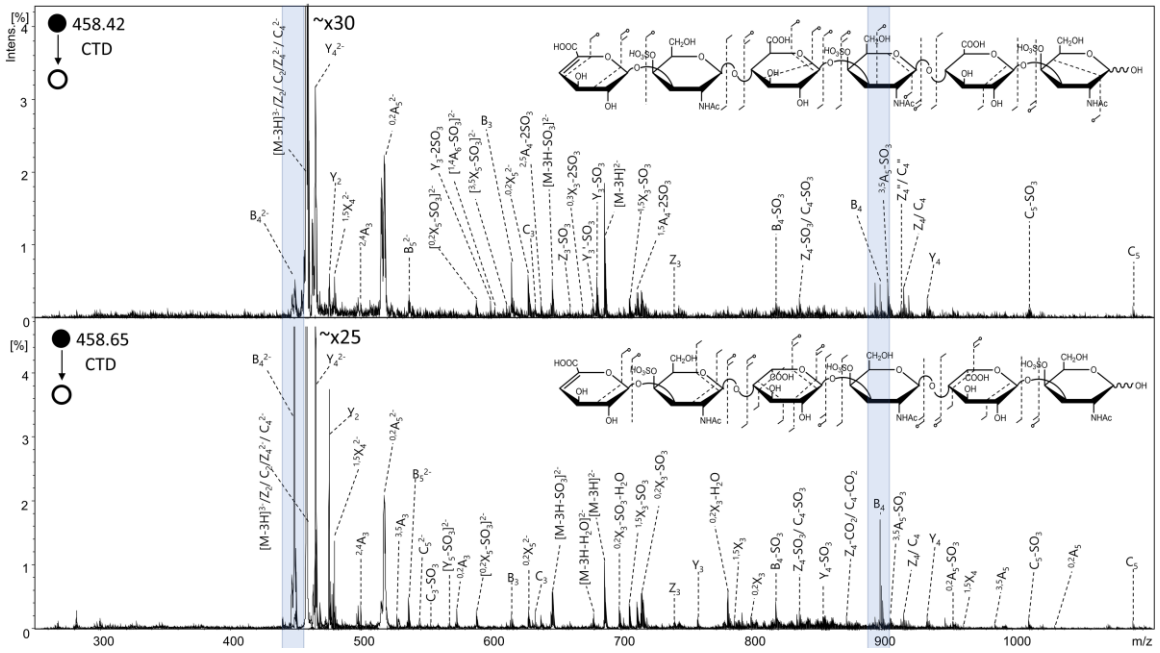

Figure 3.8. CTD spectra of the $[M-3H]^{3-}$ precursor of (top) chondroitin sulfate hexamer ΔHexA-GalNAc4S-GlcAA-GalNAc4S-GlcA-GalNAc4S-OH and (bottom) dermatan sulfate hexamer standard ΔHexA-GalNAc4S-IdoA-GalNAc4S-IdoA-GalNAc4S-OH. Molecular structure inset represents fragmentation seen from CTD MS/MS results of chondroitin sulfate (top) and dermatan sulfate (bottom). Blue highlights indicate the B_4 fragment ions shown to have a higher intensity for dermatan sulfate than chondroitin sulfate.

Conclusions

The data shows that charge transfer dissociation (CTD) is a powerful tool for sequencing GAG polysaccharides with minimal sulfate decomposition. CTD uses a 100 ms activation time with 1.5-2 min of signal averaging, making it more efficient to collect a data set for CTD than EDD. For CS, DS and HS standards investigated here, CTD performance was comparable to that of EDD, and both methods were able to establish the location of sulfate modifications from cross-ring cleavages. For CS/DS standards, CTD and EDD both fell short of being able to assign the site of sulfation as 4-*O* versus 6-*O* in the amino sugar residues.

In addition to a reduction in cross-ring fragmentation, CTD produces fewer product ions than EDD, however the products formed by CTD in general yield the same structural information. For additional information, CTD can be paired with resonance ejection to observe lower-abundance product ions. CTD as implemented here produces a chemical background which interferes with the observation of fragments in the low *m/z* region (i.e. *m/z* 200-350). This results in loss of information in this mass range; however, this was overcome in the resonance ejection experiments, which did yield fragment ions in the low *m/z* region. The necessity of a properly ionized precursor ion was shown for highly sulfated GAG standards, where both EDD and CTD are susceptible to sulfate decomposition from the activation of less-than-optimal precursor species. The extent of deprotonation of the precursors can be overcome by using solution-phase Na-H exchange to ionize acidic sites. For this preliminary test of CTD for GAG analysis, no additional Na^+ was added to the GAG standards. Further studies to investigate the ability for sodiated precursors to produce a higher abundance of informative cross-ring fragments will be performed.

Using an ion trap instrument presents an additional difficulty for GAG analysis. The low resolution of ion trap spectrometers increases the difficulty in confidently assigning fragment ions. In many cases multiple fragment ions can fall within a few Da of each other, thereby creating the need for high resolution MS in combination with CTD. CTD has been achieved with linear ion trap mass spectrometers,[41-42] so coupling with an Orbitrap should be a relatively trivial exercise. CTD with high resolution MS would alleviate the resolution discrepancies between CTD and EDD in the present manuscript. Overall, the product ions produced by CTD of GAG standards does yield informative structure information for characterizing GAGs, and presents an additional approach for the analysis of this challenging compound class.

Acknowledgments

LEP and IJA gratefully acknowledge financial support from the National Institutes of Health, P41GM103390 and U01CA231074. GPJ acknowledges financial support from the National Science Foundation (NSF) under Grant No. CHE-1710376 and the National Institutes of Health (NIH) under Grant No. 1R01GM114494-01. Any opinions, findings, and conclusions or recommendations expressed in this material are those of the authors and do not necessarily reflect the views of the NSF or NIH. The authors would like to acknowledge Geert- Jan Boons (Complex Carbohydrate Research Center, University of Georgia) for providing synthetic heparan sulfate samples that were utilized during this study, as well as Robert Linhardt and Fuming Zhang (Rensselaer Polytechnic Institute) for providing CS-A and DS samples that were utilized during this study.

References

(1) Clegg, D. O.; Reda, D. J.; Harris, C. L.; Klein, M. A.; O'Dell, J. R.; Hooper, M. M.; Bradley, J. D.; Bingham, C. O.; Weisman, M. H.; Jackson, C. G.; Lane, N. E.; Cush, J. J.; Moreland, L. W.; Schumacher, H. R.; Oddis, C. V.; Wolfe, F.; Molitor, J. A.; Yocum, D. E.; Schnitzer, T. J.; Furst, D. E.; Sawitzke, A. D.; Shi, H.; Brandt, K. D.; Moskowitz, R. W.; Williams, H. J., Glucosamine, Chondroitin Sulfate, and the Two in Combination for Painful Knee Osteoarthritis. *New Engl J Med* **2006,** *354*, 795-808.

(2) Sugahara, K.; Kitagawa, H., Recent advances in the study of the biosynthesis and functions of sulfated glycosaminoglycans. *Curr Opin Struct Biol* **2000,** *10*, 518-527.

(3) Watanabe, H.; Yamada, Y.; Kimata, K., Roles of Aggrecan, a Large Chondroitin Sulfate Proteoglycan, in Cartilage Structure and Function. *J Biochem* **1998,** *124*, 687-693.

(4) Esko, J. D.; Lindahl, U., Molecular diversity of heparan sulfate. *J Clin Invest* **2001,** *108*, 169-173.

(5) Varki, A.; Cummings, R. D.; Esko, J. D.; Freeze, H. H.; Stanley, P.; Bertozzi, C. R.; Hart, G. W.; Etzler, M. E., *Essentials of Glycobiology*. NY, 2009; Vol. 2.

(6) Ly, M.; Laremore, T. N.; Linhardt, R. J., Proteoglycomics: Recent Progress and Future Challenges. *Omics* **2010,** *14*, 389-399.

(7) Zhao, Y.; Singh, A.; Li, L.; Linhardt, R. J.; Xu, Y.; Liu, J.; Woods, R. J.; Amster, I. J., Investigating changes in the gas-phase conformation of Antithrombin III upon binding of Arixtra using traveling wave ion mobility spectrometry (TWIMS). *Analyst* **2015,** *140*, 6980-9.

(8) Sugahara, K.; Mikami, T.; Uyama, T.; Mizuguchi, S.; Nomura, K.; Kitagawa, H., Recent advances in the structural biology of chondroitin sulfate and dermatan sulfate. *Curr Opin Struct Biol* **2003,** *13*, 612-620.

(9) Zhou, W.; Hakansson, K., Structural Characterization of Carbohydrates by Fourier Transform Tandem Mass Spectrometry. *Curr Proteomics* **2011,** *8*, 297-308.

(10) Zaia, J., Glycosaminoglycan glycomics using mass spectrometry. *Mol Cell Proteomics* **2013,** *12*, 885-92.

(11) Staples, G. O.; Zaia, J., Analysis of Glycosaminoglycans Using Mass Spectrometry. *Curr Proteomics* **2011,** *8*, 325-336.

(12) Turiák, L.; Tóth, G.; Ozohanics, O.; Révész, Á.; Ács, A.; Vékey, K.; Zaia, J.; Drahos, L., Sensitive method for glycosaminoglycan analysis of tissue sections. *Journal of Chromatography A* **2018,** *1544*, 41-48.

(13) Sun, X.; Li, L.; Overdier, K. H.; Ammons, L. A.; Douglas, I. S.; Burlew, C. C.; Zhang, F.; Schmidt, E. P.; Chi, L.; Linhardt, R. J., Analysis of total human urinary glycosaminoglycan disaccharides by liquid chromatography–tandem mass spectrometry. *Anal Chem* **2015,** *87*, 6220-6227.

(14) Zaia, J., Principles of mass spectrometry of glycosaminoglycans. *J Biomacromol Mass Spectrom* **2005,** *1*, 3-36.

(15) Amster, I. J., Fourier Transform Mass Spectrometry. *J Mass Spectrom* **1996,** *31*, 1325-1337.

(16) Agyekum, I.; Pepi, L.; Yu, Y.; Li, J.; Yan, L.; Linhardt, R. J.; Chen, S.; Amster, I. J., Structural elucidation of fucosylated chondroitin sulfates from sea cucumber using FTICR-MS/MS. *Eur J Mass Spectrom* **2017,** *24*, 157-167.

(17) Agyekum, I.; Patel, A. B.; Zong, C.; Boons, G.-J.; Amster, I. J., Assignment of hexuronic acid stereochemistry in synthetic heparan sulfate tetrasaccharides with 2-O-sulfo uronic acids using electron detachment dissociation. *Int J Mass Spectrom* **2015,** *390*, 163-169.

(18) Agyekum, I.; Zong, C.; Boons, G.-J.; Amster, I. J., Single Stage Tandem Mass Spectrometry Assignment of the C-5 Uronic Acid Stereochemistry in Heparan Sulfate Tetrasaccharides using Electron Detachment Dissociation. *J. Am Soc Mass Spectrom* **2017,** *28*, 1741-1750.

(19) Chi, L.; Wolff, J. J.; Laremore, T. N.; Restaino, O. F.; Xie, J.; Schiraldi, C.; Toida, T.; Amster, I. J.; Linhardt, R. J., Structural Analysis of Bikunin Glycosaminoglycan. *J Am Chem Soc* **2008,** *130*, 2617-2625.

(20) Laremore, T. N.; Leach, F. E.; Solakyildirim, K.; Amster, I. J.; Linhardt, R. J., Glycosaminoglycan Characterization by Electrospray Ionization Mass Spectrometry Including Fourier Transform Mass Spectrometry. *Method Enzymol* **2010,** *478*, 79-108.

(21) Leach, F. E., 3rd; Arungundram, S.; Al-Mafraji, K.; Venot, A.; Boons, G. J.; Amster, I. J., Electron Detachment Dissociation of Synthetic Heparan Sulfate Glycosaminoglycan Tetrasaccharides Varying in Degree of Sulfation and Hexuronic Acid Stereochemistry. *Int J Mass Spectrom* **2012,** *330*, 152-159.

(22) Kailemia, M. J.; Li, L.; Ly, M.; Linhardt, R. J.; Amster, I. J., Complete Mass Spectral Characterization of a Synthetic Ultralow-Molecular-Weight Heparin Using Collision-Induced Dissociation. *Anal Chem* **2012,** *84*, 5475-5478.

(23) Kailemia, M. J.; Ruhaak, L. R.; Lebrilla, C. B.; Amster, I. J., Oligosaccharide analysis by mass spectrometry: a review of recent developments. *Anal Chem* **2014,** *86*, 196-212.

(24) Leach, F. E.; Xiao, Z.; Laremore, T. N.; Linhardt, R. J.; Amster, I. J., Electron detachment dissociation and infrared multiphoton dissociation of heparin tetrasaccharides. *Int J Mass Spectrom* **2011,** *308*, 253-259.

(25) Wolff, J. J.; Amster, I. J.; Chi, L.; Linhardt, R. J., Electron detachment dissociation of glycosaminoglycan tetrasaccharides. *J Am Soc Mass Spectrom* **2007,** *18,* 234-44.

(26) Wolff, J. J.; Laremore, T. N.; Busch, A. M.; Linhardt, R. J.; Amster, I. J., Influence of charge state and sodium cationization on the electron detachment dissociation and infrared multiphoton dissociation of glycosaminoglycan oligosaccharides. *J Am Soc Mass Spectrom* **2008,** *19,* 790-798.

(27) Wolff, J. J.; Laremore, T. N.; Leach, F. E.; Linhardt, R. J.; Amster, I. J., Electron Capture Dissociation, Electron Detachment Dissociation and Infrared Multiphoton Dissociation of Sucrose Octasulfate. *Eur J Mass Spectrom* **2009,** *15,* 275-281.

(28) Wolff, J. J.; Laremore, T. N.; Busch, A. M.; Linhardt, R. J.; Amster, I. J., Electron detachment dissociation of dermatan sulfate oligosaccharides. *J Am Soc Mass Spectrom* **2008,** *19,* 294-304.

(29) Wolff, J. J.; Chi, L.; Linhardt, R. J.; Amster, I. J., Distinguishing glucuronic from iduronic acid in glycosaminoglycan tetrasaccharides by using electron detachment dissociation. *Anal Chem* **2007,** *79,* 2015-2022.

(30) Yu, Y.; Duan, J.; Leach, F. E.; Toida, T.; Higashi, K.; Zhang, H.; Zhang, F.; Amster, I. J.; Linhardt, R. J., Sequencing the Dermatan Sulfate Chain of Decorin. *J Am Chem Soc* **2017,** *139,* 16986-16995.

(31) Wolff, J. J.; Laremore, T. N.; Aslam, H.; Linhardt, R. J.; Amster, I. J., Electron-induced dissociation of glycosaminoglycan tetrasaccharides. *J Am Soc Mass Spectrom* **2008,** *19,* 1449-58.

(32) Leach, F. E.; Ly, M.; Laremore, T. N.; Wolff, J. J.; Perlow, J.; Linhardt, R. J.; Amster, I. J., Hexuronic Acid Stereochemistry Determination in Chondroitin Sulfate Glycosaminoglycan

Oligosaccharides by Electron Detachment Dissociation. *J. Am Soc Mass Spectrom* **2012,** *23*, 1488-1497.

(33) Leach, F. E.; Wolff, J. J.; Laremore, T. N.; Linhardt, R. J.; Amster, I. J., Evaluation of the experimental parameters which control electron detachment dissociation, and their effect on the fragmentation efficiency of glycosaminoglycan carbohydrates. *Int J Mass Spectrom* **2008,** *276*, 110-115.

(34) Wolff, J. J.; Leach, F. E.; Laremore, T. N.; Kaplan, D. A.; Easterling, M. L.; Linhardt, R. J.; Amster, I. J., Negative electron transfer dissociation of glycosaminoglycans. *Anal Chem* **2010,** *82*, 3460-3466.

(35) Leach, F. E.; Wolff, J. J.; Xiao, Z.; Ly, M.; Laremore, T. N.; Arungundram, S.; Al-Mafraji, K.; Venot, A.; Boons, G.-J.; Linhardt, R. J.; Amster, I. J., Negative electron transfer dissociation Fourier transform mass spectrometry of glycosaminoglycan carbohydrates. *Eur J Mass Spectrom* **2011,** *17*, 167-176.

(36) Leach, F. E.; Riley, N. M.; Westphall, M. S.; Coon, J. J.; Amster, I. J., Negative Electron Transfer Dissociation Sequencing of Increasingly Sulfated Glycosaminoglycan Oligosaccharides on an Orbitrap Mass Spectrometer. *J. Am Soc Mass Spectrom* **2017,** *28*, 1844-1854.

(37) Klein, D. R.; Leach, F. E.; Amster, I. J.; Brodbelt, J. S., Structural Characterization of Glycosaminoglycan Carbohydrates Using Ultraviolet Photodissociation. *Anal Chem* **2019,** *91*, 6019-6026.

(38) Bari, S.; Sobocinski, P.; Postma, J.; Alvarado, F.; Hoekstra, R.; Bernigaud, V.; Manil, B.; Rangama, J.; Huber, B.; Schlathölter, T., Fragmentation of α-and β-alanine molecules by ions at Bragg-peak energies. *The Journal of Chemical Physics* **2008,** *128*, 02B623.

(39) Bari, S.; Hoekstra, R.; Schlathölter, T., Peptide fragmentation by keV ion-induced dissociation. *Physical Chemistry Chemical Physics* **2010,** *12*, 3376-3383.

(40) Maclot, S.; Capron, M.; Maisonny, R.; Ławicki, A.; Méry, A.; Rangama, J.; Chesnel, J. Y.; Bari, S.; Hoekstra, R.; Schlathölter, T., Ion-Induced Fragmentation of Amino Acids: Effect of the Environment. *ChemPhysChem* **2011,** *12*, 930-936.

(41) Chingin, K.; Makarov, A.; Denisov, E.; Rebrov, O.; Zubarev, R. A., Fragmentation of Positively-Charged Biological Ions Activated with a Beam of High-Energy Cations. *Anal Chem* **2014,** *86*, 372-379.

(42) Hoffmann, W. D.; Jackson, G. P., Charge Transfer Dissociation (CTD) Mass Spectrometry of Peptide Cations Using Kiloelectronvolt Helium Cations. *J. Am Soc Mass Spectrom* **2014,** *25*, 1939-1943.

(43) Li, P.; Jackson, G. P., Charge Transfer Dissociation (CTD) Mass Spectrometry of Peptide Cations: Study of Charge State Effects and Side-Chain Losses. *J. Am Soc Mass Spectrom* **2017,** *28*, 1271-1281.

(44) Ropartz, D.; Li, P.; Fanuel, M.; Giuliani, A.; Rogniaux, H.; Jackson, G. P., Charge Transfer Dissociation of Complex Oligosaccharides: Comparison with Collision-Induced Dissociation and Extreme Ultraviolet Dissociative Photoionization. *J. Am Soc Mass Spectrom* **2016,** *27*, 1614-1619.

(45) Ropartz, D.; Li, P.; Jackson, G. P.; Rogniaux, H., Negative Polarity Helium Charge Transfer Dissociation Tandem Mass Spectrometry: Radical-Initiated Fragmentation of Complex Polysulfated Anions. *Anal Chem* **2017,** *89*, 3824-3828.

(46) Li, P.; Kreft, I.; Jackson, G. P., Top-Down Charge Transfer Dissociation (CTD) of Gas-Phase Insulin: Evidence of a One-Step, Two-Electron Oxidation Mechanism. *J. Am Soc Mass Spectrom* **2018,** *29*, 284-296.

(47) Li, P.; Jackson, G. P., Charge transfer dissociation of phosphocholines: gas-phase ion/ion reactions between helium cations and phospholipid cations. *J Mass Spectrom* **2017,** *52*, 271-282.

(48) Li, P.; Hoffmann, W. D.; Jackson, G. P., Multistage Mass Spectrometry of Phospholipids using Collision-Induced Dissociation (CID) and Metastable Atom-Activated Dissociation (MAD). *Int J Mass Spectrom* **2016,** *403*, 1-7.

(49) Berkout, V. D.; Doroshenko, V. M., Fragmentation of phosphorylated and singly charged peptide ions via interaction with metastable atoms. *Int J Mass Spectrom* **2008,** *278*, 150-157.

(50) Cook, S. L.; Collin, O. L.; Jackson, G. P., Metastable atom-activated dissociation mass spectrometry: leucine/isoleucine differentiation and ring cleavage of proline residues. *J Mass Spectrom* **2009,** *44*, 1211-1223.

(51) Cook, S. L.; Jackson, G. P., Metastable atom-activated dissociation mass spectrometry of phosphorylated and sulfonated peptides in negative ion mode. *J. Am Soc Mass Spectrom* **2011,** *22*, 1088-1099.

(52) Ceroni, A.; Maass, K.; Geyer, H.; Geyer, R.; Dell, A.; Haslam, S. M., GlycoWorkbench: a tool for the computer-assisted annotation of mass spectra of glycans. *J Proteome Res* **2008,** *7*, 1650-1659.

(53) Duan, J.; Jonathan Amster, I., An Automated, High-Throughput Method for Interpreting the Tandem Mass Spectra of Glycosaminoglycans. *J. Am Soc Mass Spectrom* **2018,** *29*, 1802-1811.

(54) Domon, B.; Costello, C. E., A systematic nomenclature for carbohydrate fragmentations in FAB-MS/MS spectra of glycoconjugates. *Glycoconjugate J* **1988,** *5*, 397-409.

(55) Zaia, J.; Costello, C. E., Tandem Mass Spectrometry of Sulfated Heparin-Like Glycosaminoglycan Oligosaccharides. *Anal Chem* **2003,** *75*, 2445-2455.

(56) Thacker, B. E.; Xu, D.; Lawrence, R.; Esko, J. D., Heparan sulfate 3-O-sulfation: a rare modification in search of a function. *Matrix Biol* **2014,** *35*, 60-72.

(57) Rabenstein, D. L., Heparin and heparan sulfate: structure and function. *Nat Prod Rep* **2002,** *19*, 312-331.

(58) Williams, J. D.; Cox, K. A.; Cooks, R. G.; McLuckey, S. A.; Hart, K. J.; Goeringer, D. E., Resonance Ejection Ion Trap Mass Spectrometry and Nonlinear Field Contributions: The Effect of Scan Direction on Mass Resolution. *Anal Chem* **1994,** *66*, 725-729.

(59) Charles, M. J.; McLuckey, S. A.; Glish, G. L., Competition between resonance ejection and ion dissociation during resonant excitation in a quadrupole ion trap. *J. Am Soc Mass Spectrom* **1994,** *5*, 1031-1041.

(60) Zaia, J.; Li, X.-Q.; Chan, S.-Y.; Costello, C. E., Tandem mass spectrometric strategies for determination of sulfation positions and uronic acid epimerization in chondroitin sulfate oligosaccharides. *J. Am Soc Mass Spectrom* **2003,** *14*, 1270-1281.

(61) Kailemia, M. J.; Patel, A. B.; Johnson, D. T.; Li, L. Y.; Linhardt, R. J.; Amster, I. J., Differentiating chondroitin sulfate glycosaminoglycans using collision-induced dissociation; uronic acid cross-ring diagnostic fragments in a single stage of tandem mass spectrometry. *Eur J Mass Spectrom* **2015,** *21*, 275-285.

CHAPTER 4

Investigation of the Experimental Parameters of Ultraviolet Photodissociation for the Structural Characterization of Chondroitin Sulfate Glycosaminoglycan Isomers

Pepi, L. E., Leach, F. E. III, Klein, D. R., Brodbelt, J. S., & Amster, I. J., To be submitted to *J Am. Soc. Mass Spectrom.*

Abstract

Glycosaminoglycans (GAGs) are linear polysaccharides that participate in a broad range of biological functions. Their incomplete biosynthesis pathway leads to nonuniform chains and complex mixtures. For this reason, the characterization of GAGs has been a difficult hurdle for the analytical community. Recently, ultraviolet photodissociation (UVPD) has emerged as a useful tool for determining sites of modification within a GAG chain. Here we investigate the ability for UVPD to distinguish chondroitin sulfate epimers and the effects of UVPD experimental parameters on fragmentation efficiency. Chondroitin sulfate A (CS-A) and dermatan sulfate (DS) differ only in C-5 uronic acid stereochemistry. This uronic acid difference can influence GAG-protein binding and therefore can alter the specific biological function of a GAG chain. Prior tandem mass spectrometry methods investigated for the elucidation of GAG structures have difficulty differentiating 4-*O* from 6-*O* sulfation in chondroitin sulfate GAGs. Preliminary data using UVPD to characterize GAGs showed a promising ability to characterize 4-*O* sulfation in CS-A GAGs. Here, we look in depth at the capability of UVPD to distinguish chondroitin sulfate C-5 diastereomers and the role of key experimental parameters in making this distinction. Results using a 193 nm excimer laser and a 213 nm solid-state laser are compared for this study. The effect of precursor ionization state, the number of laser pulses (193 nm UVPD), activation time (213 nm UVPD), and background pressure in the region of activation are investigated.

Introduction

Ultraviolet photodissociation (UVPD) coupled with mass spectrometry has been utilized for a variety of biological analyses.[1-5] UV lasers were first coupled with mass spectrometers almost 40 years ago, however due to low signal-to-noise (S/N) and limitations in ionization methods and mass spectrometers at that time, it was not widely used for biological samples until decades later.[6-7] Although a large proportion of UVPD research has focused on proteins and protein complexes, there has also been successful efforts made with the UVPD characterization of lipids, nucleotides and carbohydrates.[8-18] This type of photodissociation utilizes a single wavelength for activation, with the most widely used wavelength being 193 nm from excimer lasers. Ion-activation by UVPD occurs from the absorption of one or more high-energy photons. Upon absorption of a UV photon, ions reach excited electronic states that access dissociation pathways that can be quite different from those resulting from vibrational excitation, as in collision induced dissociation (CID).[19] Following electronic excitation, ions can dissociate by direct dissociation from excited states, which is a unique feature of UVPD. Laser irradiation can also result in electron detachment from multiply deprotonated ions, leading to radically-driven dissociation.[20-22] Ions can also undergo internal conversion to the ground electronic state and intramolecular vibrational energy redistribution (IVR), which result in low-energy fragmentation pathways, similar to those commonly observed for conventional collisional-activation methods.[4, 23-26]

Glycosaminoglycans (GAGs) are linear polysaccharides covalently bound to a protein backbone. GAGs are involved in a variety of biological functions.[27-30] Structural characterization of these carbohydrates are challenging, as they are expressed as heterogeneous mixtures. GAGs are highly modified by varying degrees of sulfation, acetylation and uronic acid C-5

epimerization, and are also heterogeneous in chain length (degree of polymerization or dp). Due to the complex nature of GAG mixtures, mass spectrometry is well suited for their structural characterization. Other analytical methods, such as nuclear magnetic resonance (NMR), can determine locations of modifications; however, this requires high purity samples in much greater amounts than are required for mass spectrometry, which uses microgram quantities or less for analysis.[31] Tandem mass spectrometry of these acidic biomolecules utilize ion activation methods that are suited for negative ions, including electron detachment dissociation (EDD) and negative electron transfer dissociation (NETD). These activation methods have been shown to yield a large number of cross-ring fragment ions, which are particularly useful for assigning sites of modification within a GAG chain.[31-37] One of the more challenging modifications to characterized by mass spectrometry is the stereochemistry of the C-5 position of the hexuronic acid, which distinguishes glucuronic acid from iduronic acid. Assignment of this difference has been examined for both heparin (Hp)/ heparan sulfate (HS) and chondroitin sulfate (CS)/dermatan sulfate (DS) GAG subclasses.[34, 38-43] For CS/DS GAGs, CID can distinguish this stereochemistry difference by comparing the intensities of specific glycosidic cleavages.[41-43] Electron-based methods have also been utilized for this determination, and like threshold-based methods, produce differing fragment ion intensities that can be used to determine C-5 hexuronic acid stereochemistry.[34] We have recently shown the ability of UVPD to characterize GAG standards, producing extensive cross-ring fragmentation.[15] Here, we investigate the ability for UVPD to distinguish CS-A, which contains glucuronic acid (GlcA) from DS, which contains iduronic acid (IdoA), but are otherwise identical in structure. To determine a basis for improving fragmentation efficiency of UVPD for this class of carbohydrates, we examined parameters previously found to be essential for optimizing the fragmentation of proteins and peptides. Key

parameters for UVPD fragmentation efficiency include pulse energy, number of pulses and wavelength. For this work, we investigate the effect of these parameters on fragmentation efficiency, and as a function of the ionization state of the precursor. An additional parameter examined here is the background pressure where ion activation occurs. Prior work with EDD of GAGs used ultrahigh vacuum in the analyzer cell of Fourier transform ion cyclotron resonance (FT ICR) instruments.[44] CID and NETD occur under lower vacuum (higher pressure) in a collision cell.[45] Here, we investigate the change in fragmentation efficiency when UVPD occurs in the high-pressure cell versus the low-pressure cell of a dual-pressure ion trap.

Experimental

Preparation of Chondroitin Sulfate Oligosaccharides

Chondroitin sulfate A (CS-A) was prepared using partial enzymatic depolymerization of bovine trachea chondroitin sulfate A (Celsus Laboratories, Cincinnati, OH, USA). Dermatan sulfate (DS) was prepared the same way but using porcine intestinal mucosa dermatan sulfate (Celsus Laboratories). A full explanation of the procedure has been previously reported.[34, 42]

Mass Spectrometry

All experiments were performed on a Thermo Fisher Orbitrap Fusion Lumos mass spectrometer (San Jose, CA, USA). The mass spectrometer was equipped with a Coherent Excistar 193 nm excimer laser (Santa Clara, CA) or a 213 nm CryLas solid state laser (Berlin, Germany) depending on the experiment. Samples were sprayed from a static nanoelectrospray source with a spray voltage of 0.8-1.2 kV. Samples were diluted in 50:50 MeOH:H_2O to a concentration of 50 µg/mL before ionization. Spectra were collected in negative ion mode at a resolving power of 120,000 at *m/z* 200 in full-profile mode. To minimize sulfate decomposition

in MS^1 spectra, the ion funnel RF was set to 10%. Precursor ions were isolated in the ion trap using an isolation width of 3 *m/z*. Higher-energy collisional dissociation (HCD) was performed using a normalized collision energy (NCE) of 15-25. 193 nm UVPD was performed in both the low-pressure cell and the high-pressure cell, using 4 or 8 pulses at 4mJ per pulse, and repetition rate of 500 Hz, resulting in an 8 ms or 16 ms activation period, respectively. 213 nm UVPD experiments were also performed in the low-pressure cell and high-pressure cell, varying the number of pulses from 3 to 1,000 at 3 µJ per pulse and a repetition rate of 20 kHz to result in activation periods ranging from 1 ms- 400 ms. All data presented is an average of 50 transients, resulting in an experimental time of approximately 30-60 s per spectrum.[15]

Mass spectral features were assigned using Glycoworkbench 2.0 [46] and in-house GAG analysis software.[47-48] Fragment ions are reported using a modified version of the Domon and Costello nomenclature.[49-50] Fragment ion maps use dashed lines drawn through the chemical structure to depict fragmentation, and hash marks at the end of the lines indicate the specific fragment ion. Circles at the end of the hash marks represent sulfate decomposition via loss of -SO_3 with an open circle representing one -SO_3 loss and a filled circle representing two or more -SO_3 losses. A tick mark within a hash mark represents loss of hydrogen, and two tick marks represent the loss of two hydrogen atoms. Donut plots display the percentages of the summed ion abundances for glycosidic fragment ions, cross-ring fragment ions, glycosidic fragment ions with sulfate decomposition and cross-ring fragment ions with sulfate decomposition.

Results and Discussion

Previous work using both vibrational and electronic excitation methods for the dissociation of CS/DS GAGs have shown the ability to distinguish isomers using fragment ion intensities. Initial work using CID showed that a higher abundance of Y_n and $^{0,2}X_n$ fragment ions occurs for DS samples compared to CS-A samples.[43] Further work investigated CID, infrared multiphoton dissociation (IRMPD), EDD and NETD.[34] Like the previous results, these data showed $^{0,2}X_3$ and Y_3 fragments to be diagnostic for DS; however, the newer results showed Y_1 and B_3 fragments to be diagnostic for CS-A. It was also shown that for CS-A, B_3 is more intense than C_3, and for DS C_3 is more intense than B_3. Here, we investigate the different parameters of UVPD that have been deemed essential for protein and peptide fragmentation to determine which parameters are optimal for GAG fragmentation. We also examine the utility of UVPD to distinguish CS isomers, and how these essential fragmentation parameters affect diagnostic fragment ion intensity.

Precursor Ionization State

Precursor selection for MS/MS analysis of GAGs is of primary importance for achieving effective fragmentation. When using CID, a fully ionized precursor is needed to produce structurally-informative fragmentation.[42, 51] When using EDD, a precursor with a degree of ionization that is one more than the number of sulfate modifications is needed to minimize sulfate decomposition while maintaining informative glycosidic and cross-ring fragmentation production. [50] Here we have investigated the effect that the degree of ionization of the precursor ion exerts on UVPD fragmentation efficiency and production of diagnostic fragment ions. CS-A and DS tetrasaccharides contain two sulfate modifications and two carboxyl groups, for a total of four ionizable sites. Precursors ranging from one ionized site to four ionized sites were

examined. All UVPD results discussed in this section used 8 laser pulses of the 193 nm excimer laser in the high-pressure cell unless stated otherwise.

Figure 4.1 compares UVPD results for CS-A for four different levels of deprotonation. The singly-charged precursor ion, $[M-H]^-$ (*m/z* 917.129), of CS-A contains only one site of ionization out of four potential sites, yet yields an abundance of glycosidic fragments and a modest level of cross-ring fragments by UVPD, as shown in the fragment map in Figure 4.1A. The capability of UVPD to produce structurally informative fragment ions for this singly ionized precursor is remarkable when compared to other activation methods. For example, CID would yield principally sulfate decomposition products for this singly-charged precursor. Though the fragment ion intensities are low in the UVPD spectrum, the $[M-H]^-$ precursor produced a $^{2,4}X_2$ (*m/z* 619.130) and a $^{1,4}A_4$ (*m/z* 828.105) fragment ion for both CS-A and DS dp4, which establishes the site of both sulfate modifications as 4-*O* rather than 6-*O* (mass error of 0.48 ppm and 2.3 ppm, respectively). An expanded view of these low intensity fragment ions is shown in supplemental Figures C.1 and C.2. The singly-charged precursor ion's fragment intensity distribution is mostly glycosidic fragment ions (83.6%), with a low abundance of cross-ring fragment ion intensity (6.2%) (Figure 4.1E). Percentages compare the total ion intensity of glycosidic cleavages, cross-ring cleavages, glycosidic cleavages with SO_3 loss and cross-ring cleavages with SO_3 loss to the total intensity of assigned fragment ions. In addition, the singly-charged fragment ion produced the highest intensity of sulfate decomposition via the loss of $-SO_3$ (10.2%) compared to the other precursor ions investigated. A comparison of the CS-A and DS tetramers fragmentation results for the singly-charged precursor is shown in Figure 4.2. For the $[M-H]^-$ precursor, the Y_1 (*m/z* 300.039) fragment is less intense than the Z_1 (*m/z* 282.029) for DS whereas for CS-A the Y_1 fragment is more intense than the Z_1. These results correspond with

previous data for distinguishing CS-A from DS.[34] An increased intensity of the Z_2", C_2" (*m/z* 456.045) fragment ion, where " denotes the loss of 2 -H atoms, compared to the Z_2, C_2 peak (*m/*z 458.060) is also noted for DS while these fragment ions are similar intensities for CS-A. Z_2 and C_2 fragment ions are isobaric and therefore are indistinguishable from each other. Tables C.1 and S2 contain a list of identified fragment ions for the $[M-H]^-$ precursor of DS and CS-A.

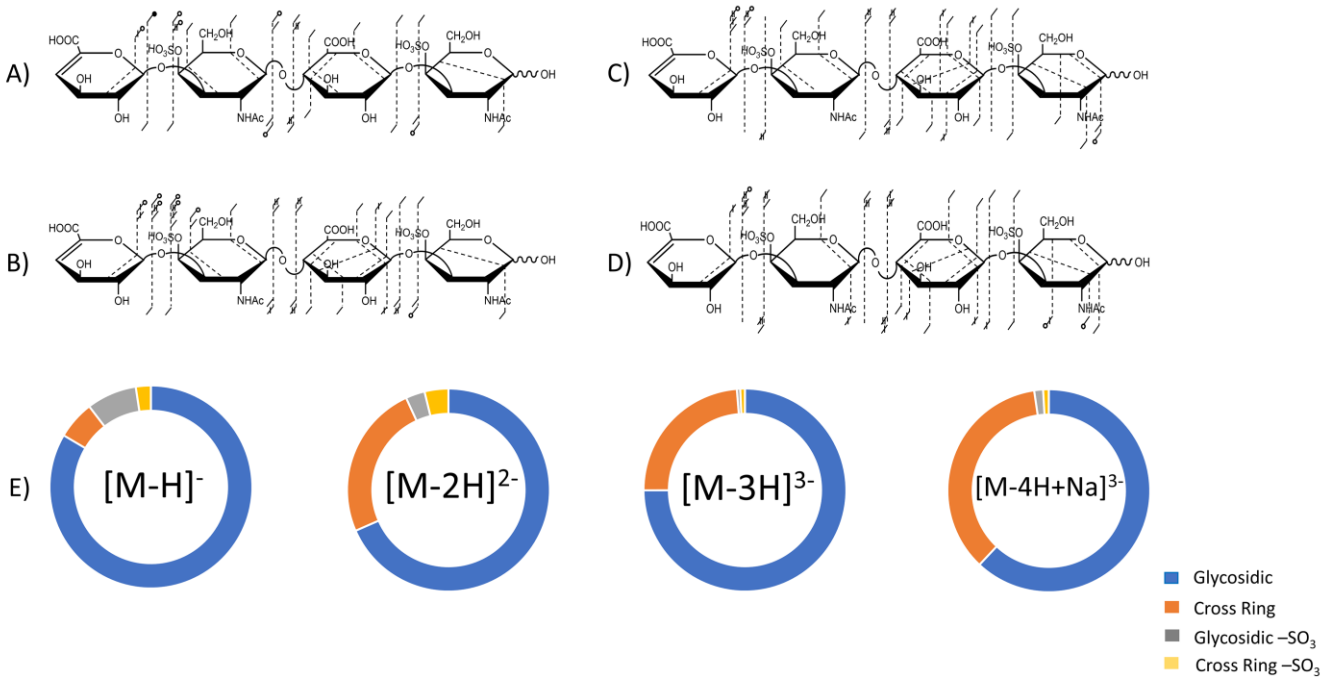

Figure 4.1. Annotated fragment maps depicting 193 nm UVPD fragment ion diversity using 8 laser pulses in the high-pressure cell for A) CS-A $[M-H]^-$ precursor, B) CS-A $[M-2H]^{2-}$ precursor, C) CS-A $[M-3H]^{3-}$ precursor and D) CS-A $[M-4H+Na]^{3-}$ precursor. E) Donut plots depicting the intensity distribution of glycosidic fragments (blue), cross-ring fragments (orange), glycosidic fragments with -SO_3 loss (grey) and cross-ring fragments with -SO_3 loss (yellow) of each precursor.

Figure 4.1B shows the fragmentation map of the $[M-2H]^{2-}$ (*m/z* 458.061) precursor ion, which exhibits a greater diversity of cross-ring fragment ion types compared to the $[M-H]^-$ precursor ion. The doubly-charged precursor is deprotonated at two of the four ionizable sites, likely the two sulfate modifications, as the sulfo half-esters are stronger acids than the carboxyl groups.[34, 52-53] The $[M-2H]^{2-}$ precursor of CS-A also produced a lower intensity of $-SO_3$ loss than the $[M-H]^-$ precursor and a higher intensity of cross-ring fragment ions (Figure 4.1E). Similar to the UVPD fragmentation of the singly-charged precursor, the doubly-charged precursor produced $^{2,4}X_2$ and $^{1,4}A_4$ for both CS-A and DS dp4, which assign both sulfate modifications to 4-*O* positions on the amino sugars. These fragment ions are more intense in the doubly-charged spectrum than in the singly-charged spectrum. A comparison of the CS-A and DS tetramers fragmentation results for the doubly-charged precursor is shown in Figure 4.3. For the $[M-2H]^{2-}$ precursor ion, the relative abundance of Y_1 versus Z_1 shows the same trend as for the singly-charged precursor, where Y_1 is more abundant than Z_1 for CS-A, and less abundant for DS. Additionally, the C_3 (*m/z* 634.093) fragment was much higher in abundance than the B_3 (*m/z* 616.083) fragment for DS (Figure 3A), which was also noted previously with EDD.[34] Past work showed that for CS-A, the B_3 fragment was more intense than C_3, however both fragment ions have very similar intensity in the UVPD results of CS-A. Both the singly and doubly-charged precursors for DS and CS-A dp4 yielded a fragment ion with the mass matching the addition of $-HSO_3$ to the C_3 fragment ion (*m/z* 715.057), which appears to arise from a rearrangement reaction of the sulfate modification. This fragment ion was not seen for the $[M-3H]^{3-}$ and $[M-4H+Na]^{3-}$ precursor ions, indicating that the location of deprotonation of acidic sites may play a role in gas-phase rearrangement processes.[15] As discussed in our previously published paper[15], MS^3 results support that sulfate migration has occurred, where the sulfate modification on the reducing end

GalNAc has moved to the underivatized uronic acid residue.[15] This is further supported by the presence of a $[Y_2/C_3]+SO_3$ (*m/z* 272.99) internal fragment which corresponds to an uronic acid containing a sulfate modification. MS^3 spectra of the *m/z* 715.057 fragment peak for DS and CS-A dp4 with additional assignments from what has previously been reported are shown in Figures C.3 and C.4.

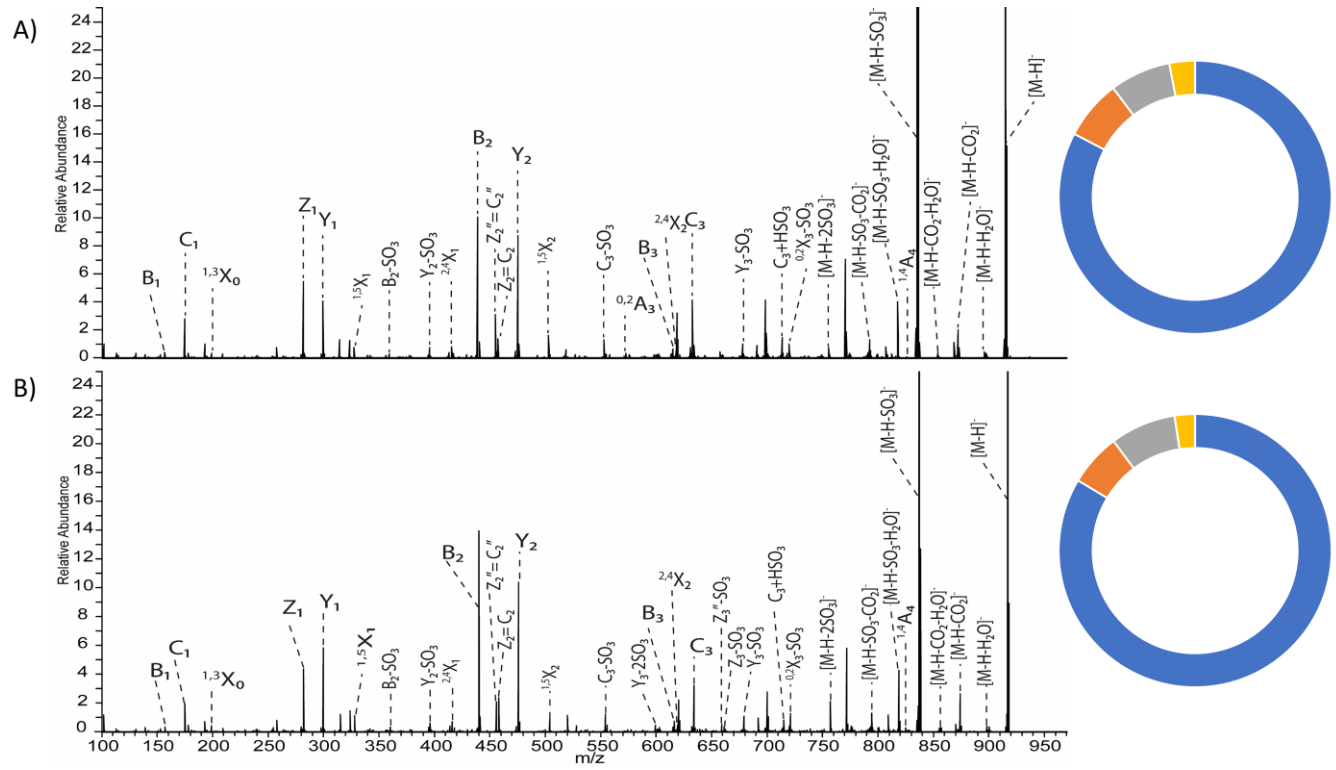

Figure 4.2. 193 nm UVPD spectra of the $[M-H]^-$ precursor and intensity donut plots using 8 laser pulses in the high-pressure cell of tetrasaccharides of A) dermatan sulfate and B) chondroitin sulfate A. Donut plots depict the intensity distribution of glycosidic fragments (blue), cross-ring fragments (orange), glycosidic fragments with $-SO_3$ loss (grey) and cross-ring fragments with $-SO_3$ loss (yellow).

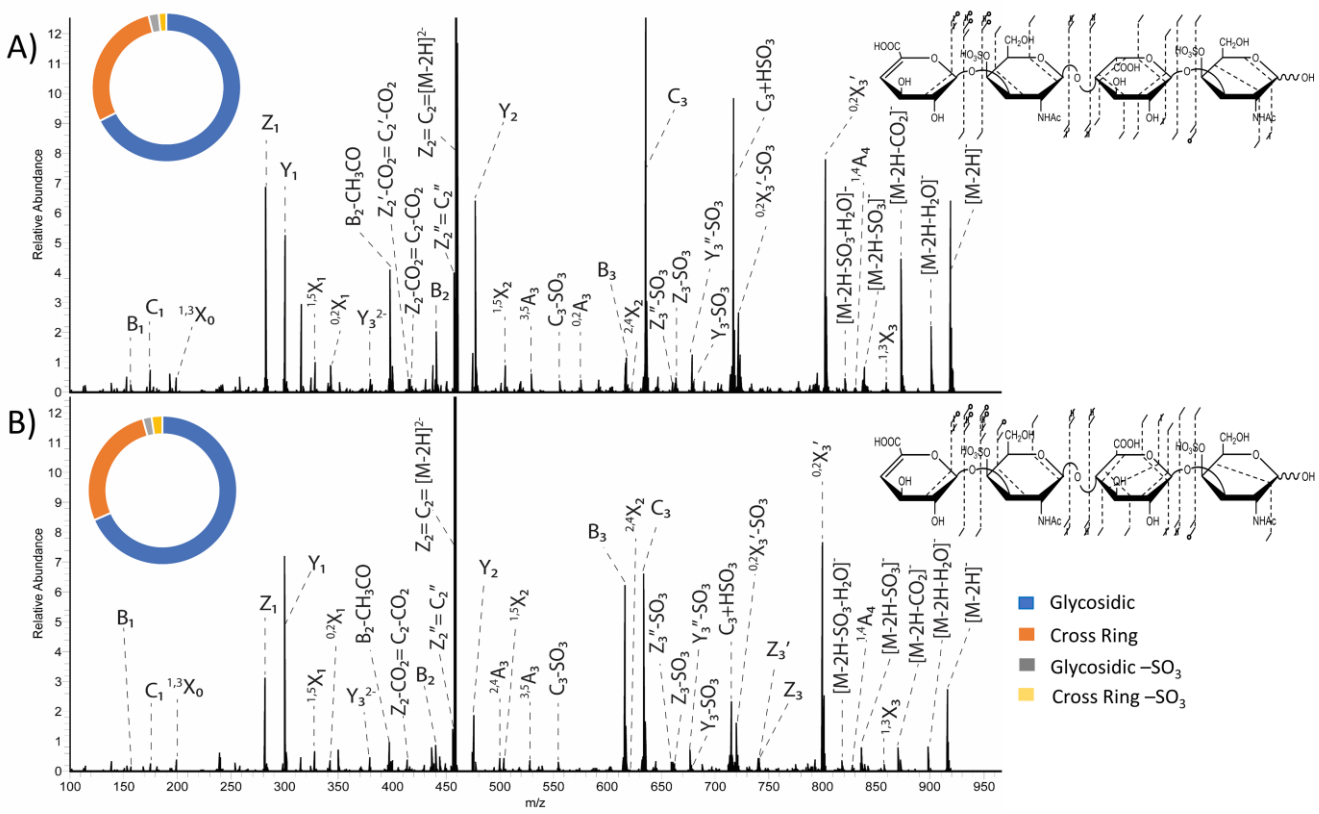

Figure 4.3. 193 nm UVPD spectra using 8 laser pulses in the high- pressure cell of the $[M-2H]^{2-}$ precursor with fragment map and intensity donut plot insets of A) dermatan sulfate and B) chondroitin sulfate A. Tables C.3-C.8 contain identified fragment ions for the $[M-2H]^{2-}$ precursor of CS-A and DS.

The triply-charged precursor of CS-A, $[M-3H]^{3-}$ (*m/z* 305.038), is deprotonated at three of the four ionizable sites. Presumably both sulfate modifications and one carboxyl group are ionized. Figure 4.1C shows the fragment ion map of the triply-charged precursor, which yielded a higher diversity of cross-ring fragment ions than the singly and doubly-charged precursors, particularly on the reducing end galactosamine and glucuronic acid residues. Like the singly and doubly-charged precursor ions, the triply-charged precursor ion also produced $^{2,4}X_2$ and $^{1,4}A_4$ fragment ions for both CS-A and DS dp4, which establish the locations of both sulfate

modifications. The triply-charged precursor however did not produce a higher intensity of cross ring fragment ions (22.6%) compared to the doubly-charged precursor (24.7%). It did however retain sulfate modifications better than both the singly and doubly-charged precursors (Figure 4.1E). A comparison of the CS-A and DS tetramers fragmentation for the $[M-3H]^{3-}$ precursor is shown in Figure 4.4. This more ionized precursor no longer exhibits a diagnostic fragment distribution for B_3 versus C_3 ions. For the singly and doubly-charged precursors, these ions had intensities that correlated with the uronic acid stereochemistry. However, for the triply-charged precursor the C_3 fragment ion is more intense than the B_3 for both CS-A and DS. As was seen previously with ion activation by EDD, the $[M-3H]^{3-}$ precursor does not produce stereospecific fragment ions.[34] However, these results differ from the EDD results for this precursor, in that the B_3 and C_3 ions are vanishingly small by EDD but have a comparable abundance relative to other fragment ions in the UVPD mass spectrum.

The fully ionized precursor, $[M-4H+Na]^{3-}$ (*m/z* 312.366), produced a similar diversity of cross-ring fragment ion types to the triply-charged precursor (Figure 4.1D). The fully ionized precursor however did not produce the necessary cross-ring fragment ions to assign either sulfate modification as 4-*O* versus 6-*O*. This may be due to the addition of Na, which adds more complexity to the spectrum and spreads signals out across additional fragmentation channels, resulting in a reduction of the overall S/N ratio.[54] It is also possible that sodium stabilizes radical intermediates from electron detachment. It has been observed in EDD studies that a significant decrease of product ion formation results from the incorporation of sodium cation in the precursor.[50] A comparison of UVPD of the $[M-4H+Na]^{3-}$ precursor of CS-A and DS tetramers is shown in Figure C.5. For the $[M-4H+Na]^{3-}$ precursor ion, the intensity of the Y_3+Na (*m/z* 781.090) fragment was more intense than the Z_3+Na (*m/z* 763.079) fragment for DS, and the

Z_3+Na fragment was more intense than the Y_1+Na for CS-A. Additionally, the doubly-charged Y_3+Na fragment had a higher intensity in DS than in CS-A; the doubly-charged Z_3+Na fragment ion was not seen for either sample. This agrees with past findings that Y_n fragment ions are diagnostic for DS.[34, 43]

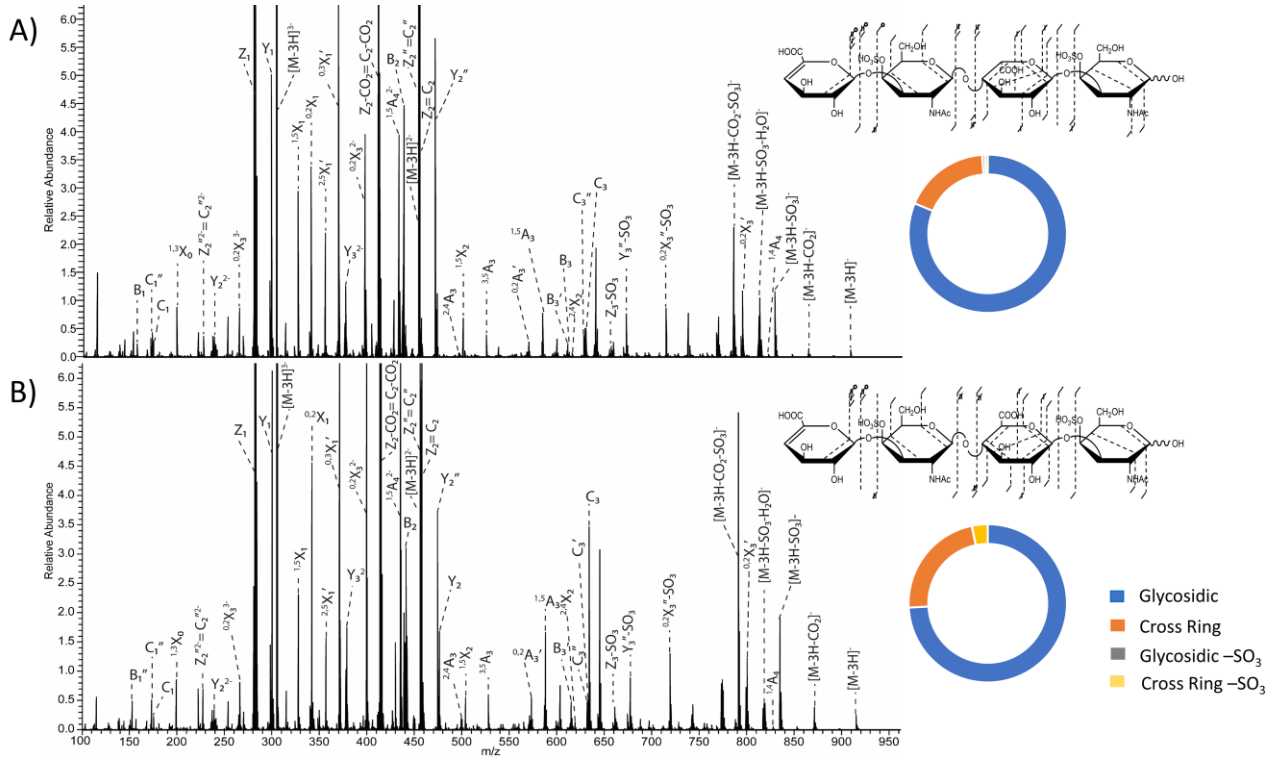

Figure 4.4. 193 nm UVPD spectra using 8 laser pulses in the high-pressure cell of the $[M-3H]^{3-}$ precursor with fragment map and donut plot insets of A) dermatan sulfate and B) chondroitin sulfate A. Donut plots depict intensity distributions if glycosidic fragments (blue), cross-ring fragments (orange), glycosidic fragments with -SO_3 loss (grey) and cross-ring fragments with -SO_3 loss (yellow). Tables C.9-C.14 show identified fragment ions for the $[M-3H]^{3-}$ precursor of CS-A and DS.

Precursor comparison for the DS tetrasaccharide, shown in Figure C.6, followed a similar trend. The fully ionized precursor produced less cross-ring fragment ion diversity than both the doubly and triply-charged precursor ions. The fully ionized precursor also produced a lower intensity of cross-ring fragment ions (15.7%) than both the doubly (23.4%) and triply-charge (17.6%) precursor ions. Neither sulfate modification could be located for the $[M-4H+Na]^{3-}$ fragment ion, however both sulfate modifications could be located for the singly, doubly and triply-charged precursor ions.

Based on these results, it can be concluded that SO_3 loss can be minimized when the ionization state is equal to one more than the number of sulfate modifications for UVPD, and product ion formation can be maximized when the ionization state is either equal to, or one more than, the number of sulfate modifications present in the precursor. This is similar to the behavior of EDD and can guide precursor selection for the analysis of a purified sample, for which one can select solution conditions to control the types of precursors that are generated in electrospray ionization. In contrast to EDD, UVPD produces informationally-rich MS/MS data from lower charge states with only a modest amount of sulfate decomposition. This is a significant result that can enable the integration of capillary zone electrophoresis (CZE) and tandem mass spectrometry for the analysis of GAG mixtures, as CZE buffers tend to produce lower charge states for GAGs that are difficult to analyze with other ion activation methods.[55]

Number of Pulses (193 nm UVPD)

The number of laser pulses used in a UVPD experiment has been shown to affect the fragmentation outcome of protein samples. Past work by Cotham *et al.* showed that an increased number of laser pulses results in higher sequence coverage of monoclonal antibodies.[56] This was

thought to be due to an enhanced energization of the polypeptide backbone, resulting in more efficient photodissociation.[56] For this study, the number of laser pulses used was varied from 4 laser pulses to 8 laser pulses at 4 mJ per pulse when using a 193 nm excimer laser. The increase in the number of laser pulses used resulted in an overall increase in fragment ion intensity, as shown for precursor ion $[M-3H]^{3-}$ of the CS-A tetramer in Figure 4.5. All signal intensity, including both glycosidic and cross-ring fragment ions, as well as neutral loss peaks, increased with an increase in pulses used. The sequence coverage however did not significantly increase, as shown in the fragment ion maps in Figure 4.5. When using 8 laser pulses, the location of both sulfate modifications were assigned by $^{2,4}X_2$ and $^{1,4}A_4$ fragment ions (Figure 4.5A). Only the $^{2,4}X_2$ fragment ion is seen when using 4 laser pulses (Figure 4.5B). This is likely due to the low intensity of these fragment ions. This trend was seen for both CS-A and DS tetramers. When comparing the intensity distribution of fragment ion types, there was minimal differences between 4 laser pulses and 8 laser pulses. With an increase in the number of pulses used, there is an expected increase in the fraction of precursor ions that undergo photoabsorption. The majority of the signal in these UVPD spectra is from undissociated precursor ions, suggesting that additional laser pulses could yield even higher yields of fragmentation. However, this must be balanced against the possibility of further fragmentation of product ions, leading to the formation of internal cleavage products that might confound the assignment of a structure.

The effect of the number of laser pulses has on diagnostic ions for distinguishing CS-A and DS were also investigated. UVPD of the $[M-2H]^{2-}$ precursor of both CS-A and DS when using 8 laser pulses in the high-pressure cell is shown in Figure 4.3. For DS, The Y_1 fragment ion is less intense than the Z_1, whereas for CS-A the Z_1 fragment is more intense than the Y_1. Additionally, for DS, the C_3 fragment ion was more intense than the B_3 fragment, whereas for

CS-A, both fragment ions were similar in intensity. These distribution difference have been noted previously for EDD.[34] When looking at UVPD of the $[M-2H]^{2-}$ precursor ion using 4 laser pulses in the high-pressure cell (Figure C.7), the same distributions for diagnostics fragments were seen. This indicates that though increasing laser pulses increases fragment ion intensity, it does not change their intensity distribution. This was also investigated for the $[M-3H]^{3-}$ precursor. As previously noted, the triply-charged precursor did not yield any diagnostic fragments. However, like the $[M-2H]^{2-}$ precursor, the $[M-3H]^{3-}$ precursor did not produce any fragmentation distribution changes when comparing UVVPD in the high-pressure cell using 8 laser pulses and 4 laser pulses (Figures 4.4 and C.8).

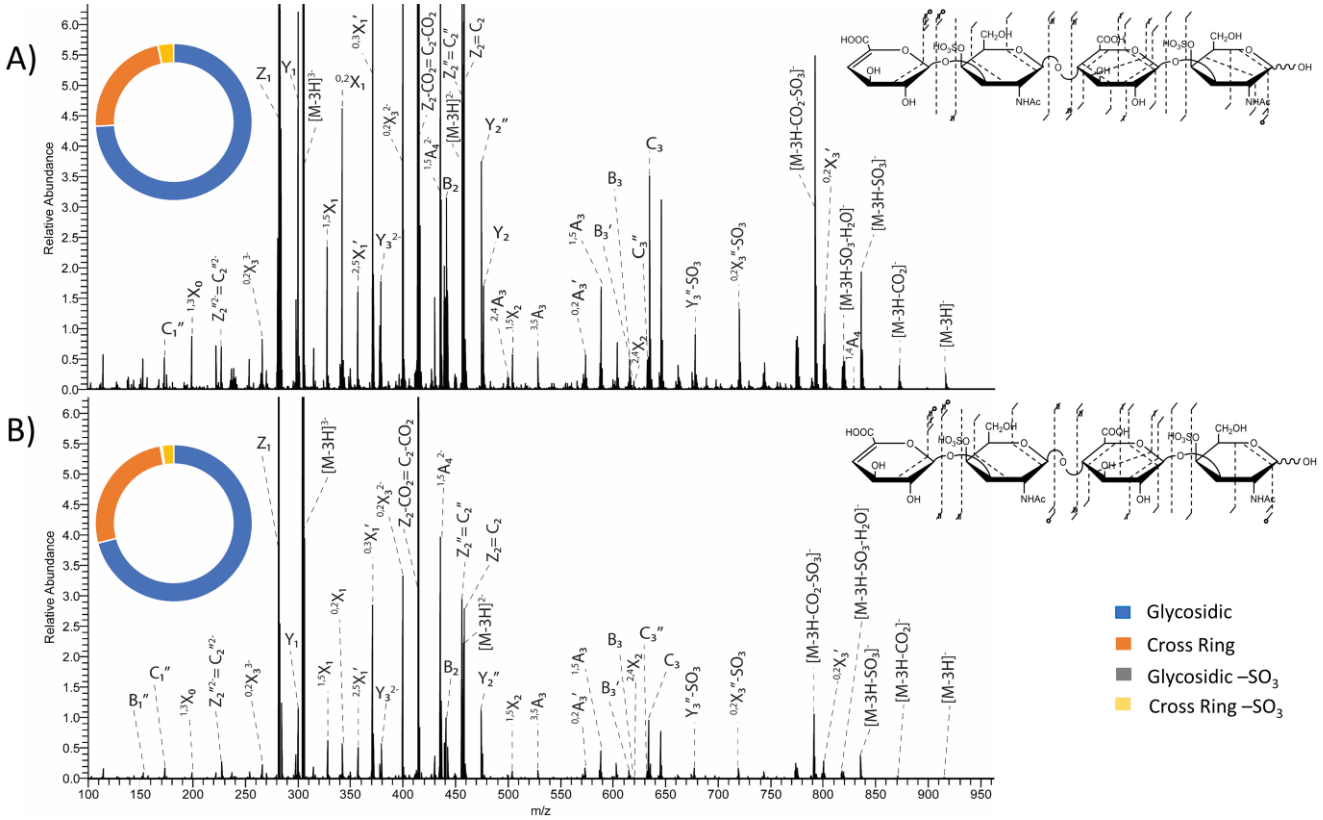

Figure 4.5. 193 nm UVPD spectra with fragment map and intensity donut plot insets of the $[M-3H]^{3-}$ precursor of chondroitin sulfate A with A) 8 laser pulses in the high-pressure cell and B) 4 laser pulses in the high-pressure cell. Donut plots depict intensity distributions if glycosidic fragments (blue), cross-ring fragments (orange), glycosidic fragments with $-SO_3$ loss (grey) and cross-ring fragments with $-SO_3$ loss (yellow).

Location of Photodissociation

A benefit of performing UVPD experiments on a mass spectrometer with a dual linear ion trap is the ability to carry out UVPD in either the high-pressure or low-pressure region. When comparing results for DS tetrasaccharide using the high-pressure cell (8 laser pulses) to the low-pressure cell (8 laser pulses), the sequence coverage did not change significantly. Both

the high-pressure cell and low-pressure cell UVPD experiments resulted in almost identical sequence coverage. However, the high-pressure cell resulted in an overall increase of fragment ion intensity and produced two cross-ring fragments needed to assign the location of both sulfate modifications, $^{2,4}X_2$ and $^{1,4}A_4$. These cross-ring fragments were not seen in the low-pressure cell results. A higher pressure in the ion trap results in a more radial condensation of the ion cloud and in increased overlap with the laser beam. This leads to a better conversion of precursor ions to fragment ions, as seen in Figure 4.6 for DS dp4. Though the fragmentation coverage of the GAG chain is almost identical between the high-pressure cell and low-pressure cell experiments, there was an increase in the intensity of cross-ring fragment ions when isolating precursor ions in the low-pressure cell. This change in intensity distribution is likely due to a few intense glycosidic fragments, specifically the Z_1, Y_1 and Z_2/C_2 fragment ions.

The influence of trapping pressure on formation of diagnostic fragments was also investigated. When activating the $[M\text{-}2H]^{2-}$ precursor (*m/z* 458.061) in the high-pressure cell with 8 laser pulses, the C_3 fragment ion was much more intense than the B_3 fragment ion, whereas for CS-A the B_3 and C_3 fragment ions have similar intensities. Additionally, the Y_1 fragment is more intense than Z_1 in CS-A, whereas for DS Z_1 is more intense (Figure 4.3). When the same precursor was activated in the low-pressure cell using 8 laser pulses, the C_3 fragment was still much more intense than the B_3 fragment in DS, but the Y_1 fragment was slightly more intense than the Z_1 fragment for CS-A (Figure C.9). These results coincide with the results from the $[M\text{-}3H]^{3-}$ precursor; activation in the high-pressure cell results in an overall increase in fragment ion intensity, however activating in the low-pressure cell does not change the intensity distribution of fragment ions.

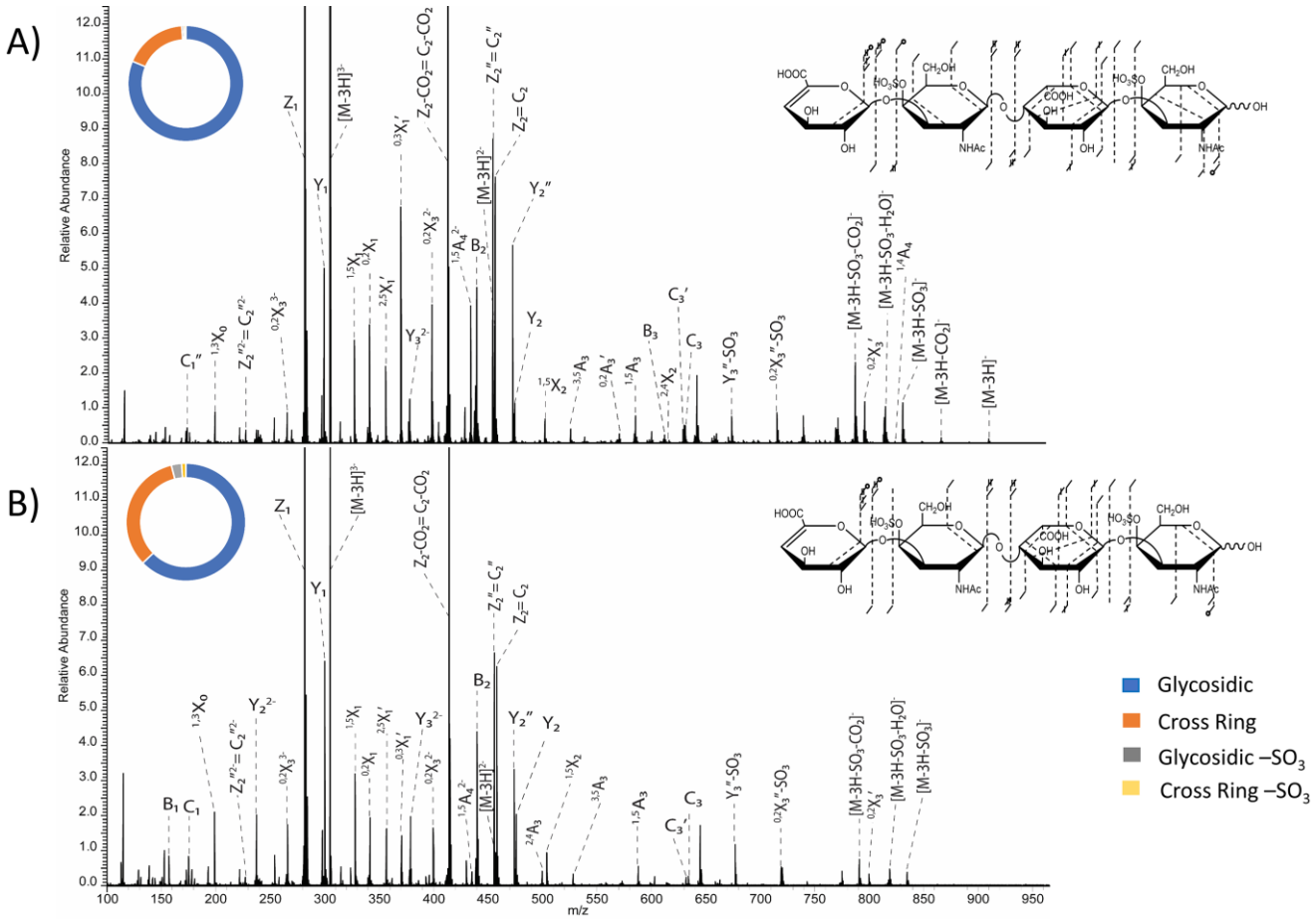

Figure 4.6. 193 nm UVPD spectra with fragment map and donut plot insets of the $[M-3H]^{3-}$ precursor of dermatan sulfate with 8 pulses in the A) high-pressure cell and B) low-pressure cell.

Laser Wavelength (193 nm v 213 nm)

193 nm UVPD has successfully been used for structural characterization of acidic saccharides, locating sulfate modifications on peptides, and recently the structural characterization of GAGs. [15, 57-58] 213 nm UVPD has recently been made a commercially available option with Orbitrap MS.[59-60] The 193 nm laser yields 6.4 eV per photon while the 213 nm laser yields 5.8 eV per photon.[23] The energy per pulse is 4 mJ for the 193 nm laser, while the

213 nm laser produces 3 μJ. We compared the two lasers for their efficiency in UVPD of GAGs. Figure 4.7 shows a comparison of fragmentation efficiency of these two wavelengths for the $[M-3H]^{3-}$ precursor of DS dp4. The red dashed lines indicate fragment ions seen only by the 193 nm laser, and blue represents fragment ions seen by only the 213 nm laser. Fragments shown in black were seen by UVPD using both wavelengths. Figure 4.7A compares 213 nm UVPD fragmentation efficiency with a 50 ms activation time (125 pulses) in the high-pressure cell to the 193 nm UVPD with 4 laser pulses (8 ms activation time) in the high-pressure cell. The 193 nm laser was able to locate one sulfate modification with a $^{2,4}X_2$ fragment ion. Figure 4.7B compares 213 nm UVPD fragmentation with a 400 ms activation time (1,000 laser pulses) in the high-pressure cell to 193 nm UVPD with 8 laser pulses in the high-pressure cell. Both wavelengths were able to assign the location of the sulfate positions under these conditions. Both produced a $^{2,4}X_2$ fragment, and 213 nm UVPD produced a $^{2,4}A_4^{2-}$ fragment while 193 nm UVPD produced a $^{1,4}A_4$ fragment. By increasing the activation time from 50 ms to 400 ms the sequence information gained from 213 nm UVPD was drastically increased (Figure 4.7A and 4.7B). When comparing 213 nm UVPD with a 50 ms activation time in the low-pressure cell to 193 nm UVPD with 4 laser pulses in the low-pressure cell, neither wavelengths were able to produce fragment ions that could assign the location of the sulfate modifications (Figure 4.7C). Both produced glycosidic fragment ions that can be used to determine the sulfate modifications are on the amino sugars and not the uronic acid residues. 213 nm UVPD with a 400 ms activation time in the low-pressure cell was able to assign both sulfate modifications with $^{2,4}X_2$ and $^{2,4}A_4^{2-}$ fragment ions, but 193 nm UVPD with 8 laser pulses in the low-pressure cell was still unable to assign the location of either sulfate modification (Figure 4.7D). For all conditions, 213 nm UVPD produced a higher intensity of cross-ring fragment ions than 193 nm UVPD. However, as

seen in the fragment maps in Figure 4.7, the higher intensity of cross-ring fragments does not mean a higher abundance and diversity of cross-ring fragment types.

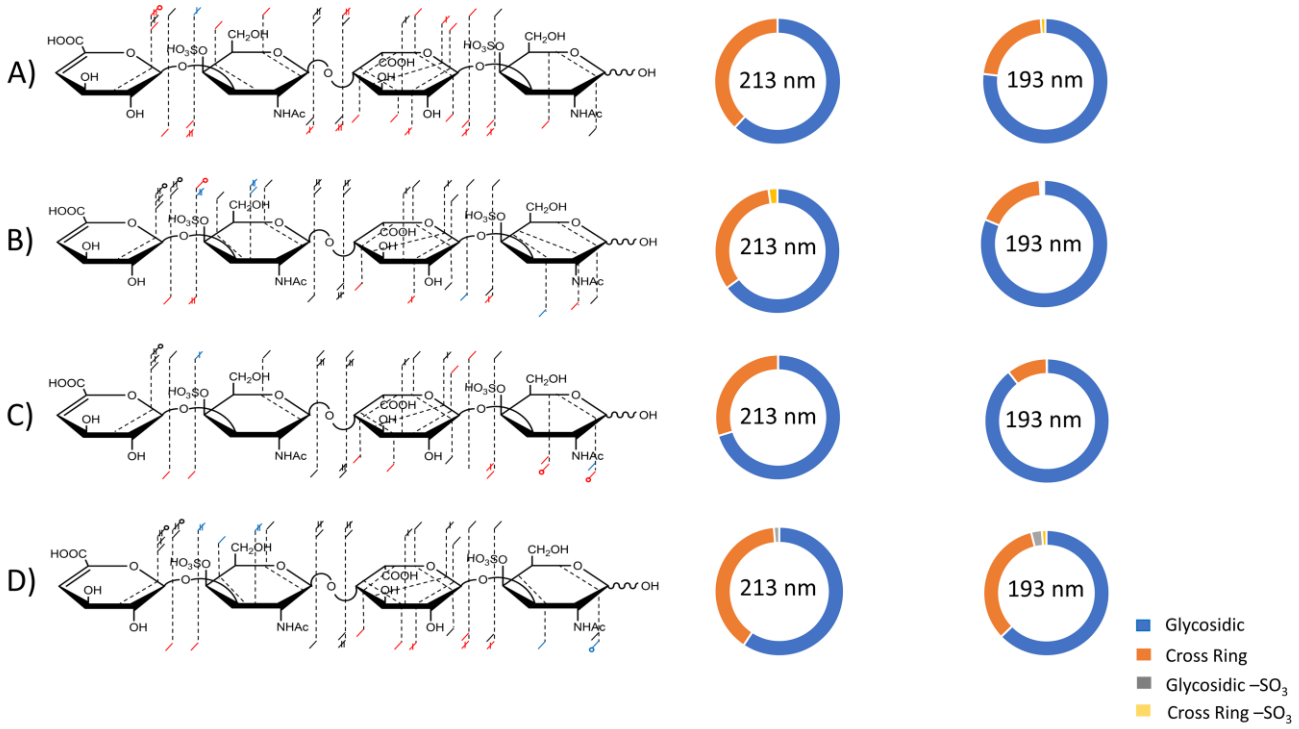

Figure 4.7. Annotated fragment maps and donut plots of the $[M-3H]^{3-}$ precursor of dermatan sulfate dp4 comparing 213 nm UVPD to 193 nm UVPD. Red fragment dashes were seen with 193 nm UVPD, blue fragment dashes were seen with 213 nm UVPD and black dashes were seen with both wavelengths. A) 213 nm UVPD with 50 ms activation in the high-pressure cell compared to 193 nm UVPD with 4 laser pulses in the high-pressure cell. B) 213 nm UVPD with 400 ms activation in the high-pressure cell compared to 193 nm UVPD with 8 laser pulses in the high-pressure cell. C) 213 nm UVPD with 50 ms activation in the low-pressure cell compared to 193 nm UVPD with 4 laser pulses in the low-pressure cell. D) 213 nm UVPD with 400 ms activation in the low-pressure cell compared to 193 nm UVPD with 8 laser pulses in the low-pressure cell.

Activation Time (213 nm UVPD)

For experiments using the 213 nm solid state laser, activation times ranging from 1 ms to 400 ms were investigated. A comparison of 50 ms, 150 ms, 300ms and 400 ms activation times of the $[M-3H]^{3-}$ precursor ion of DS dp4 is shown in Figure 4.8. By increasing the activation time there is in increase in overall signal intensity, leading to more fragment ion coverage. An activation time of 400 ms produced a more diverse fragmentation coverage than a 50 ms activation time. Neither sulfate modification could be located by the 50 ms activation time. An activation time of 150 ms was able to locate one sulfate modification with a $^{2,4}A_4^{2-}$ fragment ion, but could not locate the remaining sulfate modification. A 300 ms activation time was able to locate both sulfate modifications with $^{2,4}X_2$ and $^{2,4}A_4^{2-}$ fragment ions. A 400 ms activation time produced both $^{2,4}X_2$ and $^{2,4}A_4^{2-}$ fragments, which can locate both sulfate modifications.

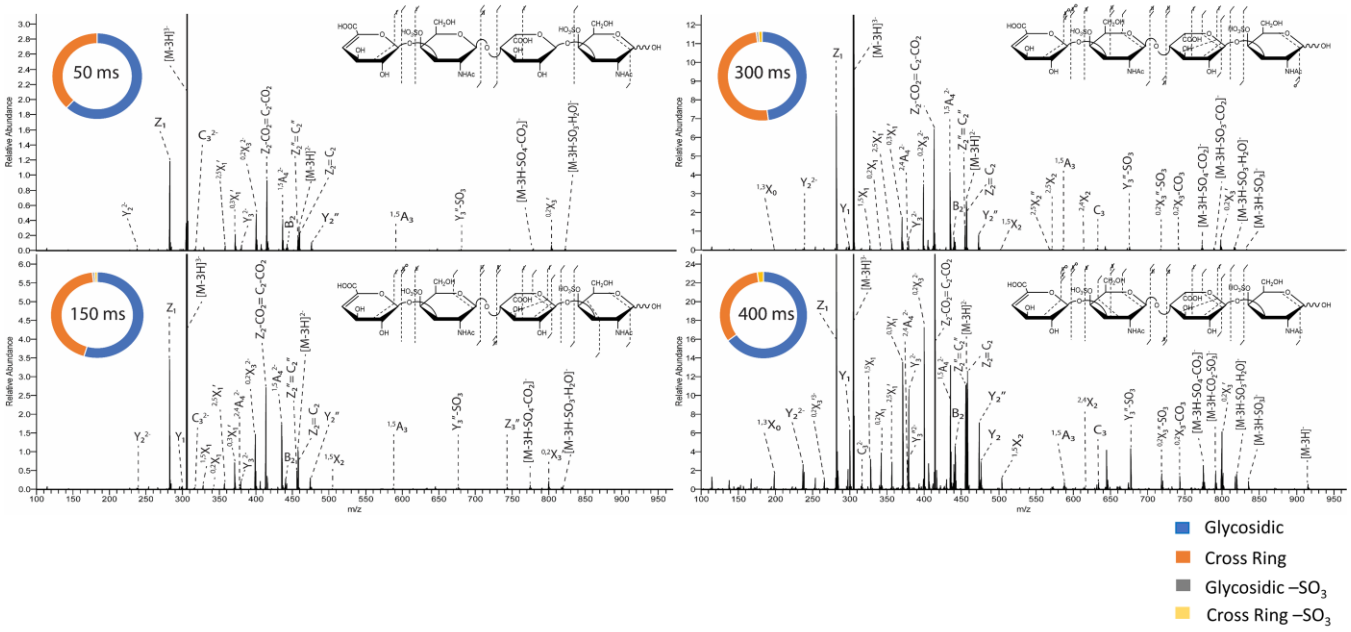

Figure 4.8. 213 nm UVPD spectra of the $[M-3H]^{3-}$ precursor of dermatan sulfate dp4 with fragment map and donut plot insets illustrating the effect of activation time on fragmentation efficiency. Fragment ion lists are shown in Tables C.17-C.22.

Conclusions

The importance of optimizing UVPD fragmentation parameters for efficiently converting precursor ions to fragment ions has been previously demonstrated for proteins and peptides. Here, we outline the effect these parameters have on fragmentation and distinction of DS and CS-A tetrasaccharide GAG standards. The parameters that were shown to be imperative for protein fragmentation efficiency, including precursor ionization state, wavelength, number of laser pulses, and pulse energy, have been shown here to play a large roll in GAG fragmentation efficiency as well. UVPD using both a 193 nm excimer laser and a 213 nm solid-state laser can yield informative fragmentation for GAG standards. Increasing the number of pulses for both

wavelengths can yield more informative fragmentation and increase the fragmentation abundance. Performing UVPD experiments in the high-pressure cell of a dual-pressure ion trap can also lead to an increase in fragmentation efficiency. However, what was shown to have the largest effect on increasing fragmentation efficiency was precursor ionization state. A precursor with one more ionized site than the number of sulfate modifications was shown to reduce sulfate decomposition while also maintaining informative fragments. Independent of these changes for fragmentation efficiency, it was noted that DS and CS-A could be distinguished from each other using UVPD in the same manner as was previously noted for other activation methods. Z_1, C_3, Y_3 and Z_2"/C_2" were shown to be indictive of DS.

Acknowledgments

Funding from the NIH (Grant RO1 GM103655 to J.S.B.) and the Welch Foundation (Grant F-1155 to J.S.B.) are gratefully acknowledged. I.J.A.,F.E.L. and L.E.P. are grateful for generous support from the National Institutes of Health and the Common Fund for Glycoscience, Grants R21HL136271, U01CA231074, and P41GM103390. Funding from the UT System for support of the UT System Proteomics Core Facility Network is gratefully acknowledged. The authors would also like to acknowledge Robert Linhardt and Fuming Zhang (Rensselaer Polytechnic Institute) for providing CS-A and DS samples that were utilized during this study.

References

(1) Shaw, J. B.; Li, W.; Holden, D. D.; Zhang, Y.; Griep-Raming, J.; Fellers, R. T.; Early, B. P.; Thomas, P. M.; Kelleher, N. L.; Brodbelt, J. S., Complete protein characterization using top-down mass spectrometry and ultraviolet photodissociation. *J Am Chem Soc* **2013,** *135*, 12646-12651.

(2) Shaw, J. B.; Robinson, E. W.; Paša-Tolić, L., Vacuum Ultraviolet Photodissociation and Fourier Transform–Ion Cyclotron Resonance (FT-ICR) Mass Spectrometry: Revisited. *Anal Chem* **2016,** *88*, 3019-3023.

(3) Madsen, J. A.; Boutz, D. R.; Brodbelt, J. S., Ultrafast ultraviolet photodissociation at 193 nm and its applicability to proteomic workflows. *J Proteome Res* **2010,** *9*, 4205-4214.

(4) Ly, T.; Julian, R. R., Ultraviolet photodissociation: developments towards applications for mass-spectrometry-based proteomics. *Angew Chem Int Edit* **2009,** *48*, 7130-7137.

(5) Guan, Z.; Kelleher, N. L.; O'Connor, P. B.; Aaserud, D. J.; Little, D. P.; McLafferty, F. W., 193 nm photodissociation of larger multiply-charged biomolecules. *Int J Mass Spectrom* **1996,** *157*, 357-364.

(6) Bowers, W. D.; Delbert, S. S.; Hunter, R. L.; McIver Jr, R. T., Fragmentation of oligopeptide ions using ultraviolet laser radiation and Fourier transform mass spectrometry. *J Am Chem Soc* **1984,** *106*, 7288-7289.

(7) Thompson, M. S.; Cui, W.; Reilly, J. P., Fragmentation of singly charged peptide ions by photodissociation at λ= 157 nm. *Angew Chem Int Edit* **2004,** *43*, 4791-4794.

(8) Devakumar, A.; Thompson, M. S.; Reilly, J. P., Fragmentation of oligosaccharide ions with 157 nm vacuum ultraviolet light. *Rapid Commun Mass Spectrom* **2005,** *19*, 2313-2320.

(9) Devakumar, A.; Mechref, Y.; Kang, P.; Novotny, M. V.; Reilly, J. P., Laser-induced photofragmentation of neutral and acidic glycans inside an ion-trap mass spectrometer. *Rapid Commun Mass Spectrom* **2007,** *21*, 1452-1460.

(10) Cui, W.; Thompson, M. S.; Reilly, J. P., Pathways of peptide ion fragmentation induced by vacuum ultraviolet light. *J Am Soc Mass Spectr* **2005,** *16*, 1384-1398.

(11) Smith, S. I.; Brodbelt, J. S., Hybrid activation methods for elucidating nucleic acid modifications. *Anal Chem* **2011,** *83*, 303-310.

(12) Pham, H. T.; Julian, R. R., Characterization of glycosphingolipid epimers by radical-directed dissociation mass spectrometry. *Analyst* **2016,** *141*, 1273-1278.

(13) Pham, H. T.; Trevitt, A. J.; Mitchell, T. W.; Blanksby, S. J., Rapid differentiation of isomeric lipids by photodissociation mass spectrometry of fatty acid derivatives. *Rapid Commun Mass Spectrom* **2013,** *27*, 805-815.

(14) Hancock, S. E.; Ailuri, R.; Marshall, D. L.; Brown, S. H.; Saville, J. T.; Narreddula, V. R.; Boase, N. R.; Poad, B. L.; Trevitt, A. J.; Willcox, M. D., Mass spectrometry-directed structure elucidation and total synthesis of ultra-long chain (O-acyl)-ω-hydroxy fatty acids. *J Lipid Res* **2018,** *59*, 1510-1518.

(15) Klein, D.; Leach, F. I.; Amster, I.; Brodbelt, J., Structural Characterization of Glycosaminoglycan Carbohydrates using Ultraviolet Photodissociation. *Anal Chem* **2019,** *91*, 6019-6026.

(16) Crittenden, C. M.; Novelli, E. T.; Xu, G.; Giles, D. H.; Fies, W. A.; Mehaffey, M. R.; Dalby, K. N.; Webb, L. J.; Brodbelt, J. S., Structural Evaluation of Protein/Metal Complexes via Native Electrospray Ultraviolet Photodissociation Mass Spectrometry. *J Am Soc Mass Spectr* **2020,** *31*, 1140-1150.

(17) Klein, D. R.; Blevins, M. S.; Macias, L. A.; Douglas, M.; Trent, M. S.; Brodbelt, J. S., Localization of Double Bonds in Bacterial Glycerophospholipids Using 193 nm Ultraviolet Photodissociation in the Negative Mode. *Anal Chem* **2020,** *92*, 5986-5993.

(18) Sipe, S. N.; Patrick, J. W.; Laganowsky, A.; Brodbelt, J. S., Enhanced Characterization of Membrane Protein Complexes by Ultraviolet Photodissociation Mass Spectrometry. *Anal Chem* **2019,** *92*, 899-907.

(19) R. Julian, R., The mechanism behind top-down UVPD experiments: making sense of apparent contradictions. *J Am Soc Mass Spectr* **2017,** *28*, 1823-1826.

(20) Racaud, A.; Antoine, R.; Joly, L.; Mesplet, N.; Dugourd, P.; Lemoine, J., Wavelength-tunable ultraviolet photodissociation (UVPD) of heparin-derived disaccharides in a linear ion trap. *J Am Soc Mass Spectr* **2009,** *20*, 1645-1651.

(21) Racaud, A.; Antoine, R.; Dugourd, P.; Lemoineb, J., Photoinduced dissociation of heparin-derived oligosaccharides controlled by charge location. *J Am Soc Mass Spectr* **2010,** *21*, 2077-2084.

(22) Gabelica, V.; Tabarin, T.; Antoine, R.; Rosu, F.; Compagnon, I.; Broyer, M.; De Pauw, E.; Dugourd, P., Electron photodetachment dissociation of DNA polyanions in a quadrupole ion trap mass spectrometer. *Anal Chem* **2006,** *78*, 6564-6572.

(23) Brodbelt, J. S.; Morrison, L. J.; Santos, I. s., Ultraviolet Photodissociation Mass Spectrometry for Analysis of Biological Molecules. *Chem Rev* **2020,** *120*, 3328-3380.

(24) Brodbelt, J. S., Shedding light on the frontier of photodissociation. *J Am Soc Mass Spectr* **2011,** *22*, 197-206.

(25) Brodbelt, J. S., Photodissociation mass spectrometry: new tools for characterization of biological molecules. *Chem Soc Rev* **2014,** *43*, 2757-2783.

(26) Reilly, J. P., Ultraviolet photofragmentation of biomolecular ions. *Mass Spectrom Rev* **2009,** *28*, 425-447.

(27) Clegg, D. O.; Reda, D. J.; Harris, C. L.; Klein, M. A.; O'Dell, J. R.; Hooper, M. M.; Bradley, J. D.; Bingham III, C. O.; Weisman, M. H.; Jackson, C. G., Glucosamine, chondroitin sulfate, and the two in combination for painful knee osteoarthritis. *New Engl J Med* **2006,** *354*, 795-808.

(28) Esko, J. D.; Lindahl, U., Molecular diversity of heparan sulfate. *Journal of Clinical Investigation* **2001,** *108*, 169-173.

(29) Varki, A.; Cummings, R. D.; Esko, J. D.; Freeze, H. H.; Stanley, P.; Bertozzi, C. R.; Hart, G. W.; Etzler, M. E., *Essentials of Glycobiology*. NY, 2009; Vol. 2.

(30) Watanabe, H.; Yamada, Y.; Kimata, K., Roles of aggrecan, a large chondroitin sulfate proteoglycan, in cartilage structure and function. *J Biochem* **1998,** *124*, 687-693.

(31) Wolff, J. J.; Leach, F. E.; Laremore, T. N.; Kaplan, D. A.; Easterling, M. L.; Linhardt, R. J.; Amster, I. J., Negative electron transfer dissociation of glycosaminoglycans. *Anal Chem* **2010,** *82*, 3460-3466.

(32) Wu, J.; Wei, J.; Hogan, J. D.; Chopra, P.; Joshi, A.; Lu, W.; Klein, J.; Boons, G.-J.; Lin, C.; Zaia, J., Negative Electron Transfer Dissociation Sequencing of 3-O-Sulfation-Containing Heparan Sulfate Oligosaccharides. *J Am Soc Mass Spectr* **2018,** *29*, 1262-1272.

(33) Leach, F. E.; Arungundram, S.; Al-Mafraji, K.; Venot, A.; Boons, G.-J.; Amster, I. J., Electron detachment dissociation of synthetic heparan sulfate glycosaminoglycan tetrasaccharides varying in degree of sulfation and hexuronic acid stereochemistry. *Int J Mass Spectrom* **2012,** *330-332*, 152-159.

(34) Leach, F. E.; Ly, M.; Laremore, T. N.; Wolff, J. J.; Perlow, J.; Linhardt, R. J.; Amster, I. J., Hexuronic Acid Stereochemistry Determination in Chondroitin Sulfate Glycosaminoglycan Oligosaccharides by Electron Detachment Dissociation. *J Am Soc Mass Spectr* **2012,** *23*, 1488-1497.

(35) Leach, F. E.; Xiao, Z.; Laremore, T. N.; Linhardt, R. J.; Amster, I. J., Electron detachment dissociation and infrared multiphoton dissociation of heparin tetrasaccharides. *Int J Mass Spectrom* **2011,** *308*, 253-259.

(36) Leach, F. E.; Riley, N. M.; Westphall, M. S.; Coon, J. J.; Amster, I. J., Negative Electron Transfer Dissociation Sequencing of Increasingly Sulfated Glycosaminoglycan Oligosaccharides on an Orbitrap Mass Spectrometer. *J Am Soc Mass Spectr* **2017,** *28*, 1844-1854.

(37) Wolff, J. J.; Amster, I. J.; Chi, L.; Linhardt, R. J., Electron detachment dissociation of glycosaminoglycan tetrasaccharides. *J Am Soc Mass Spectrom* **2007,** *18*, 234-44.

(38) Agyekum, I.; Patel, A. B.; Zong, C.; Boons, G.-J.; Amster, I. J., Assignment of hexuronic acid stereochemistry in synthetic heparan sulfate tetrasaccharides with 2-O-sulfo uronic acids using electron detachment dissociation. *Int J Mass Spectrom* **2015,** *390*, 163-169.

(39) Agyekum, I.; Zong, C.; Boons, G.-J.; Amster, I. J., Single Stage Tandem Mass Spectrometry Assignment of the C-5 Uronic Acid Stereochemistry in Heparan Sulfate Tetrasaccharides using Electron Detachment Dissociation. *J Am Soc Mass Spectr* **2017,** *28*, 1741-1750.

(40) Oh, H. B.; Leach, F. E.; Arungundram, S.; Al-Mafraji, K.; Venot, A.; Boons, G.-J.; Amster, I. J., Multivariate Analysis of Electron Detachment Dissociation and Infrared Multiphoton Dissociation Mass Spectra of Heparan Sulfate Tetrasaccharides Differing Only in Hexuronic acid Stereochemistry. *J Am Soc Mass Spectr* **2011,** *22*, 582-590.

(41) Zaia, J.; McClellan, J. E.; Costello, C. E., Tandem Mass Spectrometric Determination of the 4S/6S Sulfation Sequence in Chondroitin Sulfate Oligosaccharides. *Anal Chem* **2001,** *73*, 6030-6039.

(42) Kailemia, M. J.; Patel, A. B.; Johnson, D. T.; Li, L.; Linhardt, R. J.; Amster, I. J., Differentiating chondroitin sulfate glycosaminoglycans using collision-induced dissociation; uronic acid cross-ring diagnostic fragments in a single stage of tandem mass spectrometry. *Eur J Mass Spectrom* **2015,** *21*, 275-85.

(43) Zaia, J.; Li, X.-Q.; Chan, S.-Y.; Costello, C. E., Tandem mass spectrometric strategies for determination of sulfation positions and uronic acid epimerization in chondroitin sulfate oligosaccharides. *J Am Soc Mass Spectr* **2003,** *14*, 1270-1281.

(44) Gorshkov, M. V.; Tolic, P.; Tolić, L. P.; Udseth, H. R.; Anderson, G. A.; Huang, B. M.; Bruce, J. E.; Prior, D. C.; Hofstadler, S. A.; Tang, L., Electrospray ionization—Fourier transform ion cyclotron resonance mass spectrometry at 11.5 tesla: Instrument design and initial results. *J Am Soc Mass Spectr* **1998,** *9*, 692-700.

(45) Kaplan, D. A.; Hartmer, R.; Speir, J. P.; Stoermer, C.; Gumerov, D.; Easterling, M. L.; Brekenfeld, A.; Kim, T.; Laukien, F.; Park, M. A., Electron transfer dissociation in the hexapole collision cell of a hybrid quadrupole-hexapole Fourier transform ion cyclotron resonance mass spectrometer. *Rapid Commun Mass Spectrom* **2008,** *22*, 271-278.

(46) Ceroni, A.; Maass, K.; Geyer, H.; Geyer, R.; Dell, A.; Haslam, S. M., GlycoWorkbench: a tool for the computer-assisted annotation of mass spectra of glycans. *J Proteome Res* **2008,** *7*, 1650-1659.

(47) Duan, J.; Jonathan Amster, I., An Automated, High-Throughput Method for Interpreting the Tandem Mass Spectra of Glycosaminoglycans. *J Am Soc Mass Spectr* **2018,** *29*, 1802-1811.

(48) Duan, J.; Pepi, L.; Amster, I. J., A Scoring Algorithm for the Automated Analysis of Glycosaminoglycan MS/MS Data. *J Am Soc Mass Spectr* **2019,** *30*, 2692-3703.

(49) Domon, B.; Costello, C. E., A systematic nomenclature for carbohydrate fragmentations in FAB-MS/MS spectra of glycoconjugates. *Glycoconjugate J* **1988,** *5*, 397-409.

(50) Wolff, J. J.; Laremore, T. N.; Busch, A. M.; Linhardt, R. J.; Amster, I. J., Influence of charge state and sodium cationization on the electron detachment dissociation and infrared multiphoton dissociation of glycosaminoglycan oligosaccharides. *J Am Soc Mass Spectrom* **2008,** *19*, 790-8.

(51) Kailemia, M. J.; Li, L.; Xu, Y.; Liu, J.; Linhardt, R. J.; Amster, I. J., Structurally Informative Tandem Mass Spectrometry of Highly Sulfated Natural and Chemoenzymatically Synthesized Heparin and Heparan Sulfate Glycosaminoglycans. *Mol Cell Proteomics* **2013,** *12*, 979-990.

(52) Wolff, J. J.; Laremore, T. N.; Busch, A. M.; Linhardt, R. J.; Amster, I. J., Electron detachment dissociation of dermatan sulfate oligosaccharides. *J Am Soc Mass Spectr* **2008,** *19*, 294-304.

(53) Wolff, J. J.; Chi, L.; Linhardt, R. J.; Amster, I. J., Distinguishing glucuronic from iduronic acid in glycosaminoglycan tetrasaccharides by using electron detachment dissociation. *Anal Chem* **2007,** *79*, 2015-2022.

(54) Chi, L.; Wolff, J. J.; Laremore, T. N.; Restaino, O. F.; Xie, J.; Schiraldi, C.; Toida, T.; Amster, I. J.; Linhardt, R. J., Structural analysis of bikunin glycosaminoglycan. *J Am Chem Soc* **2008,** *130*, 2617-2625.

(55) Stickney, M.; Sanderson, P.; Leach, F. E.; Zhang, F. M.; Linhardt, R. J.; Amster, I. J., Online capillary zone electrophoresis negative electron transfer dissociation tandem mass spectrometry of glycosaminoglycan mixtures. *Int J Mass Spectrom* **2019,** *445*.

(56) Cotham, V. C.; Brodbelt, J. S., Characterization of therapeutic monoclonal antibodies at the subunit-level using middle-down 193 nm ultraviolet photodissociation. *Anal Chem* **2016,** *88*, 4004-4013.

(57) Ko, B. J.; Brodbelt, J. S., 193 nm ultraviolet photodissociation of deprotonated sialylated oligosaccharides. *Anal Chem* **2011,** *83*, 8192-8200.

(58) Robinson, M. R.; Moore, K. L.; Brodbelt, J. S., Direct identification of tyrosine sulfation by using ultraviolet photodissociation mass spectrometry. *J Am Soc Mass Spectr* **2014,** *25*, 1461-1471.

(59) Brodie, N. I.; Huguet, R.; Zhang, T.; Viner, R.; Zabrouskov, V.; Pan, J.; Petrotchenko, E. V.; Borchers, C. H., Top-down hydrogen–deuterium exchange analysis of protein structures using ultraviolet photodissociation. *Anal Chem* **2018,** *90*, 3079-3082.

(60) Fornelli, L.; Srzentić, K.; Huguet, R.; Mullen, C.; Sharma, S.; Zabrouskov, V.; Fellers, R. T.; Durbin, K. R.; Compton, P. D.; Kelleher, N. L., Accurate sequence analysis of a monoclonal antibody by top-down and middle-down orbitrap mass spectrometry applying multiple ion activation techniques. *Anal Chem* **2018,** *90*, 8421-8429.

CHAPTER 5

Advances in Negative Electron Transfer Dissociation for the Structural Characterization of Glycosaminoglycans using FTICR MS

Pepi, L. E., & Amster, I. J., To be submitted to *J Am. Soc. Mass Spectrom.*

Abstract

Glycosaminoglycan (GAG) carbohydrates have been a challenging target for the analytical community. Their acidic nature and high level of heterogeneity require powerful activation methods for determining sequence information. Electron detachment dissociation (EDD) has previously provided the largest level of structural information compared to other ion activation techniques. Aside from being restricted to Fourier transform ion cyclotron resonance mass spectrometers (FTICR MS), EDD has low convergence efficiency and long experiment times. More recently, negative electron transfer dissociation (NETD) has been used as an alternative to EDD, as it can be implemented in different mass analyzers and is a more efficient activation method. Previous work utilizing NETD on a FTICR MS for GAG sequencing required an average of 1 s reaction times. Here, we examine the efficiency of NETD compared to collision induced dissociation (CID) and EDD, while also optimizing the experimental parameters imperative for fragmentation efficiency. Reaction times for FTICR MS/MS NETD were shortened compared to previous data. The heparin-like synthetic GAG, Fondaparinux Sodium, was the focus of this study due to its many possible sites of ionization. Different charge-state and sodiated states were investigated to determine if lower charge-states with higher numbers of Na-H exchange fragment differently than higher charge-states with lower numbers of Na-H exchanges. Highly ionized precursors, independent of charge-state, were able to fully sequence Fondaparinux Sodium. Additionally, higher reagent accumulation times resulted in a large abundance of unassignable fragment peaks; however, the number of unassigned fragment ions did not affect the sequence coverage. Herein we have further optimized the experimental parameters of NETD on an FTICR instrument from previous data.

Introduction

Sulfated glycosaminoglycan (GAG) carbohydrates are linear polysaccharides, often covalently bound to a proteoglycan protein core. GAGs have a non-template, enzymatically driven biosynthesis which leads to varying degrees of polymerization, sulfate half-ester modifications and hexuronic acid stereochemistry.[1-2] Using mass spectrometry (MS) ion activation techniques, modifications can be determined and located. This allows for patterns significant for protein binding to be determined.[3-5] GAG-protein binding can influence biological processes such as wound healing, tumor growth and inflammation.[6-7] Structural characterization of GAGs has been a persistent challenge for the analytical community.[8-9] Advances in ion activation techniques have allowed for the GAG community to gain a better understanding of structure and function.

The acidic nature of GAGs, due to their sulfate and carboxyl groups, makes them ionizable in negative mode MS by electrospray ionization (ESI). Accurate mass measurement of GAGs, typically performed on a Fourier transform mass spectrometer (FTMS) instrument due to their high resolution, can determine the degrees of polymerization (dp), extent of sulfation and N-acetylation.[3] However mass measurement does not give positional information of modifications. To determine this type of structural information, tandem mass spectrometry (MS/MS) has been utilized.[10-13] Multiple MS/MS approaches such as electron-based and threshold based methods have been utilized in conjugation with computational and statistical approaches.[14-17] More recently ion-ion activation techniques such as negative electron transfer dissociation (NETD) has been utilized for the structural analysis of GAGs.[2, 18-20]

Due to its high mass accuracy and resolution, Fourier transform ion cyclotron resonance mass spectrometry (FTICR MS) is a powerful platform for GAG structural characterization.[21-23]

The Bruker solariX XR FTICR MS has the capability to perform three negative mode ESI MS/MS techniques. The first of which is collision induced dissociation (CID), which is a common approach for ion activation due to its accessibility. CID uses a collision gas, typically A, that collides with accelerated molecular ions resulting in a conversion of energy from kinetic to internal, leading to bond breakage.[24] CID is a vibrational excitation technique, resulting in the weakest bonds easily breaking. This results in high degrees of sulfate decomposition via the loss of SO_3. The second negative mode ionization technique available on the solariX XR is electron detachment dissociation (EDD), which has only been performed on FTICR MS, as it occurs in the analyzer cell. EDD irradiates a multiply charged negative ion with electrons of a moderate kinetic energy (15-20eV), causing electron detachment, leading to fragmentation.[3-4, 25-26] EDD is a powerful technique for GAG analysis, however it has low efficiency at converting precursor ions to fragment ions. This requires more signal averaging and longer experiment times. The final negative mode ionization activation technique available on the solariX XR is NETD. NETD uses electron transfer from an electron source, typically fluoranthene, to induce fragmentation in a similar manner to EDD.[2, 18-19] NETD yields informative fragment ions for locating GAG modifications and is more efficient at converting precursor ions to fragment ions than EDD. CID requires a fully ionized precursor to achieve informative fragmentation; this can be done by either deprotonation and/or hydrogen/sodium ion exchange which stabilizes sulfates from decomposition.[24] EDD and NETD both produce informative fragmentation without requiring fully ionized precursors, however EDD experiments are known for their long reaction times (greater than 0.5 s).[2, 27-28] NETD has been shown to take 10-50ms on an Orbitrap MS, giving it a liquid chromatography timescale.[2]

NETD has been demonstrated to work well for the structural analysis of GAG samples on an Orbitrap MS and FTICR MS. Past work showed the ability of an Orbitrap MS to use NETD to identify sulfate positions of GAG samples of varying sulfation and polymerization.[2] NETD of GAGs on an FTICR MS has been previously demonstrated, with more recent advancements improving NETD efficiency and generating informative fragments without complete deprotonation.[18, 29] The experimental parameters for EDD fragmentation efficiency have been examined and reported previously.[27, 30] However, a comparative analysis of the experimental parameters of NETD has yet to be reported. In this work, we revisit the use of NETD on an FTICR MS and compare the capabilities of CID, EDD and NETD on a Bruker solariX XR MS. The experimental parameters of NETD, including reagent accumulation and ionization state, are examined to determine the ideal parameters for increasing fragmentation efficiency for GAG standards.

Experimental Methods:

Materials

Fondaparinux Sodium was purchased from Fisher Scientific (Hampton, NH, USA).

Synthetic heparan sulfate oligosaccharide preparation

Heparan sulfate hexasaccharides were synthesized using a modular approach and purified using silica gel column chromatography.[31] Structures were confirmed by ^{1}H nuclear magnetic resonance (NMR) and accurate mass measurement by LC-MS. Structures were prepared as hexasaccharides with varying degrees of sulfation and hexuronic acid stereochemistry.

Chondroitin sulfate oligosaccharide preparation

Dermatan sulfate (DS) tetrasaccharide weas prepared by partial enzymatic depolymerization of porcine intestinal mucosa dermatan sulfate (Celsus Laboratories). A full description of the enzymatic depolymerization and desulfation has been previously outlined.[32-33]

Mass Spectrometry Analysis

Experiments were performed using a 9.4-T Bruker solariX XR ESI FTMS (Berman, Germany) in negative ionization mode. Each compound was dissolved in 50:50 MeOH:H_2O to a concentration of 0.1 mg/mL and ionized using nanoelectrospray at a rate of 10 µL/h (Econo12-N; New Objective, Woburn, MA). Each experiment was repeated a minimum of three times with similar results for each compound examined. Synthetic HS compounds and Fondaparinux Sodium were desalted with a 3 kDa Amicon Ultra centrifugal filter (Millipore, Temecula, CA, USA) prior to direct injection and analysis.[34] Filters are conditioned with HPLC grade water first, and the sample was then washed with 3-10 filter volumes of water (17,000 x g for 30 min each). 0.1% diethyl amine was added to Fondaparinux Sodium sample solution as needed to decrease sodiation.

Multiply deprotonated precursor anions were observed for each compound, representing a range of charge states and Na-H exchange for all tandem mass spectrometry experiments. Precursor ions were mass selected in the quadrupole and acquired at a mass resolution of 2 M for 0.5-1 s. An external calibration was performed using NaTFA clusters, resulting in a mass accuracy of 10ppm or better. Internal calibration was performed using confidently assigned glycosidic bond cleavages as calibrants. Fragment ions were assigned manually, using Glycoworkbench version 2.0 and an in-house software.[35-37] Product ions are reported based on

the Domon-Costello nomenclature [38] with graphical depictions based on a modification developed by Wolff-Amster.[28] Figure D.1 illustrates the cartoon glycan nomenclature used.

NETD experiments were performed using a 50-1400 ms reagent accumulation time and a 50 ms reaction time. Fluoranthene cation radicals were generated in the presence of Ar in the chemical ionization (CI) source. Experiments were performed in serial mode, averaging 1 scan, and presented spectra are the result of 3-5 mins of spectral averaging. Collision cell and NETD parameters were optimized for each precursor and sample to minimize sulfate loss while improving precursor isolation. EDD experiments were performed using a hollow cathode which serves as the source of electrons for EDD. Mass selected ions were irradiated with 19 eV electrons for 1 s. The extraction lens was set to 17.5 ± 0.5 V with the cathode heater set to 1.5 A. 48 signal acquisitions were averaged per EDD spectrum. CID experiments were performed in the collision cell external to the high-magnetic-field region. A collision voltage of 5-8.5 V was used, and 24 signal acquisitions were averaged per CID spectrum.

Results and discussion

Negative electron transfer dissociation (NETD) has previously been utilized for the characterization of GAG standards using FTMS and ion-trap MS instruments in our laboratory.[2, 18-19, 29] Previous work using a quadrupole ion trap mass spectrometer was limited by the resolving power, hindering the ability to analyze highly sulfated GAGs and longer chain lengths than tetrasaccharides.[19] NETD was then examined on a FTICR MS, which increased the resolving power, however was still limited by long reaction times (500-1000 ms), making coupling to on-line separations difficult.[18] Finally, NETD was performed on a hybrid Orbitrap FTMS instrument. These data showed an ability to fragment GAG standards with reaction times

below 100 ms, making pairing with on-line separation systems possible.[2] With advancements in FTICR MS instruments, NETD has since been optimized by Huang *et al.* for minimizing reaction times.[29] For these experiments, a 500 ms reaction time and 500 ms reagent time were typically used. Here, we use a Bruker FTICR solariX XR instrument to further examine the efficiency of NETD at sequencing GAG standards. NETD is compared to CID and EDD performed on the same instrument, and optimal reagent accumulation and reaction times are determined for various ionization states.

CID/EDD/NETD comparison of HS and DS Glycosaminoglycans

CID, EDD and NETD annotated spectra of the $[M-6H]^{6-}$ precursor ion (*m/z* 264.6831) of synthetic HS GlcA-GlcNS6S-GlcA-GlcNS6S-IdoA-GlcNS6S-$(CH_2)_5NH_2$ are shown in Figure D.2. Previous data has illustrated the ideal precursor for CID analysis of GAGs has all ionizable sites ionized by either deprotonation or Na-H exchange. Precursors that are not fully ionized are expected to produce minimal informative fragmentation and a high degree of sulfate decomposition by SO_3 loss.[24] Figure 5.1A displays the fragment map of CID ionization of HS hexasaccharide. The donut plots in Figure 5.1 outlines the intensity distribution of glycosidic fragments (blue), cross-ring fragments (orange), glycosidic fragments with SO_3 loss (gray) and cross-ring fragments with SO_3 loss (yellow). The donut plot in Figure 5.1A shows that majority of the fragment intensity produced by CID is glycosidic cleavages, both without (69%) and with SO_3 loss (31%). EDD of the same precursor ion (Figure 5.1B) produced a higher intensity of cross-ring cleavages than CID (9% vs 0%), however the overall same amount of SO_3 loss (31% total for glycosidic and cross-ring SO_3 loss). Additionally, both CID and EDD were able to locate one of the six total sulfate modifications. NETD fragmentation produced a much higher

intensity of cross-ring cleavages (26%) than both EDD and CID, and a lower percentage of SO_3 loss (20% total). NETD also produced the cross-ring fragment ions needed to locate three of the six sulfate modifications (Figure 5.1C). Previous data illustrates that the ideal precursor ion for EDD has one more ionized site than the number of sulfate modifications.[28] This level of ionization limits the amount of sulfate decomposition while also increasing the number of informative fragments. The HS hexasaccharide sample investigated here has 9 total ionizable sites (6 sulfate modifications and 3 carboxyl groups), meaning the ideal precursor ion for EDD of this sample would have 7 ionized sites. Even though this precursor ion is not ideal for EDD, it still displayed the ability for NETD to produce more cross-ring and informative fragment ions than both CID and EDD while also minimizing the amount of sulfate decomposition.

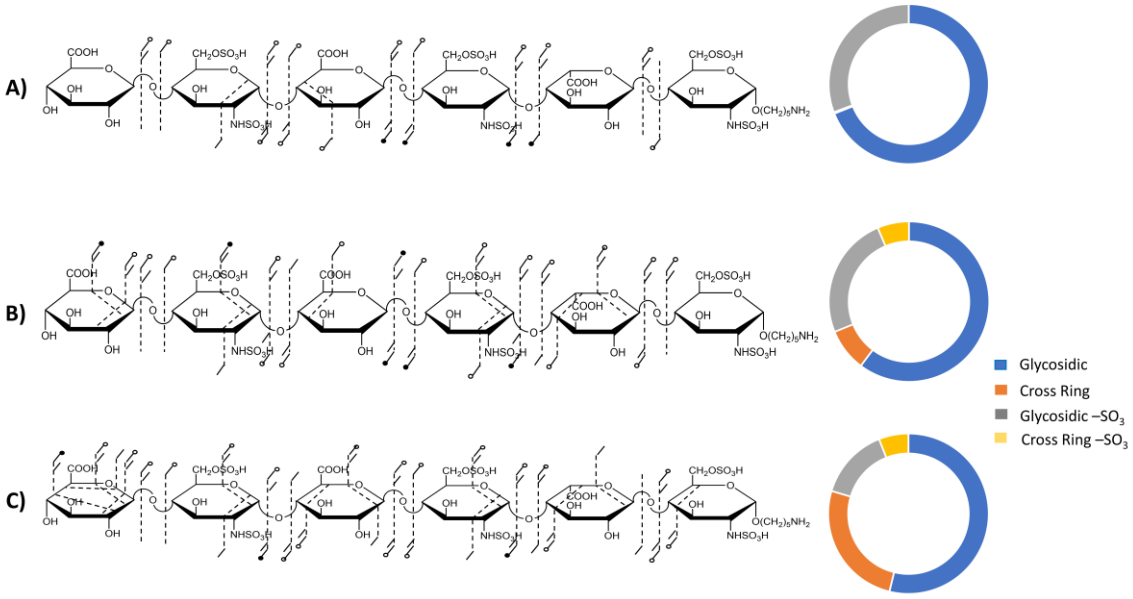

Figure 5.1. Fragment maps and donut plots for A) CID, B) EDD, and C) NETD of the $[M-6H]^{6-}$ precursor ion of GlcA-GlcNS6S-GlcA-GlcNS6S-IdoA-GlcNS6S-$(CH_2)_5NH_2$. Donut plots represent the intensity distribution of glycosidic cleavages (blue), cross-ring cleavages (orange), glycosidic cleavage with SO_3 loss (grey) and cross-ring cleavages with SO_3 loss (yellow).

CID, EDD and NETD spectra of the $[M-4H+Na]^{3-}$ precursor ion (*m/z* 312.3656) of dermatan sulfate tetrasaccharide ΔUA-GalNAc4S-IdoA-GalNAc4S-OH are shown in Figure D.3. DS tetrasaccharide has four ionizable sites (2 sulfate modifications and 2 carboxyl groups). CID had minimal sulfate decomposition and produced 95% intensity from glycosidic fragment ions and 5% intensity from cross-ring fragment ions (Figure 5.2A). EDD and NETD produced similar intensity from cross-ring fragments (17% and 23% respectively). NETD produced a $^{1,4}A_2$ fragment ion which can locate one of the sulfate modifications (Figure 5.2C). Past work

investigating fragmentation of CS/DS GAGs has shown that majority of cross-ring fragments occur on the uronic acids, which for DS does not contain sulfate modifications. The proposed mechanism states that the radical site forms on the uronic acid carboxylate instead of the sulfate modification.[5, 11, 39] Additionally, the change in linkage from β-1,4 in HS standards to β-1,3 in CS/DS standards appears to be a major factor in the differences in fragmentation between the two GAG subclasses. This is seen here with all three activation methods, where majority of cross-ring fragments occur on the IdoA residue. Though cross-ring fragment ions mainly occur on the IdoA residue, glycosidic fragment ions produced from all three activation methods allows for the determination that there is 1 sulfate modification on each amino sugar residue.

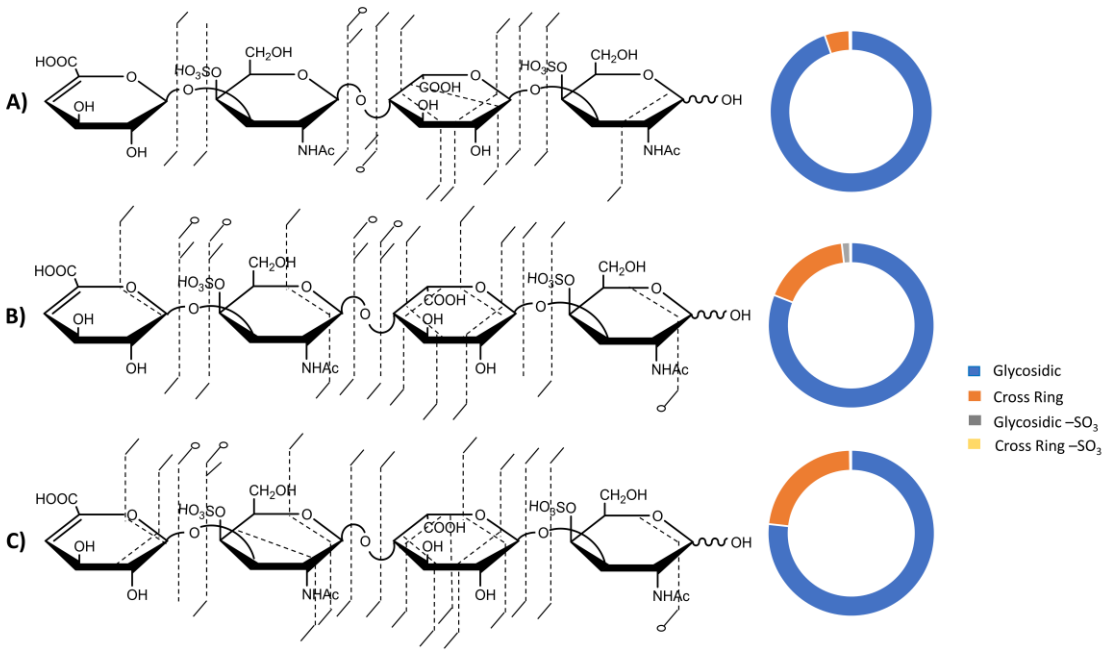

Figure 5.2. Fragment maps and donut plots for A) CID, B) EDD, and C) NETD of the $[M4H+Na]^{4-}$ precursor ion of ΔHexUA-GalNAc4S-IdoA-GalNAc4S-OH. Donut plots represent the intensity distribution of glycosidic cleavages (blue), cross-ring cleavages (orange), glycosidic cleavage with SO_3 loss (grey) and cross-ring cleavages with SO_3 loss (yellow).

NETD Parameter Optimization for Fragmentation Efficiency

The main parameters for optimizing NETD are reagent accumulation and reaction time. To determine how these parameters effect fragmentation efficiency, one was held constant while the other was increased in increments of 50 ms. When holding the reagent accumulation parameter constant at 50 ms and increasing the reaction time, no difference in fragmentation was seen (Figure D.4). However, when holding the reaction time constant at 50 ms and increasing the reagent accumulation time an increase in fragmentation was seen. This includes both the number

of fragments and the intensity of fragment ions. To determine how ionization state effects fragmentation, various precursor ions of Fondaparinux Sodium were investigated. Various sodiated states of three different charge states were tested to determine not only how ionization state effects fragmentation, but also how charge state effects fragmentation. Annotated spectra for the fully ionized precursor of the 4-charge state $[M-10H+6Na]^{4-}$ (*m/z* 408.7035) produced the necessary fragment ions to locate all 8 sulfate modifications when using a reagent accumulation time of 800 ms. This reagent accumulation time was determined to produce the most informative fragment ions for this precursor ion and is compared to 50 ms in Figure 5.3. NETD with a reagent accumulation time of 800 ms produced $^{0,2}A_5$ and $^{2,4}A_5$ fragment ions which locate the 2 sulfate modifications on the reducing end amino sugar as being at the 6-*O* and *N*-positions. Z_2 and B_4 fragment ions can locate the third sulfate modification on the iduronic acid residue. The biosynthesis of GAGs restricts sulfate modifications in uronic acid to the 2-*O* position.[40] Y_3 and C_3 fragment ions can locate 3 sulfate modifications at the central amino sugar. Since there are only 3 possible locations the sulfate modifications can be, cross-ring cleavages are not necessary for determining their location. Finally, $^{1,5}X_4$ and $^{2,4}X_4$ fragment ions locate the final 2 sulfate modifications on the nonreducing end amino sugar at the 6-*O* and *N*-positions. NETD with a 50 ms reagent accumulation also produced the B_4 and Y_3 fragment ions, but none of the other fragment ions used to locate the sulfate modifications.

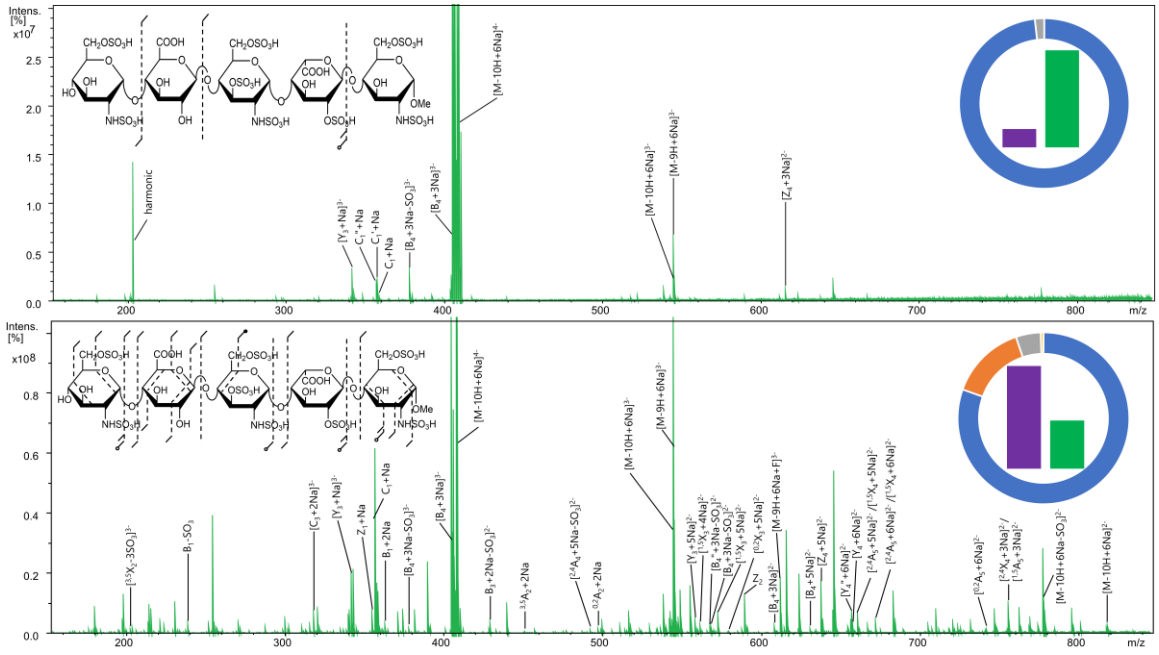

Figure 5.3. NETD spectra of the $[M-10H+6Na]^{4-}$ precursor ion of Fondaparinux Sodium with a reagent accumulation time of 50 ms (top) and 800 ms (bottom). Fragment map insets display the fragmentation distribution. Donut plots display the intensity distribution of glycosidic fragments (blue), cross-ring fragments (orange), glycosidic fragments with SO_3 loss (grey) and cross-ring fragments with SO_3 loss (yellow). Bar graphs display the intensity of assigned fragment ions (green) and unassigned fragment ions (purple).

Alternatively, the NETD of the fully ionized precursor for the 5-charge state $[M-10H+5Na]^{5-}$ (*m/z* 322.3649) with a reagent accumulation time of 800 ms was also able to locate all sulfate modifications (Figure D.5). However, this reagent accumulation time resulted in decomposition of the precursor. This could produce more internal fragments and therefore a higher percentage of unassigned fragments. The ideal reagent accumulation time for the [M-

10H+5Na]$^{5-}$ precursor ion was determined to be 350 ms. A comparison of NETD with a reagent accumulation time of 50 ms and 350 ms is shown in Figure 5.4. Like the [M-10H+6Na]$^{4-}$ precursor ion, the [M-10H+5Na]$^{5-}$ precursor ion yielded $^{1,5}X_4$ and $^{2,4}X_4$ fragment ions locate 2 sulfate modifications on the nonreducing end amino sugar at the 6-*O* and *N*-positions. The necessary glycosidic fragment ions to locate the sulfate modification on the iduronic acid (C_4 and C_3) as well as the 3 sulfate modifications on the central amino sugar (C_3 and Y_3/Z_3) were produced. Finally, $^{1,5}A_5$ and $^{2,4}A_5$ fragment ions were yielded, locating 2 sulfate modifications on the reducing end amino sugar at the 6-*O* and *N*-positions. Comparatively, the [M-10H+6Na]$^{4-}$ precursor with a reagent accumulation time of 350 ms was also able to locate the 8 sulfate modifications, however produced less fragmentation overall than the 800 ms reagent accumulation time (Figure D.6). To view the 3-charge precursor ions, 0.1% diethyl amine was added to the sample solution. Diethyl amine has been shown to remove Na ions from GAG samples and shift the charge-state of precursor ions seen to lower charge-states.[41] Due to this, we were unable to visualize the [M-10H+7Na]$^{3-}$ precursor ion.

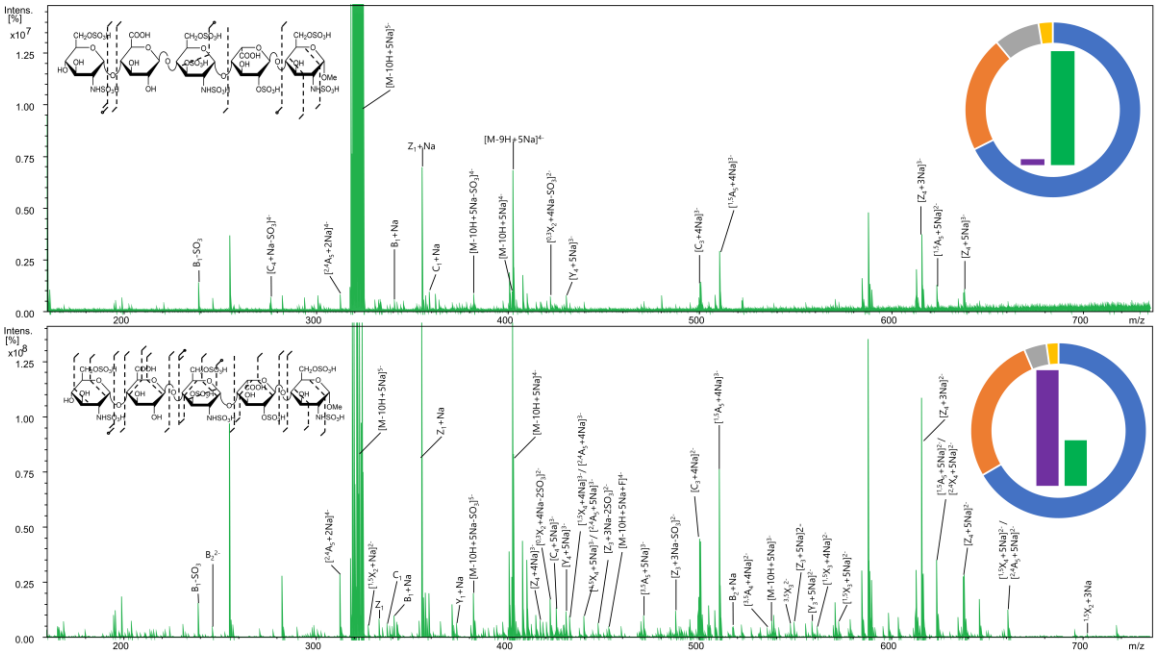

Figure 5.4. NETD spectra of the $[M\text{-}10H\text{+}5Na]^{5-}$ precursor ion of Fondaparinux Sodium with a reagent accumulation time of 50 ms (top) and 350 ms (bottom). Fragment map insets display the fragmentation distribution. Donut plots display the intensity distribution of glycosidic fragments (blue), cross-ring fragments (orange), glycosidic fragments with SO_3 loss (grey) and cross-ring fragments with SO_3 loss (yellow). Bar graphs display the intensity of assigned fragment ions (green) and unassigned fragment ions (purple).

Precursor ions where the sulfate modifications are ionized but the carboxyl groups are not were also investigated. Based on pKa, the sulfate modifications are hypothesized to be ionized when the number of ionized sites equals the number of sulfate groups. Electron transfer can occur on a carboxyl group when a proton is mobilized, resulting in a protonated sulfate group.[18] Annotated spectra of the $[M\text{-}8H\text{+}4Na]^{4-}$ precursor ion (*m/z* 397.7125) comparing a 50 ms reagent

accumulation time to a 350 ms reagent accumulation time is shown in Figure 5.5. NETD with a 350 ms reagent accumulation was able to locate 6 of the 8 sulfate modifications. Glycosidic cleavages can be used to locate the sulfate on the iduronic acid (C_4 and C_3) and the 3 sulfates on the central amino sugar (C_3 and Y_3). $^{0,2}A_5$ and $^{2,4}A_5$ cross-ring cleavages can be used to locate the 2 sulfate modifications on the reducing end amino sugar at the 6-*O* and *N*-positions. A $^{1,5}X_4$ cross-ring fragment ion and B_1/C_1 glycosidic fragment ions can determine there are 2 sulfate modifications on the nonreducing end amino sugar. These can also be used to determine that one of the sulfate modifications is at the *N*-position due to the lack of acetylation. The final sulfate modification could be located at either the 3-*O* or 6-*O* position. It is more likely that the sulfate modification is at the 6-*O* position, however the possibility it is located at the 3-*O* position cannot be dismissed.[42]

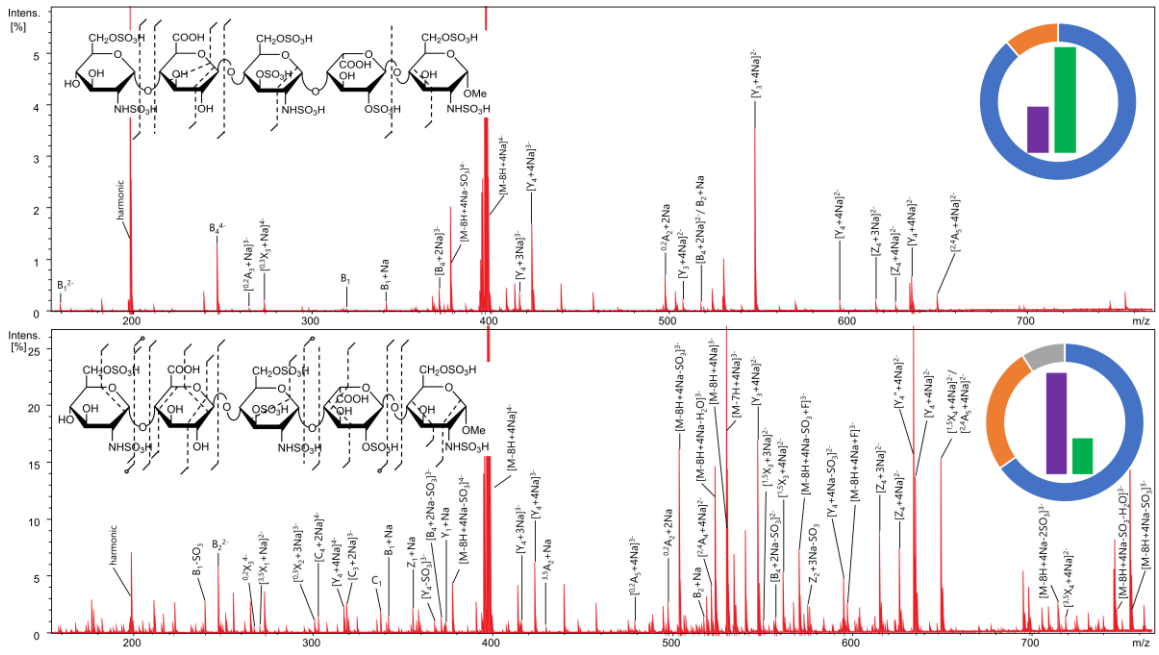

Figure 5.5. NETD spectra of the $[M-8H+4Na]^{4-}$ precursor ion of Fondaparinux Sodium with a reagent accumulation time of 50 ms (top) and 350 ms (bottom). Fragment map insets display the fragmentation distribution. Donut plots display the intensity distribution of glycosidic fragments (blue), cross-ring fragments (orange), glycosidic fragments with SO_3 loss (grey) and cross-ring fragments with SO_3 loss (yellow). Bar graphs display the intensity of assigned fragment ions (green) and unassigned fragment ions (purple).

The 5-charge precursor ion with ionized sulfate groups $[M-8H+3Na]^{5-}$ (*m/z* 313.5722) was also investigated. This precursor ion was able to locate all sulfate modifications with a reagent accumulation time of 350 ms. A comparison of NETD of the $[M-8H+3Na]^{5-}$ precursor ion with a 50 ms reagent accumulation time and a 350 ms reagent accumulation time is shown in Figure 5.6. NETD with a 350 ms reagent accumulation time yielded $^{1,5}X_4$, $^{2,4}X_4$ and $^{0,2}A_1$

fragment ions which can locate 2 sulfate modifications on the nonreducing end amino sugar. Glycosidic cleavages can be used to locate 1 sulfate modification on the iduronic acid (C_3 and C_4) and 3 sulfate modifications on the central amino sugar (C_3 and Y_3). A B_4 fragment ion can be used to determine the 2 remaining sulfate modifications are on the reducing end amino sugar. A $^{2,4}A_5$ fragment ion eliminates the 3-*O* position as a possible location for either sulfate modification, locating the sulfates at the 6-*O* and *N*-positions. The $[M-8H+5Na]^{3-}$ precursor ion (*m/z* 537.9464) was also investigated. Ideal fragmentation for this precursor ion was seen with a 950 ms reagent accumulation time. Unlike the higher charge-states, the $[M-8H+5Na]^{3-}$ precursor ion was unable to locate majority of the sulfate modifications. B_1 and $^{3,5}X_4$ fragment ions can locate 1 sulfate modification at the 6-*O* position of the nonreducing end amino sugar. The B_1 fragment ion also indicates a second sulfate modification is located on this amino sugar, however there is not enough information to distinguish between 3-*O* and *N*-positions. B_2/C_2 and Y_3 fragment ions can determine the remaining 5 sulfate modifications are on the central and reducing end amino sugars, and the iduronic acid. However, no further fragmentation was produced to determine where the sulfates are located within these three residues (Figure D.7).

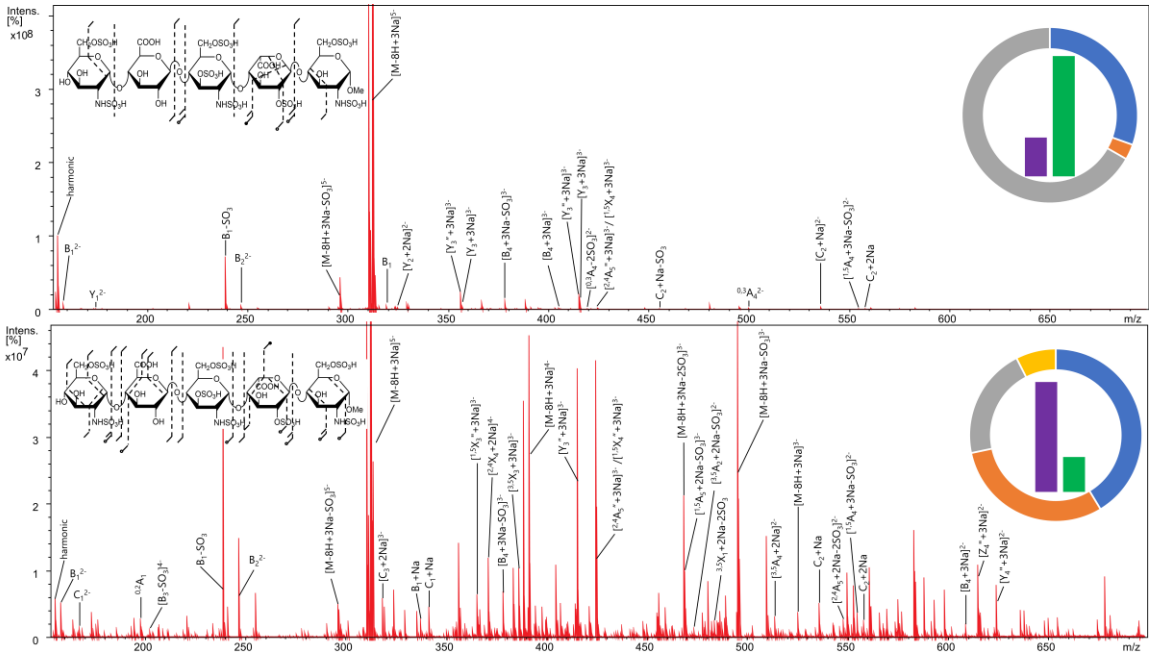

Figure 5.6. NETD spectra of the $[M-8H+3Na]^{5-}$ precursor ion of Fondaparinux Sodium with a reagent accumulation time of 50 ms (top) and 350 ms (bottom). Fragment map insets display the fragmentation distribution. Donut plots display the intensity distribution of glycosidic fragments (blue), cross-ring fragments (orange), glycosidic fragments with SO_3 loss (grey) and cross-ring fragments with SO_3 loss (yellow). Bar graphs display the intensity of assigned fragment ions (green) and unassigned fragment ions (purple).

Precursors that are known to be unideal for GAG activation were also investigated. NETD of the $[M-4H]^{4-}$ precursor ion (*m/z* 375.7306) which only has 4 of the 10 ionizable sites ionized is shown in Figure 5.7. A reagent accumulation time of 500 ms was determined to produce the best fragmentation for this precursor ion. A high percentage of fragment types produced were attributed to sulfate decomposition for both a reagent accumulation time of 50 ms

and 500 ms (46% and 56%, respectively), which agrees with past MS/MS studies of GAGs.[24, 28] However, the fragment ions produced with a 500 ms reagent accumulation time were still able to locate 6 of the 8 sulfate modifications, as shown in the fragment map inset of Figure 5.7B. The $[M-6H+Na]^{5-}$ precursor ion (*m/z* 304.7794) which has 6 of the 8 sulfate modifications ionized was also investigated. When comparing a reagent accumulation time of 50 ms to 500 ms there were minimal differences seen in the fragmentation, both in the distribution of fragments produced and the intensity of fragment ions produced (Figure D.8). Additionally, the $[M-3H]^{3-}$ precursor ion (*m/z* 501.3098) was tested. A reagent accumulation time of 1200 ms was determined to produce the most efficient fragmentation for this precursor ion. Though there was a high number of sulfate decomposition (74% for 50 ms and 21% for 1200 ms), this precursor was able to locate 6 out of 8 sulfated modifications. The 2 sulfates that could not be located are on the nonreducing end amino sugar, which had no cross-ring cleavages (Figure D.9).

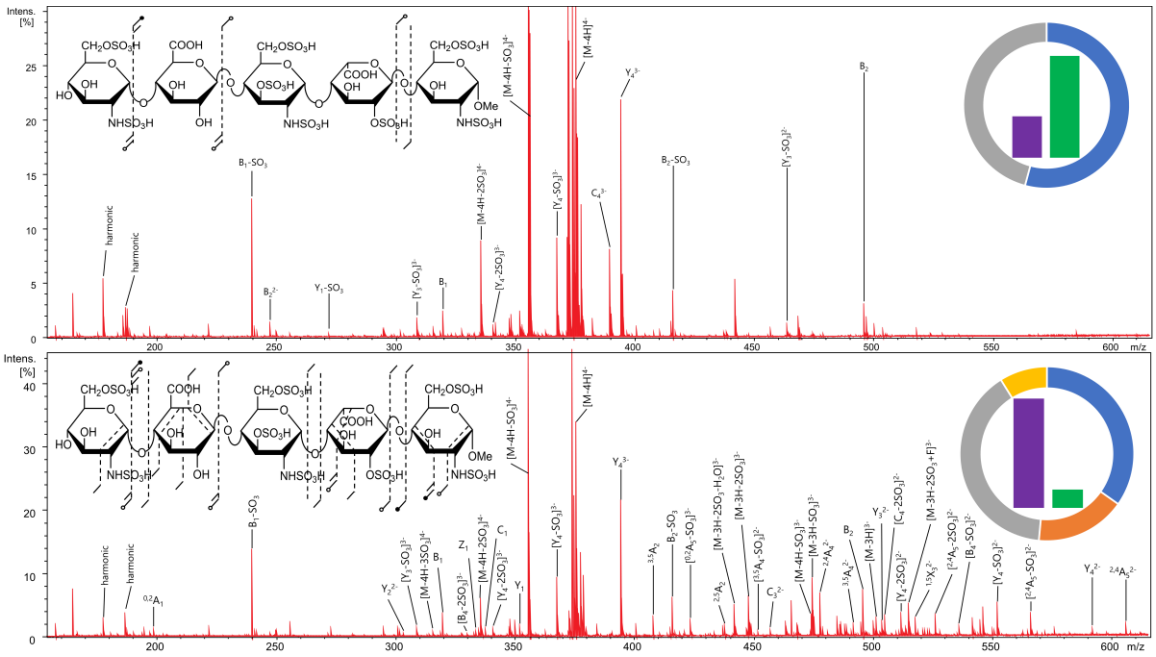

Figure 5.7. NETD spectra of the $[M-4H]^{4-}$ precursor ion of Fondaparinux Sodium with a reagent accumulation time of 50 ms (top) and 500 ms (bottom). Fragment map insets display the fragmentation distribution. Donut plots display the intensity distribution of glycosidic fragments (blue), cross-ring fragments (orange), glycosidic fragments with SO_3 loss (grey) and cross-ring fragments with SO_3 loss (yellow). Bar graphs display the intensity of assigned fragment ions (green) and unassigned fragment ions (purple).

Comparison of Assigned and Unassigned Fragment Ions

When increasing the reagent accumulation time, the precursor ion decreases in intensity as fragment ions increase in intensity. With less precursor ion, there is a higher chance of fragmenting fragments, resulting in internal fragmentation. The percentage of assigned fragment ion intensity has been compared to unassigned fragment ion intensity. Precursor ions, including

sulfate loss from the precursor, charge reduced peaks, sulfate loss from charge reduced peaks, fluoranthene adducts and harmonic peaks have been removed from the comparison. The amount of unassigned fragment ions increases as the reagent accumulation time increases. This is possibly due to an increase in internal fragment ions as the precursor ion is depleted. The bar graphs in Figure 5.3 show a comparison of assigned fragments (green) and unassigned fragments (purple) for the $[10H+6Na]^{4-}$ precursor ion. With a reagent accumulation time of 50 ms, the unassigned fragment ion intensity is about $1/5^{th}$ of the assigned fragment ion intensity. For a reagent accumulation time of 800 ms the unassigned intensity shifts to about double of the assigned fragment ion intensity. For the $[10H+5Na]^{5-}$ precursor ion the unassigned fragment ion intensity is much less than the assigned fragment ion intensity with a reagent accumulation time of 50 ms (Figure 5.4). However, with a reagent accumulation time of 350 ms the assigned intensity is just under half the unassigned intensity. The same trend was seen for the $[M-8H+4Na]^{4-}$ and $[M-8H+3Na]^{5-}$ precursor ions (Figures 5.5 and 5.6). Therefore, the amount of unassigned intensity increased with a longer reagent accumulation time. For the $[M-4H]^{4-}$ precursor ion there was no overall increase in unassigned fragment ions seen between 50 ms and 500 ms (Figure 5.7).

The intensity of assigned and unassigned fragment ions for the different reagent accumulation time points were graphed. Figure 5.8 shows these graphs for precursors of the 4- and 5-charge state with all sulfates ionized. For both precursor ions, the assigned intensity started more intense than the unassigned intensity. For the $[M-8H+4Na]^{4-}$ precursor ion this switches around 200 ms, whereas for the $[M-10H+3Na]^{5-}$ precursor ion the switch occurs at 300 ms. The same trend was seen for the fully ionized precursor ions for the 4- and 5-charge states (Figure D.10). To determine how much of the unassigned intensity corresponded to internal fragment

ions, this was also graphed. The graph in Figure D.11 compares the total assigned intensity of glycosidic ions, cross-ring ions, and SO_3 loss from both, to the total unassigned intensity (all fragment peaks that do not fall in these categories) and to unassigned intensity excluding uninformative, assignable fragments including internal fragments and neutral losses (H, 2H, H_2O, CO_2, etc.). Majority of the remaining unassigned intensity is shown to be neutral losses from fragment ions (excluding SO_3 loss), such as H loss and CO_2 loss and internal fragments. Neutral losses are expected in NETD spectra, as they occur with radical formation.

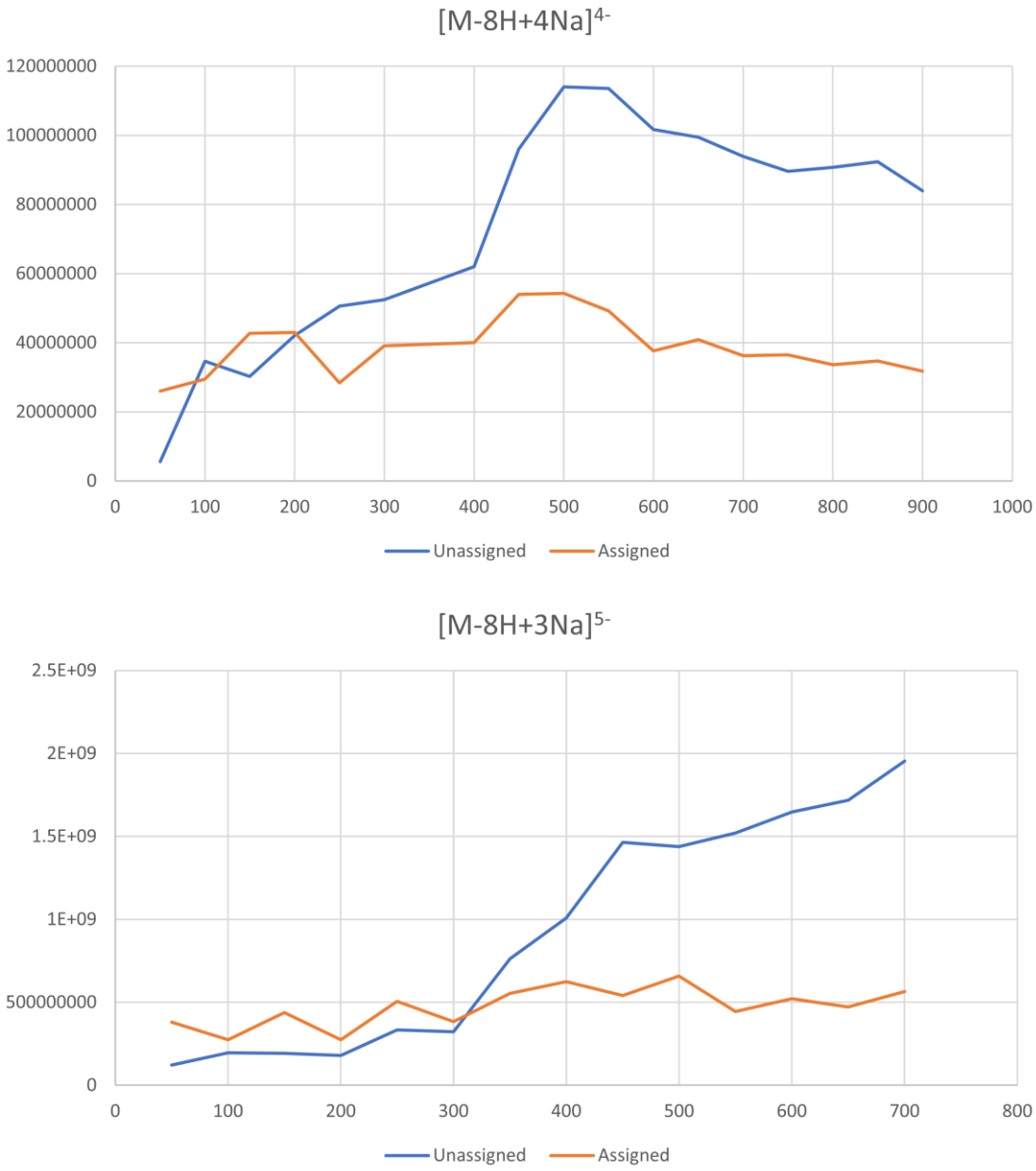

Figure 5.8. Comparison of unassigned fragment ion intensity (blue) and assigned fragment ion intensity (orange) produced from NETD of sulfate ionized precursors, with 8 H exchanges at different reagent accumulation times (X-axis).

Conclusions

Ion activation methods for sequencing sulfated GAGs have been advancing over the past few decades. Collision induced dissociation (CID) is a widely available MS/MS technique that yields high abundances of glycosidic fragment ions. Glycosidic ions can determine which sugar residue contains modifications; however, the exact location of modifications can only be determined with cross-ring cleavages. Electron detachment dissociation (EDD) has been utilized extensively and results in cross-ring cleavages, which locate sulfate modifications. Though powerful, EDD has a low conversion efficiency and long ion activation periods. Negative electron transfer dissociation (NETD) is an ion-ion reaction that produces high abundances of cross-ring cleavages. Unlike EDD, NETD parameters can be optimized to fit on-line separation timeframes. Herein, the timeframe of NETD on an FTICR MS has been optimized further than what was previously reported.[18, 29] The reaction time was determined to be independent of efficient fragmentation, whereas the reagent accumulation time was determined to be directly related. The exact reagent accumulation time needed to produce efficient fragmentation depended on ionization state and charge-state of the precursor ion. Precursor ions with lower charge-states required a longer reagent accumulation time than those with higher charge-states. Additionally, fully ionized precursor ions and precursor ions with only sulfate modifications ionized were able to locate all sulfate modifications, independent of charge-state. Ionization states without all sulfates ionized were also able to locate majority of the modifications, outperforming both CID and EDD.

With longer reagent accumulation times the number and intensity of unassigned fragment ions also increased. A large portion of this intensity can be attributed to internal fragmentation. The remaining intensity is due to neutral losses such as H loss and CO_2 loss from fragment ions.

Though the number of unassigned fragment ions increases with longer reagent accumulation, so does the extent of informative fragmentation. NETD has the fragmentation efficiency advantages of EDD, yielding a diminished extent of sulfate loss and an increase in cross-ring cleavages compared to CID. NETD can also be coupled to a multitude of mass spectrometers, including ion-trap instruments, Orbitrap instruments and FTICR instruments. The ability to couple NETD with high resolution FTMS systems makes it advantageous for GAG characterization.

Acknowledgments

LEP and IJA gratefully acknowledge financial support from the National Institutes of Health, P41GM103390 and U01CA231074. The authors would like to acknowledge Geert- Jan Boons (Complex Carbohydrate Research Center, University of Georgia) for providing synthetic heparan sulfate samples that were utilized during this study, as well as Robert Linhardt and Fuming Zhang (Rensselaer Polytechnic Institute) for providing DS samples that were utilized during this study.

References

(1) Ernst, S.; Langer, R.; Cooney, C. L.; Sasisekharan, R., Enzymatic Degradation of GlycosaminogIycans. *Critical Reviews in Biochemistry and Molecular Biology* **1995,** *30*, 387-444.

(2) Leach, F. E.; Riley, N. M.; Westphall, M. S.; Coon, J. J.; Amster, I. J., Negative Electron Transfer Dissociation Sequencing of Increasingly Sulfated Glycosaminoglycan Oligosaccharides on an Orbitrap Mass Spectrometer. *Journal of The American Society for Mass Spectrometry* **2017,** *28*, 1844-1854.

(3) Wolff, J. J.; Amster, I. J.; Chi, L.; Linhardt, R. J., Electron detachment dissociation of glycosaminoglycan tetrasaccharides. *J Am Soc Mass Spectrom* **2007,** *18*, 234-44.

(4) Leach, F. E.; Xiao, Z.; Laremore, T. N.; Linhardt, R. J.; Amster, I. J., Electron detachment dissociation and infrared multiphoton dissociation of heparin tetrasaccharides. *International Journal of Mass Spectrometry* **2011,** *308*, 253-259.

(5) Klein, D.; Leach, F. I.; Amster, I.; Brodbelt, J., Structural Characterization of Glycosaminoglycan Carbohydrates using Ultraviolet Photodissociation. *Analytical chemistry* **2019,** *19*, 6019-6026.

(6) Fannon, M.; Forsten, K. E.; Nugent, M. A., Potentiation and Inhibition of bFGF Binding by Heparin: A Model for Regulation of Cellular Response. *Biochemistry* **2000,** *39*, 1434-1445.

(7) Linhardt, R. J.; Toida, T., Role of Glycosaminoglycans in Cellular Communication. *Accounts of Chemical Research* **2004,** *37*, 431-438.

(8) Zaia, J., Glycosaminoglycan glycomics using mass spectrometry. *Mol Cell Proteomics* **2013,** *12*, 885-892.

(9) Zaia, J., Mass spectrometry and the emerging field of glycomics. *Chem Biol* **2008,** *15*, 881-892.

(10) Miller, M. J. C.; Costello, C. E.; Malmström, A.; Zaia, J., A tandem mass spectrometric approach to determination of chondroitin/dermatan sulfate oligosaccharide glycoforms. *Glycobiology* **2006,** *16*, 502-513.

(11) Wolff, J. J.; Laremore, T. N.; Busch, A. M.; Linhardt, R. J.; Amster, I. J., Electron detachment dissociation of dermatan sulfate oligosaccharides. *J Am Soc Mass Spectrom* **2008,** *19*, 294-304.

(12) Wolff, J. J.; Laremore, T. N.; Aslam, H.; Linhardt, R. J.; Amster, I. J., Electron-induced dissociation of glycosaminoglycan tetrasaccharides. *J Am Soc Mass Spectrom* **2008,** *19*, 1449-1458.

(13) Agyekum, I.; Pepi, L.; Yu, Y.; Li, J.; Yan, L.; Linhardt, R. J.; Chen, S.; Amster, I. J., Structural elucidation of fucosylated chondroitin sulfates from sea cucumber using FTICR-MS/MS. *European Journal of Mass Spectrometry* **2017,** *24*, 157-167.

(14) Duan, J.; Pepi, L.; Amster, I. J., A Scoring Algorithm for the Automated Analysis of Glycosaminoglycan MS/MS Data. *Journal of The American Society for Mass Spectrometry* **2019**.

(15) Oh, H. B.; Leach, F. E.; Arungundram, S.; Al-Mafraji, K.; Venot, A.; Boons, G.-J.; Amster, I. J., Multivariate Analysis of Electron Detachment Dissociation and Infrared Multiphoton Dissociation Mass Spectra of Heparan Sulfate Tetrasaccharides Differing Only in Hexuronic acid Stereochemistry. *Journal of The American Society for Mass Spectrometry* **2011,** *22*, 582-590.

(16) Leach, F. E.; Arungundram, S.; Al-Mafraji, K.; Venot, A.; Boons, G.-J.; Amster, I. J., Electron detachment dissociation of synthetic heparan sulfate glycosaminoglycan tetrasaccharides varying in degree of sulfation and hexuronic acid stereochemistry. *International Journal of Mass Spectrometry* **2012,** *330-332*, 152-159.

(17) Agyekum, I.; Zong, C.; Boons, G.-J.; Amster, I. J., Single Stage Tandem Mass Spectrometry Assignment of the C-5 Uronic Acid Stereochemistry in Heparan Sulfate Tetrasaccharides using Electron Detachment Dissociation. *Journal of The American Society for Mass Spectrometry* **2017,** *28*, 1741-1750.

(18) Leach, F. E.; Wolff, J. J.; Xiao, Z.; Ly, M.; Laremore, T. N.; Arungundram, S.; Al-Mafraji, K.; Venot, A.; Boons, G.-J.; Linhardt, R. J.; Amster, I. J., Negative electron transfer dissociation Fourier transform mass spectrometry of glycosaminoglycan carbohydrates. *European Journal of Mass Spectrometry (Chichester, England)* **2011,** *17*, 167-176.

(19) Wolff, J. J.; Leach, F. E.; Laremore, T. N.; Kaplan, D. A.; Easterling, M. L.; Linhardt, R. J.; Amster, I. J., Negative electron transfer dissociation of glycosaminoglycans. *Analytical chemistry* **2010,** *82*, 3460-3466.

(20) Wu, J.; Wei, J.; Hogan, J. D.; Chopra, P.; Joshi, A.; Lu, W.; Klein, J.; Boons, G.-J.; Lin, C.; Zaia, J., Negative Electron Transfer Dissociation Sequencing of 3-O-Sulfation-Containing Heparan Sulfate Oligosaccharides. *Journal of The American Society for Mass Spectrometry* **2018,** *29*, 1262-1272.

(21) Agyekum, I.; Patel, A. B.; Zong, C.; Boons, G.-J.; Amster, I. J., Assignment of hexuronic acid stereochemistry in synthetic heparan sulfate tetrasaccharides with 2-O-sulfo uronic acids using electron detachment dissociation. *International Journal of Mass Spectrometry* **2015,** *390*, 163-169.

(22) Amster, I. J., Fourier Transform Mass Spectrometry. *Journal of Mass Spectrometry* **1996,** *31*, 1325-1337.

(23) Zhou, W.; Hakansson, K., Structural Characterization of Carbohydrates by Fourier Transform Tandem Mass Spectrometry. *Current Proteomics* **2011,** *8*, 297-308.

(24) Kailemia, M. J.; Li, L.; Ly, M.; Linhardt, R. J.; Amster, I. J., Complete Mass Spectral Characterization of a Synthetic Ultralow-Molecular-Weight Heparin Using Collision-Induced Dissociation. *Analytical Chemistry* **2012,** *84*, 5475-5478.

(25) Wolff, J. J.; Laremore, T. N.; Leach, F. E.; Linhardt, R. J.; Amster, I. J., Electron Capture Dissociation, Electron Detachment Dissociation and Infrared Multiphoton Dissociation of Sucrose Octasulfate. *European Journal of Mass Spectrometry* **2009,** *15*, 275-281.

(26) Kailemia, M. J.; Park, M.; Kaplan, D. A.; Venot, A.; Boons, G. J.; Li, L.; Linhardt, R. J.; Amster, I. J., High-field asymmetric-waveform ion mobility spectrometry and electron detachment dissociation of isobaric mixtures of glycosaminoglycans. *J Am Soc Mass Spectrom* **2014,** *25*, 258-68.

(27) Leach, F. E.; Wolff, J. J.; Laremore, T. N.; Linhardt, R. J.; Amster, I. J., Evaluation of the experimental parameters which control electron detachment dissociation, and their effect on the fragmentation efficiency of glycosaminoglycan carbohydrates. *International Journal of Mass Spectrometry* **2008,** *276*, 110-115.

(28) Wolff, J. J.; Laremore, T. N.; Busch, A. M.; Linhardt, R. J.; Amster, I. J., Influence of charge state and sodium cationization on the electron detachment dissociation and infrared multiphoton dissociation of glycosaminoglycan oligosaccharides. *J Am Soc Mass Spectrom* **2008,** *19*, 790-8.

(29) Huang, Y.; Yu, X.; Mao, Y.; Costello, C. E.; Zaia, J.; Lin, C., De novo sequencing of heparan sulfate oligosaccharides by electron-activated dissociation. *Anal Chem* **2013,** *85*, 11979-86.

(30) Yang, J.; Håkansson, K., Characterization and optimization of electron detachment dissociation Fourier transform ion cyclotron resonance mass spectrometry. *International Journal of Mass Spectrometry* **2008,** *276*, 144-148.

(31) Arungundram, S.; Al-Mafraji, K.; Asong, J.; Leach, F. E.; Amster, I. J.; Venot, A.; Turnbull, J. E.; Boons, G.-J., Modular Synthesis of Heparan Sulfate Oligosaccharides for Structure-Activity Relationship Studies. *Journal of the American Chemical Society* **2009,** *131*, 17394-17405.

(32) Munoz, E.; Xu, D.; Avci, F.; Kemp, M.; Liu, J.; Linhardt, R. J., Enzymatic synthesis of heparin related polysaccharides on sensor chips: rapid screening of heparin–protein interactions. *Biochemical and biophysical research communications* **2006,** *339*, 597-602.

(33) Leach, F. E.; Ly, M.; Laremore, T. N.; Wolff, J. J.; Perlow, J.; Linhardt, R. J.; Amster, I. J., Hexuronic Acid Stereochemistry Determination in Chondroitin Sulfate Glycosaminoglycan Oligosaccharides by Electron Detachment Dissociation. *Journal of The American Society for Mass Spectrometry* **2012,** *23*, 1488-1497.

(34) Sanderson, P.; Stickney, M.; Leach, F. E.; Xia, Q.; Yu, Y.; Zhang, F.; Linhardt, R. J.; Amster, I. J., Heparin/heparan sulfate analysis by covalently modified reverse polarity capillary zone electrophoresis-mass spectrometry. *Journal of Chromatography A* **2018,** *1545*, 75-83.

(35) Ceroni, A.; Maass, K.; Geyer, H.; Geyer, R.; Dell, A.; Haslam, S. M., GlycoWorkbench: a tool for the computer-assisted annotation of mass spectra of glycans. *Journal of proteome research* **2008,** *7*, 1650-1659.

(36) Duan, J.; Jonathan Amster, I., An Automated, High-Throughput Method for Interpreting the Tandem Mass Spectra of Glycosaminoglycans. *Journal of The American Society for Mass Spectrometry* **2018,** *29*, 1802-1811.

(37) Duan, J.; Pepi, L.; Amster, I. J., A Scoring Algorithm for the Automated Analysis of Glycosaminoglycan MS/MS Data. *Journal of the American Society for Mass Spectrometry* **2019,** *30*, 2692-2703.

(38) Domon, B.; Costello, C. E., A systematic nomenclature for carbohydrate fragmentations in FAB-MS/MS spectra of glycoconjugates. *Glycoconjugate Journal* **1988,** *5*, 397-409.

(39) Wolff, J. J.; Chi, L.; Linhardt, R. J.; Amster, I. J., Distinguishing glucuronic from iduronic acid in glycosaminoglycan tetrasaccharides by using electron detachment dissociation. *Analytical chemistry* **2007,** *79*, 2015-2022.

(40) Rabenstein, D. L., Heparin and heparan sulfate: structure and function. *Natural Product Reports* **2002,** *19*, 312-331.

(41) Pepi, L. E.; Sanderson, P.; Stickney, M.; Amster, I. J., Developments in Mass Spectrometry for Glycosaminoglycan Analysis: A Review. *Molecular & Cellular Proteomics* **2020**.

(42) Thacker, B. E.; Xu, D.; Lawrence, R.; Esko, J. D., Heparan sulfate 3-O-sulfation: a rare modification in search of a function. *Matrix biology : journal of the International Society for Matrix Biology* **2014,** *35*, 60-72.

CHAPTER 6

Conclusions

Glycosaminoglycans (GAGs) are complex, heterogenous polysaccharides with high extents of modifications, including sulfation, acetylation and uronic acid C-5 epimerization. Due to their complex nature, obtaining sequencing information is inherently complex. Electron based ion activation methods produce an abundance of informative glycosidic and cross-ring cleavages with minimized sulfate decomposition. Electron detachment dissociation (EDD) has been previously optimized to yield complete sequence information of sulfated GAGs. Though a powerful tool for GAG characterization, EDD has its limits, including low conversion efficiency and long reaction times. Additionally, chondroitin sulfate (CS) GAG characterization has presented as an even more challenging endeavor. Majority of cross-ring fragmentation occurs on the uronic acid residues in CS samples, a phenomenon not seen with heparin/heparan sulfate (Hp/HS) samples. Wolff *et al.* proposed a mechanism which suggests radical formation initiating at the carboxylate rather than the sulfate, either from hydrogen rearrangement or at the initiation of electron detachment. It is also hypothesized that the change in linkage from β-1,4 in HS standards to β-1,3 in CS standards is a factor in the change in fragmentation between the two GAG classes. This presents as a challenge for CS characterization, as sulfate modifications are often located on the amino sugar, not the uronic acid. For these reasons other ion activation techniques have been investigated for GAG characterization.

Charge transfer dissociation (CTD) which had previously been utilized for algal polysaccharides, however until now had not been utilized for GAG samples. CTD is shown to produce EDD like fragmentation on an ion-trap instrument. CTD is also shown to be a more efficient than EDD. Similar to EDD, CTD is unable to distinguish 4-*O* from 6-*O* sulfation in CS standards, with majority of cross-ring fragmentation occurring on the uronic acid residues. Though CTD can produce EDD like fragmentation in an ion-trap instrument, ion-traps are limited by their low resolving power. Previously, CTD has been implemented on linear ion-trap spectrometers, so coupling with an Orbitrap MS should be a trivial exercise. Implementing CTD on an FTMS instrument would dissolve the resolution discrepancies presented here between CTD and EDD.

Ultraviolet Photodissociation (UVPD) was previously shown as a powerful tool for sequencing of both CS and Hp/HS GAGs. Here we take a closer look at the effect UVPD fragmentation parameters, which have previously been shown to be imperative for converting precursor ions to fragment ions of proteins, have on sequencing GAGs. Chondroitin sulfate A (CS-A) and dermatan sulfate (DS), which are isomers differing only in uronic acid C-5 stereochemistry, were examined. It was determined that both 193 nm and 213 nm laser wavelengths can produce informative fragmentation for GAGs. Additionally, increasing the number of laser pulses for 193 nm UVPD and increasing the activation time for 213 nm UVPD increases the fragmentation efficiency. UVPD experiments were performed on an Orbitrap Fusion Lumos MS, which contains a dual-pressure ion trap. Analyte ions can be stored in either the low-pressure cell or high-pressure cell before being exposed to UV photons. Activation occurring in the high-pressure cell resulted in a higher intensity and diversity of fragment ions, making it the ideal location for UVPD. UVPD could distinguish CS-A from DS. Diagnostic

fragment ions previously determined to distinguish CS-A from DS when using EDD were seen in the UVPD spectrum, making it a viable tool for determining uronic acid stereochemistry. The ability to distinguish CS-A from DS was noted to be independent of the experimental parameters investigated. The most notable benefit to utilizing UVPD fragmentation is the ability to distinguish 4-*O* from 6-*O* sulfation. Low-intensity cross-ring fragments were seen when utilizing UVPD in the high-pressure cell with a higher number of laser pulses. These conditions allow for lower intensity fragment ions to be visualized.

Finally, negative electron transfer dissociation (NETD) experimental parameters were optimized for NETD on a FTICR mass analyzer. NETD has been utilized for GAG sequencing on ion-trap and FTMS instruments. Previous data using NETD on a FTICR instrument had shortened the experimental time frame making it compatible with on-line separation techniques. However, this still resulted in experiment times of 1 s (500 ms reaction time and 500 ms reagent accumulation time). To better optimize reaction times, different ionization states were tested. It was determined that higher charge-states and higher ionization states result in shorter reaction times (50 ms reaction time and 350-500 ms reagent accumulation time). It was also determined that the reaction time NETD parameter on NETD instruments does not need to exceed 50 ms to achieve informative fragmentation. This allows for overall shorter reaction times than previously reported, even for low charge-states. NETD experiments on FTICR instruments occur at shorter time frames than EDD and produce more informative cross-ring fragment ions than CID.

The presented work examines the capabilities of alternative electron-based ion activation methods to EDD (CTD, UVPD and NETD). EDD is a low efficiency method, requiring high degrees of signal averaging and long experiment times. This adds an extra level of difficulty for pairing EDD with on-line separation methods. EDD is also an instrument specific technique and

is almost exclusively performed on FTICR mass spectrometers, as it occurs within the analyzer cell of the instrument. The ability to produce abundant cross-ring cleavages and locate sulfate modifications on highly-sulfated GAGs without the need for an FTICR mass analyzer makes GAG sequencing more widely available. CTD was shown here to produce informative fragmentation from GAG standards in an ion trap instrument, however the low resolution of the mass spectrometer made fragment assignment difficult. If CTD can be effectively paired with an Orbitrap MS, this problem would be resolved. Additionally, CTD produced chemical background that fell in the low m/z region, limiting the ability to activate ideal GAG precursors for sulfate retention. UVPD was shown to produce ample cross-ring and glycosidic fragment ions from GAG standards while also producing the necessary cross-ring cleavages to distinguish 4-*O* from 6-*O* sulfation in CS/DS standards. Until now this distinction was not achieved consistently by any other method investigated thus far. Additionally, UVPD has been paired successfully with ion trap and Orbitrap instruments, making it available on a wider range of mass analyzers than most electronic-activation methods. NETD produced informative cross-ring and glycosidic fragment ions, however an increase in uninformative fragment ions is seen as the reagent accumulation time is increased. This increases the difficulty to use this method for unknown compound identification; however, does not hinder from confirming the sequence of known structures. NETD is commercially available on FTICR instruments, and has been implemented on Orbitrap MS. Overall, all methods discussed herein are suitable for the analysis of GAG standards, however further optimization may be required before applying these methods to unknown complex biological samples. Further experiments pairing these methods with capillary zone electrophoresis (CZE) can further close the gap between GAG standard optimization and analyzing biological GAG mixtures.

APPENDIX A

Electron Detachment Dissociation (EDD) and Negative Electron Transfer Dissociation (NETD): A Review

Pepi, L. E., & Amster, I. J. In *Advanced Fragmentation Methods in Biomolecular Mass Spectrometry: Probing Primary and Higher Order Structure with Electrons, Photons and Surfaces.* Lermyte, F.; Royal Society of Chemistry. (Accepted for publication)

Abstract

Oligonucleotides, oligosaccharides, and proteins with acidic post translational modifications (PTMs) are more effectively ionized in negative ion mode than as positive ions. Informative fragmentation data is required to determine the structural details for these sample types. Polarity insensitive activation methods such as collision induced dissociation (CID) can be applied to both positive and negative ions, but often do not provide enough detail to fully characterize the structures of these molecules. Electron-based activation methods can provide data that is complementary to that produced by CID, and in many cases, more complete. These electron-based methods were developed principally for the characterization of positive ions but have great applicability to the dissociation of negative ions as well. Electron detachment dissociation (EDD) and negative electron transfer dissociation (NETD) are electron-based activation methods that have been developed for the analysis of multiply-charged negative ions. This chapter presents a brief history of the evolution of the positive ion activation methods, electron capture dissociation (ECD) and electron transfer dissociation (ETD), into related methods for negative ions, namely EDD and NETD. A comprehensive description of EDD and NETD is presented, and their application to a variety of biologically-relevant compound classes is reviewed.

A Brief History of Electron Capture Dissociation

Electron capture dissociation (ECD) was first reported in 1998 by Zubarev, Kelleher, and McLafferty.[1] ECD produces odd-electron ions by the recombination of a low-energy electron (<1 eV) with a multiply-charged precursor cation.[2, 3] Electron capture by a singly-charged precursor results in a neutral product that is invisible to the mass spectrometer. The electron energy range can be increased (3-13 eV) to implement hot electron capture dissociation (HECD) which produces secondary ion fragments not found in conventional ECD, including some useful side chain cleavages that can distinguish isomeric or isobaric residues, for example leucine and isoleucine.[4] This experiment is performed in positive ion mode. This is a non-ergodic process and therefore produces extensive fragmentation of peptide backbones while maintaining labile post-translational modifications (PTMs).[3] ECD is an ideal tool for determining structural details for positively charged analytes such as proteins and some oligosaccharides. Until recently, ECD was considered an instrument-specific technique mostly utilized in Fourier transform ion cyclotron resonance (FTICR) mass spectrometers. The capability of ECD to efficiently fragment peptides and proteins, and to identify PTMs by both top-down and bottom-up approaches has created great interest in this activation method. Recent innovations provide the means to implement ECD in other widely used mass spectrometers. ECD has been implemented in ion-trap mass spectrometers by applying an external magnetic field, or by pulsing electrons into the ion trap during a node in the radio-frequency (RF) amplitude.[5, 6] In recent years atmospheric pressure electron capture dissociation (AP-ECD) has gained popularity due to its ability to be applied to virtually any electrospray ionization (ESI) source. The success of AP-ECD has been demonstrated on a Quadrupole Time of Flight (Q-ToF) MS.[7] In 2009, an electromagnetostatic ECD cell was developed, and implemented on a triple quadrupole MS.[8] Since then the

electromagnetostatic ECD cell has been implemented on a variety of mass spectrometers.[9, 10] This cell utilizes a high density of electrons to provide high fragmentation efficiency in a short time scale (microseconds), and has been integrated into beam-instruments such as time-of-flight, triple quadrupoles, and Orbitrap hybrid mass spectrometers.[11] For Orbitrap MS instruments, the cell is mounted on the front end of the higher energy collisional dissociation (HCD)-cell connecting to the exit lens of the C-trap, as shown in Figure A.1. Ubiquitin and myoglobin were both investigated, and both yielded a higher sequence coverage (80% and 60% respectively) than collision energy alone and yielded a significantly higher percentage of explained fragments (69% and 74% respectively). This data shows the ability to successfully implement ECD on mass spectrometry platforms other than an FTICR MS.

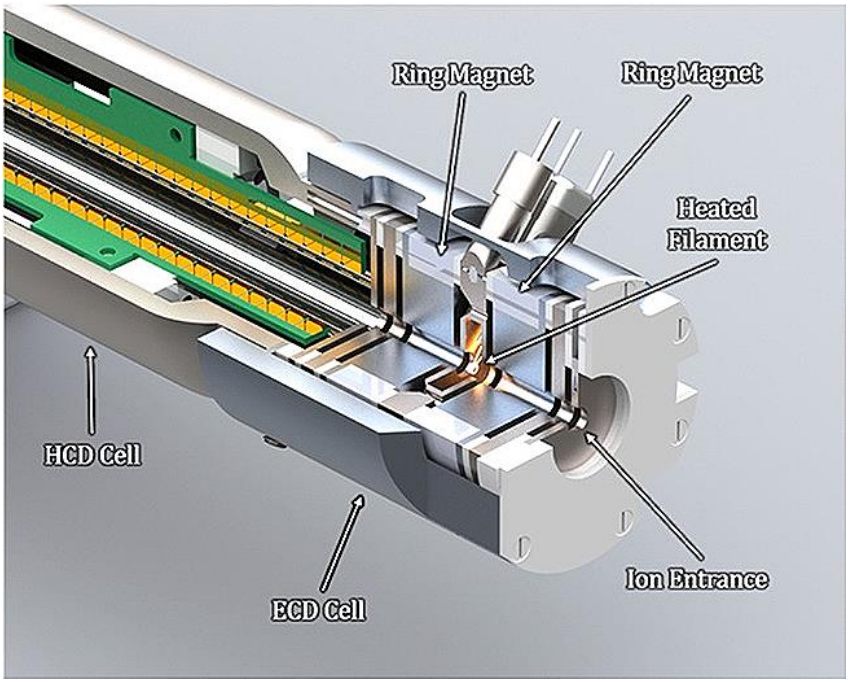

Figure A.1. Schematic of the electromagnetostatic ECD cell attached to the front of an HCD-cell in an Orbitrap mass spectrometer. Electrons are generated using a heated rhenium filament. Reproduced with permission from ref 9. Copyright 2017 American Chemical Society. Further permissions related to the material excerpted should be directed to the ACS. https://pubs.acs.org/doi/10.1021/acs.jproteome.7b00622

Electron Detachment Dissociation

Highly anionic compounds such as sulfated polysaccharides and nucleic acids are most efficiently ionized in negative ion mode. Electron detachment dissociation (EDD) serves as a useful activation method for the structural characterization of multiply-charged negative ions. EDD was first introduced in 2001 by Zubarev and co-workers as an alternative to ECD, with particular applicability to the dissociation of acidic polypeptides.[12] EDD can be thought of as the negative ion complement of ECD, sharing several characteristics. For both ECD and EDD, the

precursor ion must be multiply-charged, the reactant is an electron, and one product of the reaction between the precursor and electron is a charge-reduced odd-electron ion. EDD is accomplished by irradiating multiply-charged precursor anions with electrons of a moderate kinetic energy (15-20 eV), leading to electron detachment and ion fragmentation.[3] The range of electron energies reported for EDD has been as low as 10 eV for di-anions and as high as 30 eV for carbohydrates.[12-17] Initial work investigated sulfo-peptide di-anions and produced minimal sulfate decomposition while also producing backbone cleavages (*a*-, *c*- and *z*-ions). Radical species of these backbone fragments were produced, and CO_2 and SO_3 loss from the radical precursor species were observed. These odd-electron products are pivotal fragment ions for confirming that EDD has occurred.[12] EDD, to date, has been performed only on FTICR MS instruments.

EDD occurs in the analyzer cell of FTICR instruments and uses a heated cathode for the generation of electrons. A typical EDD experiment begins by selecting the precursor ions with a quadrupole mass filter, followed by accumulation in an RF hexapole collision cell (at sub-threshold kinetic energies for fragmentation by collisions) before injection into the ICR analyzer cell. An in-cell isolation can also be implemented for a better defined precursor, although this last step is optional.[18] The electron beam is then introduced in a pulse, leading to irradiation of the precursors by the energetic electrons. After a defined period of irradiation, the electron beam is turned off, and the product ions are detected by the standard FTICR process of chirp excitation and image current detection.

EDD Experimental Parameters

As for any tandem mass spectrometry (MS/MS) experiment, EDD parameter settings are crucial to obtaining the best fragmentation. The most critical parameters for EDD (optimal values shown in parentheses) are the cathode heater current (1.5 A), which controls the number of electrons released by the cathode, the pulse duration (1 s), the extraction lens voltage (-17 to -20 V), which also controls the rate at which electrons are extracted from the cathode, and the cathode bias (-19 V), which determines the kinetic energy of the electrons. A drawback to EDD is the low efficiency of converting precursor ions to fragment ions. Both the precursor ions and electrons bear negative charges in EDD, and so one would expect that the reaction cross-section will be lower than for positive ions reacting with electrons, as in ECD. As a result, the optimal electron flux and the resulting product ion yield for EDD is quite different than for ECD. These parameters for EDD activation were investigated for the dissociation of anionic oligosaccharides by Amster and coworkers[19] and for oligonucleotides by Håkansson and coworkers.[20] Leach *et al.* examined a variety of EDD parameters for the dissociation of glycosaminoglycans. For these studies, a circuit was designed and constructed to measure the electron current produced by the indirectly heated cathode, and the current impinging on the extraction lens. The difference between these two values is the electron current that passes through the ICR analyzer cell. This circuit allowed the electron flux in the analyzer cell to be monitored while other parameters (heater current, cathode and lens potentials) were varied. Leach varied the heater current from 1.3 A to 1.6 A and found that this parameter does not affect the product ion yield if the electron current at the cell is kept constant by adjustment of the extraction lens voltage.[19] Yang *et al.* also found this to be true for oligonucleotides.[20] With a lower heater current, a higher extraction voltage will produce the same fragmentation efficiency as can be obtained with a higher heater

current and lower extraction voltage. This is significant because lower heater currents correlate with an extended lifetime for the cathode. Careful measurements were made of the electron current as a function of the extraction lens voltage. Changing the extraction lens by 0.2 V led to a doubling of electron current, while a 1 V increment resulted in an eightfold increase in current.[20]

Leach *et al.* also investigated the pulse duration needed for EDD fragmentation. It was found that increasing the pulse length does increase the product yield, however in less than linear fashion.[19] Yang *et al.* found that the flux of electrons passing through the analyzer cell increases linearly as the cathode bias is increased from -20 to -80 V. This means that increasing the cathode bias voltage also increases the electron energy and number. However, increasing the number of electrons beyond the lowest optimal value did not result in greater fragmentation yield. In fact, the efficiency of product ion formation seemed to decrease with a higher flux of electrons through the cell. The trapped ions appear to be repelled by the beams of electrons, pushing them out of the region of interaction when the electron flux is too high.[20] The benefit of identifying an ideal electron energy is seen in Figure A.2, for a dermatan sulfate octasaccharide. Leach *et al.* also noticed limited gains in product yield when increasing the precursor accumulation time in the external hexapole. An accumulation time of approximately 3 s was ideal for increasing precursor intensity and product ion yield, whereas when this time was increased beyond 3 s, product ion yield reached a plateau even though the precursor ion intensity increased.[19] These data suggested that the larger number of trapped ions assumed a spatial distribution that did not overlap well with the electron beam.

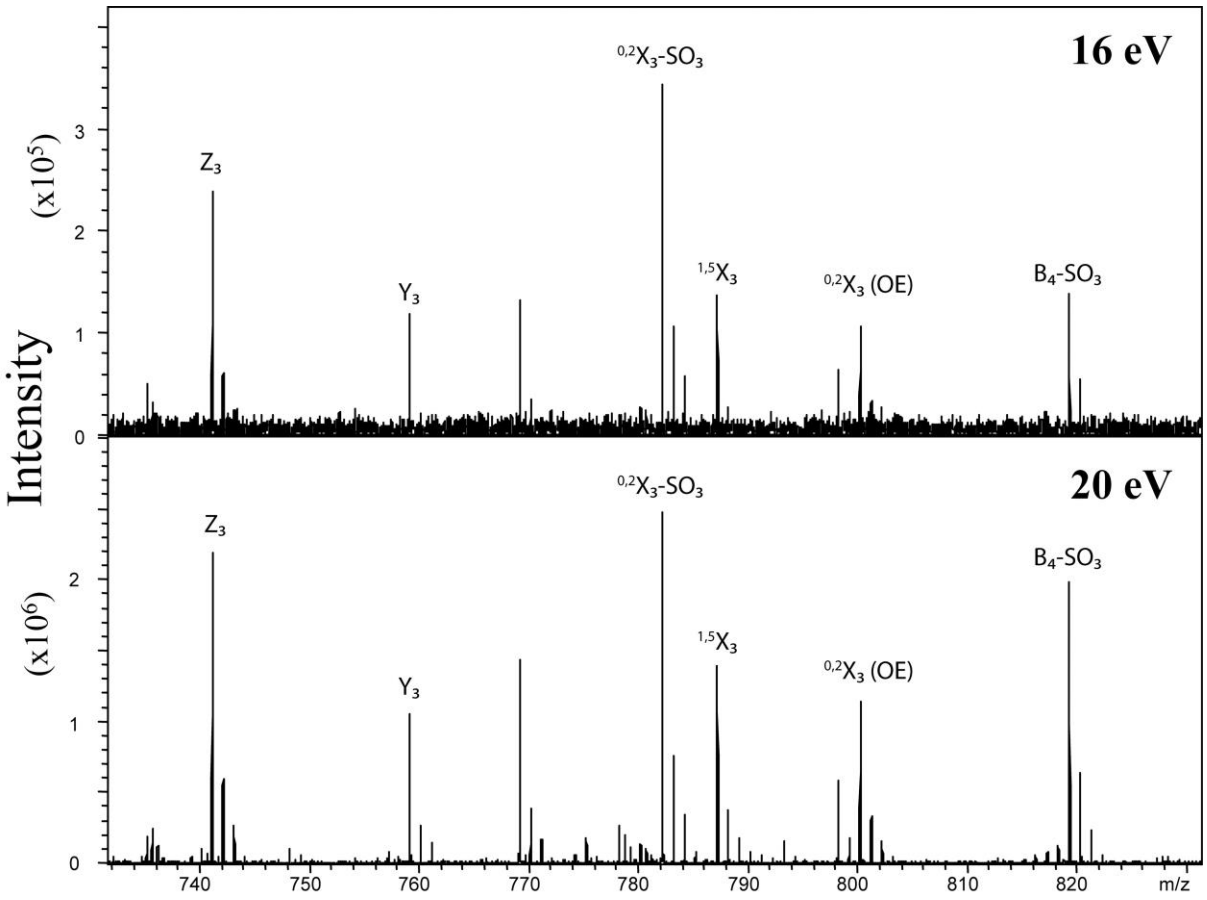

Figure A.2. EDD mass spectra of dermatan sulfate dp8, $[M-4H]^{4-}$, using an electron energy of 16 eV and 20 eV, showing similar product ions. Reproduced with permission from ref 19. Copyright Elsevier 2008.

Initial EDD experiments were performed with a Bruker Apex FTMS instrument, while more recent work used a Bruker solariX. Two differences in their design have a significant impact on the data that can be obtained for EDD experiments. First is the method for transferring ions through the fringe field of the magnet and into the high field region where the analyzer cell is located. The Apex instrument uses an electrostatic ion guide (EIG), which first accelerates ions to a high kinetic energy before focusing them into a paraxial ion beam with an Einzel lens. Once

inside the high field region of the instrument, the kinetic energy is reduced to a few eV so that ions may be trapped by the analyzer cell.[21, 22] A disadvantage of the EIG is that the ions are not well collimated around the central axis of the analyzer cell.[21-23] As a consequence, there is incomplete overlap between the electron beam and the precursor ions, with a need for long EDD activation times. The Bruker solariX FTMS instrument improved upon this by replacing the EIG with a RF-only quadrupole for guiding ions through the fringe field of the magnet.[24, 25] RF-only ion guides efficiently focus low kinetic energy ions to the central axis of the ion guide.[26] The quadrupole ion guide is better at transferring ions to the principal axis of the analyzer cell, resulting in a better overlap of the electron beam with the precursor ions, with a higher efficiency for EDD. The Bruker Apex and solariX FTMS systems also differ in the design of the analyzer cell. The Apex system utilizes an infinity cell while the newer generation solariX XR instruments utilize a dynamically harmonized Paracell.[27] The solariX XR, standing for eXtreme Resolution, is an upgrade to the original solariX instrument, which like the Apex utilizes an infinity cell. The Paracell produces a more ideal trapping electric field and longer coherent motion of the ions during detection. The experimental impact is a longer transient, which provides higher mass resolving power and better signal-to-noise.[28-30] EDD does not efficiently convert precursor ions to product ions, and many significant product ions exhibit low abundance. With higher resolution and signal-to-noise, more of the low intensity fragments can be observed, providing more complete structural detail.

Application to Oligosaccharides

Glycosaminoglycans (GAGs) have been extensively characterized using EDD. GAGs are linear polysaccharides with a repeating disaccharide unit composed of an amino sugar and an uronic acid. Both heparin (Hp)/heparan sulfate (HS) and chondroitin (CS)/dermatan sulfate (DS) have sugar residues that are modified by sulfo-half esters, making them highly acidic, and thus more efficiently mass analyzed as negative ions. The biosynthesis of GAGs occurs through a series of incomplete enzymatic transformations, resulting in highly heterogeneous products. Mass spectrometry plays a crucial role for characterizing the structural features of such complex mixtures. The structural properties of GAGs that can vary are the sites and extent of sulfation, acetylation versus sulfation of nitrogen in the amino sugars, and stereochemistry at the C-5 position of the uronic acid.[31] Mass spectrometry can provide compositional information such as chain length, the number of sulfo modifications, or the number of acetylated amine groups, but to discern their location in an oligosaccharide, MS/MS is required. Early activation studies used collision induced dissociation (CID), but this activation method produced mostly glycosidic fragmentation, and a high yield of the loss of SO_3, which confounds the assignment of its location within an oligosaccharide.[32-34] The first use of EDD for GAG structure analysis was reported by Wolff *et al.* for HS tetrasaccharides.[3] This work was later extended to longer chain lengths (<10) and higher degrees of sulfation (3-4 per disaccharide).[15, 18, 35-39] EDD has proven itself an ideal fragmentation technique for GAGs due to its ability to produce glycosidic and cross-ring fragmentation with little degradation of the labile sulfate half esters. EDD has been shown not only to determine sulfate location but also to distinguish C-5 stereochemistry for the uronic acid.[15, 38-40] It is important to note that the efficiency of EDD for GAG samples and other sulfated oligosaccharides depends on the ionization state of the oligosaccharide. Electron

detachment occurs at a site of negative charge. For GAGs, negative charge arises by deprotonation of sulfate and carboxyl groups. If both anions are present in a precursor, the preferred site of electron detachment is carboxylate, as the energy required for detachment from this functional group is over 100 kJ mol^{-1} lower than from a sulfate group. However, in solution, sulfate is more acidic than carboxylate, and is thus more likely to be a site of ionization in the gas phase. Electron detachment from a sulfate anion leads to SO_3 loss. Thus, it is important to control sample solution conditions and ionization parameters to ensure that a carboxylate is present to serve as the site of electron detachment. The optimal precursor of an oligosaccharide for EDD has an ionization state of one more than the number of sulfate groups, thus ensuring the presence of at least one carboxylate anion. For example, a tetrasaccharide with 2 sulfate groups would have an ideal precursor with 3 ionized sites.[41] Experiments with EDD have shown that a fully ionized precursor eliminates or substantially reduces sulfate decomposition, but also decrease the number of informative fragments produced. This is different from CID which relies on a fully ionized precursor to produce informative fragment ions.[42]

A challenging task for mass spectrometry is to distinguish glucuronic acid (GlcA) versus iduronic acid (IdoA) residues in GAG oligomers. These two residues have the same molecular mass and differ only by the stereochemistry of the C-5 position. Costello and coworkers were the first to address diastereomers that differ in chirality of the uronic acid C-5 center.[32] By using CID, they observed correlations in glycosidic cleavages for CS (which contains GlcA) versus DS (which contains IdoA) and were able to assign the composition of mixtures. Later experiments conducted by Leach *et. al.* showed the ability to distinguish C-5 stereochemistry in uronic acid residues of 4-*O*-sulfated CS epimers (CS-A and DS) using EDD.[36] This was based on diagnostic ion intensities in EDD mass spectra. Fragmentation of GAG samples is reported using the Domon and Costello

nomenclature.[15] These EDD results showed $^{0,2}X_n$ and Y_3 to be indictive of CS-A containing GlcA, which agreed with CID data obtained previously by Costello and coworkers. Further EDD experiments were done that led to the ability to assign C-5 stereochemistry in uronic acid residues of 4-*O*-sulfo CS epimers. These assignments were based on diagnostic cross-ring ions $^{2,4}A_n$ and $^{0,2}X_n$ using CID.[43]

A similar approach was taken to examine HS samples. Early work by Wolff *et al.* on pairs of epimeric HS tetramers, found diagnostic peaks that distinguished GlcA from IdoA for the residue nearest the reducing end.[15] A few fragments were found to correlate with the presence of GlcA near the reducing end of tetrameric HS; $^{0,2}A_3$, B_3' (the ' denotes a fragment with the loss of an additional H compared to the conventional glycosidic cleavage), and a B_3'-CO_2. These product ions were rationalized with a radical mechanism, originating by electron detachment from a carboxylate anion on the uronic acid closest to the reducing end of the tetrasaccharide. The GlcA carboxy radical could undergo hydrogen rearrangement by abstraction of -H· from ring position C4, and this radical site undergoes □-□ cleavage to produce the $^{0,2}A_3$ product. The C4 hydrogen is inaccessible to the carboxy radical of IdoA, and therefore is blocked from producing the $^{0,2}A_3$ product. In addition to the diagnostic fragment ions, some of the other peaks found in the spectra of both epimers exhibited differences in intensities.

A more comprehensive study investigating HS tetramers showed that in the presence of a sulfo group at the 2-*O* position of the uronic acid, the B_3'-CO_2 ion is not observed in GlcA containing epimers.[38] Later work focused on the application of principal component analysis (PCA) to find statistically significant differences in ion abundances in the EDD mass spectra of GAG epimers.[44] When looking at EDD data of four HS GAG standards, with uronic acids GG, GI, IG, and II, where "G" denotes GlcA and "I" denotes IdoA, PCA was able to distinctively

separate each of these four samples across PC1 (52% of variance) and PC2 (33% of variance). This shows that even though the raw data of the four samples is difficult to distinguish visually, PCA readily distinguishes replicates of these four samples with only two principal components. More recent work by Agyekum *et al.* established a diagnostic ratio from various fragment ion intensities which distinguished HS epimers for more than 30 different HS tetrasaccharides.[39] PCA analysis of standards established the fragment ions that had the strongest correlation to the reducing end uronic acid stereochemistry. During their studies, the researchers found B_3'-CO_2 present in HS samples containing GlcA near the reducing end of the tetramer, supporting the previously reported data. It was also determined by using PCA analysis that B_3, Y_1, C_2 and Z_2 were diagnostic peaks for GlcA2S, while Y_2 and $^{1,5}X_2$ were diagnostic peaks for IdoA2S. The abundances of the diagnostic ions serve as input for an equation that yields a positive output for GlcA containing samples and a negative output for IdoA containing standards. While this equation has 100% predictive power for assigning uronic acid stereochemistry (GlcA versus IdoA and GlcA-2S versus IdoA2S), it is limited to the assignment of the single uronic acid residue closest to the reducing end of HS tetrasaccharides. Furthermore, the standards used for this study were prepared with an alkyl amine linker at the reducing end, limiting the general utility of this approach.

Although the early EDD studies on GAGs focused on purified standards, later efforts were directed to mixtures of GAGs. There are frequently large numbers of isomeric structures possible for GAG oligomers of a given composition, and so precursor mass selection is often inadequate for fully characterizing all the components of mixtures by MS/MS. Given the long time necessary for an EDD experiment (1-3 s), chromatographic or electrophoretic methods of separation are not well matched with this method of ion activation. Amster and co-workers

utilized high-field asymmetric ion mobility spectrometry (FAIMS) as an on-line separation method with EDD for resolving mixtures of isomers, and even epimers, and obtaining structural details by MS/MS.[45] FAIMS separates ions spatially rather than temporally, and allows one to select one component by its compensation voltage, effectively removing other components, as can be seen in Figure A.3. This allows the user to examine the selected component for an extended period, so that high-quality EDD spectra can be obtained for each component of the mixture.

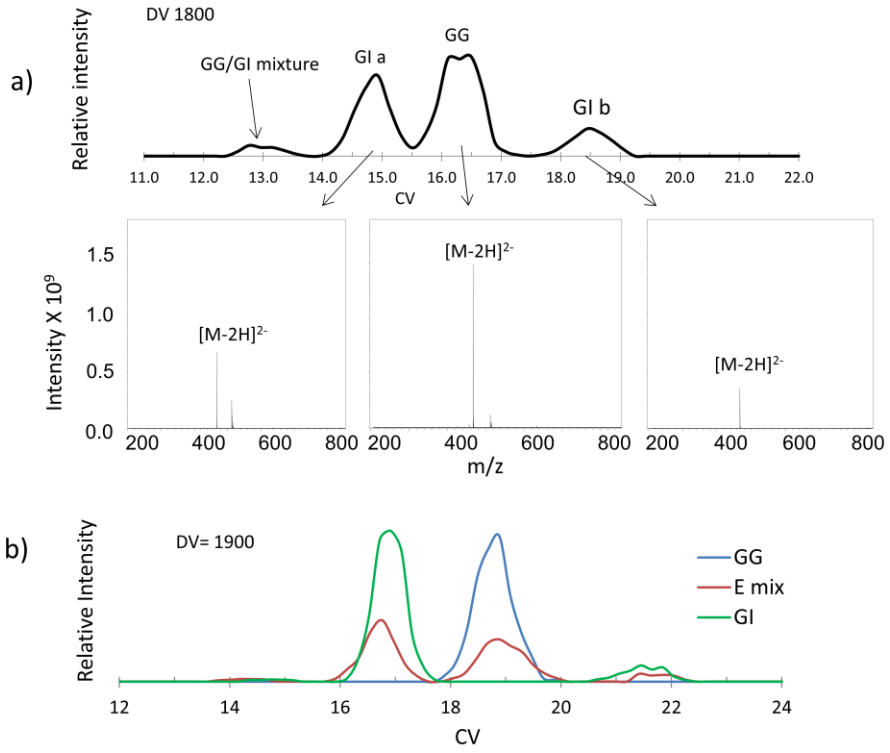

Figure A.3. FAIMS separation of a mixture of epimeric heparan sulfate tetramers. (a) Extracted ion chromatogram (EIC) at m/z 467.06, $[M-2H]^{2-}$, of a GG and GI mixture. Mass spectra at different compensation voltages show the separation of ions with the same mass-to-charge ratio. (b) EIC of a GG standard, a GI standard and a mixture of the two. GG molecular ion appears as a single peak while GI molecular ion appears as two individual peaks. Reproduced with permission from ref 45. Copyright American Chemical Society 2014. Further permissions related to the material excerpted should be directed to the ACS.

Following the early success of EDD for obtaining structural details of GAG standards[3], other oligosaccharides were quickly investigated. Håkansson and coworkers investigated neutral and sialylated oligosaccharides.[16] Neutral oligosaccharides had been extensively investigated in positive ion mode using CID, which produces B- and Y-type glycosidic ions. Negative ion mode for neutral oligosaccharides using CID produces C-type glycosidic fragmentation and A-type cross-ring fragmentation. Sialic acid contains a carboxyl group and therefore produces an abundant ion signal in negative ion mode. For the oligosaccharide maltoheptaose, which is neutral, fragmentation by CID and infrared multiphoton dissociation (IRMPD) were complementary to each other, and EDD was as well, but had a few additional cross-ring fragments. In this case, the doubly-charged precursor was used for EDD, however it had only ~50% the intensity of the singly-charged precursor. Both mono- and disialylated standards were examined; it was found in the cases where there is more than one sialic acid it is more difficult to produce the doubly-charged precursor that is necessary for EDD. This drawback was overcome in later work by the Håkansson group.[46] The ability for EDD to produce a higher product ion intensity and more diverse fragment types compared to IRMPD is shown in Figure A.4. Only $^{0,2}A_n$ or $^{2,4}A_n$ type cleavages were seen via CID and IRMPD of these oligosaccharides. EDD produced not only these cleavages, but also additional cross-ring cleavages ($^{3,5}A/X_n$, $^{1,5}A/X_n$), resulting in more complete structural details. Further work on these sample types investigated the EDD fragmentation of the doubly-charged precursor with a single chloride-adduct, $[M-H+Cl]^{2-}$.[47] The chloride-adducted precursor produced complementary fragmentation to the doubly-charged precursor studied previously, however the chloride-adducted precursor did produce a greater diversity in the type of glycosidic and cross-ring cleavages produced. It was observed that, for

acidic oligosaccharides, it was more difficult to obtain high abundance of the chloride-adducted precursor in comparison to neutral oligosaccharides.

In addition to oligosaccharides, EDD has also been used for structure analysis of other glycoconjugates, such as glycosphingolipids. This class of molecules is typically analyzed as positive ions, however gangliosides which contain a sialic acid have been shown to ionize well in negative mode.[48, 49] Gangliosides structure includes a ceramide tail of various lengths, saturation, and hydroxylation. This tail is linked to a polar carbohydrate head containing sialic acid. Grouping of gangliosides is determined by the number of sialic acid residues; M, D and T correspond to one, two and three sialic acids respectively. Nilsson and coworkers used both positive and negative ion mode to investigate the fragmentation of gangliosides using ECD, EDD and IRMPD. [50] As expected, they found that ECD produced an abundance of fragmentation with minimal secondary fragmentation. They were also able to identify both halves of the ceramide tail, which is a fatty acid N-linked to a sphingosine.[50] ECD also resulted in complementary polysaccharide fragment ions for M-sugar fragments and loss of the acetyl moiety which is used to confirm the N-linkage. EDD produced similar fragment ions to ECD; however, it also produced a significant number of uninformative water and hydrogen loss peaks. IRMPD of the gangliosides in both positive and negative ion mode yielded fewer informative fragment ions, but in negative ion mode IRMPD saw fragment ions representing the two halves of the ceramide tail, which was not seen via IRMPD in positive ion mode.[50] This work shows the ability to fragment gangliosides in negative ion mode; however, due to the low efficiency of converting precursor to fragment ions via EDD, the best approach combined EDD results with IRMPD results.[50]

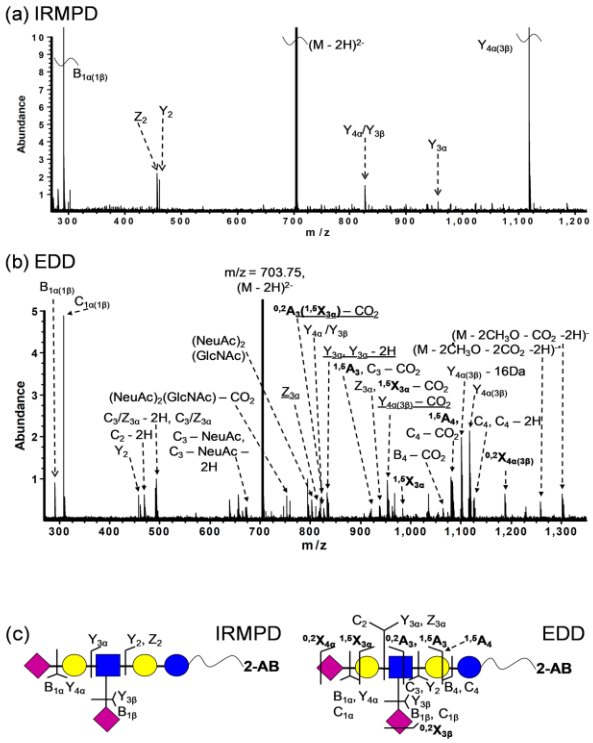

Figure A.4. (a) IRMPD and (b) EDD spectra of $[M-2H]^{2-}$ 2-AB-labeled DSLNT at *m/z* 703.75. Cross ring fragments are in bold, and reducing end product ions lacking 2-AB are underlined. (c) Fragmentation patterns from IRMPD and EDD. Reproduced with permission from ref 46. Copyright John Wiley and Sons 2011.

Application to Proteins

Proteins are typically ionized in positive ion mode; however, when a protein has a high proportion of acidic residues, phosphorylation, or sulfation PTMs present there are advantages to using negative ion mode for analysis. Matrix assisted laser desorption/ionization (MALDI) and ESI have both been used for the analysis of sulfated proteins in positive ion mode. Though these

ionization methods are considered soft ionization techniques, sulfate decomposition is commonly seen.[51] Collisional activation techniques result in a high abundance of sulfate decomposition, making it difficult to locate sulfate modifications. Phosphorylation is another important PTM, found in a third of eukaryotic proteins.[52] Phosphorylation is typically analyzed in positive ion mode using MS/MS techniques such as CID. However due to the lability of phosphate bonds, CID can often lead to phosphate decomposition.[53] Electron-based methods present a viable alternative for sequencing proteins while maintaining PTMs. Negative-mode ESI holds higher potential for acidic protein analysis due to the higher efficiency for making stable gas-phase ions.[54]

Ion-electron reactions maintain labile PTMs while producing extensive backbone fragmentation. Unlike CID, or other ion activation methods that proceed by vibrational excitation, ion-electron reactions form a radical site. These odd-electron species undergo reactions similar to those observed for electron ionization mass spectra, specifically a-b cleavage. Zubarev and coworkers detected a dominance of C_α-C backbone cleavages when using EDD, resulting in $a^{\cdot}$ and *x*-ions.[55] Previously, this was only reported as a dominant fragment when using ultraviolet photodissociation (UVPD) with a 157 nm wavelength.[56] The dominance of C_α-C fragment ions was seen for both basic and acidic peptides, as well as peptides with PTMs.[55] EDD fragmentation of peptide polyanions results in an abundance of C-terminal species. This is complementary to ECD fragmentation of polycations, which yields an abundance of N-terminal c-ions. Therefore, backbone bonds (N-C_α or C_α-C bonds) can be selectively cleaved based on which ion-electron reaction is used.[55] The biggest drawback to using EDD fragmentation for peptides is the low efficiency at converting precursor ion to fragment ions. This low efficiency was later improved upon to reduce the number of summed spectra needed and to permit EDD to

operate on a timescale suitable for liquid chromatography (LC) separations. Jensen and coworkers were able to increase the fragmentation efficiency of EDD by optimizing instrument parameters.[57] It had previously been shown that a low electron current (3-10 μA) and low-energy electrons (8-18 eV) are important parameters for EDD of peptide anions. However, in this study it was shown that electron irradiation time (150-170 ms), electron energy (18 eV), electron current (6-8 μA), and irradiation delay (40 ms), also known as the electron-ion phase correlation, all needed to be optimized (optimal parameters shown in parentheses).[57] With the optimized parameters, the fragmentation efficiency of EDD increased, making it a compatible MS/MS technique for LC-MS. Even with this increase in fragmentation efficiency, EDD still provides complementary information to ECD for peptides; thus, combining the two ion-electron reactions increases the overall sequence coverage of proteins.[57] This work was later expanded to longer peptide chains by Breuker and coworkers. EDD provided sequence information in top-down mass spectrometry of acidic proteins with up to 147 amino acid residues.[58] EDD of the ubiquitin 11- precursor ion was found to produce complementary $a^{-\cdot}$ and *x*-ions, along with neutral loss of $-CO_2$ from the same fragments, presumably lost from aspartic and glutamic side chains. Compared to ECD of the complementary positive ions, EDD yielded a lower percentage of backbone cleavage ions relative to the neutral loss peaks. Cysteine-rich proteins were found to yield *c*-ions in addition to $a^{-\cdot}$ and *x*-ions.

In a region of multiple acidic modifications, electrostatic forces can contribute to the unfolding of the tertiary structure and enhance the presence of backbone cleavages.[59] Activated ion electron detachment dissociation (AI-EDD) uses gas collisions to activate deprotonated protein anions. Håkansson and coworkers used AI-EDD and IRMPD in negative mode and compared this to AI-ECD and IRMPD in positive mode for top-down proteomics of acidic

proteins.[59] Overall, negative mode produced lower sequence coverage than positive mode. Positive-mode fragmentation did not yield backbone cleavages of proteins with multiple phosphorylation sites close to each other. These cleavages were seen in negative mode while using IRMPD.[59]

Some proteins and peptides contain disulfide bonds, which is a PTM. Disulfide bonds are known to stabilize native structures of proteins. Disulfide linkages can be identified by comparing proteolytic peptide spectra with and without reduction of the S-S bonds.[60] An alternative to this technique is using MS/MS methods. MALDI post-source decay (PSD), MALDI in-source decay (ISD), electron transfer dissociation (ETD), high-energy CID and ECD have been shown to cleave disulfide bonds.[2, 60-65] All of these are performed in positive ion mode, and therefore are not optimal for acidic proteins. Many proteins have phosphorylation and sulfation which makes them ideal for ionization in negative ion mode. For acidic proteins, EDD can produce more informative peptide backbone fragmentation than CID. Kalli *et al.* investigated multiple peptides containing disulfide bridges and found that in many cases, EDD resulted in the cleavage of C-S and S-S bonds. Researchers also found that the presence of tryptophan can enhance the fragmentation pathway at this residue, therefore suppressing disulfide cleavage. Tryptophan exhibits abundant product ions from loss of the sidechains.[60]

Application to Oligonucleotides

Oligonucleotides, including both DNA and RNA, have also been shown to dissociate well with electron-based activation methods. One level of characterization of oligonucleotides is to determine the sequence of the nucleotide residues. Oligonucleotides have been analyzed using ECD; however, since nucleic acids undergo facile deprotonation at the phosphate backbone, a

higher sensitivity is obtained in negative ion mode. Håkansson and coworkers demonstrated that EDD could produce fragmentation patterns similar to ECD for hexamer oligonucleotides.[13] EDD data of the oligonucleotides tested was extremely similar to previously obtained ECD spectra, however the EDD spectra contained a few more *c*/*x*-type ions and one more (*d*/*w*-*B*) ion (fragment types use the McLuckey convention).[66] They also found the formation of *a*/*z*-ion radicals in EDD, which were present as even-electron species in ECD. These results also showed that EDD can cleave covalent bonds without disrupting labile noncovalent interactions, just as ECD does.[13]

Hairpins are a common structural motif in nucleic acids. The assignment of hairpin structures provides valuable information for nucleic acid structure and folding predictions. Previous work has used MS/MS techniques, specifically CID and IRMPD to determine hydrogen bonding in DNA duplexes and the binding sites of RNA ligands. Mo *et al.* investigated AI-EDD, EDD, IRMPD and EDD/IRMPD MS^3 in negative ion mode to differentiate between different DNA sequences.[67] DNA samples with higher-order structures in the gas phase were investigated for this study. The more stable solution-phase nucleic acid structures generated fewer product ions in AI-EDD and EDD/ IRMPD MS^3. IRMPD was not able to differentiate between the different structures; however, it produces backbone cleavages at a higher extent than other methods.[67] For nucleic acid sequencing, EDD is a valuable complementary MS/MS method, as it provides additional structural information than traditional MS/MS techniques.

Breuker and coworkers investigated 22-76 nt RNA and examined vibrational ion activation and its effect on EDD fragmentation.[68, 69] A 34 nt RNA yielded *d*- and *w*- ions that covered 33 of the residues. The use of collisional activation of a 22 nt RNA before EDD did not produce additional sequence coverage, suggesting that higher-order gas-phase structure is not a

limiting factor in EDD of RNA oligonucleotides. Researchers found that an increased net charge on the precursor ion played a significant role in increasing sequence coverage. Increasing the net charge increases the Coulombic repulsion, therefore lowering the energy needed for dissociation. This should facilitate fragment ion formation and produce more backbone cleavages. The opposite behavior is observed for CID of RNA ions, which is most informative when the net negative charge is low. Taucher *et al.*[68] found that when combining CID and EDD data, almost complete sequence coverage can be obtained. CID produces *c*- and *y*- fragments while EDD produces *d*- and *w*- fragments. With CID, fragmentation occurs via even-electron pathways, and complementary *c*- and *y*- fragments are produced. However, EDD has a more unusual fragmentation pathway, producing an uncharged radical nucleoside and noncomplementary *d*- and *w*- fragments. Combining CID and EDD data provided full sequence coverage of a 76 nt tRNA sample.[41] The combined CID and EDD data can provide the presence, location and type of PTMs, however these techniques cannot distinguish residues of the same mass.

Ion-Ion Reactions

The first investigation of gas-phase electron transfer reactions using ion-ion reactions was reported in 1995 by McLuckey and coworkers,[70] who examined argon, krypton and xenon as singly-charged cations to serve as an electron acceptor. Polyadenylate anions served as the multiply-charged analytes in this study. Polyadenylate anions produced principally even-electron product ions, presumably from proton transfer reactions with acidic neutrals present in the background. However, some odd-electron product ions were observed, proving that electron transfer occurred between the oppositely-charged ions. This work showed that using this electron transfer reaction, even-electron precursor ions in the form or multiply-charged anions, could

yield odd-electron product ions, a behavior not seen by other activation methods.[70] These findings established a new field of dissociation methods utilizing ion-ion reactions. ETD was developed as an alternative to ECD by Syka *et al.* in 2004.[71] ETD is an ion-ion reaction that utilizes a source of anions, commonly fluoranthene, and analyte multiply-charged cations, resulting in electron transfer. The reagent anion works as a vehicle for electron delivery, where ECD utilizes a heated hollow cathode as the source for electrons. Like ECD, ETD requires multiply-charged precursor ions. This typically results in *c*- and *z*- type fragments for proteins and peptides. One of the major benefits to ETD is a capability to be implemented in many types of mass spectrometers. Initial reports of ETD were performed on phosphopeptides, using a linear ion trap mass spectrometer. ETD experiments occur as rapidly as CID and ECD experiments, occurring on the ms timescale. Therefore, ETD is easily paired with separation techniques such as LC and capillary zone electrophoresis (CZE).

Coon *et al.* investigated the ability for electron transfer reactions to perform similarly to EDD and produce backbone fragmentation for peptide anions in negative ion mode.[72] This work used xenon cations as the reagent ions. Deprotonated phosphopeptide anions produced both extensive fragmentation and associated charge reduction peaks. Both *a*- and *x*-type fragments were prevalent, and neutral losses of carbon dioxide and phosphoric acid were observed.[72] The fragmentation scheme for *a*- and *x*-ion production when using Xe^+ cations for electron abstraction is illustrated in Figure A.5. The ion-ion reaction resulted in a charge-reduced peptide, containing a radical site at the carboxyl group. Extraction of a hydrogen radical from a backbone amide nitrogen results in cleavage of adjacent C-C bond, producing *a*- and *x*-type product ions. At the C-terminus an electron is most likely lost to Xe^+ followed by free-radical-driven chemistry resulting in loss of CO_2. A second hydrogen radical loss then induces peptide

backbone fragmentation to generate *x*-type fragments. In comparison to what was originally reported for EDD of a deprotonated peptide, the ion-ion reaction produced similar results. Both methods saw neutral loss of CO_2 from the precursor as well as fragment ions. The main difference was the resultant fragment ion types; EDD produced *a*-, *c*-, and *z*-type fragments whereas electron transfer reactions produced *a*- and *x*-type fragments with minimal *c*- and *z*-type fragment production.[12, 72] Though the authors referred to this reaction as ETD, this, in fact, was the first example of the ion-ion reaction that later was named negative electron transfer dissociation (NETD).

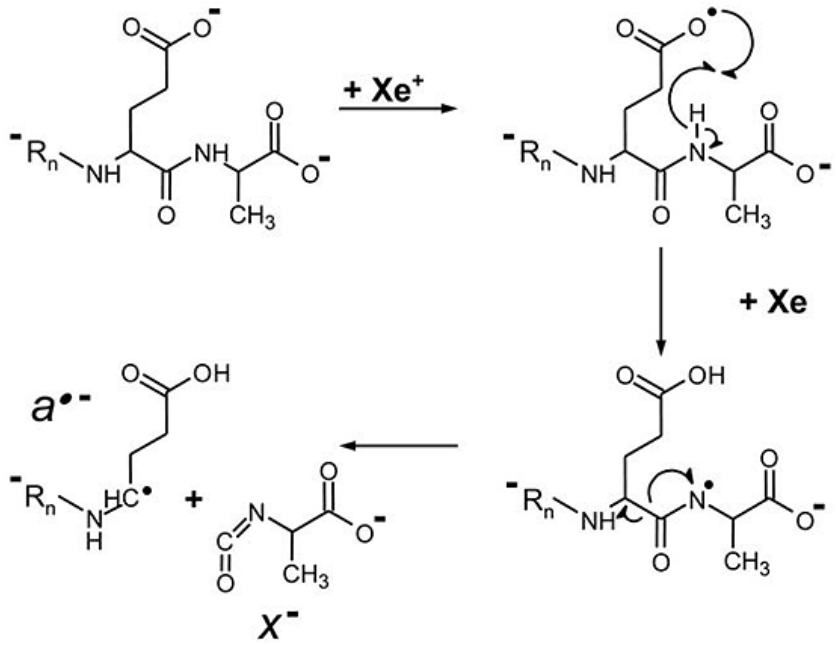

Figure A.5. Fragmentation scheme for production of a- and x-type ions by NETD using Xe^+ cations for electron abstraction from multiply deprotonated peptide, X_nEA, where X represents any amino acid. Reproduced with permission from ref 72. Copyright American Chemical Society 2005. Further permissions related to the material excerpted should be directed to the ACS.

Negative Electron Transfer Dissociation

One of the major appeals of ETD/NETD is the wider array of mass spectrometers that can be utilized compared to ECD and EDD, which originally were restricted to FTICR MS instruments. ETD/NETD experiments can be performed on several MS instrument platforms,

including ion trap and Orbitrap mass spectrometers, as well as FTICR instruments. Originally demonstrated by McLuckey and coworkers, a gas-phase electron transfer from a multiply-charged anion of interest to a rare gas cation results in the production of odd-electron product ions.[70] Singly-charged xenon and fluoranthene cations are commonly used as the electron acceptor; however, metal ions have also been used.[73] Another attractive feature of NETD compared to EDD is a higher reaction efficiency. In EDD, the two reactants (electrons and multiply-charged anions) bear the same polarity, and therefore repel each other, leading to a low reaction cross-section. On the other hand, with NETD (as well as for ETD), the two reactants have opposite polarity, and therefore have an attractive force between them, leading to a larger cross-section and a higher reaction rate. Another feature of NETD that distinguishes it from EDD is better control over the energetics of the reaction. The enthalpy of the electron transfer reaction is deposited in the precursor, resulting in a narrow energy distribution for the charge-reduced precursor, which then decomposes via various channels to yield an array of product ions. For NETD, all products must arise from the charge-reduced precursor ion. In comparison, EDD involves a collision between an electron and a precursor anion. The energy transferred depends on the impact factor (closest distance of approach between the electron and precursor ion), yielding intermediates with a broad range of internal energies. Some of these lead to charge reduced species, but others can decompose directly to products, without electron detachment of the precursor.

NETD Experimental Parameters

NETD has not been studied as systematically as EDD for fragmentation of negative ions. There is some data that examines the experimental parameters for NETD and how they affect fragmentation.[74-77] The two principal instrument parameters in NETD are reagent accumulation time and reaction time. For the solariX FTICR MS, the reagent accumulation time is typically set between 200-500 ms, and the reaction time is set between 50-500 ms.[74-77] Recent studies have shown that when using fluoranthene as an electron acceptor, less time is needed for both reagent accumulation and reaction time, making the experiment more time efficient (200 ms and 50 ms respectively).[74] When using an Orbitrap MS, reaction time is usually set between 10-110 ms, with higher charge state precursors needing less time to react with the reagent.[78, 79]

Another important experimental parameter is the choice of the reagent ion. Fluoranthene is commonly used in both FTICR MS and Orbitrap MS instruments, both for ETD and for NETD; however, fluoranthene is not the only reagent ion option. Coon and coworkers[80] implemented sulfur pentafluoride as a reagent cation for NETD experiments. Sulfur pentafluoride cation is produced by electron ionization of sulfur hexafluoride and has a higher ionization energy (9.6 eV) than fluoranthene (7.9 eV). The increased ionization energy impacts the enthalpy of the ion-ion reaction, which is equal to the difference in the electron affinity of the charge-reduced product and the recombination energy of the reagent ion. When using sulfur pentafluoride for proteomics they found an increase in informative fragmentation and a decrease in non-dissociative negative electron transfer compared to fluoranthene cation as the reagent. Thus far this reagent cation has only been tested for proteomics; however, it would in theory help improve fragmentation results for other negative ion analytes as well. Xenon has also been extensively studied as a reagent ion for both ETD and NETD. Xenon also has a higher ionization

energy (12.1 eV) than fluoranthene which makes the ion-ion reaction more energetic. With sulfated carbohydrates, this led to a higher yield of cross-ring fragmentation, but also produced more of the undesirable neutral loss products from sulfo-degradation.[76] NETD of phosphopeptides by Huzarska *et al.* also found a higher yield of undesirable neutral loss products when the reagent ion was Xe^+ compared to fluoranthene cation.[81] This work is discussed in greater detail below.

Application to Oligosaccharides

Amster and coworkers performed the seminal studies of the application of NETD to glycosaminoglycans to obtain structural information. Initial work using NETD on GAG standards utilized both fluoranthene and xenon cations as the electron acceptor.[76] Both produced EDD-like fragmentation; however, loss of the sulfate half ester was minimized when using fluoranthene compared to xenon, due to the lower recombination energy of fluoranthene (7.9 eV) versus xenon (12.1 eV). Overall, more sulfate loss was seen using NETD than EDD; however, this could be minimized with a higher charge state or addition of sodium atoms, resulting in a more ionized precursor. NETD was also shown to distinguish the epimers GlcA and IdoA in HS tetramers. All diagnostic fragments determined previously using EDD (B_3', B_3'-CO_2 and $^{0,2}A_3$ only present in GlcA spectra) were present in NETD spectra.[76] The initial work was performed on an ion trap mass spectrometer, which demonstrated a significant feature of NETD compared to EDD, namely that it can be implemented on a broader array of mass spectrometry platforms. However, for the structural characterization of GAGs larger than tetrasaccharides, higher resolution is required than can be obtained on an ion trap instrument. Amster and coworkers extended their exploration of the utility of NETD for GAG analysis first to FTICR MS,[77] and

then later to the Orbitrap platform.[79] When using NETD for the structural characterization of GAG standards on an FTICR MS, Leach *et al.* found that NETD provides sufficient cross-ring cleavages enabling the identification of sulfate position.[77] By utilizing an FTICR MS, the mass resolution was high enough to confidently assign product ions. NETD and EDD spectra were not identical due to the lack of electronic excitation products seen with NETD. However, this allows for NETD experiments to occur on a much shorter timescale than EDD (50 ms versus 1-3 seconds), making it more suitable for coupling with online separations. Lin and coworkers conducted a comparison of NETD and EDD for Hp and HS oligosaccharides as well as the heparin-like synthetic highly sulfated pentasaccharide, Arixtra™, by FTICR MS. They were able to optimize EDD so that they could obtain data on the LC timescale. This was done by replacing a conventional ESI source with a nanoelectrospray source, which made it possible to minimize sample consumption while maximizing precursor ion intensity.[82] They showed that NETD was faster and far more efficient and produced higher intensity fragment ions with less neutral loss of SO_3, and was better suited for online LC separations.[82] Figure A.6 shows the ability for NETD to produce EDD-like fragmentation while more efficiently converting precursor ion to fragment ions.

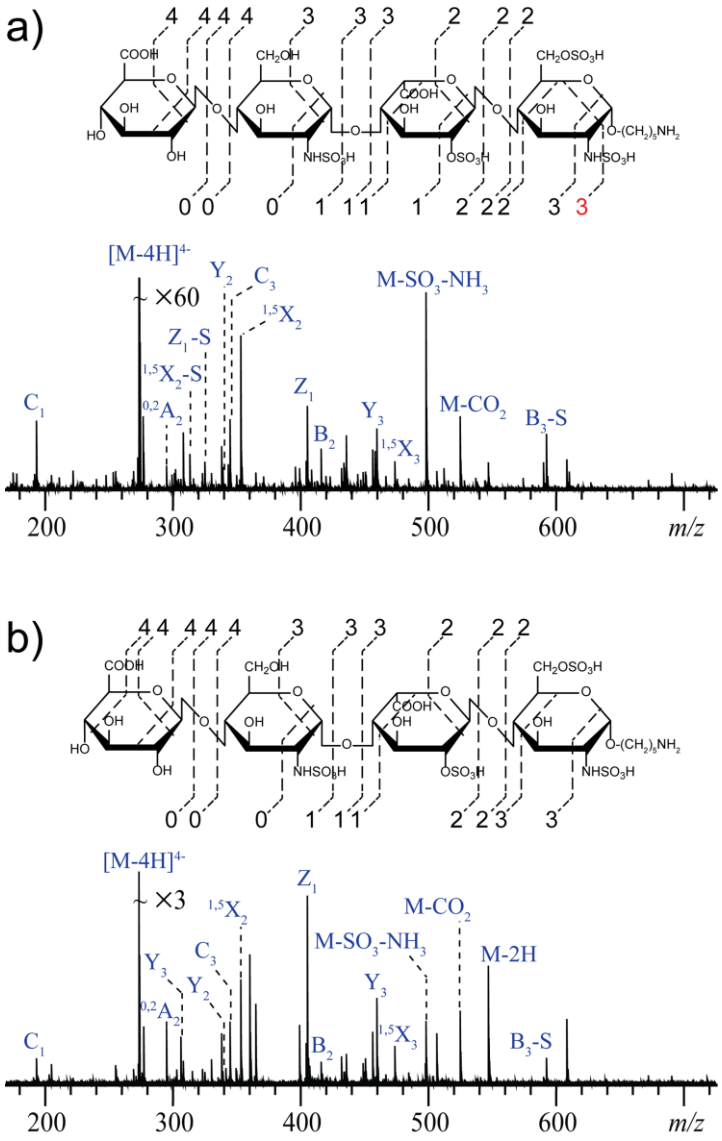

Figure A.6. (a) EDD and (b) NETD spectra and cleavage maps of synthetic HS tetrasaccharide GlcA-GlcNS-IdoA2S- GlcNS6S-O$(CH_2)_5NH_2$. Reproduced with permission from ref 82. Copyright American Chemical Society 2013. Further permissions related to the material excerpted should be directed to the ACS.

ETD and NETD are options on some Thermo Fisher Orbitrap mass spectrometers. Orbitrap analyzers provide much higher mass resolution compared to ion trap mass spectrometers and are more widely available than FTICR instruments. Amster and Coons tested NETD on an Orbitrap Elite for the fragmentation of GAG oligosaccharides, and compared these data to results of EDD and CID on an FTICR MS.[79] This work examined GAG standards ranging from tetrasaccharides to decasaccharides, including Arixtra™. NETD on the Orbitrap MS produced similar fragmentation to EDD by FTICR MS, with a reduction in sulfate decomposition compared to CID. Figure A.7 shows the ability for NETD to produce both a higher intensity and diversity of cross-ring cleavages than EDD. CID also requires a highly ionized precursor to produce informative fragmentation, whereas NETD requires less deprotonation of the precursor. NETD has a high efficiency for converting precursor and can be executed on a millisecond timescale with the Orbitrap Elite. Alternatively, EDD experiments requires a 1 s pulse length, making it difficult to pair to online separation techniques. This makes NETD a good choice for activation of negative ions when coupled to separation methods such as LC or CZE.

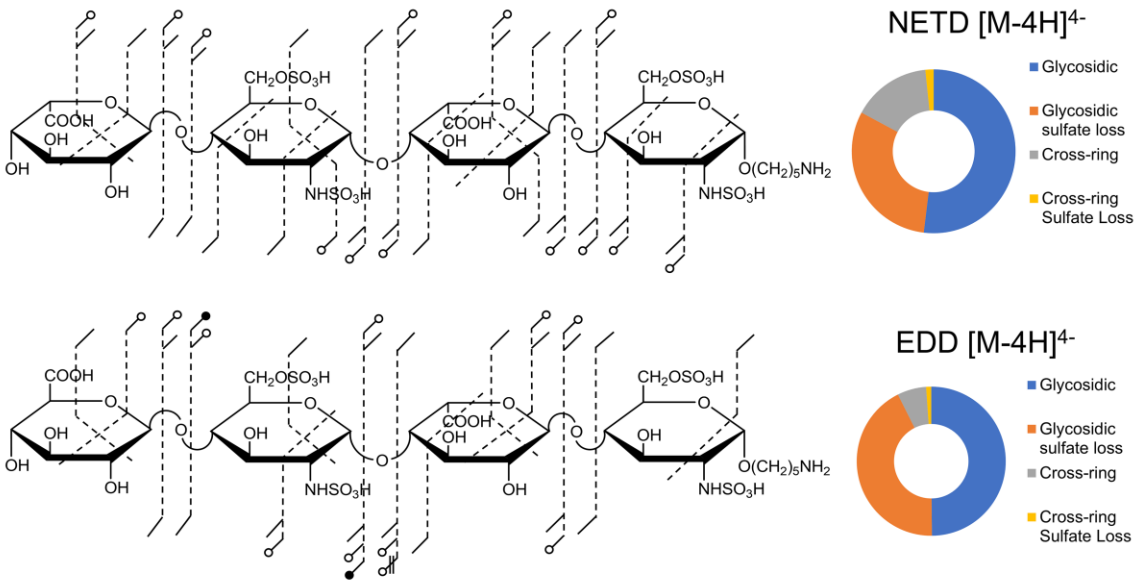

Figure A.7. Cleavage maps comparing NETD and EDD activation for the $[M-4H]^{4-}$ precursor of the synthetic tetrasaccharide GlcA-GlcNS6S-IdoA-GlcNS6S-$O(CH_2)_5NH_2$. Donut plots represent the intensity distribution of fragment ion types. Reproduced with permission from ref 79. Copyright American Chemical Society 2017. Further permissions related to the material excerpted should be directed to the ACS.

The pharmaceutical product, enoxaparin, is a complex mixture of low molecular weight Hp. Using CZE-MS, enoxaparin was separated into its individual components that migrated within a 15-20 min window.[78, 83] This resulted in 37 unique compositions being identified. These compositions were then confirmed using MS/MS, specifically NETD in this study. Pairing

NETD with online CZE resulted in lower charge state precursors than direct infusion, which makes CID a less ideal match for sequencing GAGs by CZE-MS/MS. Enough information from lower charge states is obtained when using NETD, and sites of sulfo-modifications can be identified. It was also seen that as the degree of sulfation increased, the charge states seen using CZE-MS/MS increased as well.

Zaia and coworkers have successfully paired hydrophobic interaction liquid chromatography (HILIC) with NETD.[74] MS/MS sequencing of GAGs has been widely studied over several decades, as shown within this chapter. However, LC-MS/MS of GAGs has remained a challenge. By utilizing an ion suppressor, more highly-charged precursor ions are produced. NETD has been previously shown to successfully fragment GAGs of lower charge state than can be tolerated by other MS/MS techniques. By utilizing both an ion suppressor and NETD, Zaia and coworkers successfully demonstrated complete characterization of a range of GAG standards, varying in degree of polymerization and sulfation. A separate assessment of NETD for the characterization of GAGs conducted by Zaia and coworkers investigated synthetic HS hexasaccharides with 3-*O* sulfation.[75] Though 3-*O* sulfation is a rare modification, it is a critical feature in several binding motifs with biological functions such as anticoagulation and glycoprotein binding. Their work showed the ability of NETD to produce informative fragmentation needed to identify sulfation locations while using a less deprotonated precursor ion than previously observed for NETD. Neither CID nor EDD could provide this level of structural assignment for the same precursors.

Ion mobility spectrometry (IMS) has emerged as an alternative for separation of GAG isomers. IMS sorts analyte ions based on their size and charge. Isomers show differences in their collision cross sections (CCS) and their mobilities as a function of their gas-phase

conformations. The CCS of an analyte provides additional information for identification. FAIMS has been previously used to separate and characterize HS tetrasaccharide epimers using EDD data.[45] However, FAIMS does not provide a CCS value, and is also restricted by low sensitivity and limited peak capacity. FAIMS separates ions based on their differential mobilities in strong and weak electric fields.[84] In contrast, trapped ion mobility mass spectrometry (TIMS) allows for high mobility resolution and ion transmission efficiency.[85, 86] TIMS occurs in a modified dual ion funnel near the ESI interface region of a mass spectrometer, and has been implemented with both time-of-flight and FTICR mass spectrometers. TIMS has been successfully paired with NETD for the analysis of glycosaminoglycans by FTICR MS.[87] Gated-TIMS selects ions of a specific mobility by a pulsed voltage which releases the desired ions for storage in a low pressure collision cell. The advantage of this arrangement over the original implementation of TIMS, called selective accumulation (SA) TIMS, is that the ions undergo less collisional heating. For thermally labile analytes, this is an important feature that reduces the decomposition of sulfo modifications in GAGs. When pairing gated-TIMS with NETD, not only were labile sulfate groups retained, but also isomeric structures were resolved. Tetramers and hexamers were examined, that were both isomeric in the location of sulfo modifications and stereoisomeric differing by IdoA/GlcA. Figure A.8 shows gated-TIMS NETD MS/MS of a mixture of three isomeric GAG hexamers. Online gated-TIMS NETD MS/MS yielded a high degree of fragmentation and sulfo retention. NETD also yielded many diagnostic fragments for differentiating isomer pairs. These fragment ions in combination with gated-TIMS yielding unique CCS values for the isomers allowed for differentiation of isomers and stereoisomers. Scrivens and coworkers utilized travelling-wave ion mobility mass spectrometry (TWIMS) and CID in negative ion mode to distinguish high-mannose N-glycans.[88] The use of TWIMS allowed

for separation of isomeric compounds and the use of negative ion mode increased the detection ability of the isomers. By combining TWIMS with CID, a more complete story can be told. TWIMS can separate isomers and CID can determine the differences between the isomers as well as allow for structural characterization.

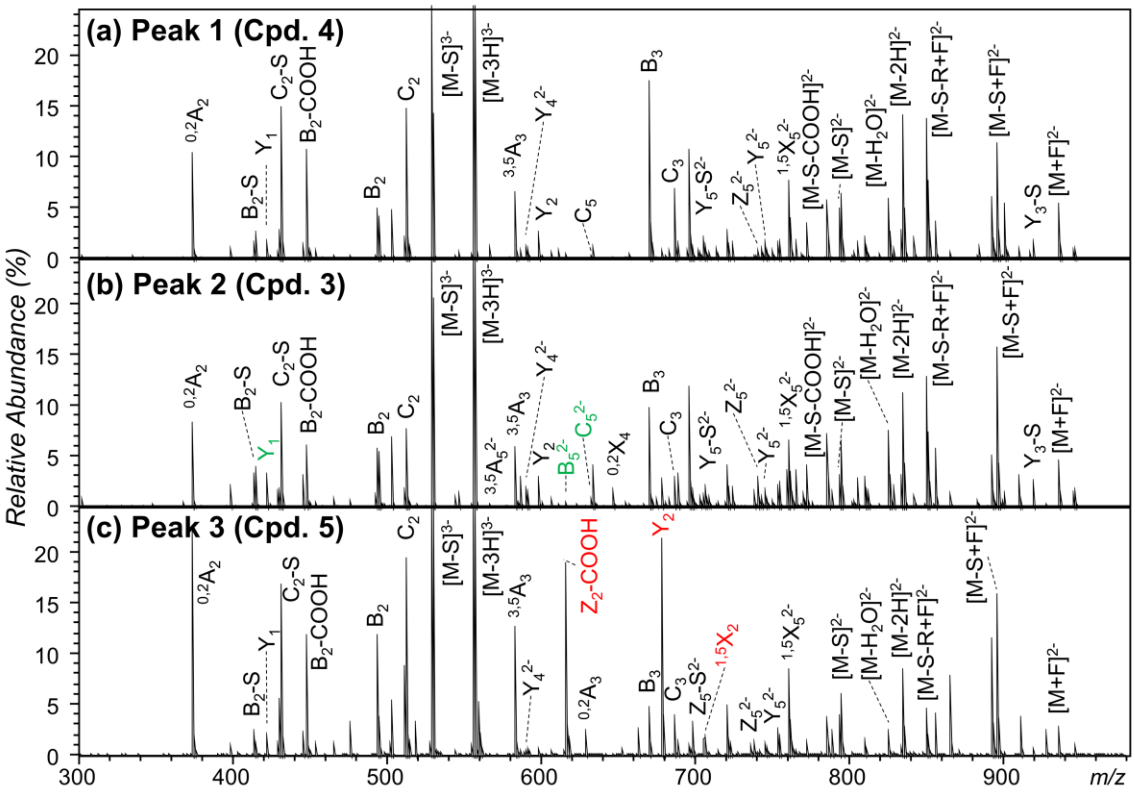

Figure A.8. Gated-TIMS NETD MS/MS of a mixture of three isomeric heparan sulfate hexamers, for the $[M-3H]^{3-}$ precursor ion. Sulfo losses are labeled as -S, fluoranthene adducts are labeled as +F, losses of the aminopentyl group are labeled as -R. Reproduced with permission from ref 87. Copyright American Chemical Society 2019. Further permissions related to the material excerpted should be directed to the ACS.

Application to Proteins

MS/MS of peptide anions has been studied far less than for their positive ion counterparts. Work by Huzarska *et al.* explored different cationic reagent ions when using NETD.[81] Researchers found that when using fluoranthene cations for NETD, *a*- and *x*-fragments arise by cleavage at the C_α-C bond, creating similar products to those observed by EDD. This leaves the phosphorylation modification intact and enables the localization of the PTM site. When using Xe^+ cations as the electron acceptor, neutral loss accompanies the formation of *a*- and *x*-type fragment ions, resulting in more complex spectra with no additional information. The increase in neutral loss is due to the higher enthalpy of the ion-ion reaction from using a reagent ion with a higher ionization potential, Xe^+ (12.1 eV) versus fluoranthene (7.9 eV). It was also seen that proton transfer was a minor channel in the case of fluoranthene (20%), but very abundant when using Xe^+ (up to 82%). The high abundance of proton transfer when using Xe^+ cations is most likely due to Xe^+ radicals ionizing other molecules within the ion trap, and these ionized molecules then react with the peptide anion. Proton transfer is highly exothermic and can result in non-ETD-type products. Addition of the fluoranthene ion to the charge-reduced radical product ion was reported and has since been reported by others when using fluoranthene for NETD.

Coon and coworkers showed the capability of NETD to produce sequence information for peptide anions.[89] However, positive ion mode experiments produced approximately three times as many informative fragments as negative ion mode. The authors postulated this to be a result of a lower flux of peptide anions and a propensity to form lower charge states in negative mode. On the other hand, negative-mode proteomics was found to access acidic portions of the

proteome that were not covered in positive ion mode. To improve negative-mode performance, NETD was coupled with concurrent or supplemental activation. Supplemental activation can separate product ions that are held together by intramolecular noncovalent interactions, giving rise to non-dissociative negative electron transfer. This approach is based on the success of activated ion ETD (AI-ETD), a powerful tool for proteomics applications.[90] Coon and coworkers designed a multipurpose dissociation cell (MDC) which allows for faster ETD reaction times and larger precursor ion populations.[90] The MDC replaces the HCD cell in an ETD-enabled Orbitrap MS, which is the ideal placement for implementing activated ion NETD (AI-NETD). A continuous wave CO_2 laser can be easily introduced to the MDC. When coupling AI-NETD experiments with a high-pH solvent system anion flux increases, providing a better distribution of precursor charge states. This work also utilized a reverse phase LC system. LC-MS/MS using AI-NETD characterized more than 80% of the yeast proteome, a substantial improvement over results obtained using positive ion mode and implementing multiple fragmentation techniques, producing approximately 45% proteome coverage. Figure A.9 shows the ability for AI-NETD to improve precursor to product ion conversion resulting in enhanced peptide dissociation compared to NETD. AI-NETD also resulted in improved protein sequence coverage (12% improvement on average) compared to what can be achieved with positive ion mode methods. Negative ion mode methods can provide complementary information with continued implementation of robust fragmentation techniques to information obtained using positive ion mode.

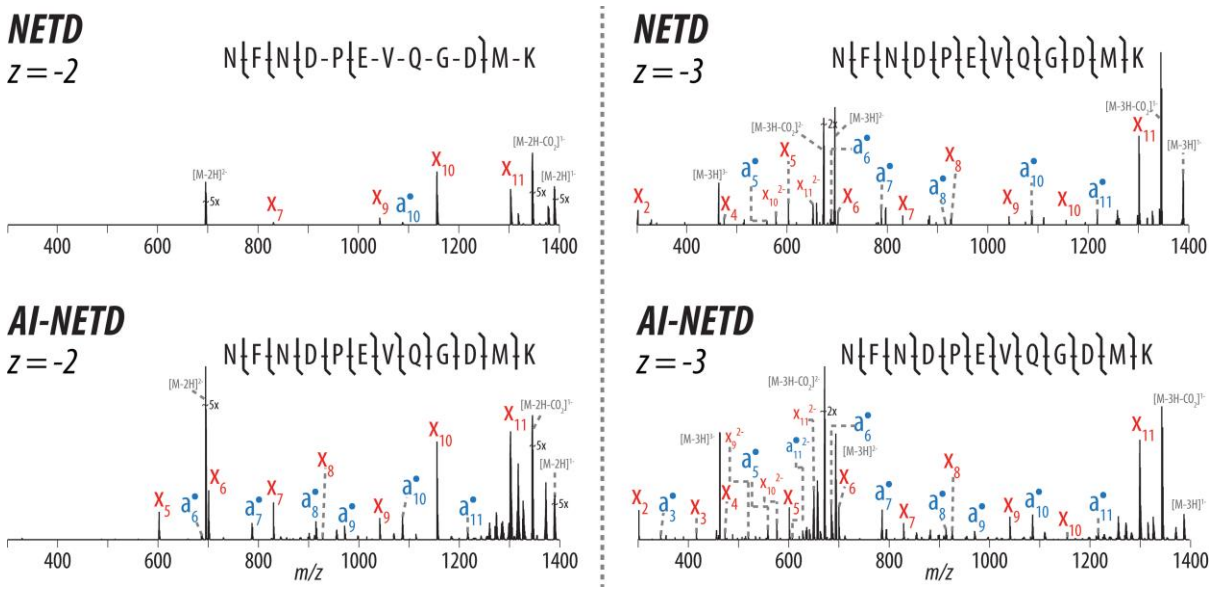

Figure A.9. NETD and AI-NETD MS/MS spectra for the $[M-2H]^{2-}$ and $[M-3H]^{3-}$ precursor ions of the same peptide. AI-NETD shows improved precursor to product ion conversion for low charge state precursors, in this case increasing sequence coverage from 45% to 100%. At higher charge both NETD and AI-NETD produced 100% sequence coverage. Republished with permission of The American Society for Biochemistry and Molecular Biology (2015) from ref 90. Copyright The American Society for Biochemistry and Molecular Biology 2015.

With the emergence of NETD as a powerful analysis tool for protein and peptide anions, there is a need for a more comprehensive data analysis tool. Riley *et al.* developed a search algorithm specifically for AI-NETD and NETD data sets.[91] This algorithm does not require preprocessing of spectra, and utilizes features from the ByOnic database search software package, including rank-based scoring, *m/z* errors, predicted intensities based on longer or more acidic precursor peptide sequences, and two-dimensional false discovery rate (2D-FDR) protein-aware calculations. 2D-FDR provides half of the sensitivity gain of this new algorithm, whereas

the other half sensitivity gained is attributed to the other three aforementioned features. This software advance makes the data analysis process more streamlined and robust for proteomics users.

CID is the most popular activation method for peptide sequencing, due in large part to its wide availability. However, phospho- and sulfo-half esters are labile, and CID often leads to the loss of these PTMs.[53] Other techniques in positive mode, specifically ETD and ECD, have also been used for this analysis and both these activation methods maintain these labile PTMs while producing fragmentation along the peptide backbone. NETD and EDD of negatively charged precursors have also been examined and present promising complementary tools for peptide anion analysis. McLuckey and coworkers recently investigated the ability to distinguish phosphopeptides and sulfopeptides from each other.[52] They used a gas-phase ion-ion charge inversion technique. Guanidinium exhibits a strong noncovalent interaction to phosphate and sulfate groups in the gas phase. Ion-ion reactions are induced between singly-charged peptide anion mixtures and a guanidinium-containing peptide. This cationic peptide complex is exposed to a broadband collisional activation using dipolar direct current (DDC).[52] Due to the binding strength between the two peptides being dependent on functional group interactions, DDC serves as an energy filter. The strengths of the electrostatic interactions of guanidinium and acidic sites' conjugate bases were determined to increase from carboxylate < phosphonate < sulfonate. When a doubly protonated reagent peptide containing at least two arginine residues was reacted with singly deprotonated peptides in the gas phase, a peptide complex was formed. The DDC amplitude and time could then be selectively chosen to fragment specific complexes. With a lower DDC amplitude, unmodified peptide complexes were fragmented while retaining a majority of complexes with sulfo- or phosphopeptides. A higher DDC amplitude was then able

to fragment phosphopeptide complexes while retaining the sulfopeptide complexes. This illustrated the importance of non-covalent interactions affecting complex ion stabilities.[52]

Application to Oligonucleotides

McLuckey and coworkers[92] investigated rubrene radical cations as an electron acceptor for deprotonated RNA and DNA samples. Rubrene is a polycyclic aromatic hydrocarbon with elemental formula of $C_{42}H_{28}$ and an ionization energy of 6.4 eV. Researchers saw NETD products, complex formation, and NET-no-D products (electron transfer with no dissociation). They found that the relative abundances of NET-no-D products (G > A > C > T) were inversely proportional to the nucleobase ionization potential (G < A < C < T). Complex formation however was directly related to the ionization potential of the nucleobase. NETD products included *w*/*d*- ions and *a*/*z*- radical ions. These products were only seen with highly deprotonated precursor ions. Which reaction channel occurs is not only dependent on the degree of precursor deprotonation but also the oligonucleotide composition and length. The same trends were seen with DNA 6-mer and RNA 8-mer analyte samples. Improved coverage can be achieved by simultaneous activation of the NET-no-D radical anion products (termed negative electron transfer collision induced dissociation). This leads to abundant *w*/*d*-ions and *a*/*z* radical ions, which are the expected products when successfully performing NETD.

Brodbelt and coworkers performed a comprehensive comparison of various ion activation methods for the ability to generate the most informative sequence-specific fragment ions for DNA/cisplatin adducts including cisplatin-modified oligodeoxynucleotides (ODNs).[93] This study examined CID, IRMPD, UVPD, ETD, electron transfer ultraviolet photodissociation (ET-UVPD), electron transfer collision activated dissociation (ETcaD) and electron transfer IRMPD

(ET-IRMPD). This work was performed in both positive and negative ion mode to provide a full systematic comparison of MS/MS spectra. ODNs contain an acidic phosphodiester backbone that is readily deprotonated to produce negative precursor ions. ODNs also undergo protonation of their nucleobases, making it feasible to use both polarities for their analysis. Overall CID produced mostly base loss products, as well as *a-B*, *w*- and internal fragment ions. IRMPD and UVPD both were more proficient when used in negative ion mode for locating platinum modifications. IRMPD and UVPD also produced increased fragment ion diversity, including fragment ions which maintained the cisplatin modification. Both ETD and NETD resulted in limited backbone cleavages and charge reduction. ETcaD produced similar fragmentation to CID, however with *a*/*z*- ions present. ET-IRMPD produced fragmentation similar to IRMPD. UVPD, IRMPD and ET-UVPD/ET-IRMPD can be employed to evaluate sequence-selective reactivities of cisplatin with ODNs and characterize resulting adducts. To obtain full structure elucidation of DNA crosslinks, these MS/MS methods should be combined with enzymatic digestion.

Other Methods

Electron induced dissociation (EID), also known as electron-impact excitation of ions from organics (EIEIO), and electronic excitation dissociation (EED) results in ECD-/EDD-like fragmentation for singly-charged ions.[4] This technique utilizes 6-20 eV electrons to irradiate singly-charged precursor ions. This was originally presented as a useful tool for molecules that do not typically produce multiply-charged ions. EID was first applied to small molecules and peptides, resulting in fragmentation comparable to IRMPD and CID.[94] This was unexpected, as the fragmentation pathway of EID occurs via electronic excitation, whereas IRMPD and CID

both produce vibrational excitation. Wolff *et al.* used EID to examine HS and DS GAG tetrasaccharides.[95] These data show that EID of singly-charged GAGs produces many similar fragment ions to those formed by EDD. These results suggest that some product ions in NETD are also produced by electronic excitation but without electron detachment. Many of the product ions produced by EID, specifically cross-ring fragments, and odd-electron products, were not seen when using IRMPD, as shown in Figure A.10. A similar consensus was seen when using EID to dissociate negatively charged peptides.[96] Many *b*-, *y*-, *a*-, *c*-, and a handful of *x*- and *z*-type ions were seen in both EID and CID for peptide anions. However, both CID and EID spectra had unique fragment ions. This would suggest that ions activated by EID and CID not only undergo different fragmentation pathways, but that EID produces both electronic and vibrational excitation of the precursor ion. EID has been used for many other sample types, including polyketides, amino acids, small pharmaceuticals and non-ribosomal peptides.[97-101]

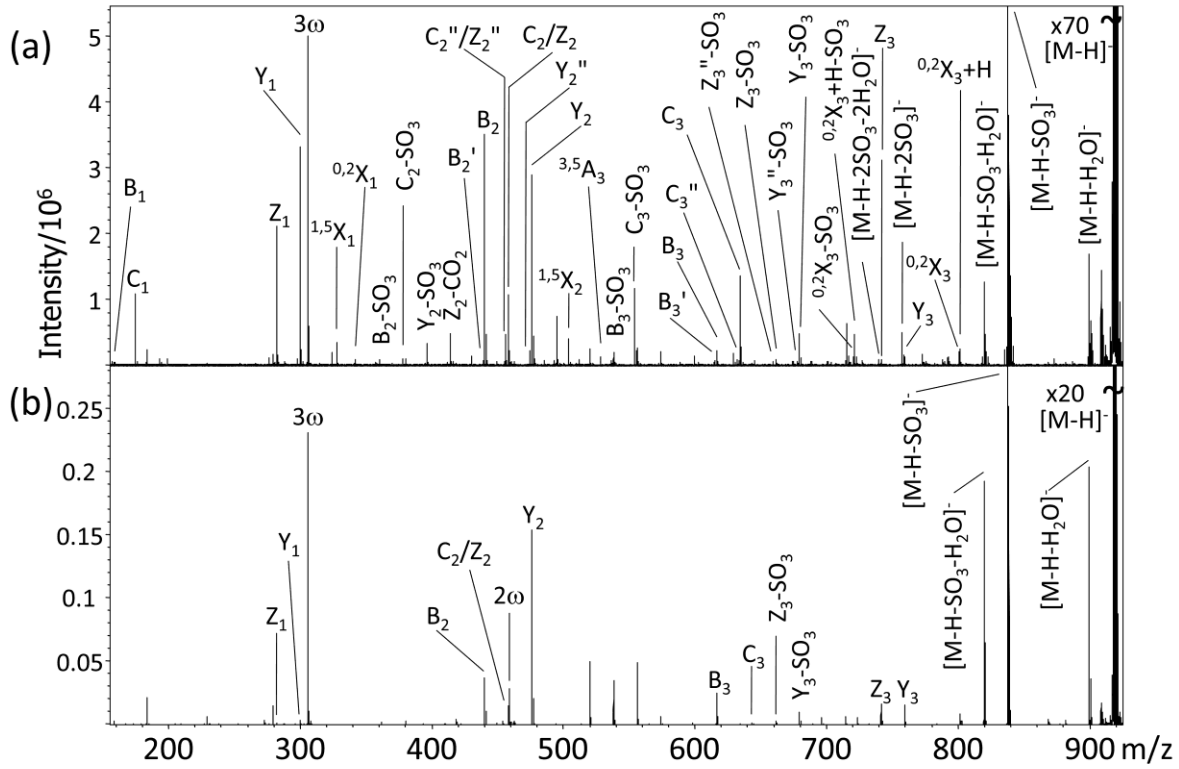

Figure A.10. (a) EID and (b) IRMPD tandem mass spectra of the $[M-H]^-$ precursor ion of a dermatan sulfate tetrasaccharide. Odd-electron product ions are shown with a box surrounding the annotation. Reproduced with permission from ref 95. Copyright American Chemical Society 2008. Further permissions related to the material excerpted should be directed to the ACS.

Negative ion ECD (niECD) is a particularly unexpected outcome of a reaction between an anionic precursor and an electron that results in electron capture, and an increase in the charge state of the precursor. niECD uses long irradiation times (10-20 s) with a narrow range of electron energy (3.5-6.5 eV). This reaction was first introduced by Yoo *et al.* who observed that

peptide anions capture an electron,[102] resulting in charge-increased radical species that undergo ECD-like fragmentation.[97] The hypothesis for the unexpected anion reaction is that the electron is attracted to a positively charged region of a gas-phase zwitterionic structure. Acetylation of the primary amine of peptides decreases niECD efficiency while the presence of quaternary amines with a fixed positive charge promotes niECD. Further work on sulfopeptides showed that niECD can fragment precursors with complete sulfonate retention, and provide full sequence information.[103] niECD was superior to NETD and EDD for this sample type due to its ability to produce minimal neutral loss in the formation of fragment ions. Additionally, niECD was shown to minimize hydrogen migration and demonstrated moderate hydrogen/deuterium scrambling when investigating the extent of intramolecular H/D scrambling using negative ion mode MS/MS techniques.[104] There was a reduced amount of H/D scrambling compared to that produced by CID and free radical-initiated peptide sequencing (FRIPS). EDD produced a similar degree of scrambling to CID while in contrast, niECD was better than EDD and CID at minimizing hydrogen migration. The negative ion methods tested were not considered to be better than positive ion mode hydrogen/deuterium exchange (HDX) MS/MS experiments. The incompatibility specifically of niECD for HDX is most likely due to the energetics being too high.

Electron photodetachment dissociation (EPD) has been studied for the structural characterization of oligonucleotide anions. EPD of nucleic acids was first introduced by Gabelica *et al.* for the analysis of DNA strands.[105] A laser irradiation event causes electron detachment. Both EPD and EDD involve electron detachment from multiply deprotonated species, which leads to radically-driven dissociation of the oxidized species. In the initial EPD work, DNA strands containing guanine were found to dissociate well using 260 nm from a Nd^{3+}:YAG-

pumped OPO laser. Once photodetachment has occurred, CID could be used to fragment the sample further. Figure A.11 shows the benefit of using EPD-CID compared to CID alone for the activation of DNA strands. This concept is known as activated-EPD (a-EPD) which implies subsequent collisional activation of the radical oxidized species.[106] More structurally informative peaks were observed in the EPD spectra than by CID. However, when comparing EPD to EDD of oligonucleotides, it appeared that EDD did not require the presence of guanine for electron detachment, an advantage over EPD which does require the presence of guanine residues. EPD has been shown to be highly dependent on the base sequence of oligonucleotides, and electron detachment is inversely related to the ionization potentials of the bases.[107] EPD and EDD have different fragmentation pathways and therefore can provide complementary information for oligonucleotides. De Pauw and coworkers investigated the effect of chain length on the fragmentation pathways of EDD and EPD.[108] Fragmentation pathways that are ergodic become less favored as the chain length increases, whereas non-ergodic and low-threshold ergodic fragmentation pathways are favored as the chain length increases. Previous work by Håkansson and coworkers proposed that incomplete sequence coverage can be due to gas-phase intramolecular folding.[67] Complete sequence coverage of unstructured oligonucleotides with up to 20 thymine nucleobases was achieved using EPD, further validating the proposal by Håkansson and coworkers. EPD has also been analyzed for peptide anions.[106, 109] Radical species formed by EPD have modest excess internal energy, making it significantly less prone to dissociation. This can be overcome by using a-EPD. When investigating lasso peptide anions, which are bacteria-produced bioactive peptides, EDD and a-EPD produced informative fragment ions unlike CID.[106] By utilizing FTICR MS, ion identities can be confidently assigned. There is a benefit in using both EDD and a-EPD since the data complement each other. Lasso peptides are

entangled structures, and these electron dissociation techniques can produce two-peptide product ions, which result from either a mechanical interlock or an unknown stabilization mode. Entangled structures also are more prone to H radical transfers and consecutive dissociation.[106]

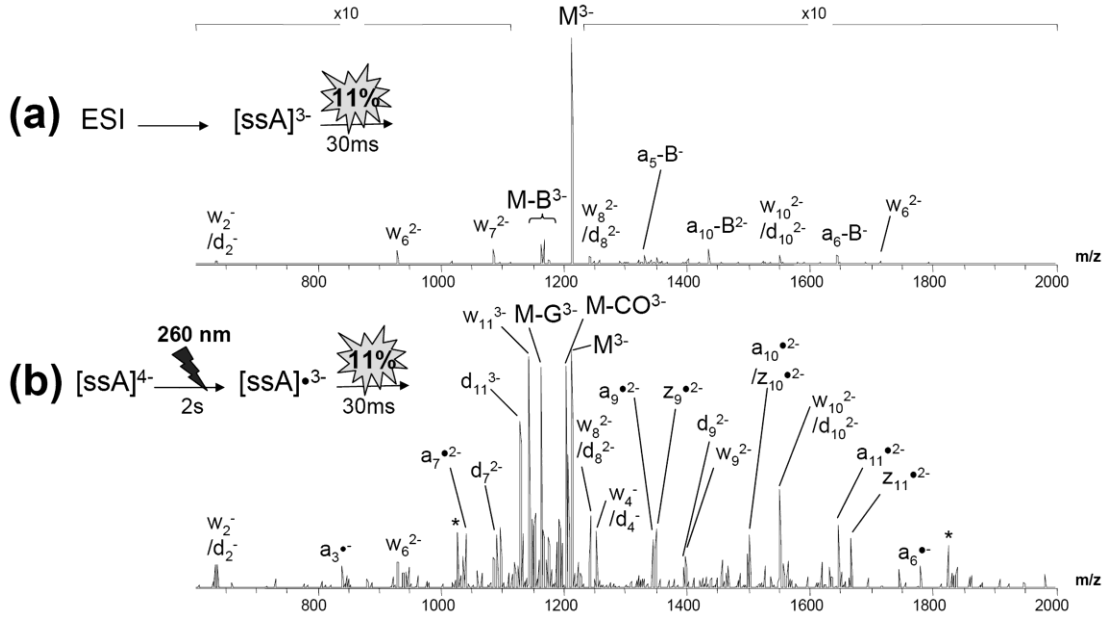

Figure A.11. (a) CID spectrum of $[ssA\text{-}3H]^{3-}$ with 11% activation amplitude for 30 ms. (b) EPD-CID spectrum of $[ssA\text{-}4H]^{\cdot 3-}$ produced by electron photodetachment of a single-stranded DNA, $[ssA\text{-}4H]^{4-}$, using the same CID parameters as in the top panel. Parent ion is shown as M in both spectra. Asterisks indicate two electronic noise spikes. Reproduced with permission from ref 105. Copyright American Chemical Society 2006. Further permissions related to the material excerpted should be directed to the ACS.

Summary

Here we have presented a review of electron-based methods for the dissociation of negative ions. Following the success of ECD for positively-charged ions, a negative ion mode complement, termed electron detachment dissociation (EDD), was developed for acidic compounds. Multiply-charged negative ions are activated by collisions with electrons, leading to electron detachment and the production of a charge-reduced radical species that can undergo fragmentation that is quite different than observed for the dissociation of even-electron species. EDD provides good structural details for acidic proteins, oligosaccharides, and oligonucleotides; however, it is inefficient at converting precursor ions into fragment ions. Negative electron transfer dissociation (NETD) is an ion-ion reaction that produces fragmentation similar to that found in EDD mass spectra. NETD is more efficient at converting precursor ion to fragment ions than EDD and can be implemented with a wider array of mass spectrometer types than EDD. It produces a higher abundance and diversity of fragment ions for acidic compounds. Though EDD and NETD are the most investigated negative ion electron-based activation methods, other methods including negative ion electron capture dissociation (niECD) and electron photodetachment dissociation (EPD) have also shown promise for the analysis of negative ions.

Acknowledgements

The authors are grateful for the financial support of the National Institutes of Health, grants U01-CA231074, S10-OD025118, and P41-GM103390.

References

(1) Zubarev, R. A.; Kelleher, N. L.; McLafferty, F. W., Electron Capture Dissociation of Multiply Charged Protein Cations. A Nonergodic Process. *J Am Chem Soc* **1998,** *120*, 3265-3266.

(2) Zubarev, R. A., Electron-capture dissociation tandem mass spectrometry. *Curr Opin Biotechnol* **2004,** *15*, 12-16.

(3) Wolff, J. J.; Amster, I. J.; Chi, L.; Linhardt, R. J., Electron detachment dissociation of glycosaminoglycan tetrasaccharides. *J Am Soc Mass Spectrom* **2007,** *18*, 234-44.

(4) Haselmann, K. F.; Budnik, B. A.; Kjeldsen, F.; Nielsen, M. L.; Olsen, J. V.; Zubarev, R. A., Electronic excitation gives informative fragmentation of polypeptide cations and anions. *Eur J Mass Spectrom* **2002,** *8*, 117-121.

(5) Baba, T.; Hashimoto, Y.; Hasegawa, H.; Hirabayashi, A.; Waki, I., Electron capture dissociation in a radio frequency ion trap. *Anal Chem* **2004,** *76*, 4263-4266.

(6) Ding, L.; Brancia, F. L., Electron capture dissociation in a digital ion trap mass spectrometer. *Anal Chem* **2006,** *78*, 1995-2000.

(7) Robb, D. B.; Brown, J. M.; Morris, M.; Blades, M. W., Tandem mass spectrometry using the atmospheric pressure electron capture dissociation ion source. *Anal Chem* **2014,** *86*, 4439-4446.

(8) Voinov, V. G.; Deinzer, M. L.; Barofsky, D. F., Radio-Frequency-Free cell for electron capture dissociation in tandem mass spectrometry. *Anal Chem* **2009,** *81*, 1238-1243.

(9) Fort, K. L.; Cramer, C. N.; Voinov, V. G.; Vasil'ev, Y. V.; Lopez, N. I.; Beckman, J. S.; Heck, A. J. R., Exploring ECD on a Benchtop Q Exactive Orbitrap Mass Spectrometer. *J Proteome Res* **2018,** *17*, 926-933.

(10) Voinov, V. G.; Otis, C.; Beckman, J. S.; Vasil'ev, Y. Reflectron-electromagnetostatic cell for ECD fragmentation in mass spectrometers. 10,283,335, 2019.

(11) Voinov, V. G.; Deinzer, M. L.; Beckman, J. S.; Barofsky, D. F., Electron capture, collision-induced, and electron capture-collision induced dissociation in Q-TOF. *J Am Soc Mass Spectrom* **2011,** *22*, 607-611.

(12) Budnik, B. A.; Haselmann, K. F.; Zubarev, R. A., Electron detachment dissociation of peptide di-anions: an electron–hole recombination phenomenon. *Chem Phys Lett* **2001,** *342*, 299-302.

(13) Yang, J.; Mo, J. J.; Adamson, J. T.; Hakansson, K., Characterization of oligodeoxynucleotides by electron detachment dissociation Fourier transform ion cyclotron resonance mass spectrometry. *Anal Chem* **2005,** *77*, 1876-1882.

(14) Yang, J.; Hakansson, K., Fragmentation of oligoribonucleotides from gas-phase ion-electron reactions. *J Am Soc Mass Spectrom* **2006,** *17*, 1369-1375.

(15) Wolff, J. J.; Chi, L.; Linhardt, R. J.; Amster, I. J., Distinguishing glucuronic from iduronic acid in glycosaminoglycan tetrasaccharides by using electron detachment dissociation. *Analytical chemistry* **2007,** *79*, 2015-2022.

(16) Adamson, J. T.; Hakansson, K., Electron detachment dissociation of neutral and sialylated oligosaccharides. *J Am Soc Mass Spectrom* **2007,** *18*, 2162-2172.

(17) Wolff, J. J.; Laremore, T. N.; Busch, A. M.; Linhardt, R. J.; Amster, I. J., Electron detachment dissociation of dermatan sulfate oligosaccharides. *J Am Soc Mass Spectrom* **2008,** *19*, 294-304.

(18) Leach, F. E.; Arungundram, S.; Al-Mafraji, K.; Venot, A.; Boons, G. J.; Amster, I. J., Electron detachment dissociation of synthetic heparan sulfate glycosaminoglycan

tetrasaccharides varying in degree of sulfation and hexuronic acid stereochemistry. *Int J Mass Spectrom* **2012,** *330*, 152-159.

(19) Leach, F. E.; Wolff, J. J.; Laremore, T. N.; Linhardt, R. J.; Amster, I. J., Evaluation of the experimental parameters which control electron detachment dissociation, and their effect on the fragmentation efficiency of glycosaminoglycan carbohydrates. *Int J Mass Spectrom* **2008,** *276*, 110-115.

(20) Yang, J.; Hakansson, K., Characterization and optimization of electron detachment dissociation Fourier transform ion cyclotron resonance mass spectrometry. *Int J Mass Spectrom* **2008,** *276*, 144-148.

(21) Limbach, P. A.; Marshall, A. G.; Wang, M., An electrostatic ion guide for efficient transmission of low energy externally formed ions into a Fourier transform ion cyclotron resonance mass spectrometer. *Int J Mass Spectrom Ion Proc* **1993,** *125*, 135-143.

(22) Tang, L.; Hettich, R. L.; Hurst, G. B.; Buchanan, M. V., An electrostatic ion guide interface for combining electrospray with Fourier transform ion cyclotron resonance mass spectrometry. *Rapid Comm Mass Spectrom* **1995,** *9*, 731-734.

(23) Guan, S.; Marshall, A. G., Stacked-ring electrostatic ion guide. *J Am Soc Mass Spectrom* **1996,** *7*, 101-106.

(24) McIver Jr, R. T.; Hunter, R. L.; Bowers, W. D., Coupling a quadrupole mass spectrometer and a Fourier transform mass spectrometer. *Int J Mass Spectrom Ion Proc* **1985,** *64*, 67-77.

(25) Harkewicz, R.; Belov, M. E.; Anderson, G. A.; Paša-Tolić, L.; Masselon, C. D.; Prior, D. C.; Udseth, H. R.; Smith, R. D., ESI-FTICR mass spectrometry employing data-dependent external ion selection and accumulation. *J Am Soc Mass Spectrom* **2002,** *13*, 144-154.

(26) Jones, R. M.; Gerlich, D.; Anderson, S. L., Simple radio-frequency power source for ion guides and ion traps. *Rev Sci Instrum* **1997,** *68*, 3357-3362.

(27) Caravatti, P.; Allemann, M., The 'infinity cell': A new trapped-ion cell with radiofrequency covered trapping electrodes for fourier transform ion cyclotron resonance mass spectrometry. *Org Mass Spectrom* **1991,** *26*, 514-518.

(28) Nikolaev, E. N.; Boldin, I. A.; Jertz, R.; Baykut, G., Initial experimental characterization of a new ultra-high resolution FTICR cell with dynamic harmonization. *J Am Soc Mass Spectrom* **2011,** *22*, 1125-1133.

(29) Kostyukevich, Y. I.; Vladimirov, G. N.; Nikolaev, E. N., Dynamically harmonized FT-ICR cell with specially shaped electrodes for compensation of inhomogeneity of the magnetic field. Computer simulations of the electric field and ion motion dynamics. *J Am Soc Mass Spectrom* **2012,** *23*, 2198-2207.

(30) Nikolaev, E. N.; Kostyukevich, Y. I.; Vladimirov, G. N., Fourier transform ion cyclotron resonance (FT ICR) mass spectrometry: Theory and simulations. *Mass Spectrom Rev* **2016,** *35*, 219-258.

(31) Zaia, J., Glycosaminoglycan Glycomics Using Mass Spectrometry. *Mol Cell Proteomics* **2013,** *12*, 885-892.

(32) Zaia, J.; Li, X.-Q.; Chan, S.-Y.; Costello, C. E., Tandem mass spectrometric strategies for determination of sulfation positions and uronic acid epimerization in chondroitin sulfate oligosaccharides. *Journal of the American Society for Mass Spectrometry* **2003,** *14*, 1270-1281.

(33) Zaia, J.; Costello, C. E., Compositional analysis of glycosaminoglycans by electrospray mass spectrometry. *Anal Chem* **2001,** *73*, 233-239.

(34) Desaire, H.; Leary, J. A., Detection and quantification of the sulfated disaccharides in chondroitin sulfate by electrospray tandem mass spectrometry. *J Am Soc Mass Spectrom* **2000,** *11*, 916-920.

(35) Wolff, J. J.; Laremore, T. N.; Busch, A. M.; Linhardt, R. J.; Amster, I. J., Influence of charge state and sodium cationization on the electron detachment dissociation and infrared multiphoton dissociation of glycosaminoglycan oligosaccharides. *J Am Soc Mass Spectrom* **2008,** *19*, 790-8.

(36) Leach, F. E.; Ly, M.; Laremore, T. N.; Wolff, J. J.; Perlow, J.; Linhardt, R. J.; Amster, I. J., Hexuronic Acid Stereochemistry Determination in Chondroitin Sulfate Glycosaminoglycan Oligosaccharides by Electron Detachment Dissociation. *J Am Soc Mass Spectr* **2012,** *23*, 1488-1497.

(37) Leach, F. E.; Xiao, Z.; Laremore, T. N.; Linhardt, R. J.; Amster, I. J., Electron detachment dissociation and infrared multiphoton dissociation of heparin tetrasaccharides. *Int J Mass Spectrom* **2011,** *308*, 253-259.

(38) Agyekum, I.; Patel, A. B.; Zong, C.; Boons, G.-J.; Amster, I. J., Assignment of hexuronic acid stereochemistry in synthetic heparan sulfate tetrasaccharides with 2-O-sulfo uronic acids using electron detachment dissociation. *Int J Mass Spectrom* **2015,** *390*, 163-169.

(39) Agyekum, I.; Zong, C.; Boons, G.-J.; Amster, I. J., Single Stage Tandem Mass Spectrometry Assignment of the C-5 Uronic Acid Stereochemistry in Heparan Sulfate Tetrasaccharides using Electron Detachment Dissociation. *J Am Soc Mass Spectr* **2017**, 1-10.

(40) Bielik, A. M.; Zaia, J., Multistage tandem mass spectrometry of chondroitin sulfate and dermatan sulfate. *Int J Mass Spectrom* **2011,** *305*, 131-137.

(41) Wolff, J. J.; Laremore, T. N.; Busch, A. M.; Linhardt, R. J.; Amster, I. J., Influence of charge state and sodium cationization on the electron detachment dissociation and infrared multiphoton dissociation of glycosaminoglycan oligosaccharides. *J Am Soc Mass Spectr* **2008,** *19*, 790-798.

(42) Kailemia, M. J.; Li, L. Y.; Ly, M.; Linhardt, R. J.; Amster, I. J., Complete Mass Spectral Characterization of a Synthetic Ultralow-Molecular-Weight Heparin Using Collision-Induced Dissociation. *Anal Chem* **2012,** *84*, 5475-5478.

(43) Kailemia, M. J.; Patel, A. B.; Johnson, D. T.; Li, L. Y.; Linhardt, R. J.; Amster, I. J., Differentiating chondroitin sulfate glycosaminoglycans using collision-induced dissociation; uronic acid cross-ring diagnostic fragments in a single stage of tandem mass spectrometry. *Eur J Mass Spectrom* **2015,** *21*, 275-285.

(44) Bin Oh, H.; Leach, F. E.; Arungundram, S.; Al-Mafraji, K.; Venot, A.; Boons, G. J.; Amster, I. J., Multivariate Analysis of Electron Detachment Dissociation and Infrared Multiphoton Dissociation Mass Spectra of Heparan Sulfate Tetrasaccharides Differing Only in Hexuronic acid Stereochemistry. *J Am Soc Mass Spectr* **2011,** *22*, 582-590.

(45) Kailemia, M. J.; Park, M.; Kaplan, D. A.; Venot, A.; Boons, G. J.; Li, L. Y.; Linhardt, R. J.; Amster, I. J., High-Field Asymmetric-Waveform Ion Mobility Spectrometry and Electron Detachment Dissociation of Isobaric Mixtures of Glycosaminoglycans. *J Am Soc Mass Spectr* **2014,** *25*, 258-268.

(46) Zhou, W.; Hakansson, K., Electron detachment dissociation of fluorescently labeled sialylated oligosaccharides. *Electrophoresis* **2011,** *32*, 3526-3535.

(47) Kornacki, J. R.; Adamson, J. T.; Hakansson, K., Electron Detachment Dissociation of Underivatized Chloride-Adducted Oligosaccharides. *J Am Soc Mass Spectr* **2012,** *23*, 2031-2042.

(48) Werner, I.; Odin, L., On the presence of sialic acid in certain glycoproteius and in gangliosides. *Acta Soc Bot Pol* **1952,** *57*, 230-241.

(49) Juhasz, P.; Costello, C. E., Matrix-assisted laser desorption ionization time-of-flight mass spectrometry of underivatized and permethylated gangliosides. *J Am Soc Mass Spectr* **1992,** *3*, 785-796.

(50) McFarland, M. A.; Marshall, A. G.; Hendrickson, C. L.; Nilsson, C. L.; Fredman, P.; Mansson, J. E., Structural characterization of the GM1 ganglioside by infrared multiphoton dissociation/electron capture dissociation, and electron detachment dissociation electrospray ionization FT-ICR MS/MS. *J Am Soc Mass Spectrom* **2005,** *16*, 752-762.

(51) Monigatti, F.; Hekking, B.; Steen, H., Protein sulfation analysis - A primer. *Bba-Proteins Proteom* **2006,** *1764*, 1904-1913.

(52) Shih, M.; McLuckey, S. A., Ion/ion charge inversion/attachment in conjunction with dipolar DC collisional activation as a selective screen for sulfo- and phosphopeptides. *Int J Mass Spectrom* **2019,** *444*, 116181.

(53) Brodbelt, J. S., Ion activation methods for peptides and proteins. *Anal Chem* **2016,** *88*, 30-51.

(54) Flora, J. W.; Muddiman, D. C., Selective, sensitive, and rapid phosphopeptide identification in enzymatic digests using ESI-FTICR-MS with infrared multiphoton dissociation. *Anal Chem* **2001,** *73*, 3305-3311.

(55) Kjeldsen, F.; Silivra, O. A.; Ivonin, I. A.; Haselmann, K. F.; Gorshkov, M.; Zubarev, R. A., C-alpha-C backbone fragmentation dominates in electron detachment dissociation of gas-phase polypeptide polyanions. *Chem-Eur J* **2005,** *11*, 1803-1812.

(56) Thompson, M. S.; Cui, W.; Reilly, J. P., Fragmentation of singly charged peptide ions by photodissociation at λ= 157 nm. *Angew Chem Int Edit* **2004,** *43*, 4791-4794.

(57) Kjeldsen, F.; Horning, O. B.; Jensen, S. S.; Giessing, A. M. B.; Jensen, O. N., Towards liquid chromatography time-scale peptide sequencing and characterization of post-translational modifications in the negative-ion mode using electron detachment dissociation tandem mass spectrometry. *J Am Soc Mass Spectrom* **2008,** *19*, 1156-1162.

(58) Ganisl, B.; Valovka, T.; Hartl, M.; Taucher, M.; Bister, K.; Breuker, K., Electron Detachment Dissociation for Top-Down Mass Spectrometry of Acidic Proteins. *Chem-Eur J* **2011,** *17*, 4460-4469.

(59) Song, H. T.; Hakansson, K., Electron Detachment Dissociation and Negative on Infrared Multiphoton Dissociation of Electrosprayed Intact Proteins. *Anal Chem* **2012,** *84*, 871-876.

(60) Kalli, A.; Hakansson, K., Preferential cleavage of S-S and C-S bonds in electron detachment dissociation and infrared multiphoton dissociation of disulfide-linked peptide anions. *Int J Mass Spectrom* **2007,** *263*, 71-81.

(61) Asakawa, D.; Smargiasso, N.; Quinton, L.; De Pauw, E., Peptide backbone fragmentation initiated by side-chain loss at cysteine residue in matrix-assisted laser desorption/ionization in-source decay mass spectrometry. *J Mass Spectrom* **2013,** *48*, 352-360.

(62) Asakawa, D.; Takayama, M., C-alpha - C Bond Cleavage of the Peptide Backbone in MALDI In-Source Decay Using Salicylic Acid Derivative Matrices. *J Am Soc Mass Spectrom* **2011,** *22*, 1224-1233.

(63) Jones, M. D.; Patterson, S. D.; Lu, H. S., Determination of disulfide bonds in highly bridged disulfide-linked peptides by matrix-assisted laser desorption/ionization mass spectrometry with postsource decay. *Anal Chem* **1998,** *70*, 136-143.

(64) Zubarev, R. A.; Kruger, N. A.; Fridriksson, E. K.; Lewis, M. A.; Horn, D. M.; Carpenter, B. K.; McLafferty, F. W., Electron capture dissociation of gaseous multiply-charged proteins is favored at disulfide bonds and other sites of high hydrogen atom affinity. *J Am Chem Soc* **1999,** *121*, 2857-2862.

(65) Chrisman, P. A.; Pitteri, S. J.; Hogan, J. M.; McLuckey, S. A., SO 2−· electron transfer ion/ion reactions with disulfide linked polypeptide ions. *J Am Soc Mass Spectrom* **2005,** *16*, 1020-1030.

(66) McLuckey, S. A.; Van Berkel, G. J.; Glish, G. L., Tandem mass spectrometry of small, multiply charged oligonucleotides. *J Am Soc Mass Spectrom* **1992,** *3*, 60-70.

(67) Mo, J. J.; Hakansson, K., Characterization of nucleic acid higher order structure by high-resolution tandem mass spectrometry. *Anal Bioanal Chem* **2006,** *386*, 675-681.

(68) Taucher, M.; Breuker, K., Characterization of Modified RNA by Top-Down Mass Spectrometry. *Angew Chem Int Edit* **2012,** *51*, 11289-11292.

(69) Taucher, M.; Breuker, K., Top-Down Mass Spectrometry for Sequencing of Larger (up to 61 nt) RNA by CAD and EDD. *J Am Soc Mass Spectrom* **2010,** *21*, 918-929.

(70) Herron, W. J.; Goeringer, D. E.; Mcluckey, S. A., Gas-Phase Electron-Transfer Reactions from Multiply-Charged Anions to Rare-Gas Cations. *J Am Chem Soc* **1995,** *117*, 11555-11562.

(71) Syka, J. E. P.; Coon, J. J.; Schroeder, M. J.; Shabanowitz, J.; Hunt, D. F., Peptide and protein sequence analysis by electron transfer dissociation mass spectrometry. *Proc Natl Acad Sci USA* **2004,** *101*, 9528.

(72) Coon, J. J.; Shabanowitz, J.; Hunt, D. F.; Syka, J. E. P., Electron transfer dissociation of peptide anions. *J Am Soc Mass Spectrom* **2005,** *16*, 880-882.

(73) Payne, A. H.; Glish, G. L., Gas-phase ion/ion interactions between peptides or proteins and iron ions in a quadrupole ion trap. *Int J Mass Spectrom* **2001,** *204*, 47-54.

(74) Wu, J. D.; Wei, J.; Chopra, P.; Boons, G. J.; Lin, C.; Zaia, J., Sequencing Heparan Sulfate Using HILIC LC-NETD-MS/MS. *Anal Chem* **2019,** *91*, 11738-11746.

(75) Wu, J. D.; Wei, J.; Hogan, J. D.; Chopra, P.; Joshi, A.; Lu, W. G.; Klein, J.; Boons, G. J.; Lin, C.; Zaia, J., Negative Electron Transfer Dissociation Sequencing of 3-O-Sulfation-Containing Heparan Sulfate Oligosaccharides. *J Am Soc Mass Spectrom* **2018,** *29*, 1262-1272.

(76) Wolff, J. J.; Leach, F. E.; Laremore, T. N.; Kaplan, D. A.; Easterling, M. L.; Linhardt, R. J.; Amster, I. J., Negative Electron Transfer Dissociation of Glycosaminoglycans. *Anal Chem* **2010,** *82*, 3460-3466.

(77) Leach, F. E.; Wolff, J. J.; Xiao, Z. P.; Ly, M.; Laremore, T. N.; Arungundram, S.; Al-Mafraji, K.; Venot, A.; Boons, G. J.; Linhardt, R. J.; Amster, I. J., Negative electron transfer dissociation Fourier transform mass spectrometry of glycosaminoglycan carbohydrates. *Eur J Mass Spectrom* **2011,** *17*, 167-176.

(78) Stickney, M.; Sanderson, P.; Leach, F. E.; Zhang, F. M.; Linhardt, R. J.; Amster, I. J., Online capillary zone electrophoresis negative electron transfer dissociation tandem mass spectrometry of glycosaminoglycan mixtures. *Int J Mass Spectrom* **2019,** *445*.

(79) Leach, F. E.; Riley, N. M.; Westphall, M. S.; Coon, J. J.; Amster, I. J., Negative Electron Transfer Dissociation Sequencing of Increasingly Sulfated Glycosaminoglycan Oligosaccharides on an Orbitrap Mass Spectrometer. *J Am Soc Mass Spectrom* **2017,** *28*, 1844-1854.

(80) Rush, M. J. P.; Riley, N. M.; Westphall, M. S.; Syka, J. E. P.; Coon, J. J., Sulfur Pentafluoride is a Preferred Reagent Cation for Negative Electron Transfer Dissociation. *J Am Soc Mass Spectrom* **2017,** *28*, 1324-1332.

(81) Huzarska, M.; Ugalde, I.; Kaplan, D. A.; Hartmer, R.; Easterling, M. L.; Polfer, N. C., Negative Electron Transfer Dissociation of Deprotonated Phosphopeptide Anions: Choice of Radical Cation Reagent and Competition between Electron and Proton Transfer. *Anal Chem* **2010,** *82*, 2873-2878.

(82) Huang, Y.; Yu, X.; Mao, Y.; Costello, C. E.; Zaia, J.; Lin, C., De Novo Sequencing of Heparan Sulfate Oligosaccharides by Electron-Activated Dissociation. *Anal Chem* **2013,** *85*, 11979-11986.

(83) Sanderson, P.; Stickney, M.; Leach, F. E.; Xia, Q. W.; Yu, Y. L.; Zhang, F. M.; Linhardt, R.; Amster, I. J., Heparin/heparan sulfate analysis by covalently modified reverse polarity capillary zone electrophoresis-mass spectrometry. *J Chromatogr A* **2018,** *1545*, 75-83.

(84) Shvartsburg, A. A.; Smith, R. D., Scaling of the resolving power and sensitivity for planar FAIMS and mobility-based discrimination in flow-and field-driven analyzers. *J Am Soc Mass Spectrom* **2007,** *18*, 1672-1681.

(85) Ridgeway, M. E.; Wolff, J. J.; Silveira, J. A.; Lin, C.; Costello, C. E.; Park, M. A., Gated trapped ion mobility spectrometry coupled to fourier transform ion cyclotron resonance mass spectrometry. *Int J Ion Mobility Spectrom* **2016,** *19*, 77-85.

(86) Benigni, P.; Porter, J.; Ridgeway, M. E.; Park, M. A.; Fernandez-Lima, F., Increasing analytical separation and duty cycle with nonlinear analytical mobility scan functions in TIMS-FT-ICR MS. *Anal Chem* **2018,** *90*, 2446-2450.

(87) Wei, J.; Wu, J. D.; Tang, Y.; Ridgeway, M. E.; Park, M. A.; Costello, C. E.; Zaia, J.; Lin, C., Characterization and Quantification of Highly Sulfated Glycosaminoglycan Isomers by Gated-Trapped Ion Mobility Spectrometry Negative Electron Transfer Dissociation MS/MS. *Anal Chem* **2019,** *91*, 2994-3001.

(88) Harvey, D. J.; Scarff, C. A.; Edgeworth, M.; Struwe, W. B.; Pagel, K.; Thalassinos, K.; Crispin, M.; Scrivens, J., Travelling-wave ion mobility and negative ion fragmentation of high-mannose N-glycans. *J Mass Spectrom* **2016,** *51*, 219-235.

(89) McAlister, G. C.; Russell, J. D.; Rumachik, N. G.; Hebert, A. S.; Syka, J. E. P.; Geer, L. Y.; Westphall, M. S.; Pagliarini, D. J.; Coon, J. J., Analysis of the Acidic Proteome with Negative Electron-Transfer Dissociation Mass Spectrometry. *Anal Chem* **2012,** *84*, 2875-2882.

(90) Riley, N. M.; Rush, M. J. P.; Rose, C. M.; Richards, A. L.; Kwiecien, N. W.; Bailey, D. J.; Hebert, A. S.; Westphall, M. S.; Coon, J. J., The Negative Mode Proteome with Activated Ion Negative Electron Transfer Dissociation (AI-NETD). *Mol Cell Proteomics* **2015,** *14*, 2644-2660.

(91) Riley, N. M.; Bern, M.; Westphall, M. S.; Coon, J. J., Full-Featured Search Algorithm for Negative Electron-Transfer Dissociation. *J Proteome Res* **2016,** *15*, 2768-2776.

(92) Huang, T. Y.; McLuckey, S. A., Gas-phase ion/ion reactions of rubrene cations and multiply charged DNA and RNA anions. *Int J Mass Spectrom* **2011,** *304*, 140-147.

(93) Xu, Z.; Shaw, J. B.; Brodbelt, J. S., Comparison of MS/MS Methods for Characterization of DNA/Cisplatin Adducts. *J Am Soc Mass Spectrom* **2013,** *24*, 265-273.

(94) Wang, B.-H.; McLafferty, F. W., Electron impact excitation of ions from larger organic molecules. *Org Mass Spectrom* **1990,** *25*, 554-556.

(95) Wolff, J. J.; Laremore, T. N.; Aslam, H.; Linhardt, R. J.; Amster, I. J., Electron-Induced Dissociation of Glycosaminoglycan Tetrasaccharides. *J Am Soc Mass Spectrom* **2008,** *19*, 1449-1458.

(96) Kalli, A.; Grigorean, G.; Håkansson, K., Electron Induced Dissociation of Singly Deprotonated Peptides. *J Am Soc Mass Spectrom* **2011,** *22*, 2209-2221.

(97) Qi, Y.; Volmer, D. A., Electron-based fragmentation methods in mass spectrometry: An overview. *Mass Spectrom Rev* **2017,** *36*, 4-15.

(98) Wills, R. H.; Tosin, M.; O'Connor, P. B., Structural Characterization of Polyketides Using High Mass Accuracy Tandem Mass Spectrometry. *Anal Chem* **2012,** *84*, 8863-8870.

(99) Mosely, J. A.; Smith, M. J.; Prakash, A. S.; Sims, M.; Bristow, A. W., Electron-induced dissociation of singly charged organic cations as a tool for structural characterization of pharmaceutical type molecules. *Anal Chem* **2011,** *83*, 4068-4075.

(100) Lioe, H.; Richard, A., Comparison of collision-induced dissociation and electron-induced dissociation of singly protonated aromatic amino acids, cystine and related simple peptides using a hybrid linear ion trap–FT-ICR mass spectrometer. *Anal Bioanal Chem* **2007,** *389*, 1429-1437.

(101) Wills, R. H.; O'connor, P. B., Structural characterization of actinomycin D using multiple ion isolation and electron induced dissociation. *J Am Soc Mass Spectrom* **2013,** *25*, 186-195.

(102) Yoo, H. J.; Wang, N.; Zhuang, S.; Song, H.; Håkansson, K., Negative-Ion Electron Capture Dissociation: Radical-Driven Fragmentation of Charge-Increased Gaseous Peptide Anions. *J Am Chem Soc* **2011,** *133*, 16790-16793.

(103) Hersberger, K. E.; Hakansson, K., Characterization of O-Sulfopeptides by Negative Ion Mode Tandem Mass Spectrometry: Superior Performance of Negative Ion Electron Capture Dissociation. *Anal Chem* **2012,** *84*, 6370-6377.

(104) Wang, Q.; Borotto, N. B.; Håkansson, K., Gas-Phase Hydrogen/Deuterium Scrambling in Negative-Ion Mode Tandem Mass Spectrometry *J Am Soc Mass Spectrom* **2019,** *30*, 855-863.

(105) Gabelica, V.; Tabarin, T.; Antoine, R.; Rosu, F.; Compagnon, I.; Broyer, M.; De Pauw, E.; Dugourd, P., Electron Photodetachment Dissociation of DNA Polyanions in a Quadrupole Ion Trap Mass Spectrometer. *Anal Chem* **2006,** *78*, 6564-6572.

(106) Perot-Taillandier, M.; Afonso, C.; Enjalbert, Q.; Antoine, R.; Dugourd, P.; Cole, R. B.; Tabet, J. C.; Rebuffat, S.; Zirah, S., Electron detachment/photodetachment dissociation of lasso peptides. *Int J Mass Spectrom* **2015,** *390*, 91-100.

(107) Gabelica, V.; Rosu, F.; Tabarin, T.; Kinet, C.; Antoine, R.; Broyer, M.; De Pauw, E.; Dugourd, P., Base-dependent electron photodetachment from negatively charged DNA strands upon 260-nm laser irradiation. *J Am Chem Soc* **2007,** *129*, 4706-4713.

(108) Kinet, C.; Gabelica, V.; Balbeur, D.; De Pauw, E., Electron detachment dissociation (EDD) pathways in oligonucleotides. *Int J Mass Spectrom* **2009,** *283*, 206-213.

(109) Perot-Taillandier, M.; Zirah, S.; Enjalbert, Q.; Antoine, R.; Lemoine, J.; Dugourd, P.; Rebuffat, S.; Tabet, J. C.; Afonso, C., Prompt and Slow Electron-Detachment-Dissociation/Electron-Photodetachment-Dissociation of a 21-Mer Peptide. *Chem-Eur J* **2013,** *19*, 350-357.

APPENDIX B

Structural Characterization of Sulfated Glycosaminoglycans Using Charge Transfer Dissociation Supplemental Data

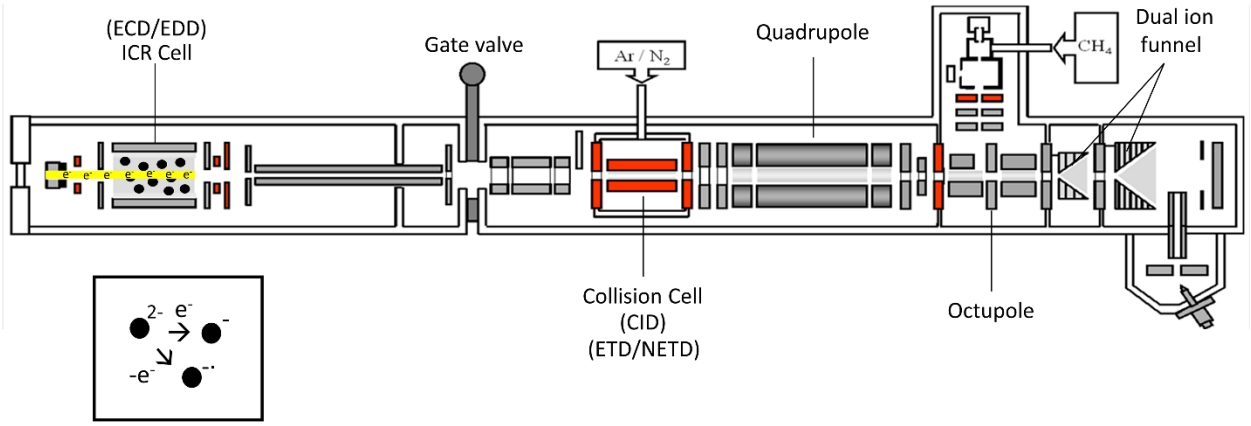

Figure B.1. EDD schematic on a Bruker solariX XR FTICR MS. A heated cathode works as a source of electrons. Multiply charged precursor anions are stored in the analyzer/ICR cell, and then bombarded with electrons (19 eV). Precursor ions can the undergo direct decomposition resulting in even-electron products, or an electron can be detached, resulting in radical formation.

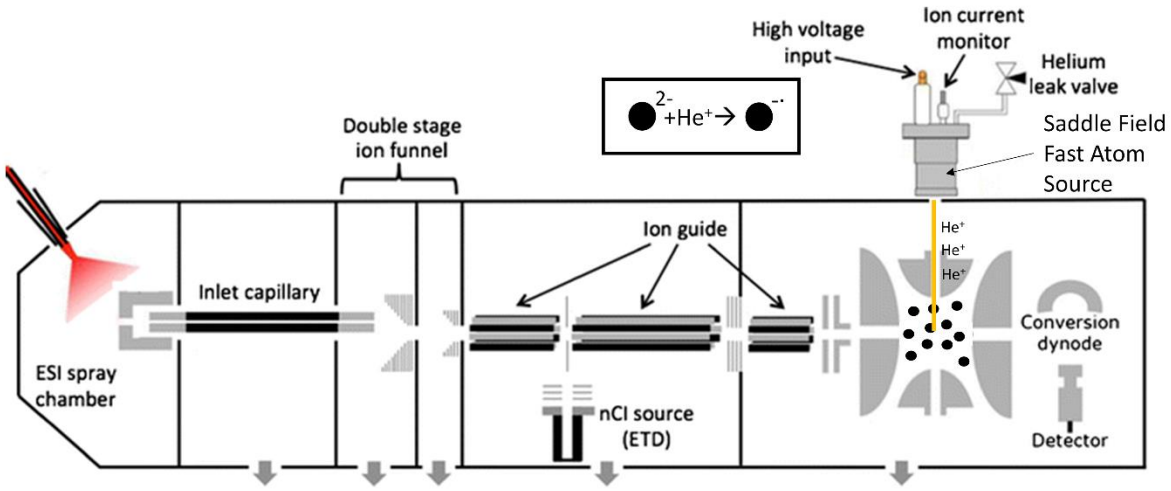

Figure B.2. CTD schematic on a Bruker AmaZon 3D IT MS. A saddle field ion source is mounted over the ring electrode. Multiply charged precursor ions are store in the ion trap, and highly energized helium cations are introduced. Both even and odd-electron products are observed. Adapted from reference 41. Copyright 2017 American Chemical Society.

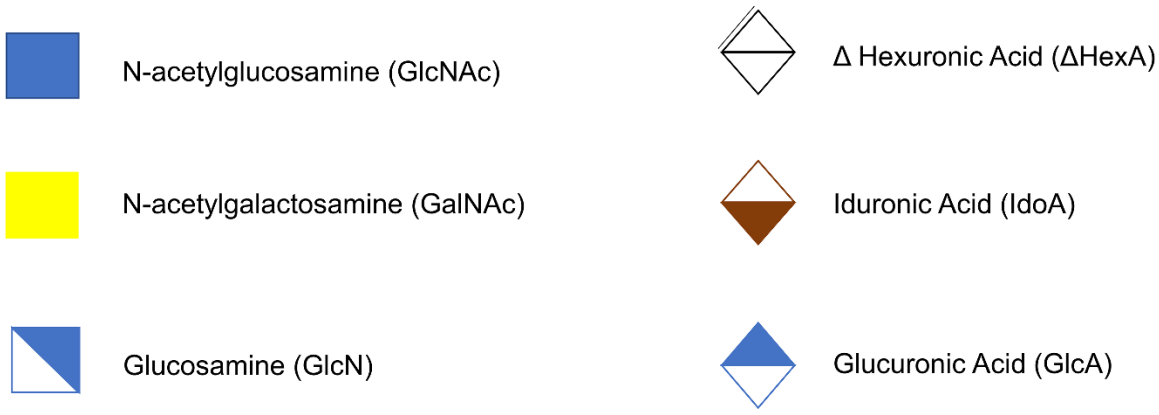

Figure B.3. Symbol nomenclature for glycans (SNFG).

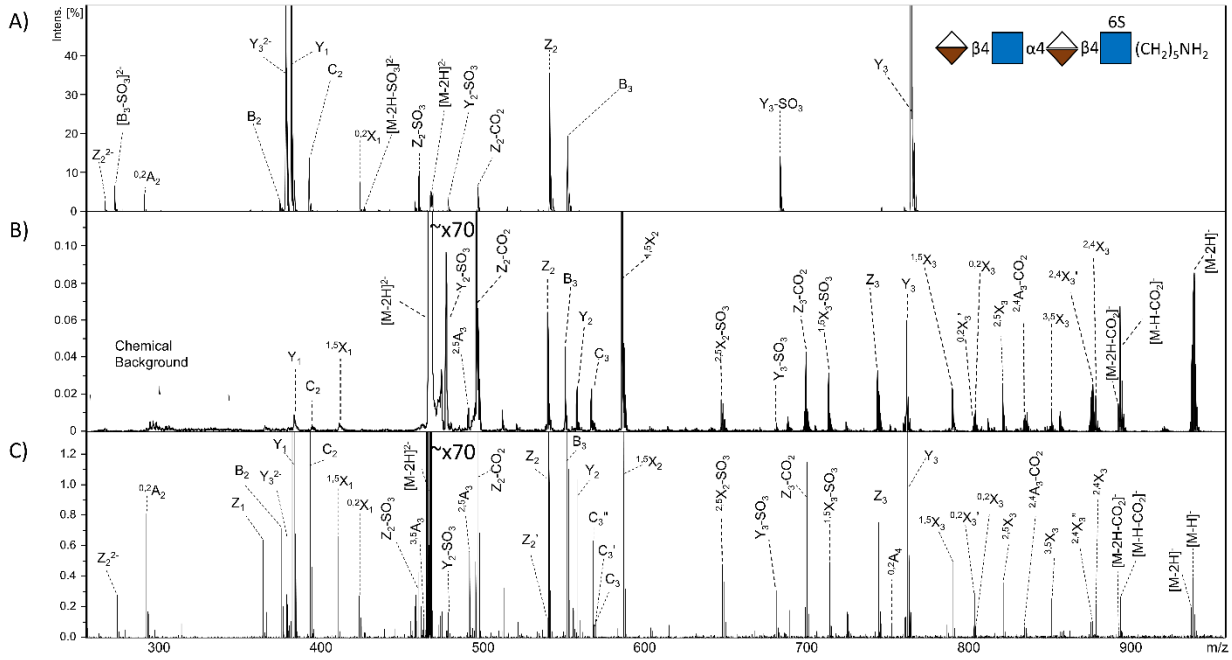

Figure B.4. A) CID, B) CTD and C) EDD spectra of the $[M-2H]^{2-}$ precursor of HS tetrasaccharide IdoA-GlcNAc-IdoA-GlcNAc6S-$(CH_2)_5NH_2$.

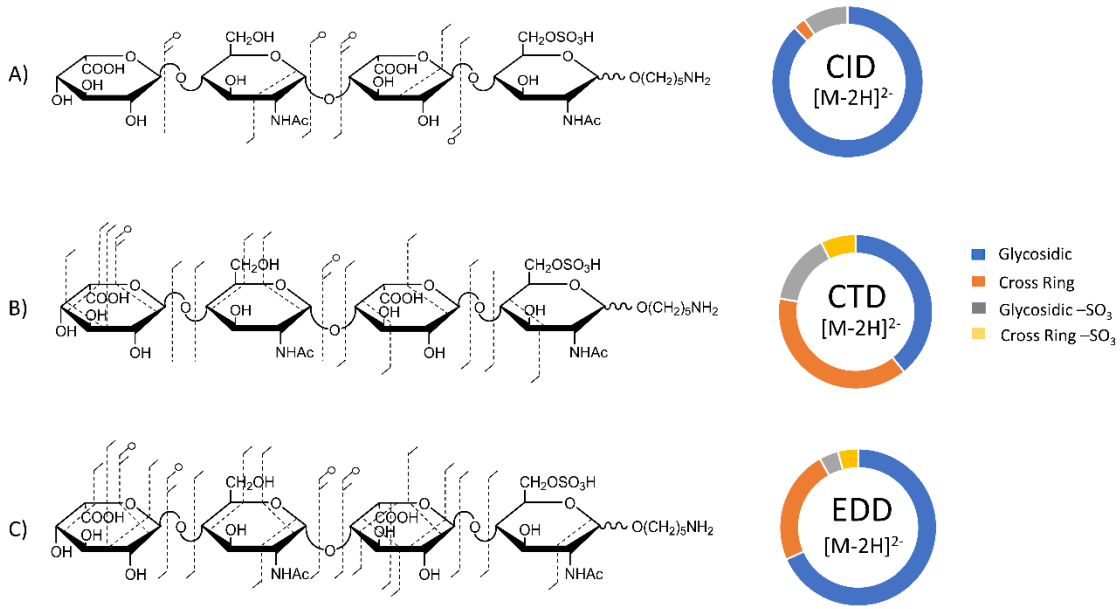

Figure B.5. Fragment maps of A) CID, B) CTD and C) EDD and corresponding donut plots of the $[M-2H]^{2-}$ precursor of HS tetrasaccharide IdoA-GlcNAc-IdoA-GlcNAc6S-$(CH_2)_5NH_2$. Donut plots show the intensity distribution of fragment ion types.

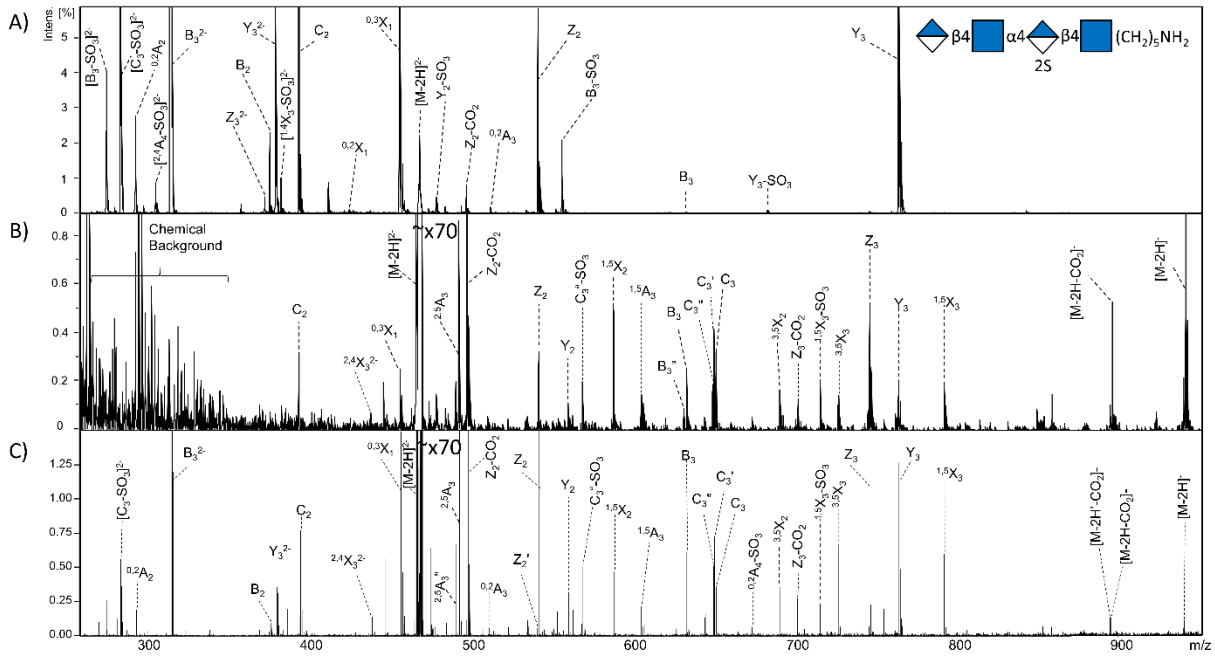

Figure B.6. A) CID, B) CTD and C) EDD spectra of the $[M-2H]^{2-}$ precursor of HS tetrasaccharide GlcA-GlcNAc-GlcA2S-GlcNAc-$(CH_2)_5NH_2$.

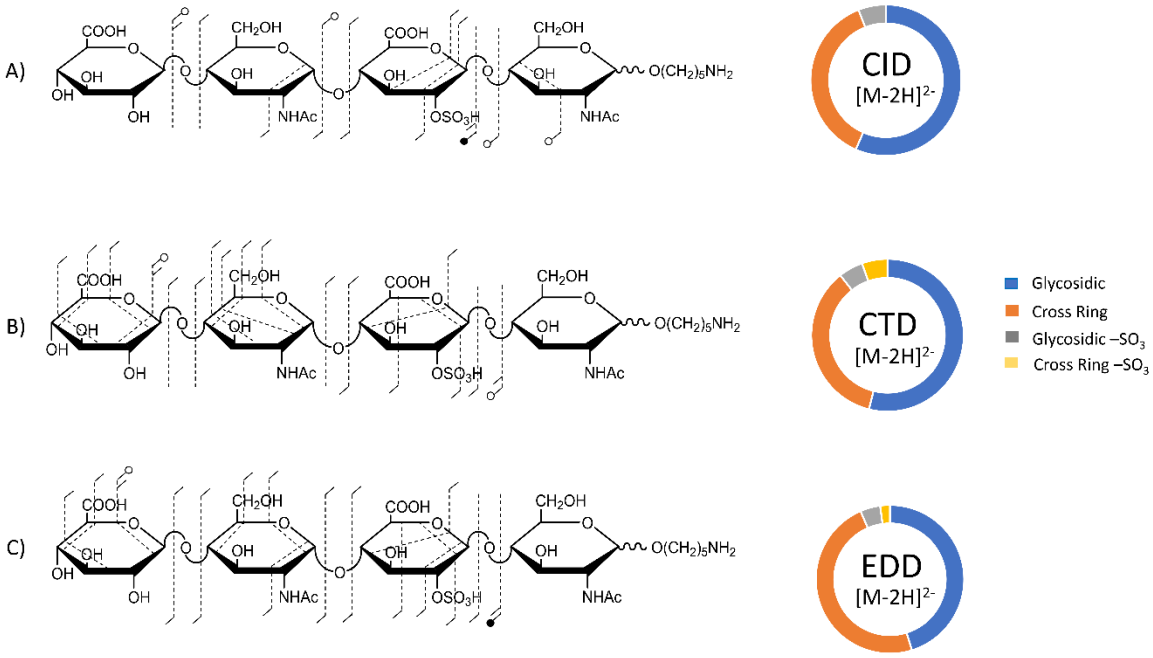

Figure B.7. Fragment maps of A) CID, B) CTD and C) EDD and corresponding donut plots of the $[M-2H]^{2-}$ precursor of HS tetrasaccharide GlcA-GlcNAc-GlcA2S-GlcNAc-$(CH_2)_5NH_2$. Donut plots show the intensity distribution of fragment ion types.

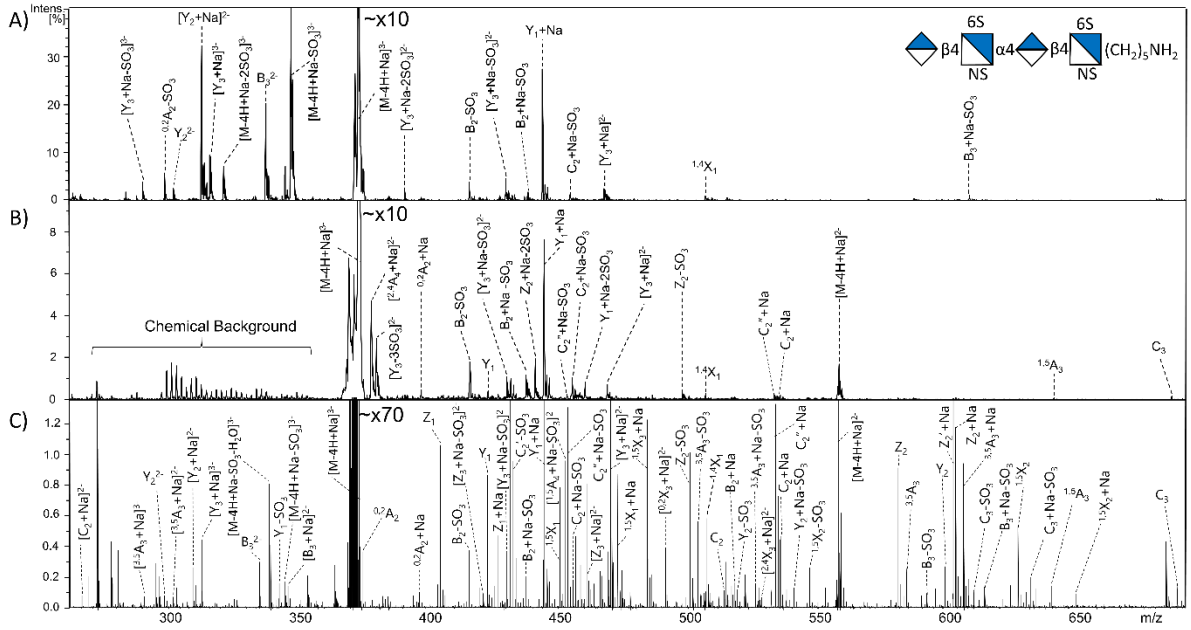

Figure B.8. A) CID, B) CTD and C) EDD spectra of the $[M-4H+Na]^{3-}$ precursor of HS tetrasaccharide GlcA-GlcNS6S-GlcA-GlcNS6S-$(CH_2)_5NH_2$.

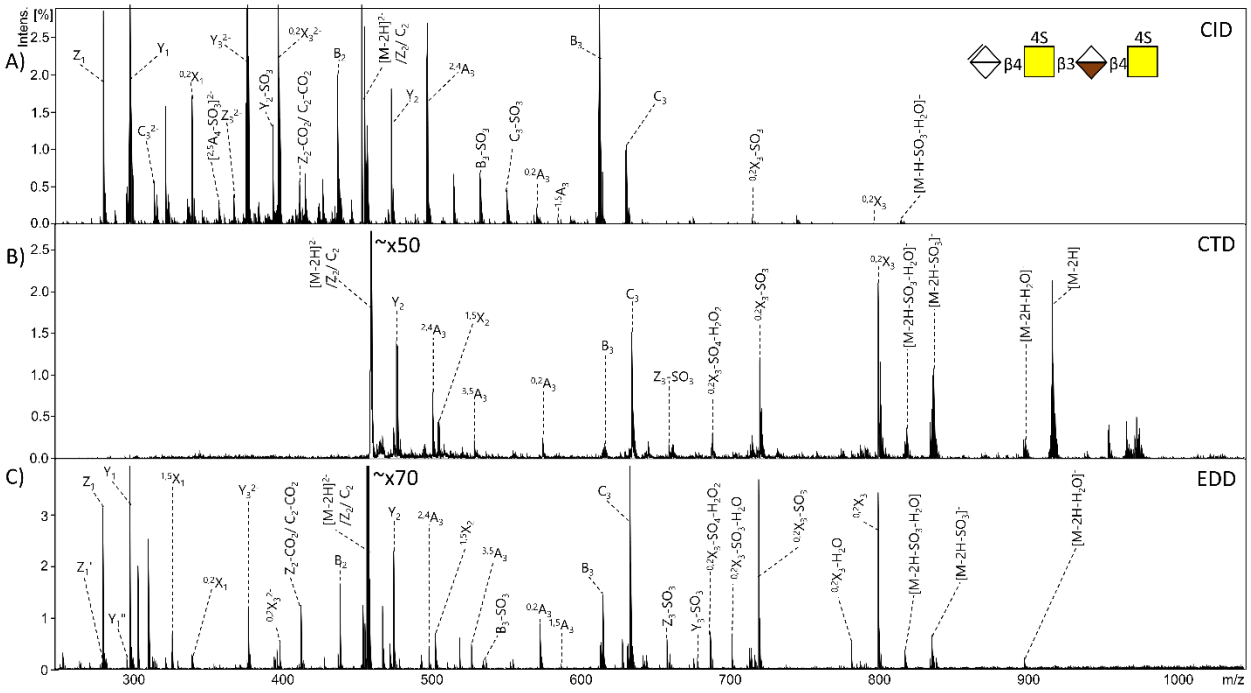

Figure B.9. A) CID, B) CTD and C) EDD spectra of the $[M-2H]^{2-}$ precursor of DS tetrasaccharide ΔHexA-GalNAc4S-IdoA-GalNAc4S-OH.

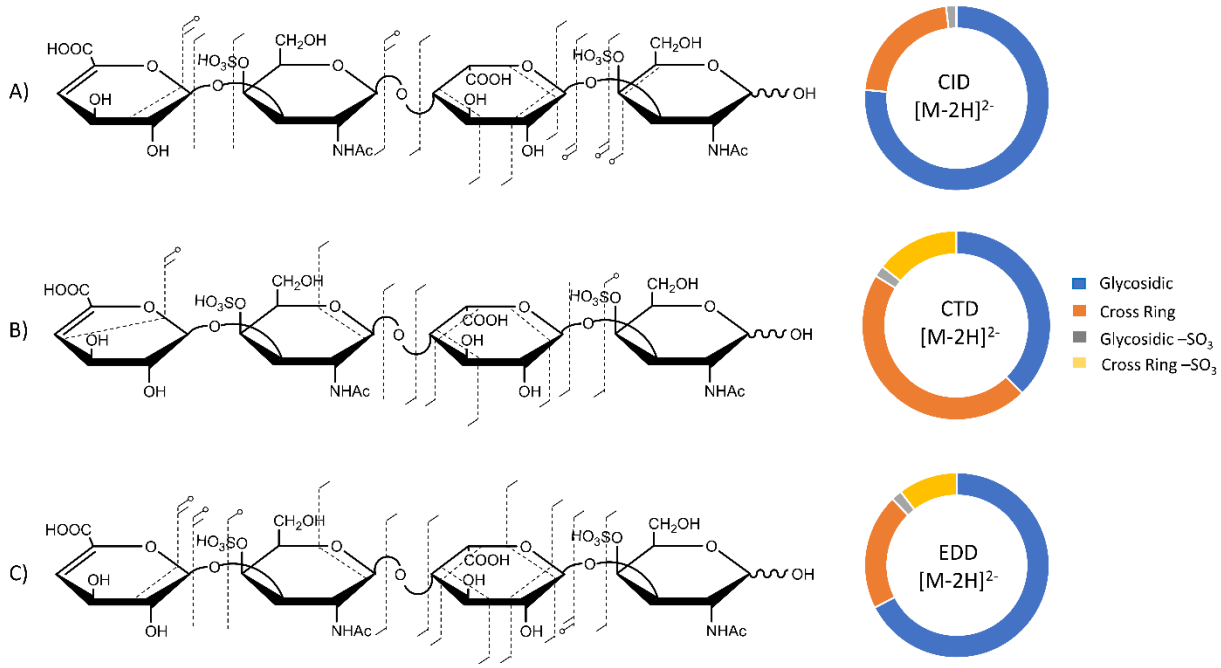

Figure B.10. Fragment maps of A) CID, B) CTD and C) EDD and corresponding donut plots of the $[M-2H]^{2-}$ precursor of DS tetrasaccharide ΔHexA-GalNAc4S-IdoA-GalNAc4S-OH. Donut plots show the intensity distribution of fragment ion types.

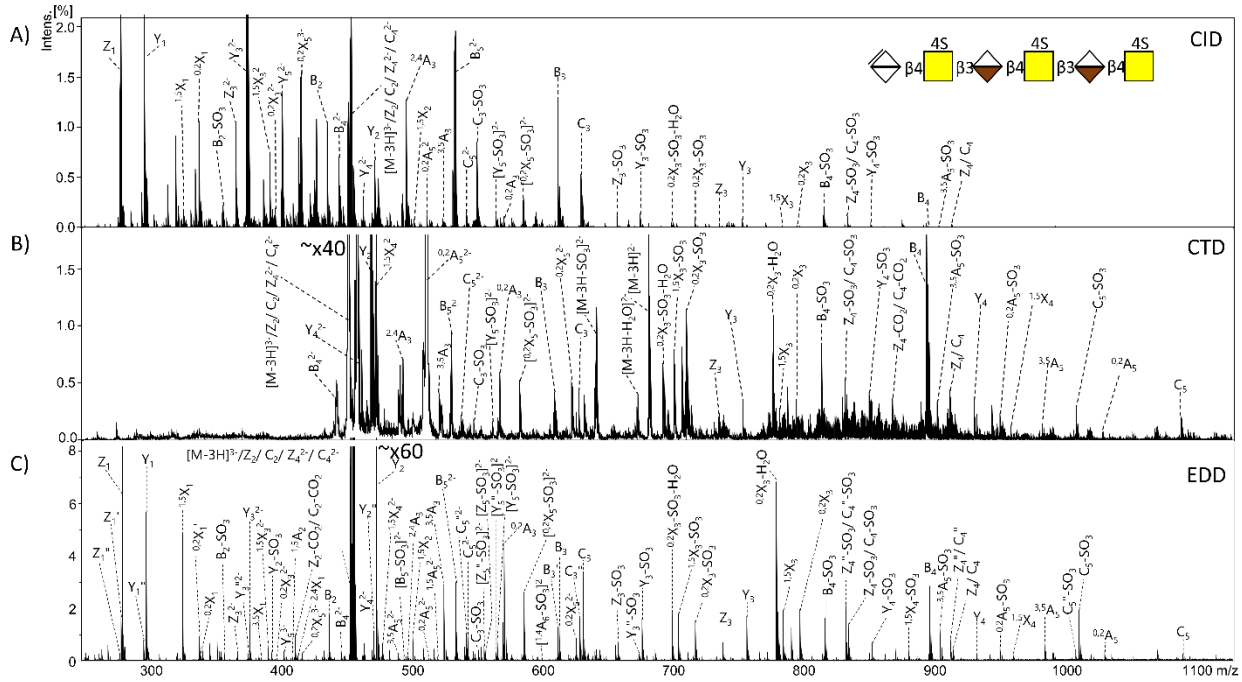

Figure B.11. A) CID, B) CTD and C) EDD spectra of the $[M-3H]^{3-}$ precursor of DS hexasaccharide ΔHexA-GalNAc4S-IdoA-GalNAc4S-IdoA-GalNAc4S-OH.

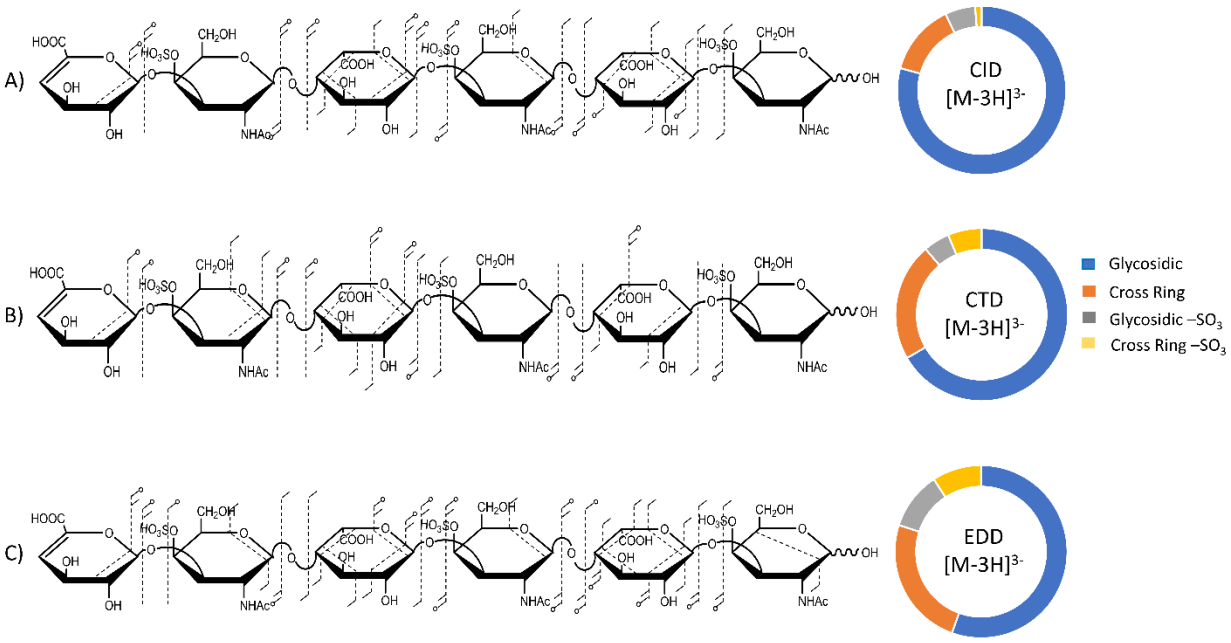

Figure B.12. Fragment maps of A) CID, B) CTD and C) EDD and corresponding donut plots of the $[M-3H]^{3-}$ precursor of DS hexasaccharide ΔHexA-GalNAc4S-IdoA-GalNAc4S-IdoA-GalNAc4S-OH. Donut plots show the intensity distribution of fragment ion types.

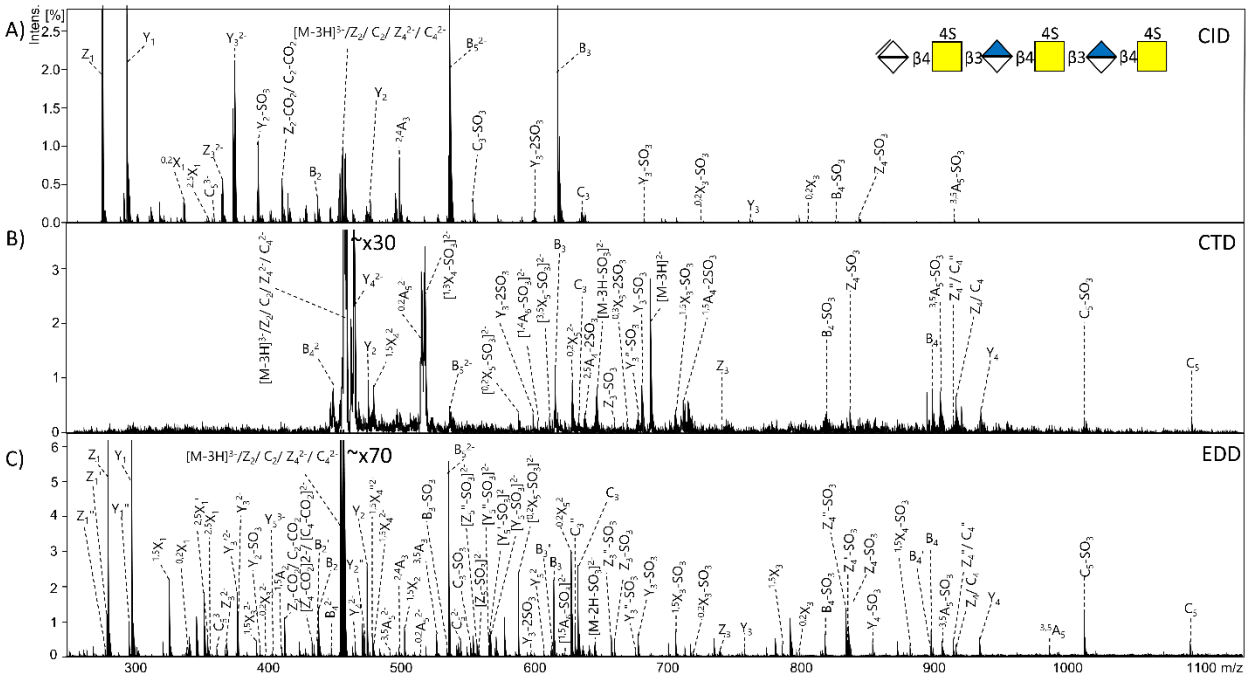

Figure B.13. A) CID, B) CTD and C) EDD spectra of the $[M-3H]^{3-}$ precursor of cS hexasaccharide ΔHexA-GalNAc4S-GlcA-GalNAc4S-GlcA-GalNAc4S-OH.

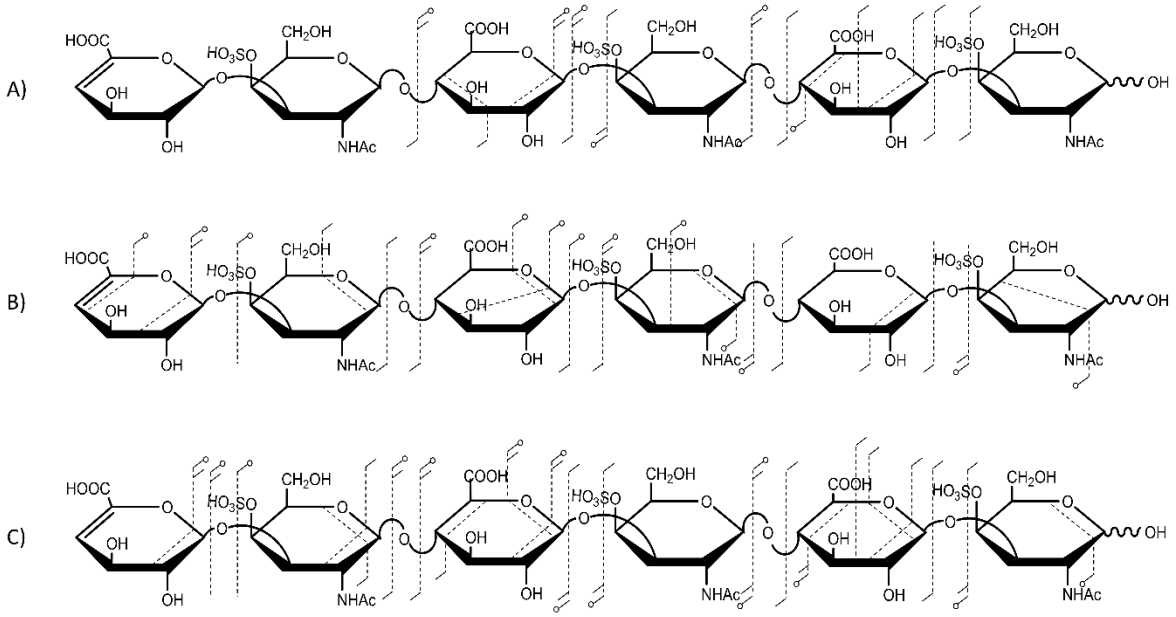

Figure B.14. Fragment maps of A) CID, B) CTD and C) EDD of the $[M-3H]^{3-}$ precursor of CS hexasaccharide ΔHexA-GalNAc4S-GlcA-GalNAc4S-GlcA-GalNAc4S-OH.

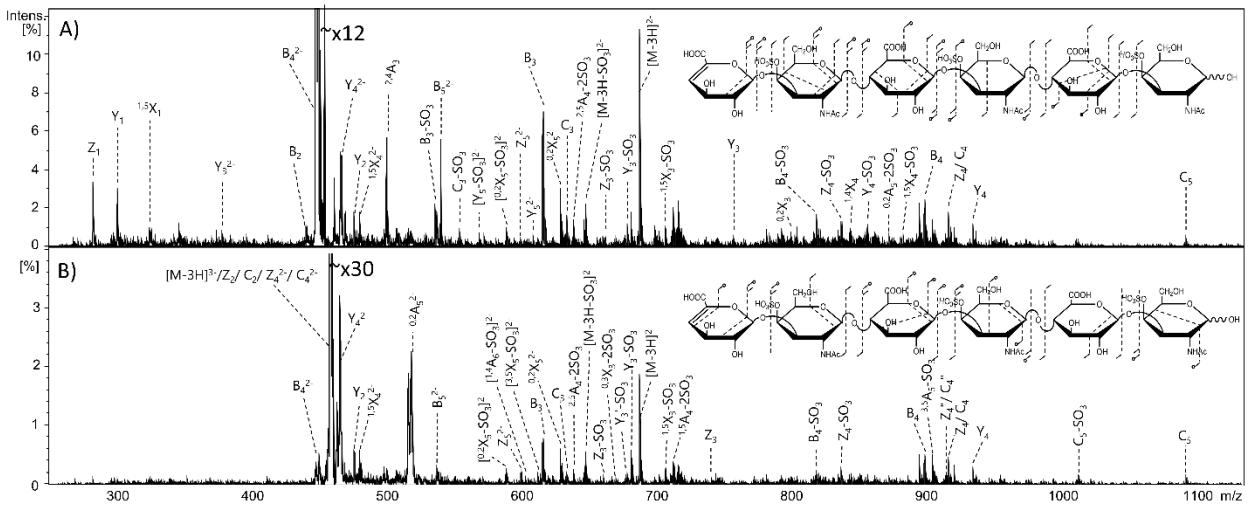

Figure B.15. MS/MS spectra of CTD with resonance ejection (A) and CTD without resonance ejection (B) of the CS hexasaccharide ΔHexA-GalNAc4S-GlcA-GalNAc4S-GlcA-GalNAc4S-OH. Fragment map inserts represent sites of fragmentation.

Table B.1. Fragment ion list for He-CTD of $[M-2H]^{2-}$ (*m/z* 470.39) of IdoA-GlcNAc-IdoA-GlcNAc6S-$(CH_2)_5NH_2$

Measured m/z	Calculated m/z	Accuracy (Da)	Intensity	Assigned Cleavage
387.42	385.1275	2.2925	222	Y_1
398.51	396.1147	2.3953	90	C_2
415.16	413.1224	2.0376	111	$^{1,5}X_1$
470.39	469.6319	0.7569	2235460	$[M-2H]^{2-}$
480.79	481.2027	-0.4131	2339	Y_2-SO_3
494.45	496.1308	-1.6808	312	$^{2,5}A_3$
499.43	499.1598	0.2702	6814	Z_2-CO_2
543.2	543.149	0.0510	1554	Z_2
554.14	554.1363	0.0037	1103	B_3
561.12	561.1596	-0.0396	585	Y_2
570.05	572.1468	-2.0968	557	C_3
589	589.1545	-0.1545	4106	$^{1,5}X_2$
683.84	684.2821	-0.4424	110	Y_3-SO_3
701.8	702.2392	-0.4392	1031	Z_3-CO_2
715.75	712.277	3.4730	765	$^{1,5}X_3$-SO_3
745.77	746.2284	-0.4587	793	Z_3
763.77	764.2389	-0.4692	1452	Y_3
791.79	792.2339	-0.4441	564	$^{1,5}X_3$
804.82	805.2425	-0.4225	192	$^{0,2}X_3'$
805.82	806.2495	-0.4297	281	$^{0,2}X_3$
822.84	822.2444	0.5952	627	$^{2,5}X_3$
835.87	836.2609	-0.3909	175	$^{2,4}A_3$-CO_2
852.84	852.255	0.5846	303	$^{3,5}X_3$
878	879.2429	-1.2429	615	$^{2,4}X_3'$
879.98	880.2499	-0.2700	468	$^{2,4}X_3$
940.25	940.271	-0.0210	2067	$[M-2H]^-$

Table B.2. Fragment ion list for He-CTD of $[M-2H]^{2-}$ (*m/z* 469.14) of GlcA-GlcNAc-GlcA2S-GlcNAc-$(CH_2)_5NH_2$

Measured m/z	Calculated m/z	Accuracy (Da)	Intensity	Assigned Cleavage
395.24	396.1147	-0.8767	382	C_2
439.22	439.6213	-0.4013	87	$^{2,4}X_3^{2-}$
457.45	457.1486	0.3012	303	$^{0,3}X_1$
469.14	469.6319	-0.4924	178949	$[M-2H]^{2-}$
493.51	496.1308	-2.6208	1033	$^{2,5}A_3$
498.58	499.16	-0.5800	4189	Z_2-CO_2
542.71	543.149	-0.4394	388	Z_2
560.9	561.1596	-0.2596	135	Y_2
569.77	570.1318	-0.3618	238	C_3"-SO_3
588.88	589.1545	-0.2746	622	$^{1,5}X_2$
605.87	606.0982	-0.2282	177	$^{1,5}A_3$
631.93	632.0781	-0.1481	105	B_3"
633.91	634.0931	-0.1831	307	B_3
649.92	650.0897	-0.1697	229	C_3"
650.95	651.0967	-0.1467	498	C_3'
651.97	652.1037	-0.1337	384	C_3
691.13	690.2022	0.9266	199	$^{3,5}X_2$
702.21	702.2394	-0.0294	153	Z_3-CO_2
716.24	712.277	3.9630	249	$^{1,5}X_3$-SO_3
746.37	746.2284	0.1416	629	Z_3
764.35	764.2389	0.1110	246	Y_3
792.47	792.2339	0.2361	237	$^{1,5}X_3$
895.77	896.282	-0.5120	632	$[M-2H-CO_2]^-$
940.9	940.271	0.6286	1495	$[M-2H]^-$

Table B.3. Fragment ion list for He-CTD of $[M-4H+Na]^{3-}$ (*m/z* 372.45) of GlcA-GlcNS6S-GlcA-GlcNS6S-$(CH_2)_5NH_2$

Measured m/z	Calculated m/z	Accuracy (Da)	Intensity	Assigned Cleavage
372.45	372.0292	0.4203	34651	$[M-4H+Na]^{3-}$
377.53	376.5176	1.0097	1746	$[^{2,4}A_4+Na]^{2-}$
379.5	379.5837	-0.0837	1089	$[Y_3-2SO_3]^{2-}$
397.04	397.0058	0.0342	171	$^{0,2}A_2+Na$
416.05	416.0504	-0.0004	667	B_2-SO_3
423.07	423.0737	-0.0037	162	Y_1
430.55	430.5531	-0.0031	399	$[Y_3+Na-SO_3]^{2-}$
438.05	438.0324	0.0176	434	$B_2+Na-SO_3$
441.59	443.1636	-1.5792	727	$Z_2+Na-2SO_3$
445.11	445.0557	0.0543	2830	Y_1+Na
454.1	454.0279	0.0721	99	$C_2"+Na-SO_3$
456.15	456.0429	0.1070	391	$C_2+Na-SO_3$
461.17	461.1741	-0.0041	314	$Y_1+Na-2SO_3$
469.8	470.5315	-0.7326	275	$[Y_3+Na]^{2-}$
499.13	501.1384	-2.0084	176	Z_2-SO_3
508.22	509.0741	-0.8556	111	$^{1,4}X_1$
535.19	533.9848	1.2052	86	$C_2"+Na$
537.3	535.9998	1.3002	82	C_2+Na
560.31	558.5475	1.7570	632	$[M-4H+Na]^{2-}$
644.49	644.0444	0.4456	32	$^{1,5}A_3$
690.41	690.0499	0.3599	62	C_3

Table B.4. Fragment ion list for He-CTD of $[M-3H]^{3-}$ (*m/z* 378.47) of IdoA2S-GlcNS6S-IdoA-GlcNAc6S-$(CH_2)_5NH_2$

Measured m/z	Calculated m/z	Accuracy (Da)	Intensity	Assigned Cleavage
378.47	378.7054	-0.2356	220698	$[M-3H]^{3-}$
383.05	384.4997	-1.4552	1584	C_3^{2-}
384.55	385.1275	-0.5783	1211	Y_1
400.08	400.589	-0.5096	2154	$[Y_3\text{-}SO_3]^{2-}$
412.6	413.1224	-0.5231	918	$^{1,5}X_1$
415.54	416.0504	-0.5111	1917	$B_2\text{-}2SO_3$
431.58	431.5621	0.0179	966	Z_3^{2-}
440.15	440.5674	-0.4178	824	Y_3^{2-}
454.69	454.5648	0.1251	500	$^{1,5}X_3^{2-}$
461.31	463.1922	-1.8899	237	$Z_2\text{-}SO_3$
481.2	481.2027	-0.0027	849	$Y_2\text{-}SO_3$
499.45	501.5511	-2.1011	754	$^{2,4}X_1$
512.58	512.1257	0.4539	518	$B_3\text{-}3SO_3$
514.64	516.5563	-1.9235	380	$^{0,3}X_3^{2-}$
520.3	522.2293	-1.9365	274	$^{0,2}X_2\text{-}2SO_3$
529.53	530.1363	-0.6070	730	$C_3\text{-}3SO_3$
539.76	538.5512	1.2060	390	$^{2,4}X_3^{2-}$
544.46	543.149	1.3078	308	Z_2
563	561.1596	1.8344	699	Y_2
570.11	568.5618	1.5440	848	$[M-3H]^{2-}$
586.6	586.1625	0.4372	309	$^{3,5}A_4\text{-}4SO_3$
596.89	593.9746	2.9154	472	C_2
688.07	690.0499	-1.9856	258	$C_3\text{-}SO_3$
712.45	713.1375	-0.6875	93	$^{1,4}X_2$
832.49	830.1801	2.3099	85	$^{1,5}X_3\text{-}2SO_3$
847.56	847.1238	0.4362	136	$^{1,5}A_4\text{-}2SO_3$
875.85	874.2063	1.6437	134	$^{0,3}X_3\text{-}2SO_3$
884.51	883.0544	1.4556	99	$^{1,4}A_4$
899.96	898.2605	1.6995	131	$[M\text{-}2H\text{-}3SO_3]^{-}$
919.73	918.1961	1.5339	207	$^{2,4}X_3\text{-}2SO_3$

Table B.5. Fragment ion list for He-CTD of $[M-2H]^{2-}$ (*m/z* 458.46) of ΔHexA-GalNAc4S-IdoA-GalNAc4S-OH

Measured m/z	Calculated m/z	Accuracy (Da)	Intensity	Assigned Cleavage
458.46	458.0610	0.3987	1.30E+07	C_2
458.46	458.0610	0.3987	1.30E+07	$[M-2H]^{2-}$
458.46	458.0610	0.3987	1.30E+07	Z_2
474.12	476.0716	-1.9596	32665	Y_2
500.23	500.0716	0.1584	75233	$^{2,4}A_3$
504.25	504.0665	0.1835	42641	$^{1,5}X_2$
528.33	528.0665	0.2634	19387	$^{3,5}A_3$
574.33	574.0720	0.2579	21538	$^{0,2}A_3$
616.33	616.0825	0.2474	14386	B_3
634.34	634.0931	0.2468	147359	C_3
661.38	661.1404	0.2395	13935	Z_3-SO_3
720.3	721.1615	-0.8625	113294	$^{0,2}X_3$-SO_3
800.2	801.1183	-0.9194	205728	$^{0,2}X_3$
819.21	819.1641	0.0459	32786	$[M-2H-SO_3-H_2O]^-$
837.21	836.1661	1.0439	104116	$[M-2H-SO_3]^-$
899.15	899.1203	0.0297	19615	$[M-2H-H_2O]^-$
917.17	916.1223	1.0477	208707	$[M-2H]^-$

Table B.6. Fragment ion list for He-CTD of $[M-3H]^{3-}$ (*m/z* 458.65) of ΔHexA-GalNAc4S-IdoA-GalNAc4S-IdoA-GalNAc4S-OH

Measured m/z	Calculated m/z	Accuracy (Da)	Intensity	Assigned Cleavage
450.32	449.0557	1.2607	4962	B_4^{2-}
458.65	458.0610	0.5882	2003394	C_2
458.65	458.0610	0.5882	2003394	C_4^{2-}
458.65	458.0610	0.5882	2003394	$[M-3H]^{3-}$
458.65	458.0610	0.5882	2003394	Z_4^{2-}
458.65	458.0610	0.5882	2003394	Z_2
465.63	467.0663	-1.4407	157308	Y_4^{2-}
476.26	476.0716	0.1884	74936	Y_2
480.24	481.0637	-0.8252	27491	$^{1,5}X_4^{2-}$
500.33	500.0716	0.2583	6780	$^{2,4}A_3$
518.46	516.0665	2.3935	41148	$^{0,2}A_5^{2-}$
528.15	528.0665	0.0835	3994	$^{3,5}A_3$
537.15	537.0718	0.0782	9143	B_5^{2-}
545.16	546.0770	-0.9170	1886	C_5^{2-}
554.25	554.1363	0.1137	1488	C_3-SO_3
568.69	568.6060	0.0840	1351	$[Y_5$-$SO_3]^{2-}$
574.14	574.0720	0.0680	5643	$^{0,2}A_3$
589.19	589.6112	-0.4216	4974	$[^{0,2}X_5$-$SO_3]^{2-}$
616.14	616.0825	0.0575	3902	B_3
629.16	629.5897	-0.4300	4989	$^{0,2}X_5^{2-}$
634.14	634.0931	0.0469	4002	C_3-SO_3
647.68	647.6167	0.0633	11283	$[M-3H-SO_3]^{2-}$
679.15	678.5910	0.5590	3641	$[M-3H-H_2O]^{2-}$
687.64	687.5951	0.0449	20373	$[M-3H]^{2-}$
706.6	707.1459	-0.5463	7324	$1,5X_3$-SO_3
720.15	721.1615	-1.0129	2770	$0,2X_3$-SO_3
741.07	741.0972	-0.0272	2059	Z_3
759.11	759.1078	0.0022	3017	Y_3
782.09	783.1183	-1.0283	10952	$^{0,2}X_3$-H_2O
787.1	787.1027	-0.0027	2545	$^{1,5}X_3$
800.11	801.1183	-1.0096	3562	$^{0,2}X_3$
819.14	819.1619	-0.0219	7890	B_4-SO_3
837.14	837.1725	-0.0325	5000	C_4-SO_3
837.14	837.1725	-0.0325	5000	Z_4-SO_3
855.13	855.1830	-0.0530	3900	Y_4-SO_3
899.08	899.1187	-0.0387	33946	B_4
907.13	907.1779	-0.0479	3050	$^{3,5}A_5$-SO_3
917.08	917.1293	-0.0493	4129	C_4
917.08	917.1293	-0.0493	4129	Z_4
935.08	935.1398	-0.0598	3251	Y_4
955.01	953.1834	1.8231	2075	$^{0,2}A_5$-SO_3
963.09	963.1348	-0.0448	992	$^{1,5}X_4$
987.06	987.1348	-0.0748	1490	$^{3,5}A_5$
1013.14	1013.2045	-0.0646	2493	C_5-SO_3
1033.06	1033.1402	-0.0802	696	$^{0,2}A_5$
1093.13	1093.1614	-0.0314	1897	C_5

Table B.7. Fragment ion list for He-CTD of $[M-3H]^{3-}$ (*m/z* 458.42) of ΔHexA-GalNAc4S-GlcA-GalNAc4S-GlcA-GalNAc4S-OH

Measured m/z	Calculated m/z	Accuracy (Da)	Intensity	Assigned Cleavage
450.19	449.0557	1.1314	7502	B_4^{2-}
458.42	458.0610	0.3587	1515533	C_2
458.42	458.0610	0.3587	1515533	C_4^{2-}
458.42	458.0610	0.3587	1515533	$[M-3H]^{3-}$
458.42	458.0610	0.3587	1515533	Z_4^{2-}
458.42	458.0610	0.3587	1515533	Z_2
465.64	467.0663	-1.4306	47640	Y_4^{2-}
476.29	476.0716	0.2183	8702	Y_2
480.24	481.0637	-0.8252	8101	$^{1,5}X_4^{2-}$
537.05	537.0718	-0.0218	1953	B_5^{2-}
589.08	589.6112	-0.5317	3254	$[^{0,2}X_5\text{-}SO_3]^{2-}$
599.96	599.1941	0.7649	3069	$Y_3\text{-}2SO_3$
603.22	602.6009	0.6185	1800	$[^{1,4}A_6\text{-}SO_3]^{2-}$
612.13	612.6140	-0.4844	2270	$[^{3,5}X_5\text{-}SO_3]^{2-}$
616.05	616.0825	-0.0325	11079	B_3
629.05	629.5897	-0.5401	8445	$^{0,2}X_5^{2-}$
634.07	634.0931	-0.0231	2441	C_3
638.59	640.1731	-1.5870	2970	$^{2,5}A_4\text{-}2SO_3$
647.57	647.6167	-0.0467	7594	$[M-2H\text{-}SO_3]^{2-}$
661.09	661.1404	-0.0504	1707	$Z_3\text{-}SO_3$
670.5	671.2153	-0.7160	1523	$^{0,3}X_3\text{-}2SO_3$
678.57	678.1439	0.4261	2584	$Y_3'\text{-}SO_3$
681.5	679.1509	2.3491	1929	$Y_3\text{-}SO_3$
687.08	687.5951	-0.5155	1650	$[M-3H]^{2-}$
707	707.1459	-0.1459	3621	$^{1,5}X_3\text{-}SO_3$
712.52	711.2102	1.3074	5314	$^{1,5}A_4\text{-}2SO_3$
741	741.0972	-0.0972	1596	Z_3
819.1	819.1619	-0.0619	2824	$B_4\text{-}SO_3$
837.14	837.1725	-0.0325	3654	$Z_4\text{-}SO_3$
899.06	899.1187	-0.0587	6942	B_4
905.51	907.1779	-1.6710	1975	$^{3,5}A_5\text{-}SO_3$
915.07	915.1142	-0.0442	2346	Z_4''
915.07	915.1142	-0.0442	2346	C_4''
917.07	917.1293	-0.0593	6090	C_4
917.07	917.1293	-0.0593	6090	Z_4
935.09	935.1398	-0.0498	3675	Y_4
1013.18	1013.2045	-0.0245	1726	$C_5\text{-}SO_3$
1093.09	1093.1614	-0.0714	1914	C_5

APPENDIX C

Investigation of the Experimental Parameters of Ultraviolet Photodissociation for the Structural Characterization of Chondroitin Sulfate Glycosaminoglycan Isomers

Supplemental Data

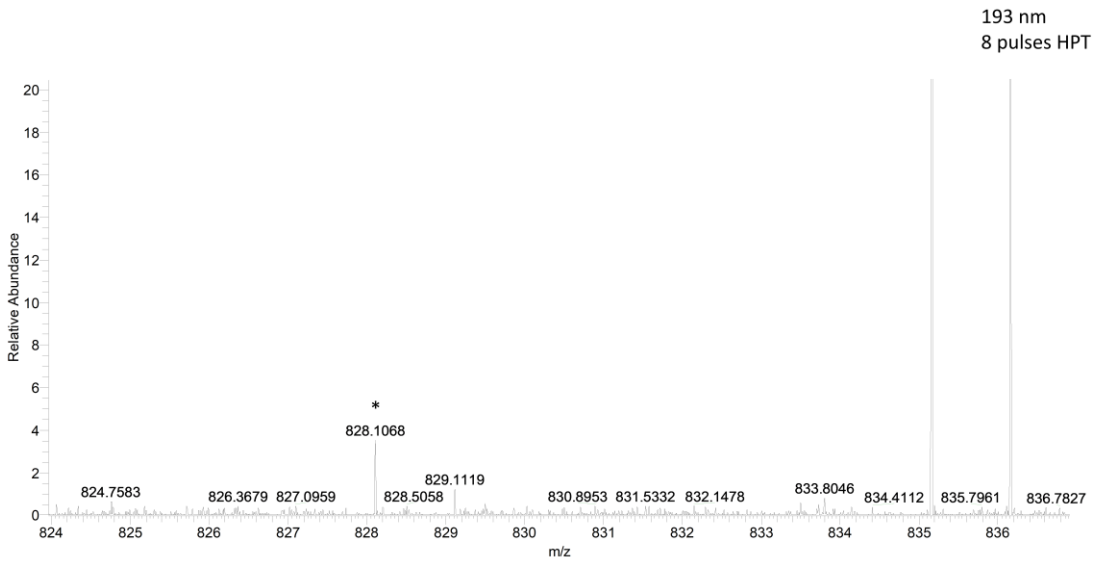

Figure C.1. Zoomed in view of $^{1,4}A_4$ fragment ion

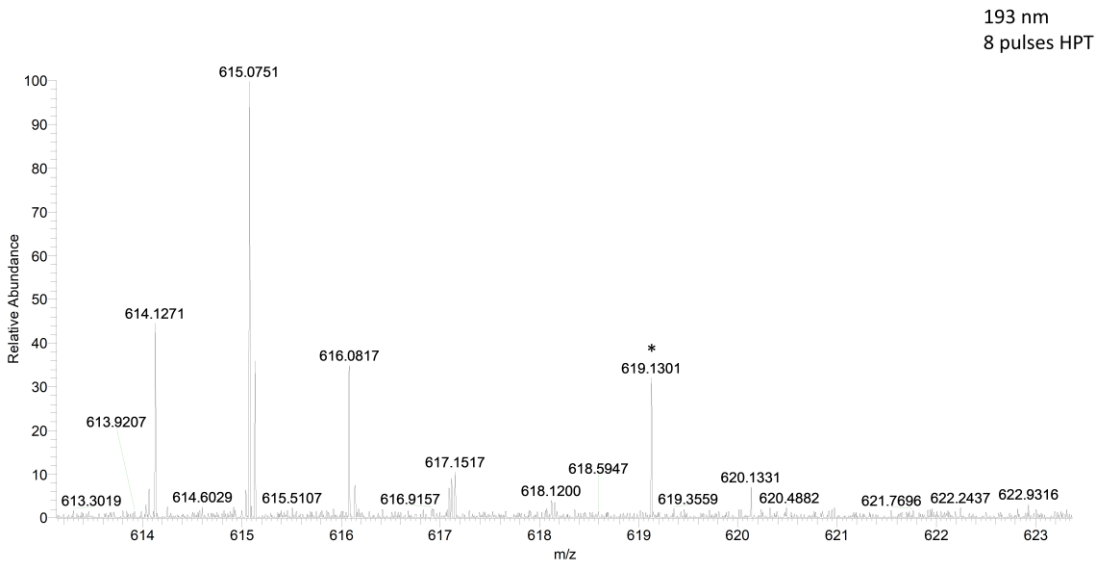

Figure C.2. Zoomed in view of $^{2,4}X_2$ fragment ion

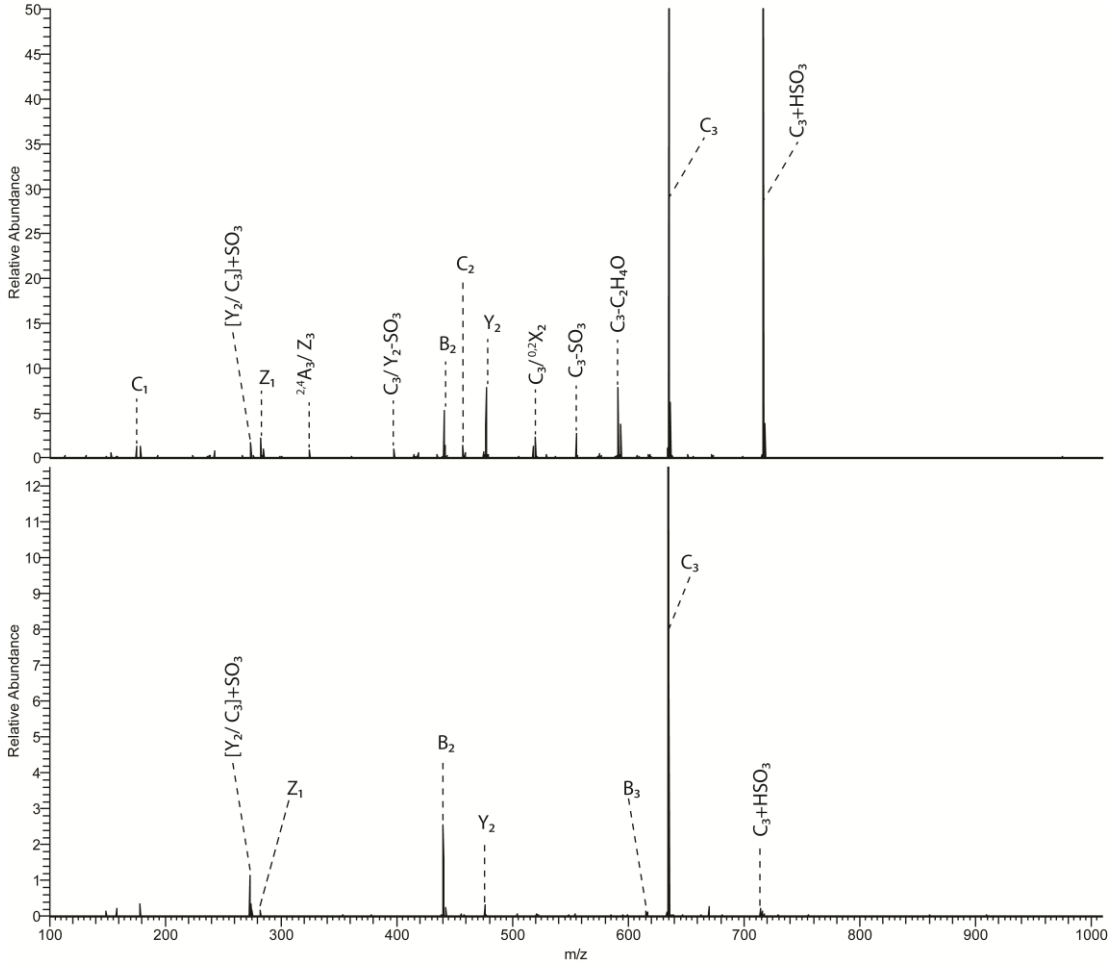

Figure C.3. MS^3 activation of the fragment ion m/z 715.05 of DS dp4 using (top) 193 nm UVPD (8 pulses, 4 mJ)/ 193 nm UVPD (8 pulses, 4 mJ) and (bottom) 193 nm UVPD (8 pulses, 4 mJ)/ HCD (NCE 20). Fragment ion lists are shown in Tables C.23 and C.24.

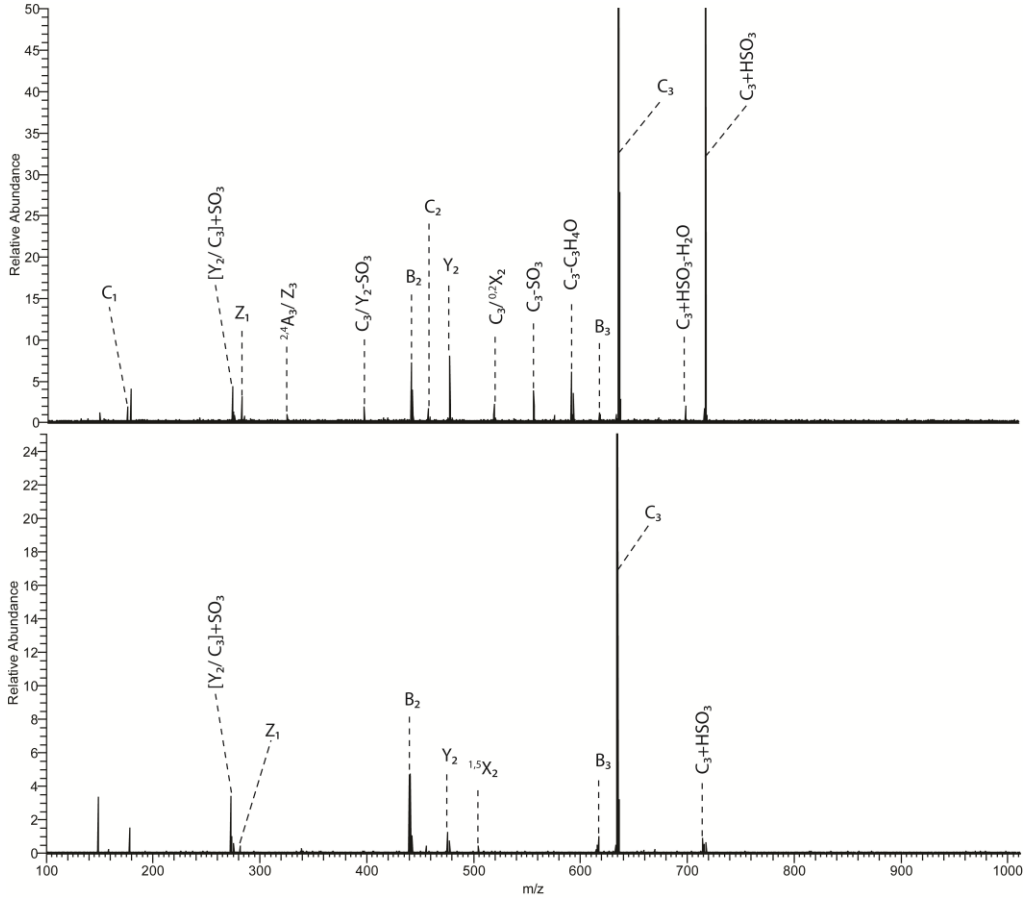

Figure C.4. MS^3 activation of the fragment ion m/z 715.05 of CS-A dp4 using (top) 193 nm UVPD (8 pulses, 4 mJ)/ 193 nm UVPD (8 pulses, 4 mJ) and (bottom) 193 nm UVPD (8 pulses, 4 mJ)/ HCD (NCE 20). Fragment ion lists are shown in Tables C.25 and C.26.

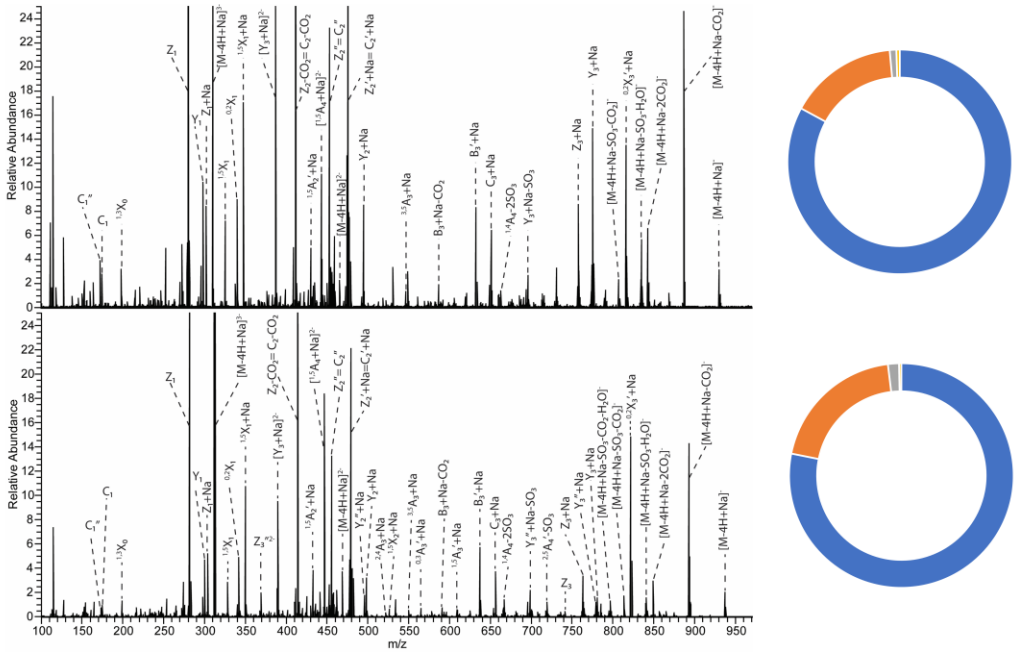

Figure C.5. 193 nm UVPD with 8 laser pulses in the high-pressure cell of the $[M-4H+Na]^{3-}$ precursor of DSdp4 (top) and CS-A dp4 (bottom). Donut plots depict intensity distributions if glycosidic fragments (blue), cross-ring fragments (orange), glycosidic fragments with SO_3 loss (grey) and cross-ring fragments with SO_3 loss (yellow). Fragment ion lists are shown in Tables C.15 and C.16.

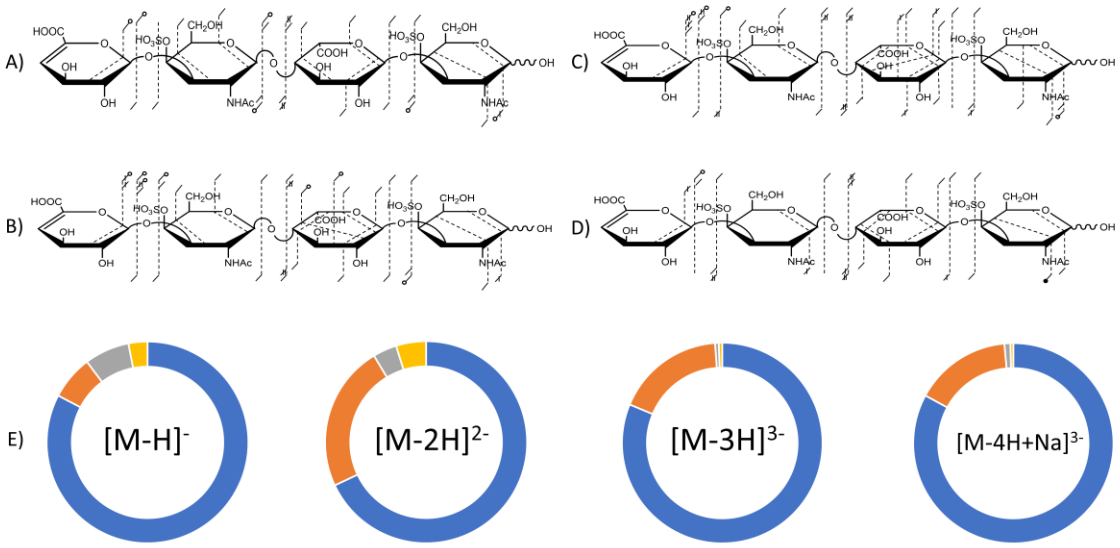

Figure C.6. Annotated fragment maps depicting 193 nm UVPD fragment ion diversity using 8 laser pulses in the high-pressure cell for A) DS $[M-H]^-$ precursor, B) DS $[M-2H]^{2-}$ precursor, C) DS $[M-3H]^{3-}$ precursor and D) DS $[M-4H+Na]^{3-}$ precursor. E) Donut plots depicting the intensity distribution of glycosidic fragments (blue), cross-ring fragments (orange), glycosidic fragments with SO_3 loss (grey) and cross-ring fragments with SO_3 loss (yellow) of each precursor.

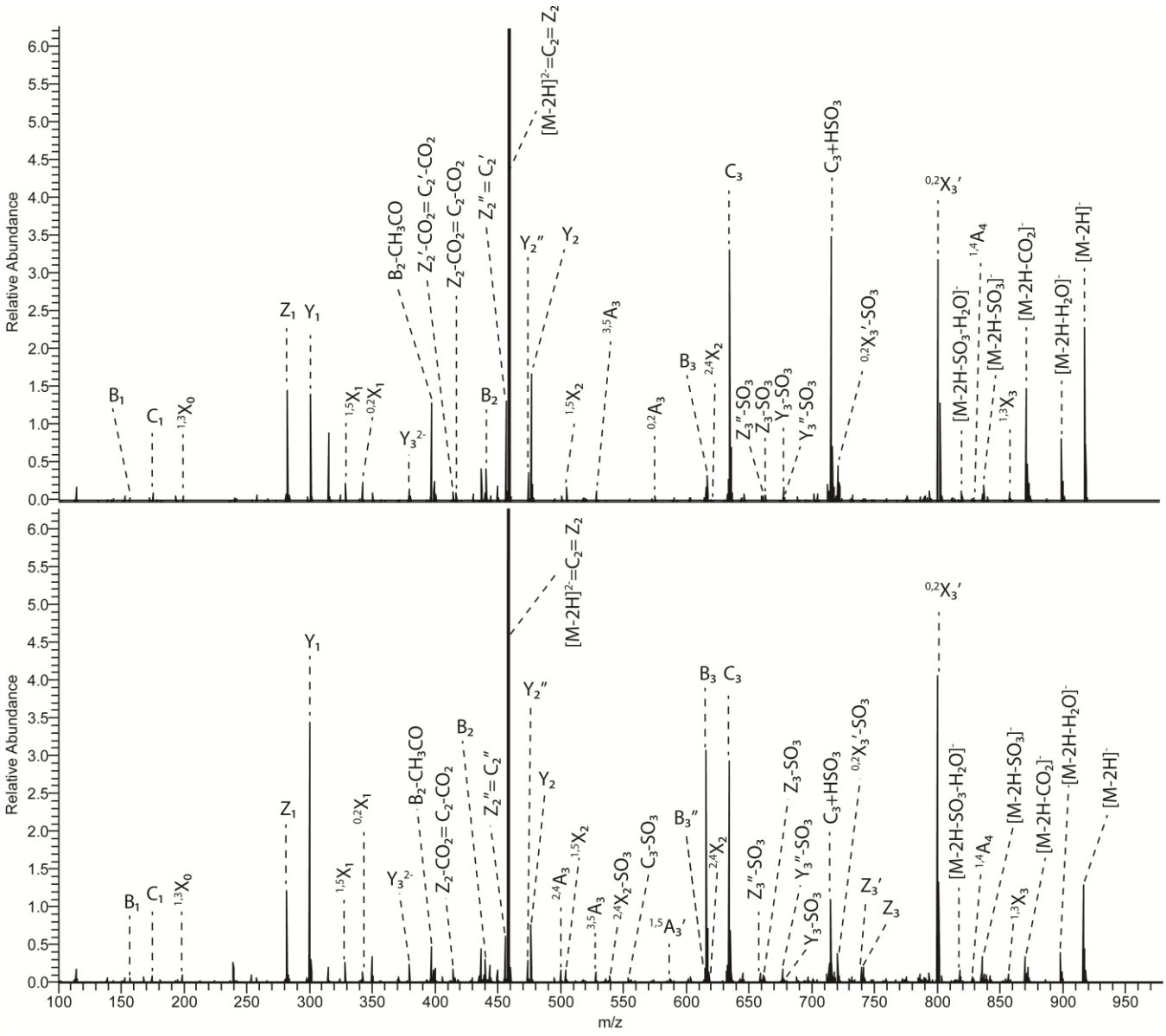

Figure C.7. 193 nm UVPD spectra of the $[M-2H]^{2-}$ precursor ion using 4 laser pulses in the high-pressure cell of (top) DS and (bottom) CS-A.

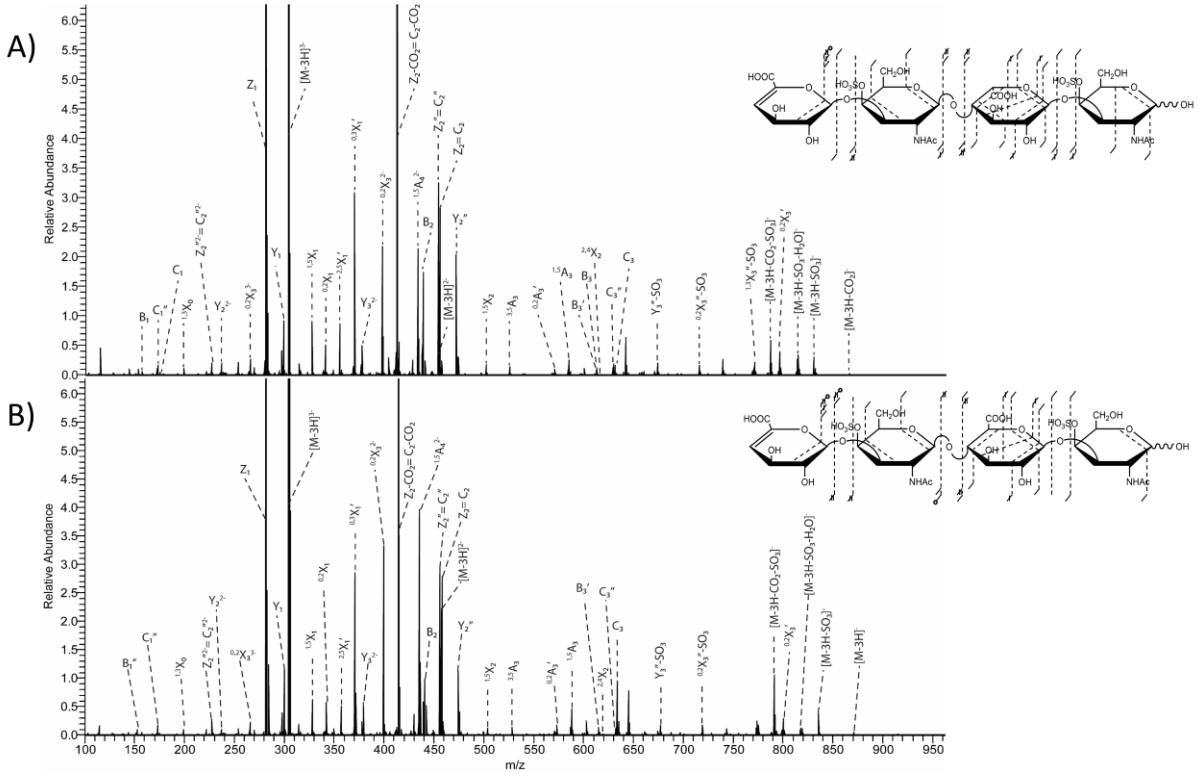

Figure C.8. 193 nm UVPD with 4 laser pulses in the high-pressure cell spectra and annotated fragment map insets of A) dermatan sulfate dp4 and B) chondroitin sulfate A dp4 using the $[M\text{-}3H]^{3-}$ precursor ion.

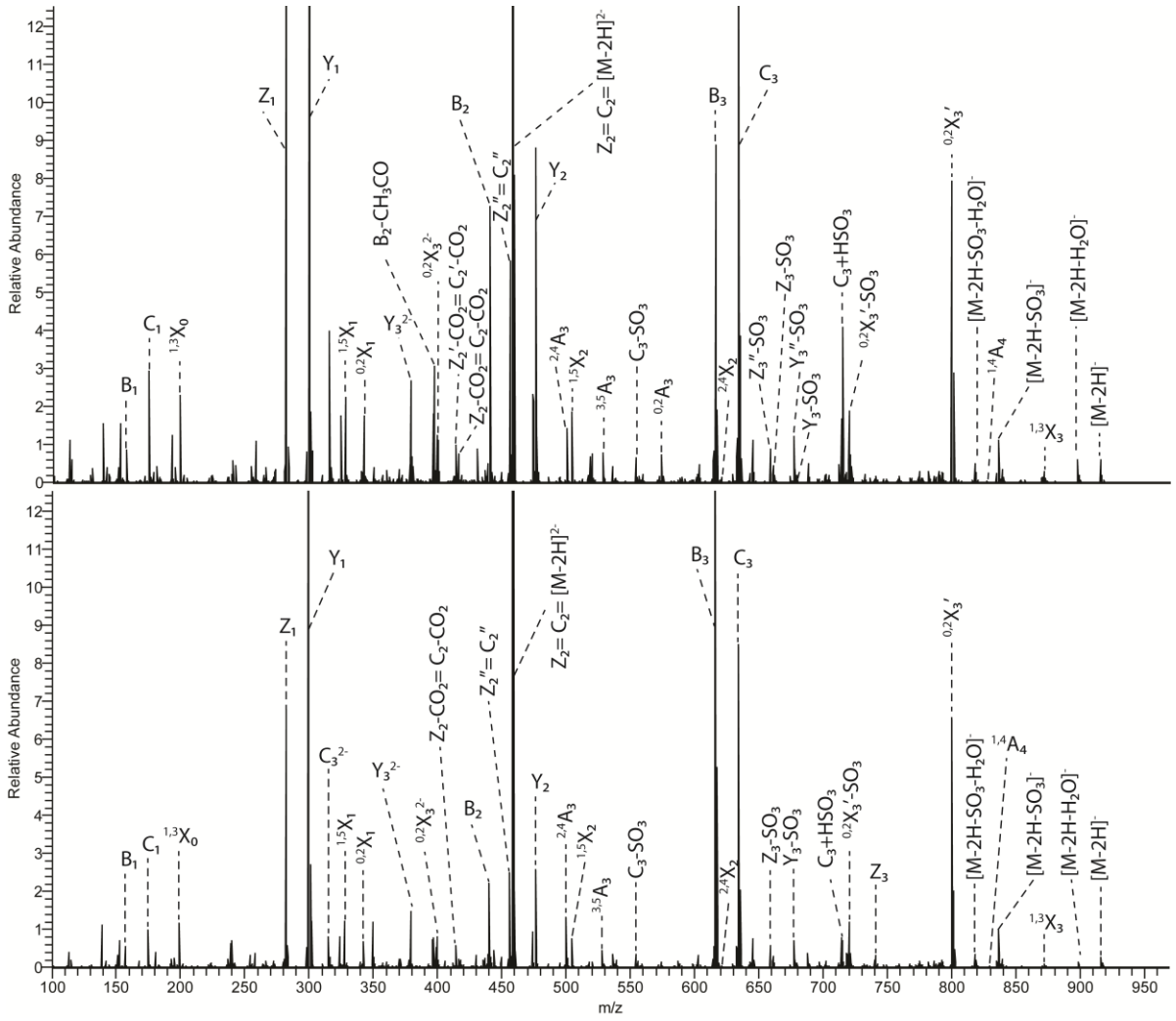

Figure C.9. 193 nm UVPD spectra of the $[M-2H]^{2-}$ precursor ion using 8 laser pulses in the low-pressure cell of (top) DS and (bottom) CS-A.

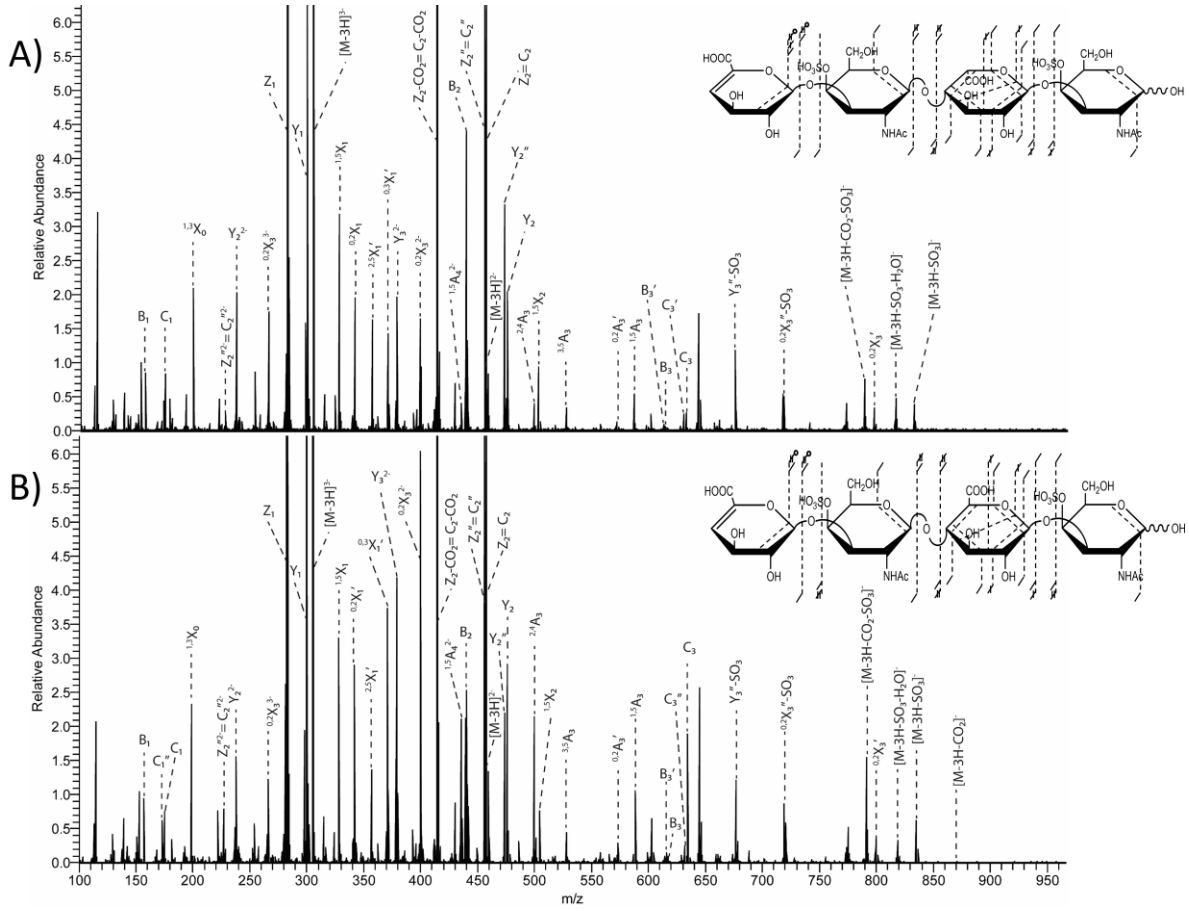

Figure C.10. 193 nm UVPD using 8 laser pulses in the low-pressure cell spectra and fragment map insets of the $[M-3H]^{3-}$ precursor of A) dermatan sulfate and B) chondroitin sulfate A.

Table C.1. Fragment ion list for 193 nm UVPD activation of the $[M-H]^-$ precursor of CS-A dp4 (8 pulses, 4 mJ)

Measured m/z	Calculated m/z	Accuracy (PPM)	Intensity	Assigned Fragment
157.0144	157.0142469	0.975261819	4754.8	B_1
175.025	175.0248116	1.076670207	27347.4	C_1
198.9921	198.9917969	1.523339177	6025.7	$^{1,3}X_0$
282.0293	282.0289107	1.380514501	63313.8	Z_1
300.0399	300.0394753	1.415343766	83608.1	Y_1
328.0348	328.03439	1.249981751	16121.5	$^{1,5}X_1$
360.0941	360.0936194	1.334650144	4561.8	B_2-SO_3
396.1153	396.1147488	1.391584135	8744.8	Y_2-SO_3
416.051	416.050434	1.360515348	10277.6	$^{2,4}X_1$
440.051	440.050434	1.286313925	206886.1	B_2
456.0459	456.045898	0.004385523	29959.4	Z_2"
456.0459	456.045898	0.004385523	29959.4	C_2"
458.0616	458.0609986	1.312831703	33634.5	Z_2
458.0616	458.0609986	1.312831703	33634.5	C_2
476.0721	476.0715633	1.127290606	145963.3	Y_2
504.0672	504.066478	1.432447966	12921.9	$^{1,5}X_2$
554.137	554.1362721	1.313620921	17647.9	C_3-SO_3
599.195	599.1941213	1.466462986	6341.5	Y_3-$2SO_3$
616.0833	616.0825219	1.262907114	10504	B_3
619.1306	619.1298065	1.281656919	6574.7	$^{2,4}X_2$
634.0939	634.0930866	1.282728068	45667.9	C_3-SO_3
659.1258	659.12537	0.652379683	7025.5	Z_3"-SO_3
661.1414	661.1403712	1.556138522	4845.1	Z_3-SO_3
679.152	679.1509359	1.566868194	15239.8	Y_3-SO_3
715.059	715.0564	3.636076818	11169.5	C_3+HSO_3
721.1627	721.1615005	1.663225226	17917.1	$^{0,2}X_3$-SO_3
757.2169	757.2156446	1.657908165	29523.8	$[M-H-2SO_3]^-$
793.1836	793.1832	0.504297116	2483.7	$[M-H-SO_3-CO_2]^-$
819.1631	819.162459	0.782506563	61997.5	$[M-H-SO_3-H_2O]^-$
827.0969	827.0975797	-0.821741009	187.8	$^{1,4}A_4$
837.1736	837.1724592	1.362727581	1448867.4	$[M-H-SO_3]^-$
873.1342	873.13999	-6.631239053	1528	$[M-H-CO_2]^-$
899.1179	899.11927	-1.523713311	1730.4	$[M-H-H_2O]^-$
917.1305	917.1292737	1.337087405	872408.2	$[M-H]^-$

Table C.2. Fragment ion list for 193 nm UVPD activation of the $[M-H]^-$ precursor of DS dp4 (8 pulses, 4 mJ)

Measured m/z	Calculated m/z	Accuracy (PPM)	Intensity	Assigned Fragment
157.0139	157.0142469	-2.209162588	1766.1	B_1
175.0246	175.0248116	-1.208720056	13065.1	C_1
198.9913	198.9917969	-2.496927048	1559.4	$^{1,3}X_0$
282.0282	282.0289107	-2.519794858	26137.3	Z_1
300.0388	300.0394753	-2.250840488	19226.8	Y_1
328.0339	328.03439	-1.493633027	3473.2	$^{1,5}X_1$
360.0932	360.0936194	-1.16469989	1391.2	B_2-SO_3
396.1143	396.1147488	-1.132936861	3578.2	Y_2-SO_3
416.0499	416.050434	-1.283394885	3842.2	$^{2,4}X_1$
440.0498	440.050434	-1.440646231	48973.7	B_2
456.0447	456.045898	-2.626928573	14909.7	Z_2"
456.0447	456.045898	-2.626928573	14909.7	C_2"
458.0604	458.0609986	-1.306906724	6574.3	Z_2
458.0604	458.0609986	-1.306906724	6574.3	C_2
476.0708	476.0715633	-1.603391292	40616.8	Y_2
504.0657	504.066478	-1.543350001	7956.5	$^{1,5}X_2$
554.1354	554.1362721	-1.573755489	6185.4	C_3-SO_3
574.0715	574.0719573	-0.796518614	424.7	$^{0,2}A_3$
616.0817	616.0825219	-1.334147571	3080.5	B_3
619.129	619.1298065	-1.302615367	2409.7	$^{2,4}X_2$
634.092	634.0930866	-1.713677413	20116.8	C_3
679.15	679.1509359	-1.377985291	4901	Y_3-SO_3
715.0565	715.0564	0.139849108	6828.5	C_3+HSO_3
721.1603	721.1615005	-1.66473945	4935.5	$^{0,2}X_3$-SO_3
757.2144	757.2156446	-1.643661233	3623.9	$[M-H-2SO_3]^-$
793.1798	793.1832	-4.286525484	6211.2	$[M-H-SO_3-CO_2]^-$
819.1605	819.162459	-2.391467014	18817	$[M-H-SO_3-H_2O]^-$
828.1042	828.1049	-0.845303536	397	$^{1,4}A_4$
837.1713	837.1724592	-1.384615544	475284.8	$[M-H-SO_3]^-$
873.1326	873.13999	-8.463705803	9581.9	$[M-H-CO_2]^-$
899.1152	899.11927	-4.526651954	1583.4	$[M-H-H_2O]^-$
917.1278	917.1292737	-1.60688143	216655.7	$[M-H]^-$

Table C.3. Fragment ion list for 193 nm UVPD activation of the $[M-2H]^{2-}$ precursor of DS dp4 in the high-pressure cell (8 pulses, 4 mJ)

Measured m/z	Calculated m/z	Accuracy (PPM)	Intensity	Assigned Fragment
157.0142	157.0142469	-0.298507944	386771	B_1
175.0247	175.0248116	-0.63737249	660087.6	C_1
198.9917	198.9917969	-0.486793936	950130.3	$^{1,3}X_0$
282.0289	282.0289107	-0.037779811	7631718.5	Z_1
300.0394	300.0394753	-0.251103622	1.80E+07	Y_1
328.0343	328.03439	-0.274248682	1600171.8	$^{1,5}X_1$
342.05	342.05004	-0.117020887	833672	$^{0,2}X_1$
379.0501	379.050237	-0.361408557	1109182.6	Y_3^{2-}
414.071	414.07171	-1.714678841	939309.6	Z_2-CO_2
414.071	414.07171	-1.714678841	939309.6	C_2-CO_2
440.0505	440.050434	0.150080527	2134325.8	B_2
456.0463	456.04599	0.679756004	3582480	Z_2"
456.0463	456.04599	0.679756004	3582480	C_2"
458.0615	458.0609986	1.094520168	2.47E+08	Z_2
458.0615	458.0609986	1.094520168	2.47E+08	$[M-2H]^{2-}$
458.0615	458.0609986	1.094520168	2.47E+08	C_2
476.0714	476.0715633	-0.34307657	4630654.5	Y_2
500.0718	500.0715633	0.473274264	1065457.4	$^{2,4}A_3$
504.0664	504.066478	-0.154644283	1073665.1	$^{1,5}X_2$
528.0667	528.066478	0.420494408	894172.8	$^{3,5}A_3$
554.1364	554.1362721	0.230854767	701168.8	C_3-SO_3
616.0828	616.0825219	0.451327525	1.56E+07	B_3
619.1304	619.1298065	0.958622883	102350.4	$^{2,4}X_2$
634.0933	634.0930866	0.336494758	1.71E+07	C_3
659.125	659.12537	-0.56134996	7.65E+05	Z_3"-SO_3
661.1411	661.1403712	1.102377092	715256	Z_3-SO_3
677.1356	677.135935	-0.494730796	1.75E+06	Y_3"-SO_3
679.1539	679.1509359	4.364479004	169428.4	Y_3-SO_3
715.0581	715.05635	2.447359568	5721797	C_3+HSO_3
720.154	720.1545	-0.69429546	4002868.8	$^{0,2}X_3$'-SO_3
740.0898	740.0901	-0.405356051	1088177.6	Z_3'
741.0971	741.0971857	-0.115679833	1063499.8	Z_3
801.1146	801.1183151	-4.637394914	6340332	$^{0,2}X_3$'
818.1544	818.15545	-1.283374694	876701.9	$[M-2H-SO_3-H_2O]^-$
827.0975	827.0975797	-0.096312699	99521.7	$^{1,4}A_4$
836.1647	836.1654	-0.837154946	2034560.1	$[M-2H-SO_3]^-$
857.108	857.1081443	-0.168410486	516611.3	$^{1,3}X_3$
872.1333	872.13327	0.034398412	898920.7	$[M-2H-CO_2]^-$
898.1113	898.11227	-1.080043144	2054511.9	$[M-2H-H_2O]^-$
916.1216	916.12227	-0.731343426	6796009	$[M-2H]^-$

Table C.4. Fragment ion list for 193 nm UVPD activation of the $[M-2H]^{2-}$ precursor of DS dp4 in the low-pressure cell (8 pulses, 4 mJ)

Measured m/z	Calculated m/z	Accuracy (PPM)	Intensity	Assigned Fragment
157.0141	157.0142469	-0.935392825	17872.5	B_1
175.0248	175.0248116	-0.066024925	58180.2	C_1
198.9917	198.9917969	-0.486793936	45844.3	$^{1,3}X_0$
282.0285	282.0289107	-1.456074124	339557.2	Z_1
300.0391	300.0394753	-1.250972055	704381.8	Y_1
328.0342	328.03439	-0.579094768	44679.4	$^{1,5}X_1$
342.05	342.05004	-0.117020887	35065	$^{0,2}X_1$
379.05	379.050237	-0.62522583	54292.4	Y_3^{2-}
397.0319	397.0315	1.007476737	60756.7	B_2-CH_3CO
400.0556	400.0555193	0.201634514	22921.3	$^{0,2}X_3^{2}$-
413.0633	413.0647	-3.389299546	3320.1	Z_2'-CO_2
413.0633	413.0647	-3.389299546	3320.1	C_2'-CO_2
414.071	414.07171	-1.714678841	19815.1	Z_2-CO_2
414.071	414.07171	-1.714678841	19815.1	C_2-CO_2
440.0502	440.050434	-0.531659512	148273.9	B_2
456.0453	456.04599	-1.5130053	117860	Z_2"
456.0453	456.04599	-1.5130053	117860	C_2"
458.0608	458.0609986	-0.433660581	2006954.3	Z_2
458.0608	458.0609986	-0.433660581	2006954.3	$[M-2H]^{2-}$
458.0608	458.0609986	-0.433660581	2006954.3	C_2
476.0712	476.0715633	-0.763181477	177077.2	Y_2
500.0713	500.0715633	-0.52658263	29257.2	$^{2,4}A_3$
504.0662	504.066478	-0.551417345	37637.9	$^{1,5}X_2$
554.1359	554.1362721	-0.671450361	13126.2	C_3-SO_3
574.0715	574.0719573	-0.796518614	15225.3	$^{0,2}A_3$
616.082	616.0825219	-0.847199817	182301.3	B_3
619.1295	619.1298065	-0.495030278	1388.3	$^{2,4}X_2$
634.0926	634.0930866	-0.767444103	359430.4	C_3
659.1243	659.12537	-1.623363398	17811.9	Z_3"-SO_3
661.1404	661.1403712	0.043600423	9227.2	Z_3-SO_3
677.1348	677.135935	-1.676177472	24949.8	Y_3"-SO_3
679.152	679.1509359	1.566868194	3678.1	Y_3-SO_3
715.0571	715.05635	1.048868386	81697	C_3+HSO_3
720.153	720.1545	-2.082886381	37093.3	$^{0,2}X_3$'-SO_3
800.11	800.1113	-1.624773953	166729.6	$^{0,2}X_3$'
818.1535	818.15545	-2.383410145	9743.9	$[M-2H-SO_3-H_2O]^-$
827.0982	827.0975797	0.750020331	693.7	$^{1,4}A_4$
836.1641	836.1654	-1.554716328	23056.5	$[M-2H-SO_3]^-$
857.1071	857.1081443	-1.218453011	1212.1	$^{1,3}X_3$
898.1103	898.11227	-2.193489685	11987.5	$[M-2H-H_2O]^-$
916.1208	916.12227	-1.604589309	11957	$[M-2H]^-$

Table C.5. Fragment ion list for 193 nm UVPD activation of the $[M-2H]^{2-}$ precursor of DS dp4 in the high-pressure cell (4 pulses, 4 mJ)

Measured m/z	Calculated m/z	Accuracy (PPM)	Intensity	Assigned Fragment
157.014	157.0142469	-1.572277707	6953.8	B_1
175.0249	175.0248116	0.505322641	16848.2	C_1
198.9918	198.9917969	0.015739342	10000	$^{1,3}X_0$
282.0286	282.0289107	-1.101500546	199780	Z_1
300.0392	300.0394753	-0.917682577	189802.1	Y_1
328.0343	328.03439	-0.274248682	31623.4	$^{1,5}X_1$
342.0501	342.05004	0.175333998	34777.3	$^{0,2}X_1$
379.0503	379.050237	0.16622599	22734.6	Y_3^{2-}
397.032	397.0315	1.259345921	170944.9	B_2-CH_3CO
413.0632	413.0647	-3.63139237	3858.2	Z_2'-CO_2
413.0632	413.0647	-3.63139237	3858.2	C_2'-CO_2
414.0709	414.07171	-1.956182904	17390.1	Z_2-CO_2
414.0709	414.07171	-1.956182904	17390.1	C_2-CO_2
440.0505	440.050434	0.150080527	60421.8	B_2
456.0465	456.04599	1.118308265	172432.4	Z_2''
456.0465	456.04599	1.118308265	172432.4	C_2''
458.0617	458.0609986	1.531143239	1.28E+07	Z_2
458.0617	458.0609986	1.531143239	1.28E+07	$[M-2H]^{2-}$
458.0617	458.0609986	1.531143239	1.28E+07	C_2
474.0558	474.0566	-1.687562203	5.23E+04	Y_2''
476.0714	476.0715633	-0.34307657	218874.9	Y_2
504.0662	504.066478	-0.551417345	26911.2	$^{1,5}X_2$
528.0667	528.066478	0.420494408	19263.5	$^{3,5}A_3$
574.0716	574.0719573	-0.622324424	11317.6	$^{0,2}A_3$
616.0824	616.0825219	-0.197936146	47829.5	B_3
619.1302	619.1298065	0.635588847	3900.4	$^{2,4}X_2$
634.093	634.0930866	-0.136621896	441769.4	C_3
659.1245	659.12537	-1.319930987	11566	Z_3''-SO_3
661.1411	661.1403712	1.102377092	10554.9	Z_3-SO_3
677.1351	677.135935	-1.233134969	26784.8	Y_3''-SO_3
679.1534	679.1509359	3.628265633	2733.1	Y_3-SO_3
715.0577	715.05635	1.887963095	448555.6	C_3+HSO_3
720.1536	720.1545	-1.249731828	62417	$^{0,2}X_3'$-SO_3
800.1106	800.1113	-0.874878283	424307	$^{0,2}X_3'$
818.1541	818.15545	-1.650053178	19694.3	$[M-2H-SO_3-H_2O]^-$
827.098	827.0975797	0.508210894	5531.3	$^{1,4}A_4$
836.1641	836.1654	-1.554716328	41388.1	$[M-2H-SO_3]^-$
857.108	857.1081443	-0.168410486	17270.3	$^{1,3}X_3$
872.1346	872.13327	1.524996289	32983.9	$[M-2H-CO_2]^-$
898.111	898.11227	-1.414077106	108724	$[M-2H-H_2O]^-$
916.1217	916.12227	-0.622187691	295978.7	$[M-2H]^-$

Table C.6. Fragment ion list for 193 nm UVPD activation of the $[M-2H]^{2-}$ precursor of CS-A dp4 in the high-pressure cell (8 pulses, 4 mJ)

Measured m/z	Calculated m/z	Accuracy (PPM)	Intensity	Assigned Fragment
157.0142	157.0142469	-0.298507944	386771	B_1
175.0247	175.0248116	-0.63737249	660087.6	C_1
198.9917	198.9917969	-0.486793936	950130.3	$^{1,3}X_0$
282.0289	282.0289107	-0.037779811	7631718.5	Z_1
300.0394	300.0394753	-0.251103622	1.80E+07	Y_1
328.0343	328.03439	-0.274248682	1600171.8	$^{1,5}X_1$
342.05	342.05004	-0.117020887	833672	$^{0,2}X_1$
379.0501	379.050237	-0.361408557	1109182.6	Y_3^{2-}
414.071	414.07171	-1.714678841	939309.6	Z_2-CO_2
414.071	414.07171	-1.714678841	939309.6	C_2-CO_2
440.0505	440.050434	0.150080527	2134325.8	B_2
456.0463	456.04599	0.679756004	3582480	Z_2''
456.0463	456.04599	0.679756004	3582480	C_2''
458.0615	458.0609986	1.094520168	2.47E+08	Z_2
458.0615	458.0609986	1.094520168	2.47E+08	$[M-2H]^{2-}$
458.0615	458.0609986	1.094520168	2.47E+08	C_2
476.0714	476.0715633	-0.34307657	4630654.5	Y_2
500.0718	500.0715633	0.473274264	1065457.4	$^{2,4}A_3$
504.0664	504.066478	-0.154644283	1073665.1	$^{1,5}X_2$
528.0667	528.066478	0.420494408	894172.8	$^{3,5}A_3$
554.1364	554.1362721	0.230854767	701168.8	C_3-SO_3
616.0828	616.0825219	0.451327525	1.56E+07	B_3
619.1304	619.1298065	0.958622883	102350.4	$^{2,4}X_2$
634.0933	634.0930866	0.336494758	1.71E+07	C_3
659.125	659.12537	-0.56134996	7.65E+05	Z_3''-SO_3
661.1411	661.1403712	1.102377092	715256	Z_3-SO_3
677.1356	677.135935	-0.494730796	1.75E+06	Y_3''-SO_3
679.1539	679.1509359	4.364479004	169428.4	Y_3-SO_3
715.0581	715.05635	2.447359568	5721797	C_3+HSO_3
720.154	720.1545	-0.69429546	4002868.8	$^{0,2}X_3$'-SO_3
740.0898	740.0901	-0.405356051	1088177.6	Z_3'
741.0971	741.0971857	-0.115679833	1063499.8	Z_3
801.1146	801.1183151	-4.637394914	6340332	$^{0,2}X_3$'
818.1544	818.15545	-1.283374694	876701.9	$[M-2H-SO_3-H_2O]^-$
827.0975	827.0975797	-0.096312699	99521.7	$^{1,4}A_4$
836.1647	836.1654	-0.837154946	2034560.1	$[M-2H-SO_3]^-$
857.108	857.1081443	-0.168410486	516611.3	$^{1,3}X_3$
872.1333	872.13327	0.034398412	898920.7	$[M-2H-CO_2]^-$
898.1113	898.11227	-1.080043144	2054511.9	$[M-2H-H_2O]^-$
916.1216	916.12227	-0.731343426	6796009	$[M-2H]^-$

Table C.7. Fragment ion list for 193 nm UVPD activation of the $[M-2H]^{2-}$ precursor of CS-A dp4 in the low-pressure cell (8 pulses, 4 mJ)

Measured m/z	Calculated m/z	Accuracy (PPM)	Intensity	Assigned Fragment
157.0141	157.0142469	-0.935392825	667880.4	B_1
175.0246	175.0248116	-1.208720056	1189419	C_1
198.9916	198.9917969	-0.989327214	1433519	$^{1,3}X_0$
282.0287	282.0289107	-0.746926967	8009461	Z_1
300.0392	300.0394753	-0.917682577	3.72E+07	Y_1
316.5426	316.5429051	-0.963848802	314679.3	C_3^{2-}
328.0341	328.03439	-0.883940855	1437117	$^{1,5}X_1$
342.0497	342.05004	-0.994085541	801432.8	$^{0,2}X_1$
379.0499	379.050237	-0.889043103	1757168	Y_3^{2-}
400.0553	400.0555193	-0.548261402	970361.3	$^{0,2}X_3^{2-}$
414.0708	414.07171	-2.197686966	702227.4	Z_2-CO_2
414.0708	414.07171	-2.197686966	702227.4	C_2-CO_2
440.0502	440.050434	-0.531659512	2661253	B_2
456.0455	456.04599	-1.074453039	2974363	Z_2"
456.0455	456.04599	-1.074453039	2974363	C_2"
458.0608	458.0609986	-0.433660581	1.23E+08	Z_2
458.0608	458.0609986	-0.433660581	1.23E+08	$[M-2H]^{2-}$
458.0608	458.0609986	-0.433660581	1.23E+08	C_2
476.0711	476.0715633	-0.973233931	3012829	Y_2
500.0714	500.0715633	-0.326611251	1600320	$^{2,4}A_3$
504.0661	504.066478	-0.749803876	940149.9	$^{1,5}X_2$
528.0663	528.066478	-0.336985979	530744.2	$^{3,5}A_3$
554.1359	554.1362721	-0.671450361	415093.5	C_3-SO_3
616.0823	616.0825219	-0.360252064	2.59E+07	B_3
619.1299	619.1298065	0.151037794	41896	$^{2,4}X_2$
634.0928	634.0930866	-0.452033	1.02E+07	C_3
661.1408	661.1403712	0.648615663	364385.8	Z_3-SO_3
679.1525	679.1509359	2.303081565	141212.1	Y_3-SO_3
715.0571	715.05635	1.048868386	850519.6	C_3+HSO_3
720.1534	720.1545	-1.527450012	1401252	$^{0,2}X_3$'-SO_3
741.0969	741.0971857	-0.385549972	385652	Z_3
800.1104	801.1183151	-1258.135138	8021901	$^{0,2}X_3$'
818.1537	818.15545	-2.138957823	418205.8	$[M-2H-SO_3-H_2O]^-$
828.1041	828.1049	-0.966061184	30484	$^{1,4}A_4$
836.1643	836.1654	-1.3155292	12194995	$[M-2H-SO_3]^-$
857.1077	857.1081443	-0.518424661	29294.8	$^{1,3}X_3$
898.1104	898.11227	-2.082145031	189617.8	$[M-2H-H_2O]^-$
916.121	916.12227	-1.386277838	340443.9	$[M-2H]^-$

Table C.8. Fragment ion list for 193 nm UVPD activation of the $[M-2H]^{2-}$ precursor of CS-A dp4 in the high-pressure cell (4 pulses, 4 mJ)

Measured m/z	Calculated m/z	Accuracy (PPM)	Intensity	Assigned Fragment
157.0142	157.0142469	-0.298507944	230344.6	B_1
175.0248	175.0248116	-0.066024925	316772.8	C_1
198.9918	198.9917969	0.015739342	370501.2	$^{1,3}X_0$
282.029	282.0289107	0.316793767	4713021.5	Z_1
300.0395	300.0394753	0.082185856	1.33E+07	Y_1
328.0344	328.03439	0.030597405	1025935.8	$^{1,5}X_1$
342.0501	342.05004	0.175333998	505210.3	$^{0,2}X_1$
379.0503	379.050237	0.16622599	937570.5	Y_3^{2-}
414.0711	414.07171	-1.473174779	647141.5	Z_2-CO_2
414.0711	414.07171	-1.473174779	647141.5	C_2-CO_2
440.0508	440.050434	0.831820566	1144941.4	B_2
456.0469	456.04599	1.995412787	2330769.3	Z_2"
456.0469	456.04599	1.995412787	2330769.3	C_2"
458.0619	458.0609986	1.96776631	4.08E+08	Z_2
458.0619	458.0609986	1.96776631	4.08E+08	$[M-2H]^{2-}$
458.0619	458.0609986	1.96776631	4.08E+08	C_2
474.0559	474.0566	-1.476616927	1.13E+06	Y_2"
476.0715	476.0715633	-0.133024116	2979715	Y_2
500.0721	500.0715633	1.0731884	604170.8	$^{2,4}A_4$
504.0666	504.066478	0.242128779	621596	$^{1,5}X_2$
528.067	528.066478	0.988604698	530658.8	$^{3,5}A_3$
539.1733	539.173	0.556407684	7734.6	$^{2,4}X_2$-SO_3
554.1367	554.1362721	0.772237844	240976	C_3-SO_3
587.0799	587.0806	-1.192340541	194752.9	$^{1,5}A_3$'
614.0679	614.0675	0.651394187	23024.5	B_3"
616.0831	616.0825219	0.938275279	1.19E+07	B_3
619.1314	619.1298065	2.573793061	47981.4	$^{2,4}X_2$
634.0936	634.0930866	0.809611413	1.16E+07	C_3
659.1252	659.12537	-0.257917549	5.11E+05	Z_3"-SO_3
661.1415	661.1403712	1.707392332	376637.7	Z_3-SO_3
677.1358	677.135935	-0.199369127	6.53E+05	Y_3"-SO_3
679.154	679.1509359	4.511721678	86170.9	Y_3-SO_3
715.0584	715.05635	2.866906923	4254010	C_3+HSO_3
720.1542	720.1545	-0.416577276	1496160.4	$^{0,2}X_3$'-SO_3
740.0901	740.0901	0	821365.9	Z_3'
741.0974	741.0971857	0.289125374	796138.7	Z_3
800.1113	800.1113	0	15970153	$^{0,2}X_3$'
818.1545	818.15545	-1.161148532	655793.9	$[M-2H-SO_3-H_2O]^-$
827.097	827.0975797	-0.700836291	64767	$^{1,4}A_4$
836.1651	836.1654	-0.358780691	1351615.3	$[M-2H-SO_3]^-$
857.1083	857.1081443	0.181603689	399077.3	$^{1,3}X_3$
872.1334	872.13327	0.149059788	747082.9	$[M-2H-CO_2]^-$
898.1116	898.11227	-0.746009182	1520385.9	$[M-2H-H_2O]^-$
916.122	916.12227	-0.294720485	4964973	$[M-2H]^-$

Table C.9. Fragment ion list for 193 nm UVPD activation of the $[M-3H]^{3-}$ precursor of DS dp4 in the high-pressure cell (8 pulses, 4 mJ)

Measured m/z	Calculated m/z	Accuracy (PPM)	Intensity	Assigned Fragment
173.0092	173.0098	-3.468011639	381285.4	C_1"
198.9918	198.9917969	0.015739342	779947.4	$^{1,3}X_0$
227.5187	227.51986	-5.09845602	326737.8	Z_2"$^{2-}$
227.5187	227.51986	-5.09845602	326737.8	C_2"$^{2-}$
266.3678	266.3679207	-0.453305337	7675.3	$^{0,2}X_3^{3-}$
282.0287	282.0289107	-0.746926967	9.23E+07	Z_1
300.0392	300.0394753	-0.917682577	4664430	Y_1
305.0382	305.0382403	-0.132064314	6.44E+07	$[M-3H]^{3-}$
328.0345	328.03439	0.335443491	2638980.5	$^{1,5}X_1$
342.0502	342.05004	0.467688883	3176481.5	$^{0,2}X_1$
357.0374	357.03795	-1.540452493	1947957.5	$^{2,5}X_1$'
371.0528	371.0536	-2.156022742	5988777.5	$^{0,3}X_1$'
379.0504	379.050237	0.430043264	1156924.5	Y_3^{2-}
400.0536	400.0555193	-4.797671591	1049798.8	$^{0,2}X_3^{2-}$
414.073	414.07179	2.922198588	38247732	Z_2-CO_2
414.073	414.07179	2.922198588	38247732	C_2-CO_2
435.0583	435.058259	0.094265538	274987.8	$^{1,5}A_4^{2-}$
440.0507	440.050434	0.604573886	1500656.8	B_2
456.0455	456.04699	-3.26720718	8195103.5	Z_2"
456.0455	456.04699	-3.26720718	8195103.5	C_2"
457.5572	457.55769	-1.070903212	2972730	$[M-3H]^{2-}$
458.0609	458.0609986	-0.215349046	6815683.5	Z_2
458.0609	458.0609986	-0.215349046	6815683.5	$[M-2H]^{2-}$
458.0609	458.0609986	-0.215349046	6815683.5	C_2
474.056	474.05656	-1.181293641	5208735	Y_2"
476.0717	476.0715633	0.287080791	997905.3	Y_2
504.0667	504.066478	0.44051531	624601.4	$^{1,5}X_2$
528.0666	528.066478	0.231124311	348820.6	$^{3,5}A_3$
573.0613	573.0649	-6.28201099	7014	$^{0,2}A_3$'
588.0879	588.0876073	0.497675852	684368	$^{1,5}A_3$
616.0817	616.0825219	-1.334147571	73377.5	B_3
619.1301	619.1298065	0.474071829	66204.4	$^{2,4}X_2$
633.0854	633.0861	-1.105694786	474579.1	C_3'
634.0934	634.0930866	0.49420031	450427.7	C_3
677.1357	677.1359	-0.295361684	678578.2	Y_3"-SO_3
719.1464	719.1465	-0.139053725	805124.3	$^{0,2}X_3$"-SO_3
791.1675	791.1682	-0.884767613	2156252	$[M-3H-SO_3-CO_2]^-$
800.111	800.1113	-0.374947835	1065954.3	$^{0,2}X_3$'
817.1469	817.148	-1.346145374	205586.5	$[M-3H-SO_3-H_2O]^-$
828.1068	828.1049	2.294395311	37981	$^{1,4}A_4$
835.1575	835.15803	-0.634610434	1022026.5	$[M-3H-SO_3]^-$
871.1244	871.1251	-0.803558524	134517.5	$[M-3H-CO_2]^-$
915.1144	915.1143	0.109275967	106567.8	$[M-3H]^-$

Table C.10. Fragment ion list for 193 nm UVPD activation of the $[M-3H]^{3-}$ precursor of DS dp4 in the low-pressure cell (8 pulses, 4 mJ)

Measured m/z	Calculated m/z	Accuracy (PPM)	Intensity	Assigned Fragment
157.0141	157.0142469	-0.935392825	227634.4	B_1
175.0248	175.0248116	-0.066024925	218615.2	C_1
198.9917	198.9917969	-0.486793936	541126.6	$^{1,3}X_0$
227.5187	227.51986	-5.09845602	63811.5	$C_2''^{2-}$
227.5187	227.51986	-5.09845602	63811.5	$Z_2''^{2-}$
237.5321	237.5321434	-0.182916297	525358.5	Y_2^{2-}
266.0339	266.3679207	-1253.982631	464912	$^{0,2}X_3^{3-}$
282.0285	282.0289107	-1.456074124	2.63E+07	Z_1
300.0391	300.0394753	-1.250972055	1661497.8	Y_1
305.0377	305.0382403	-1.771203065	4184672.3	$[M-3H]^{3-}$
328.0341	328.03439	-0.883940855	821421.7	$^{1,5}X_1$
342.05	342.05004	-0.117020887	506899.2	$^{0,2}X_1$
357.0371	357.03795	-2.380699307	428356.6	$^{2,5}X_1'$
371.0526	371.0536	-2.695028427	378142.3	$^{0,3}X_1'$
379.05	379.050237	-0.62522583	517511.9	Y_3^{2-}
400.0548	400.0555193	-1.798087928	245070.9	$^{0,2}X_3^{2-}$
414.0709	414.07179	-2.149385738	9353081	$Z_2\text{-}CO_2$
414.0709	414.07179	-2.149385738	9353081	$C_2\text{-}CO_2$
440.0502	440.050434	-0.531659512	1163178.1	B_2
456.0451	456.04699	-4.144309778	1724189.4	Z_2''
456.0451	456.04699	-4.144309778	1724189.4	C_2''
457.5567	457.55769	-2.163661592	64861.9	$[M-3H]^{2-}$
458.0607	458.0609986	-0.651972117	1622287.1	C_2
458.0607	458.0609986	-0.651972117	1622287.1	$[M-2H]^{2-}$
458.0607	458.0609986	-0.651972117	1622287.1	Z_2
474.0556	474.05656	-2.025074814	876162.2	Y_2''
476.0712	476.0715633	-0.763181477	533658.4	Y_2
500.0714	500.0715633	-0.326611251	106240.6	$^{2,4}A_3$
504.0662	504.066478	-0.551417345	246322.6	$^{1,5}X_2$
528.0662	528.066478	-0.526356076	88348	$^{3,5}A_3$
588.0872	588.0876073	-0.692622993	145997.2	$^{1,5}A_3$
633.0811	633.0861	-7.897819902	14447.8	C_3'
634.0929	634.0930866	-0.294327448	70532.3	C_3
677.1348	677.1359	-1.624489264	321440.4	$Y_3''\text{-}SO_3$
719.1453	719.1465	-1.668644706	138785.3	$^{0,2}X_3''\text{-}SO_3$
791.1664	791.1682	-2.27511672	196611.8	$[M-3H\text{-}SO_3\text{-}CO_2]^-$
800.1136	800.1113	2.874600071	26510.4	$^{0,2}X_3'$
817.1457	817.148	-2.8146676	16450.2	$[M-3H\text{-}SO_3\text{-}H_2O]^-$
835.1558	835.15803	-2.670153336	101698	$[M-3H\text{-}SO_3]^-$

Table C.11. Fragment ion list for 193 nm UVPD activation of the $[M-3H]^{3-}$ precursor of DS dp4 in the high-pressure cell (4 pulses, 4 mJ)

Measured m/z	Calculated m/z	Accuracy (PPM)	Intensity	Assigned Fragment
157.0143	157.0142469	0.338376937	112723	B_1
173.0094	173.0098	-2.312007759	325398	C_1"
175.0247	175.0248116	-0.63737249	93456.5	C_1
198.9917	198.9917969	-0.486793936	247650.4	$^{1,3}X_0$
227.5192	227.51986	-2.900845667	416323.8	Z_2"$^{2-}$
227.5192	227.51986	-2.900845667	416323.8	C_2"$^{2-}$
237.5322	237.5321434	0.238079357	430151.8	Y_2^{2-}
266.3676	266.3679207	-1.204146502	15420.1	$^{0,2}X_3^{3-}$
282.0288	282.0289107	-0.392353389	7.44E+07	Z_1
300.0394	300.0394753	-0.251103622	1976159.1	Y_1
305.0387	305.0382403	1.507074436	2.24E+08	$[M-3H]^{3-}$
328.0346	328.03439	0.640289578	1982057.5	$^{1,5}X_1$
342.0503	342.05004	0.760043767	1089795.6	$^{0,2}X_1$
357.0375	357.03795	-1.260370221	1835419.3	$^{2,5}X_1$'
371.053	371.0536	-1.617017056	6579420.5	$^{0,3}X_1$'
379.0506	379.050237	0.95767781	1039833.5	Y_3^{2-}
400.0539	400.0555193	-4.047775675	1381661.6	$^{0,2}X_3^{2-}$
414.0715	414.07179	-0.700361645	37404120	Z_2-CO_2
414.0715	414.07179	-0.700361645	37404120	C_2-CO_2
435.0586	435.058259	0.783828359	262323.9	$^{1,5}A_4^{2-}$
440.051	440.050434	1.286313925	1094002.9	B_2
456.0458	456.04699	-2.609380231	6997210	Z_2"
456.0458	456.04699	-2.609380231	6997210	C_2"
457.5575	457.55769	-0.415248184	3677603.3	$[M-3H]^{2-}$
458.0611	458.0609986	0.221274025	6162838.5	Z_2
458.0611	458.0609986	0.221274025	6162838.5	$[M-2H]^{2-}$
458.0611	458.0609986	0.221274025	6162838.5	C_2
474.0563	474.05656	-0.548457762	4324970	Y_2"
504.067	504.066478	1.035674904	363802.8	$^{1,5}X_2$
528.067	528.066478	0.988604698	292350.1	$^{3,5}A_3$
573.1013	573.0649	63.51811113	205772.9	$^{0,2}A_3$'
588.0883	588.0876073	1.177846621	532729.5	$^{1,5}A_3$
615.0756	615.0755	0.162581667	186421.2	B_3'
616.0819	616.0825219	-1.009515735	61322	B_3
619.1323	619.1298065	4.027446222	20744.1	$^{2,4}X_2$
632.0782	632.07808	0.189849963	246210.8	C_3"
634.094	634.0930866	1.44043362	347995.8	C_3
677.1363	677.1359	0.590723369	428713.9	Y_3"-SO_3
719.1467	719.1465	0.278107451	335221	$^{0,2}X_3$"-SO_3
775.137	775.1363	0.903066983	450231.7	$^{1,3}X_3$"-SO_3
791.1682	791.1682	0	1263949	$[M-3H-SO_3-CO_2]^-$
800.1117	800.1113	0.499930447	833865.9	$^{0,2}X_3$'
817.1481	817.148	0.122376852	114732.1	$[M-3H-SO_3-H_2O]^-$
835.1581	835.15803	0.083816472	642817.6	$[M-3H-SO_3]^-$
871.1254	871.1251	0.344382225	41361.7	$[M-3H-CO_2]^-$

Table C.12. Fragment ion list for 193 nm UVPD activation of the $[M-3H]^{3-}$ precursor of CS-A dp4 in the high-pressure cell (8 pulses, 4 mJ)

Measured m/z	Calculated m/z	Accuracy (PPM)	Intensity	Assigned Fragment
173.009	173.0098	-4.624015518	1428054.1	C_1"
198.9916	198.9917969	-0.989327214	2410980.5	$^{1,3}X_0$
227.5188	227.51986	-4.65893395	1909038.5	Z_2"$^{2-}$
227.5188	227.51986	-4.65893395	1909038.5	C_2"$^{2-}$
266.3676	266.3679207	-1.204146502	55167.8	$^{0,2}X_3^{3-}$
282.0286	282.0289107	-1.101500546	2.77E+08	Z_1
300.0393	300.0394753	-0.584393099	1.74E+07	Y_1
305.0381	305.0382403	-0.459892064	2.63E+08	$[M-3H]^{3-}$
328.0341	328.03439	-0.883940855	6353023.5	$^{1,5}X_1$
342.0497	342.05004	-0.994085541	1.24E+07	$^{0,2}X_1$
357.0368	357.03795	-3.220946121	4.24E+06	$^{2,5}X_1$'
371.0524	371.0536	-3.234034113	2.10E+07	$^{0,3}X_1$'
379.0499	379.050237	-0.889043103	4756848	Y_3^{2-}
400.0532	400.0555193	-5.797532812	6957444	$^{0,2}X_3^{2-}$
414.0708	414.07179	-2.390889754	173417392	Z_2-CO_2
414.0708	414.07179	-2.390889754	173417392	C_2-CO_2
435.0579	435.058259	-0.825151555	2015001.1	$^{1,5}A_4^{2-}$
440.0505	440.050434	0.150080527	4174323.3	B_2
456.0451	456.04699	-4.144309778	26351570	Z_2"
456.0451	456.04699	-4.144309778	26351570	C_2"
457.5568	457.55769	-1.945109916	16107254	$[M-3H]^{2-}$
458.0602	458.0609986	-1.743529795	2.41E+07	Z_2
458.0602	458.0609986	-1.743529795	2.41E+07	$[M-2H]^{2-}$
458.0602	458.0609986	-1.743529795	2.41E+07	C_2
474.0556	474.05656	-2.025074814	1.04E+07	Y_2"
476.0712	476.0715633	-0.763181477	4496472	Y_2
500.0717	500.0715633	0.273302885	501382.8	$^{2,4}A_3$
504.0662	504.066478	-0.551417345	1589974.6	$^{1,5}X_2$
528.0662	528.066478	-0.526356076	1369161.5	$^{3,5}A_3$
573.0597	573.0649	-9.074015875	24935.5	$^{0,2}A_3$'
588.0874	588.0876073	-0.352537609	4527201	$^{1,5}A_3$
615.0745	615.0755	-1.625816668	1289869.4	B_3'
616.0814	616.0825219	-1.821095324	507767.9	B_3
619.1296	619.1298065	-0.33351326	358531.8	$^{2,4}X_2$
632.0773	632.07808	-1.234024758	1338071.6	C_3"
634.0929	634.0930866	-0.294327448	9563548	C_3
677.1351	677.1359	-1.181446738	2473670.5	Y_3"-SO_3
719.1458	719.1465	-0.973376078	3517010.5	$^{0,2}X_3$"-SO_3
791.1668	791.1682	-1.769535227	14645490	$[M-3H-CO_2-SO_3]^-$
800.11	800.1113	-1.624773953	3338681	$^{0,2}X_3$'
817.146	817.148	-2.447537044	971407.4	$[M-3H-SO_3-H_2O]^-$
828.105	828.1049	0.120757648	132965.6	$^{1,4}A_4$
835.1566	835.15803	-1.712250794	5283968.5	$[M-3H-SO_3]^-$
871.1234	871.1251	-1.951499274	1028001.1	$[M-3H-CO_2]^-$
915.1132	915.1143	-1.202035636	708207.2	$[M-3H]^-$

Table C.13. Fragment ion list for 193 nm UVPD activation of the $[M-3H]^{3-}$ precursor of CS-A dp4 in the low-pressure cell (8 pulses, 4 mJ)

Measured m/z	Calculated m/z	Accuracy (PPM)	Intensity	Assigned Fragment
157.0139	157.0142469	-2.209162588	764433.8	B_1
173.0088	173.0098	-5.780019398	509262.8	C_1"
175.0245	175.0248116	-1.780067622	616644	C_1
198.9914	198.9917969	-1.99439377	1931929.1	$^{1,3}X_0$
227.5186	227.51986	-5.537978091	630660.4	$Z_2"^{2-}$
227.5186	227.51986	-5.537978091	630660.4	$C_2"^{2-}$
237.5317	237.5321434	-1.866898911	1307501.1	Y_2^{2-}
266.3674	266.3679207	-1.954987667	102129.3	$^{0,2}X_3^{3-}$
282.0284	282.0289107	-1.810647702	7.74E+07	Z_1
300.0389	300.0394753	-1.91755101	1.13E+07	Y_1
305.0377	305.0382403	-1.771203065	8.02E+07	$[M-3H]^{3-}$
328.0338	328.03439	-1.798479114	2645442	$^{1,5}X_1$
341.0416	341.043	-4.105054201	3.03E+05	$^{0,2}X_1'$
357.0364	357.03795	-4.341275206	1.16E+06	$^{2,5}X_1'$
371.052	371.0536	-4.312045483	3.12E+06	$^{0,3}X_1'$
379.0495	379.050237	-1.944312197	3390571.5	Y_3^{2-}
400.0537	400.0555193	-4.547706286	1971418.6	$^{0,2}X_3^{2-}$
414.0704	414.07179	-3.356905816	4.16E+07	Z_2-CO_2
414.0704	414.07179	-3.356905816	4.16E+07	C_2-CO_2
435.0573	435.058259	-2.204277195	233480.2	$^{1,5}A_4^{2-}$
440.0499	440.050434	-1.213399551	2026331.4	B_2
456.0444	456.04699	-5.679239326	6713159	$Z_2"$
456.0444	456.04699	-5.679239326	6713159	$C_2"$
457.5562	457.55769	-3.256419972	887101.1	$[M-3H]^{2-}$
458.0601	458.0609986	-1.96184133	8004435.5	Z_2
458.0601	458.0609986	-1.96184133	8004435.5	$[M-2H]^{2-}$
458.0601	458.0609986	-1.96184133	8004435.5	C_2
474.055	474.05656	-3.290746572	1762344	$Y_2"$
476.0706	476.0715633	-2.023496199	2468611.5	Y_2
500.0707	500.0715633	-1.726410903	1716128	$^{2,4}A_3$
504.0656	504.066478	-1.741736532	610999.5	$^{1,5}X_2$
528.0655	528.066478	-1.851946753	368275.9	$^{3,5}A_3$
588.0865	588.0876073	-1.882921839	862843.8	$^{1,5}A_3$
615.0734	615.0755	-3.414215003	49127.7	B_3'
616.0815	616.0825219	-1.658779406	120361.8	B_3
619.1285	619.1298065	-2.110200456	19601	$^{2,4}X_2$
632.0765	632.07808	-2.499691177	200389.6	$C_3"$
634.092	634.0930866	-1.713677413	1529364.6	C_3
677.1342	677.1359	-2.510574318	969444.1	$Y_3"$-SO_3
719.1447	719.1465	-2.502967059	710339.9	$^{0,2}X_3"$-SO_3
791.1657	791.1682	-3.159884333	1261714.9	$[M-3H-SO_3-CO_2]^-$
800.1089	800.1113	-2.999582683	282980.8	$^{0,2}X_3'$
817.1447	817.148	-4.038436122	56492.6	$[M-3H-SO_3-H_2O]^-$
835.1555	835.15803	-3.02936679	503955.9	$[M-3H-SO_3]^-$

Table C.14. Fragment ion list for 193 nm UVPD activation of the $[M-3H]^{3-}$ precursor of CS-A dp4 in the high-pressure cell (4 pulses, 4 mJ)

Measured m/z	Calculated m/z	Accuracy (PPM)	Intensity	Assigned Fragment
173.0091	173.0098	-4.046013579	1211537.6	C_1"
198.9917	198.9917969	-0.486793936	7.56E+05	$^{1,3}X_0$
227.5189	227.51986	-4.219411879	1958871.6	Z_2"$^{2-}$
227.5189	227.51986	-4.219411879	1958871.6	C_2"$^{2-}$
266.3672	266.3679207	-2.705828832	108060	$^{0,2}X_3^{3-}$
282.0288	282.0289107	-0.392353389	2.12E+08	Z_1
300.0396	300.0394753	0.415475333	8292346.5	Y_1
305.0386	305.0382403	1.179246686	7.54E+08	$[M-3H]^{3-}$
328.0343	328.03439	-0.274248682	4495393.5	$^{1,5}X_1$
342.0499	342.05004	-0.409375771	4077744.8	$^{0,2}X_1$
357.037	357.03795	-2.660781578	3750311.8	$^{2,5}X_1$'
371.0527	371.0536	-2.425525584	21302490	$^{0,3}X_1$'
379.0502	379.050237	-0.097591283	4104255.3	Y_3^{2-}
400.0535	400.0555193	-5.047636896	7853565	$^{0,2}X_3^{2-}$
414.0711	414.07179	-1.666377707	157626288	Z_2-CO_2
414.0711	414.07179	-1.666377707	157626288	C_2-CO_2
435.0583	435.058259	0.094265538	1531235.5	$^{1,5}A_4^{2-}$
440.051	440.050434	1.286313925	2608724	B_2
456.0454	456.04699	-3.486482829	21768876	Z_2"
456.0454	456.04699	-3.486482829	21768876	C_2"
457.5572	457.55769	-1.070903212	16673176	$[M-3H]^{2-}$
458.0605	458.0609986	-1.088595188	2.03E+07	Z_2
458.0605	458.0609986	-1.088595188	2.03E+07	$[M-2H]^{2-}$
458.0605	458.0609986	-1.088595188	2.03E+07	C_2
474.056	474.05656	-1.181293641	8.20E+06	Y_2"
504.0665	504.066478	0.043742248	850755.9	$^{1,5}X_2$
528.0667	528.066478	0.420494408	977573.4	$^{3,5}A_3$
573.0659	573.0649	1.745003053	4.27E+04	$^{0,2}A_3$'
588.0879	588.0876073	0.497675852	3291947.8	$^{1,5}A_3$
615.075	615.0755	-0.812908334	967091.1	B_3'
616.0808	616.0825219	-2.794990831	313427.3	B_3
619.1295	619.1298065	-0.495030278	106927.9	$^{2,4}X_2$
632.0778	632.07808	-0.442983247	864503.6	C_3"
634.0934	634.0930866	0.49420031	7280671	C_3
677.1356	677.1359	-0.443042527	1257629.9	Y_3"-SO_3
719.1462	719.1465	-0.417161176	1309795.9	$^{0,2}X_3$"-SO_3
791.1674	791.1682	-1.011162986	7875305.5	$[M-3H-CO_2-SO_3]^-$
800.1107	800.1113	-0.749895671	2201241.3	$^{0,2}X_3$'
817.1465	817.148	-1.835652783	509871.3	$[M-3H-SO_3-H_2O]^-$
835.157	835.15803	-1.233299523	2740336.5	$[M-3H-SO_3]^-$
871.1241	871.1251	-1.147940749	299677.5	$[M-3H-CO_2]^-$
915.1143	915.1143	0	170128	$[M-3H]^-$

Table C.15. Fragment ion list for 193 nm UVPD activation of the $[M-4H+Na]^{3-}$ precursor of CS-A dp4 in the high-pressure cell (8 pulses, 4 mJ)

Measured m/z	Calculated m/z	Accuracy (PPM)	Intensity	Assigned Fragment
173.009	173.0098	-4.624015518	256207.8	C_1"
175.0246	175.0248116	-1.208720056	321594.2	C_1"
198.9916	198.9917969	-0.989327214	440792	$^{1,3}X_0$
282.0286	282.0289107	-1.101500546	1.20E+07	Z_1
300.0392	300.0394753	-0.917682577	1607087.6	Y_1
304.0105	304.0108553	-1.168685239	1736888.6	Z_1+Na
312.3652	312.3655552	-1.13701397	3.36E+07	$[M-4H+Na]^{3-}$
328.034	328.03439	-1.188786941	1000586.1	$^{1,5}X_1$
342.0497	342.05004	-0.994085541	1696293.6	$^{0,2}X_1$
350.0159	350.0163346	-1.241659194	3717047.5	$^{1,5}X_1$+Na
369.0355	369.038	-6.774370119	661124.3	$Z_3"^{2-}$
390.0408	390.0412093	-1.049404497	3203229	$[Y_3+Na]^{2-}$
414.0707	414.07179	-2.632393769	14669782	Z_2-CO_2
414.0707	414.07179	-2.632393769	14669782	C_2-CO_2
434.0314	434.037464	-13.971082	142960	$^{1,5}A_2$'+Na
446.0487	446.0492313	-1.191142057	276977.2	$[^{1,5}A_4+Na]^{2-}$
456.0448	456.04699	-4.802136727	4493237	Z_2"
456.0448	456.04699	-4.802136727	4493237	C_2"
469.0493	469.051971	-5.694383916	450568.3	$[M-4H+Na]^{2-}$
479.0346	479.0359	-2.713784082	7654003.5	Z_2'+Na
479.0346	479.0359	-2.713784082	7654003.5	C_2'+Na
496.0374	496.0395	-4.233533821	613693.5	Y_2"+Na
498.053	498.053508	-1.019904472	1105643	Y_2+Na
522.053	522.053508	-0.973017118	120183.5	$^{2,4}A_3$+Na
526.0479	526.0484226	-0.993423754	218115.1	$^{1,5}X_2$+Na
528.0659	528.066478	-1.094466366	28116.8	$^{3,5}A_3$+Na
565.0331	565.0363	-5.663352956	4081	$^{0,3}A_3$'+Na
609.0611	609.0626	-2.462801032	200538.7	$^{1,5}A_3$'+Na
637.056	637.0575	-2.354575529	1934383.6	B_3'+Na
656.0745	656.0750313	-0.809768662	1324433.8	C_3+Na
699.1167	699.1179	-1.716448685	748532.2	Y_3"+Na-SO_3
719.1248	719.1229	2.64210749	407274.6	$^{2,5}A_4$'-SO_3
741.0984	741.0971857	1.638476065	21590.1	Z_3
763.0785	763.0791304	-0.826084706	1177829.3	Z_3+Na
779.0733	779.0747	-1.797003548	406034.2	Y_3"+Na
781.089	781.0896951	-0.889851708	530058.4	Y_3+Na
795.1592	795.1517	9.432162442	8380.3	$[M-4H+Na-SO_3-CO_2-H_2O]^-$
813.1481	813.1517	-4.427218193	579796.9	$[M-4H+Na-SO_3-CO_2]^-$
823.0952	823.1002597	-6.147173373	1539003.9	$^{0,2}X_3$'+Na
839.1268	839.1309	-4.886007654	59953	$[M-4H+Na-SO_3-H_2O]^-$
849.1151	849.1186	-4.121921249	1044659.8	$[M-4H+Na-2CO_2]^-$
893.104848	893.1079	-3.417260837	77258	$[M-4H+Na-CO_2]^-$
937.0945	937.0972	-2.881237933	705435.6	$[M-4H+Na]^-$

Table C.16. Fragment ion list for 193 nm UVPD activation of the $[M-4H+Na]^{3-}$ precursor of DS dp4 in the high-pressure cell (8 pulses, 4 mJ)

Measured m/z	Calculated m/z	Accuracy (PPM)	Intensity	Assigned Fragment
173.0089	173.0098	-5.202017458	199847.3	C_1"
175.0249	175.0248116	0.505322641	138870.5	C_1
198.9916	198.9917969	-0.989327214	160745.4	$^{1,3}X_0$
282.0284	282.0289107	-1.810647702	4998976.5	Z_1
300.0391	300.0394753	-1.250972055	518889.6	Y_1
304.0104	304.0108553	-1.497620861	418420.8	Z_1+Na
312.3649	312.3655552	-2.097427162	1477232.5	$[M-4H+Na]^{3-}$
328.0341	328.03439	-0.883940855	356449.3	$^{1,5}X_1$
342.0499	342.05004	-0.409375771	445879.2	$^{0,2}X_1$
350.0162	350.0163346	-0.384556338	857283.6	$^{1,5}X_1$+Na
390.041	390.0412093	-0.536638165	1308640.3	$[Y_3+Na]^{2-}$
414.0709	414.07179	-2.149385738	3926893	Z_2-CO_2
414.0709	414.07179	-2.149385738	3926893	C_2-CO_2
434.0379	434.037464	1.004583789	9910.1	$^{1,5}A_2$'+Na
456.045	456.04699	-4.363585428	1151781.3	Z_2"
456.045	456.04699	-4.363585428	1151781.3	C_2"
469.0496	469.051971	-5.054795941	46750	$[M-4H+Na]^{2-}$
479.0348	479.0359	-2.296278838	2121329.3	Z_2'+Na
479.0348	479.0359	-2.296278838	2121329.3	C_2'+Na
498.0531	498.053508	-0.819122832	437572.4	Y_2+Na
550.048	550.0484226	-0.768275995	67685.5	$^{3,5}A_3$+Na
637.0561	637.0575	-2.197603827	420323.8	B_3'+Na
656.0743	656.0750313	-1.114611843	334548.3	C_3+Na
701.1324	701.1328805	-0.685316597	134599	Y_3+Na-SO_3
763.0783	763.0791304	-1.088180722	435433.5	Z_3+Na
781.0889	781.0896951	-1.017877977	766180.5	Y_3+Na
813.1483	813.1517	-4.181261627	115379.3	$[M-4H+Na-SO_3-CO_2]^-$
823.0953	823.1002597	-6.025681491	221509.7	$^{0,2}X_3$'+Na
839.1274	839.1309	-4.170982144	20041.1	$[M-4H+Na-SO_3-H_2O]^-$
849.1151	849.1186	-4.121921249	328856.4	$[M-4H+Na-2CO_2]^-$
893.1049	893.1079	-3.359056616	1227829.5	$[M-4H+Na-CO_2]^-$
937.0947	937.0972	-2.667812901	158982	$[M-4H+Na]^-$

Table C.17. Fragment ion list for 213 nm UVPD activation of the $[M-3H]^{3-}$ precursor of DS dp4 in the high-pressure cell (50 ms)

Measured m/z	Calculated m/z	Accuracy (PPM)	Intensity	Assigned Fragment
237.5332	237.5321434	4.448035894	6723.1	Y_2^{2-}
282.0301	282.0289107	4.217103127	423403.3	Z_1
305.0403	305.0382403	6.752318437	3.50E+07	$[M-3H]^{3-}$
316.5452	316.5429051	7.249887655	7486.9	C_3^{2-}
357.0385	357.03795	1.540452492	20369.2	$^{2,5}X_1'$
371.0544	371.0536	2.156022742	74936.7	$^{0,3}X_1'$
379.0522	379.050237	5.178754185	25672.9	Y_3^{2-}
400.0553	400.0555193	-0.548261402	49641.2	$^{0,2}X_3^{2-}$
414.0731	414.07179	3.163702603	317054.1	Z_2-CO_2
414.0731	414.07179	3.163702603	317054.1	C_2-CO_2
435.0578	435.058259	-1.055005829	992.9	$^{1,5}A_4^{2-}$
440.053	440.050434	5.831247518	9500.1	B_2
456.0475	456.04699	1.118305813	57571.7	Z_2''
456.0475	456.04699	1.118305813	57571.7	C_2''
457.5592	457.55769	3.300130307	115132	$[M-3H]^{2-}$
458.0625	458.0609986	3.277635523	80651.5	Z_2
458.0625	458.0609986	3.277635523	80651.5	C_2
458.0625	458.0609986	3.277635523	80651.5	$[M-2H]^{2-}$
474.0582	474.05656	3.459502807	35859.6	Y_2''
588.0893	588.0876073	2.878273543	3066.1	$^{1,5}A_3$
677.1381	677.1359	3.248978529	5116	Y_3''-SO_3
775.1725	775.1739	-1.806046359	3332.4	$[M-3H-SO_4-CO_2]^-$
800.1141	800.1113	3.49951313	23743.4	$^{0,2}X_3'$

Table C.18. Fragment ion list for 213 nm UVPD activation of the $[M-3H]^{3-}$ precursor of DS dp4 in the low-pressure cell (50 ms)

Measured m/z	Calculated m/z	Accuracy (PPM)	Intensity	Assigned Fragment
237.5322	237.5321434	0.238079357	25591.9	Y_2^{2-}
282.029	282.0289107	0.316793767	376801.5	Z_1
305.0385	305.0382403	0.851418936	1.34E+07	$[M-3H]^{3-}$
357.0372	357.03795	-2.100617035	15926.8	$^{2,5}X_1'$
379.0504	379.050237	0.430043264	57966.1	Y_3^{2-}
435.0593	435.058259	2.392808272	1136.4	$^{1,5}A_4^{2-}$
440.0507	440.050434	0.604573886	18277.4	B_2
458.0608	458.0609986	-0.433660581	62375.6	Z_2
458.0608	458.0609986	-0.433660581	62375.6	$[M-2H]^{2-}$
458.0608	458.0609986	-0.433660581	62375.6	C_2
474.0561	474.05656	-0.970348348	29513.2	Y_2''
775.1706	775.1739	-4.257109276	3723.3	$[M-3H-SO_4-CO_2]^-$
800.111	800.1113	-0.374947835	21056	$^{0,2}X_3'$

Table C.19. Fragment ion list for 213 nm UVPD activation of the $[M-3H]^{3-}$ precursor of DS dp4 in the high-pressure cell (150 ms)

Measured m/z	Calculated m/z	Accuracy (PPM)	Intensity	Assigned Fragment
237.5329	237.5321434	3.185048933	76668.1	Y_2^{2-}
282.0298	282.0289107	3.153382393	7391485.5	Z_1
300.0408	300.0394753	4.414949065	125171.5	Y_1
305.0401	305.0382403	6.096662937	2.20E+08	$[M-3H]^{3-}$
316.5446	316.5429051	5.354410011	94324.7	C_3^{2-}
328.0354	328.03439	3.079058269	233104.1	$^{1,5}X_1$
342.051	342.05004	2.80652796	44843.4	$^{0,2}X_1$
357.0383	357.03795	0.98028795	335265.5	$^{2,5}X_1'$
372.058	372.0606047	-7.000776129	65620	$^{0,3}X_1'$
379.0516	379.050237	3.595850544	458945.8	Y_3^{2-}
400.055	400.0555193	-1.298157318	1026168.4	$^{0,2}X_3^{2-}$
414.0726	414.07179	1.956182526	5869078	Z_2-CO_2
414.0726	414.07179	1.956182526	5869078	C_2-CO_2
435.5638	435.058259	1162.007617	3672126	$^{1,5}A_4^{2-}$
440.0523	440.050434	4.240520761	138030.9	B_2
456.0471	456.04699	0.241203215	1099505.1	Z_2''
456.0471	456.04699	0.241203215	1099505.1	C_2''
457.5588	457.55769	2.425923603	2260667.8	$[M-3H]^{2-}$
458.0618	458.0609986	1.749454774	1614808.9	Z_2
458.0618	458.0609986	1.749454774	1614808.9	$[M-2H]^{2-}$
458.0618	458.0609986	1.749454774	1614808.9	C_2
474.0577	474.05656	2.404776341	681351	Y_2''
504.0676	504.066478	2.22599409	31038.9	$^{1,5}X_2$
588.0897	588.0876073	3.558444312	63162.5	$^{1,5}A_3$
677.1378	677.1359	2.805936002	117259.2	Y_3''-SO_3
775.172	775.1739	-2.451062916	228915.2	$[M-3H-SO_4-CO_2]^-$
800.1134	800.1113	2.624634848	452784.7	$^{0,2}X_3'$

Table C.20. Fragment ion list for 213 nm UVPD activation of the $[M-3H]^{3-}$ precursor of DS dp4 in the high-pressure cell (300 ms)

Measured m/z	Calculated m/z	Accuracy (PPM)	Intensity	Assigned Fragment
198.9921	198.9917969	1.523339177	40082.5	$^{1,3}X_0$
237.5327	237.5321434	2.343057626	72358.8	Y_2^{2-}
282.0295	282.0289107	2.089661658	9184308	Z_1
300.0404	300.0394753	3.081791154	263792.7	Y_1
305.0396	305.0382403	4.457524187	1.25E+08	$[M-3H]^{3-}$
328.0351	328.03439	2.16452001	327671.6	$^{1,5}X_1$
342.0506	342.05004	1.637108421	124282.4	$^{0,2}X_1$
358.0414	358.0449546	-9.92794048	46280.9	$^{2,5}X_1'$
372.0565	372.0606047	-11.03237738	92391.4	$^{0,3}X_1'$
377.5278	377.5265947	3.192568462	20384.1	$^{2,4}A_4^{2-}$
379.0511	379.050237	2.276764177	607442.9	Y_3^{2-}
400.0545	400.0555193	-2.547983844	1429674.9	$^{0,2}X_3^{2-}$
414.0722	414.07179	0.990166464	8176075.5	$Z_2\text{-}CO_2$
414.0722	414.07179	0.990166464	8176075.5	$C_2\text{-}CO_2$
435.0596	435.058259	3.082371092	23605.7	$^{1,5}A_4^{2-}$
440.0518	440.050434	3.104287363	163650.5	B_2
456.0466	456.04699	-0.855175034	1577052.9	Z_2''
456.0466	456.04699	-0.855175034	1577052.9	C_2''
457.5583	457.55769	1.333165223	3198577.5	$[M-3H]^{2-}$
458.0611	458.0609986	0.221274025	2480923.3	Z_2
458.0611	458.0609986	0.221274025	2480923.3	$[M-2H]^{2-}$
458.0611	458.0609986	0.221274025	2480923.3	C_2
474.0572	474.05656	1.350049876	998110.1	Y_2''
504.0675	504.066478	2.027607559	55947.7	$^{1,5}X_2$
573.0823	573.0886	-10.9930646	2330.8	$^{2,5}X_2''$
574.1074	575.1036	-1732.20964	10056.4	$^{2,5}X_2$
588.0892	588.0876073	2.708230851	93418.8	$^{1,5}A_3$
619.131	619.1298065	1.92772499	1550	$^{2,4}X_2$
634.0949	634.0930866	2.859783584	100005.6	C_3
677.1371	677.1359	1.772170107	211551.5	$Y_3''\text{-}SO_3$
719.1479	719.1465	1.946752157	37529.5	$^{0,2}X_3''\text{-}SO_3$
775.1714	775.1739	-3.225082785	348810.4	$[M-3H\text{-}SO_4\text{-}CO_2]^-$
791.1692	791.1682	1.263953733	142279.2	$[M-3H\text{-}SO_3\text{-}CO_2]^-$
800.1126	800.1113	1.624773953	687008.6	$^{0,2}X_3'$
817.1465	817.148	-1.835652783	2505.6	$[M-3H\text{-}SO_3\text{-}H_2O]^-$
835.1588	835.15803	0.921981197	33927.3	$[M-3H\text{-}SO_3]^-$

Table C.21. Fragment ion list for 213 nm UVPD activation of the $[M-3H]^{3-}$ precursor of DS dp4 in the high-pressure cell (400 ms)

Measured m/z	Calculated m/z	Accuracy (PPM)	Intensity	Assigned Fragment
198.9917	198.9917969	-0.486793936	937290.9	$^{1,3}X_0$
237.5321	237.5321434	-0.182916297	1475916.5	Y_2^{2-}
266.0339	266.0326	4.886619159	529746.9	$^{0,2}X_3'^{3-}$
282.0289	282.0289107	-0.037779811	2.65E+07	Z_1
300.0394	300.0394753	-0.251103622	3660405	Y_1
305.0382	305.0382403	-0.132064314	5.87E+07	$[M-3H]^{3-}$
316.5428	316.5429051	-0.332022921	342631.5	C_3^{2-}
328.0343	328.03439	-0.274248682	1862910.3	$^{1,5}X_1$
342.0499	342.05004	-0.409375771	2212737	$0,2X_1$
357.037	357.03795	-2.660781578	1601530.4	$2,5X_1'$
371.0526	371.0536	-2.695028427	7530043.5	$0,3X_1'$
377.5264	377.5265947	-0.515779557	42948	$^{2,4}A_4^{2-}$
378.0423	378.0435	-3.174237885	1696612.1	$Y_3''^{2-}$
379.0501	379.050237	-0.361408557	6254056	Y_3^{2-}
400.0538	400.0555193	-4.297740981	3270166.8	$^{0,2}X_3^{2-}$
414.071	414.07179	-1.907881723	26811848	Z_2-CO_2
414.071	414.07179	-1.907881723	26811848	C_2-CO_2
435.0581	435.058259	-0.365443008	202104.9	$^{1,5}A_4^{2-}$
440.0504	440.050434	-0.077166153	1519904.6	B_2
456.0452	456.04699	-3.925034129	6185014	Z_2''
456.0452	456.04699	-3.925034129	6185014	C_2''
457.5569	457.55769	-1.72655824	6338524.5	$[M-3H]^{2-}$
458.0604	458.0609986	-1.306906724	7186134	Z_2
458.0604	458.0609986	-1.306906724	7186134	$[M-2H]^{2-}$
458.0604	458.0609986	-1.306906724	7186134	C_2
474.0558	474.05656	-1.603184228	4013836	Y_2''
476.0714	476.0715633	-0.34307657	1698655.8	Y_2
504.0664	504.066478	-0.154644283	660264.5	$^{1,5}X_2$
588.0876	588.0876073	-0.012452225	426564	$^{1,5}A_3$
619.1296	619.1298065	-0.33351326	13311.4	$^{2,4}X_2$
634.0931	634.0930866	0.021083655	430736.5	C_3
677.1353	677.1359	-0.886085053	2404114	Y_3''-SO_3
719.1458	719.1465	-0.973376078	955455.3	$^{0,2}X_3''$-SO_3
775.1707	775.1739	-4.128105964	461205.3	$[M-3H-SO_4-CO_2]^-$
791.1671	791.1682	-1.390349106	1145811.9	$[M-3H-SO_3-CO_2]^-$
800.1103	800.1113	-1.249826118	3441741.3	$^{0,2}X_3'$
817.1457	817.148	-2.8146676	66057.8	$[M-3H-SO_3-H_2O]^-$
835.1567	835.15803	-1.592512976	460815.9	$[M-3H-SO_3]^-$
915.1133	915.1143	-1.092759669	305314.3	$[M-3H]^-$

Table C.22. Fragment ion list for 213 nm UVPD activation of the $[M-3H]^{3-}$ precursor of DS dp4 in the low-pressure cell (400 ms)

Measured m/z	Calculated m/z	Accuracy (PPM)	Intensity	Assigned Fragment
198.992	198.9917969	1.020805898	54469.5	$^{1,3}X_0$
237.5326	237.5321434	1.922061972	70144	Y_2^{2-}
266.0344	266.0326	6.766088066	125775.3	$^{0,2}X_3'^{3-}$
282.0294	282.0289107	1.73508808	9037220	Z_1
300.0401	300.0394753	2.081922721	414498.3	Y_1
305.0394	305.0382403	3.801868687	7.73E+07	$[M-3H]^{3-}$
316.5437	316.5429051	2.511193545	89387.4	C_3^{2-}
328.0349	328.03439	1.554827837	372294.6	$^{1,5}X_1$
342.0504	342.05004	1.052398652	221333.5	$^{0,2}X_1$
358.0411	358.0449546	-10.76582409	51533.2	$^{2,5}X_1'$
372.0562	372.0606047	-11.83869763	114927.5	$^{0,3}X_1'$
377.5275	377.5265947	2.397922458	23318	$^{2,4}A_4^{2-}$
379.0509	379.050237	1.749129631	713679.8	Y_3^{2-}
400.0543	400.0555193	-3.047914454	1561209.5	$^{0,2}X_3^{2-}$
414.0719	414.07179	0.265654417	8909531	Z_2-CO_2
414.0719	414.07179	0.265654417	8909531	C_2-CO_2
435.0592	435.058259	2.162953999	32272.3	$^{1,5}A_4^{2-}$
440.0515	440.050434	2.422547324	171774.2	B_2
456.0463	456.04699	-1.513001983	1751302.5	Z_2"
456.0463	456.04699	-1.513001983	1751302.5	C_2"
457.5581	457.55769	0.896061872	3460587.5	$[M-3H]^{2-}$
458.0608	458.0609986	-0.433660581	2780777.3	Z_2
458.0608	458.0609986	-0.433660581	2780777.3	$[M-2H]^{2-}$
458.0608	458.0609986	-0.433660581	2780777.3	C_2
476.0724	476.0715633	1.757447967	210474.1	Y_2^{2-}
504.0673	504.066478	1.630834497	85287.7	$^{1,5}X_2$
573.0821	573.0886	-11.34205078	51388.5	$^{2,5}X_2$"
588.089	588.0876073	2.368145466	110024.5	$^{1,5}A_3$
619.1309	619.1298065	1.766207972	2101.3	$^{2,4}X_2$
634.0947	634.0930866	2.544372481	120173.9	C_3
677.1367	677.1359	1.181446738	313029.1	Y_3"-SO_3
719.1473	719.1465	1.112429804	73862.1	$^{0,2}X_3$"-SO_3
775.171	775.1739	-3.74109603	112104.8	$[M-3H-SO_4-CO_2]^-$
791.1686	791.1682	0.505581493	222651.9	$[M-3H-SO_3-CO_2]^-$
800.1122	800.1113	1.124843506	807399.1	$^{0,2}X_3'$
817.1459	817.148	-2.569913896	4722.2	$[M-3H-SO_3-H_2O]^-$
835.1584	835.15803	0.443029926	47343.2	$[M-3H-SO_3]^-$
915.1148	915.1143	0.546379835	41853.7	$[M-3H]^-$

Table C.23. MS^3 activation of the fragment ion m/z 715.05 of DS dp4 using 193 nm UVPD (8 pulses, 4 mJ)/ 193 nm UVPD (8 pulses, 4 mJ)

Measured m/z	Calculated m/z	Accuracy (PPM)	Intensity	Assigned Fragment
175.0246	175.0248	-1.142695207	77009.5	C_1
272.992	272.9916	1.46524655	101466.1	$[Y_2/C_3]+SO_3$
282.0287	282.0289107	-0.746926967	132838.8	Z_1
325.032	325.0291076	8.898833773	2086.7	$[^{1,4}A_3'/Z_3']^{2-}$
396.1143	396.1147488	-1.132936861	55170.3	C_3/Y_2-SO_3
440.0499	440.050434	-1.213399551	322608.3	B_2
456.0603	456.0609986	-1.531906918	31145.2	Z_2''
456.0603	456.0609986	-1.531906918	31145.2	C_2''
476.071	476.0715633	-1.183286385	456067.5	Y_2
518.0816	518.082128	-1.019172389	134232.8	$C_3/^{0,2}X_2$
554.1356	554.1363	-1.263227116	158272.3	C_3-SO_3
590.0663	590.06744	-1.931982555	459146.9	$C_3-C_2H_4O$
634.0924	634.0931	-1.103938838	5880742	C_3
715.0571	715.05719	-0.125864059	5776643	C_3+HSO_3

Table C.24. MS^3 activation of the fragment ion m/z 715.05 of DS dp4 using 193 nm UVPD (8 pulses, 4 mJ)/ HCD (NCE 20)

Measured m/z	Calculated m/z	Accuracy (PPM)	Intensity	Assigned Fragment
272.9922	272.9916	2.197869825	218682.5	$[Y_2/C_3]+SO_3$
282.0289	282.0289107	-0.037779811	31981	Z_1
440.0503	440.050434	-0.304412832	490020.3	B_2
476.0714	476.0715633	-0.34307657	60841.8	Y_2
616.0821	616.0825	-0.649263694	11841	B_3
634.093	634.0931	-0.157705548	20435110	C_3

Table C.25. MS^3 activation of the fragment ion m/z 715.05 of CS-A dp4 using 193 nm UVPD (8 pulses, 4 mJ)/ 193 nm UVPD (8 pulses, 4 mJ)

Measured m/z	Calculated m/z	Accuracy (PPM)	Intensity	Assigned Fragment
175.0246	175.0248	-1.142695207	25957.2	C_1
272.9918	272.9916	0.732623275	58237.1	$[Y_2/C_3]+SO_3$
282.0285	282.0289107	-1.456074124	42349.1	Z_1
396.1145	396.1147488	-0.628032662	25369.6	C_3/Y_2-SO_3
440.0498	440.050434	-1.440646231	99417.8	B_2
456.0445	456.0609986	-36.17639537	23296.5	$C_2"$
456.0445	456.0609986	-36.17639537	23296.5	$Z_2"$
476.0709	476.0715633	-1.393338838	109280.8	Y_2
518.0809	518.0821	-2.316235207	29465.8	$C_3/^{0,2}X_2$
554.1354	554.1363	-1.624149149	53173.5	C_3-SO_3
590.066	590.06744	-2.440399016	81207.7	$C_3-C_3H_4O$
616.082	616.0825	-0.811579618	15116.6	B_3
634.0922	634.0931	-1.419349935	1258890.4	C_3
697.0464	697.0472	-1.147698463	26059.2	$C_3+HSO_3-H_2O$
715.056	715.05719	-1.664202551	1330775.6	C_3+HSO_3

Table C.26. MS^3 activation of the fragment ion m/z 715.05 of CS-A dp4 using 193 nm UVPD (8 pulses, 4 mJ)/ HCD (NCE 20)

Measured m/z	Calculated m/z	Accuracy (PPM)	Intensity	Assigned Fragment
272.9919	272.9916	1.098934912	168492.5	$[Y_2/C_3]+SO_3$
282.0284	282.0289107	-1.810647702	21308.3	Z_1
440.0497	440.050434	-1.66789291	234610.4	B_2
476.0708	476.0715633	-1.603391292	62210.2	Y_2
504.0658	504.0665	-1.388705657	20400.4	$^{1,5}X_2$
616.0815	616.0825	-1.623159236	23458.2	B_3
634.0922	634.0931	-1.419349935	4795857	C_3

APPENDIX D

Advances in Negative Electron Transfer Dissociation for the Structural Characterization of Glycosaminoglycans using FTICR MS Supplemental Data

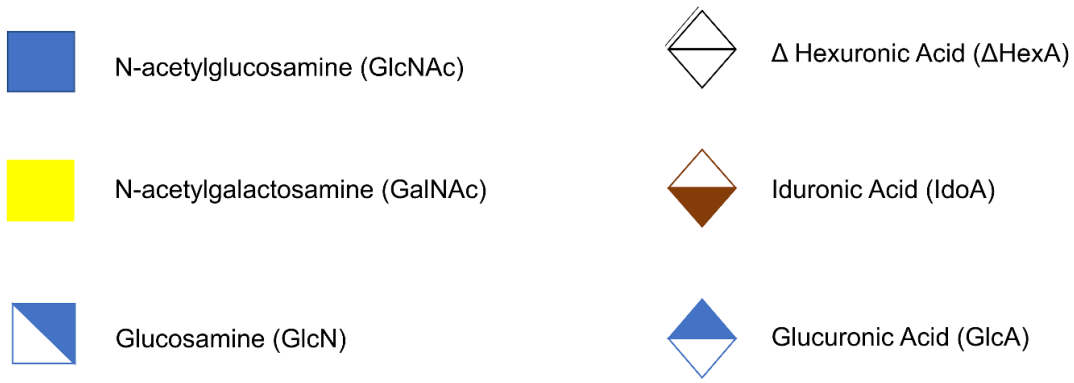

Figure D.1. Glycan symbol nomenclature

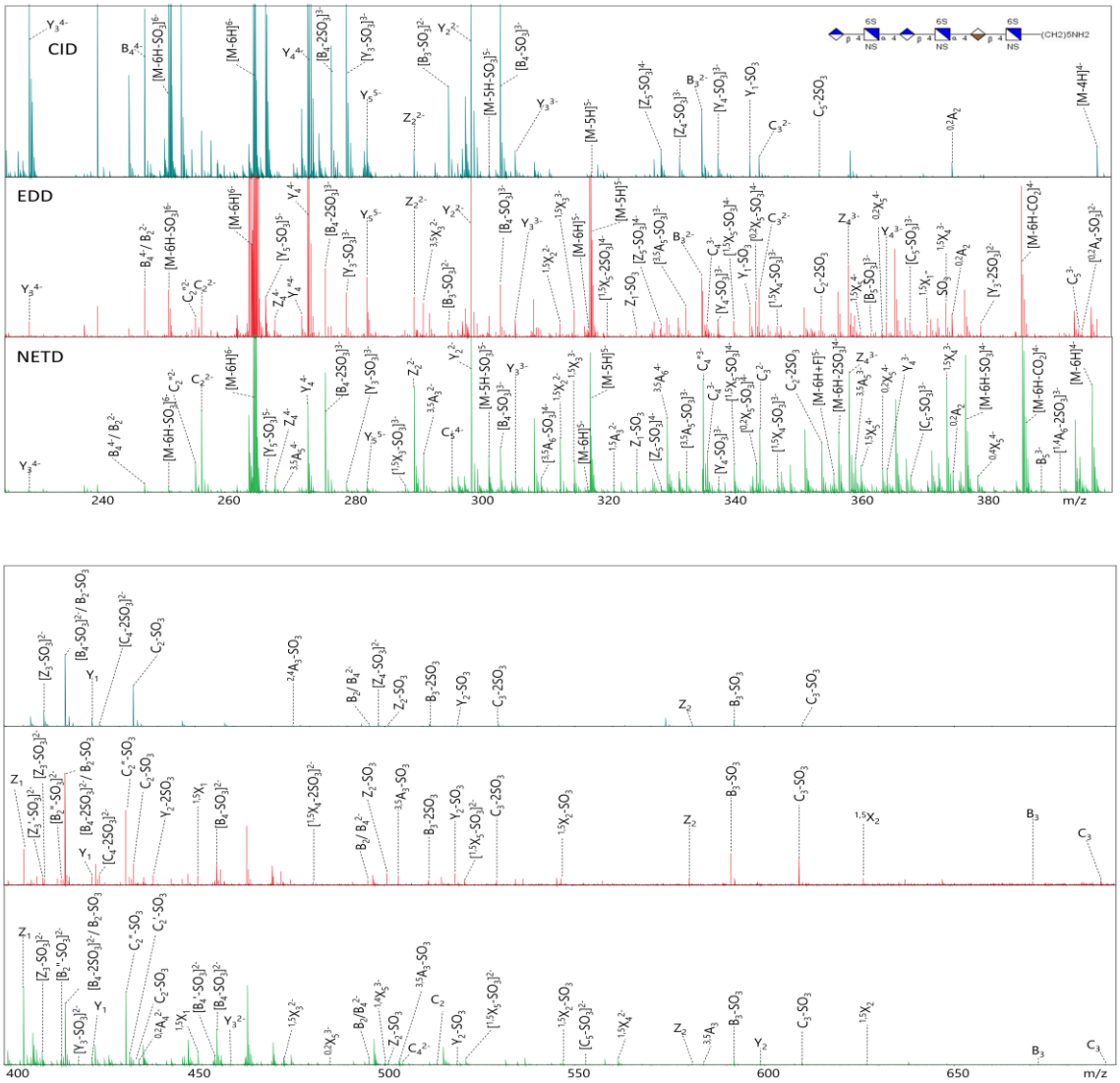

Figure D.2. Comparison of CID (top/blue), EDD (middle/red), and NETD (bottom/green) of the $[M-6H]^{6-}$ precursor ion (*m/z* 264.6831) of GlcA-GlcNS6S-GlcA-GlcNS6S-IdoA-GlcNS6S-$(CH_2)_5NH_2$.

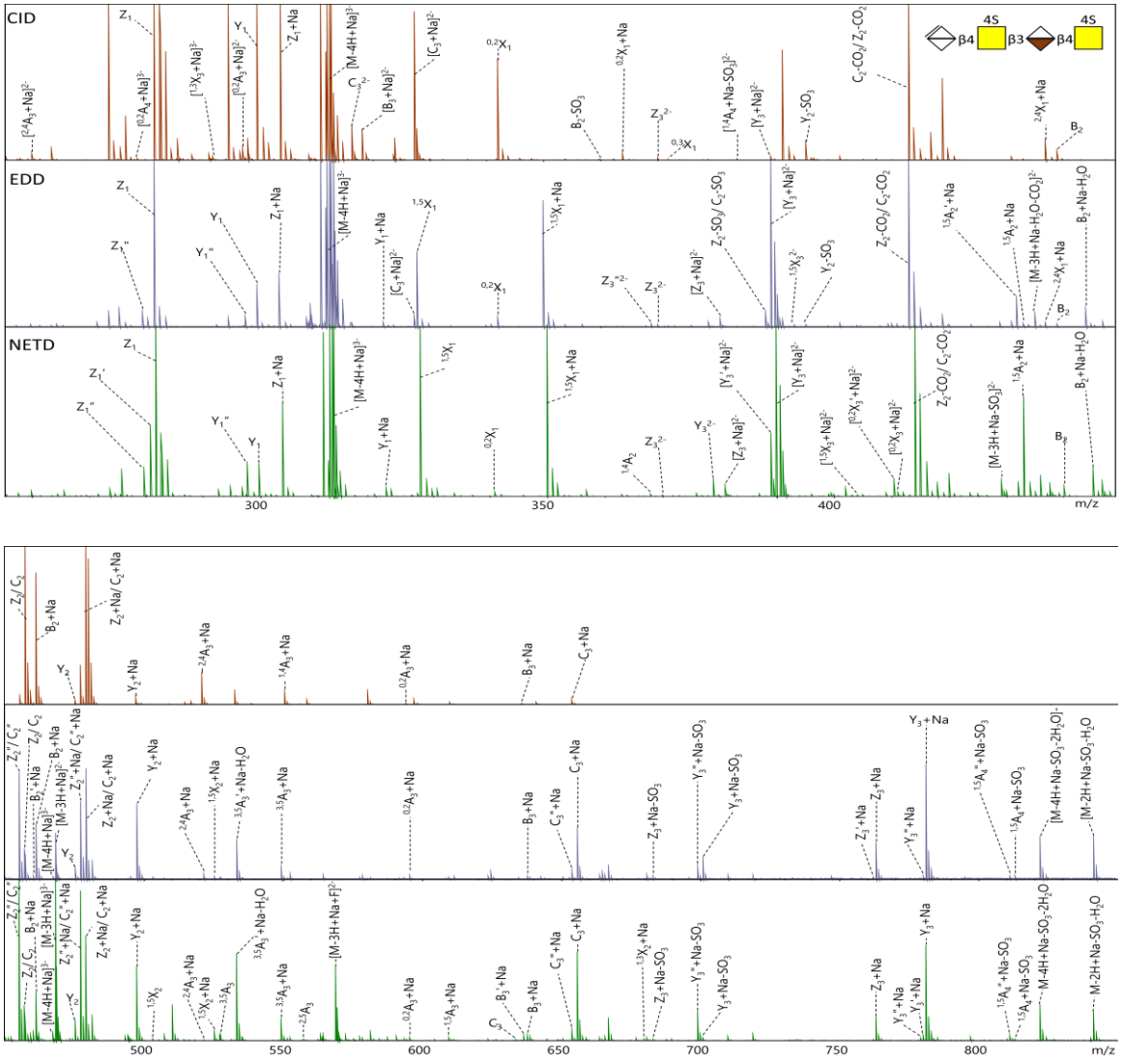

Figure D.3. Comparison of CID (top/brown), EDD (middle/blue), and NETD (bottom/green) of the $[M-4H+Na]^{3-}$ precursor ion (*m/z* 312.3656) of dermatan sulfate dp4.

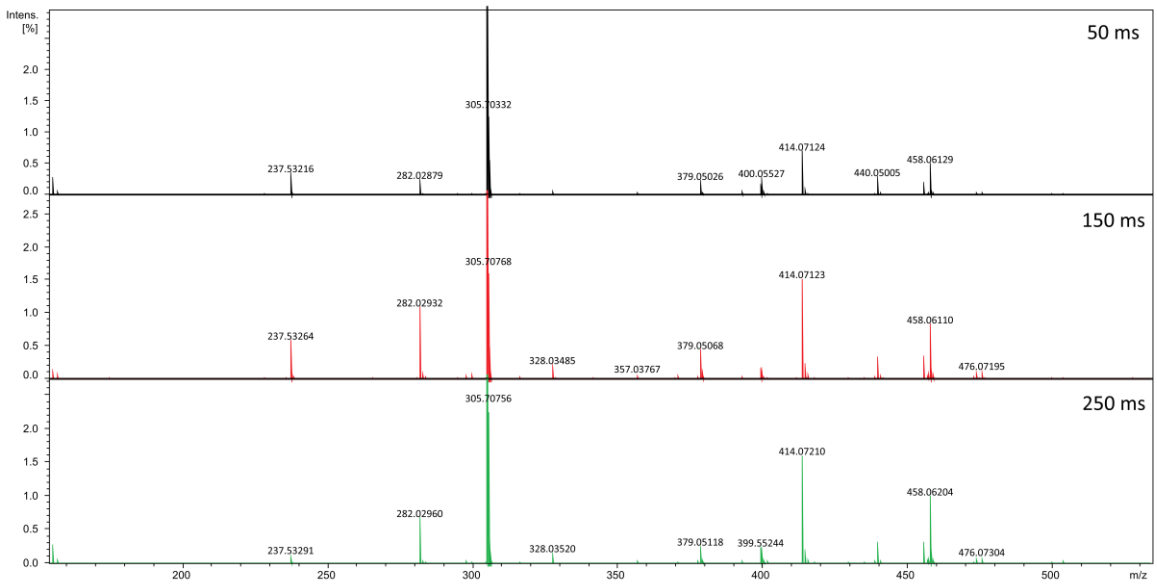

Figure D.4. NETD spectra of dermatan sulfate dp4 $[M-3H]^{3-}$ precursor ion (*m/z* 305.0382). Reagent accumulation time was held constant at 50 ms while the reaction time was increased from 50 ms (top), 150 ms (center) and 250 ms (bottom).

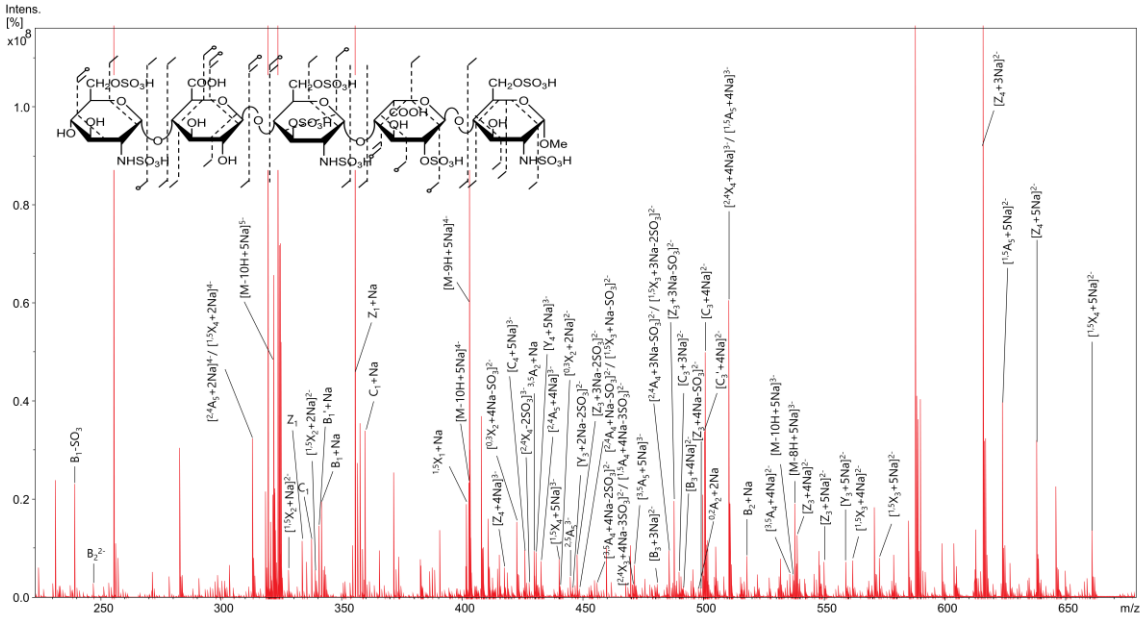

Figure D.5. NETD spectrum of Fondaparinux Sodium precursor ion $[M\text{-}10H+5Na]^{5-}$ (*m/z* 322.3649) with a reaction time of 50 ms and a reagent accumulation time of 800 ms. Inset displays fragment map.

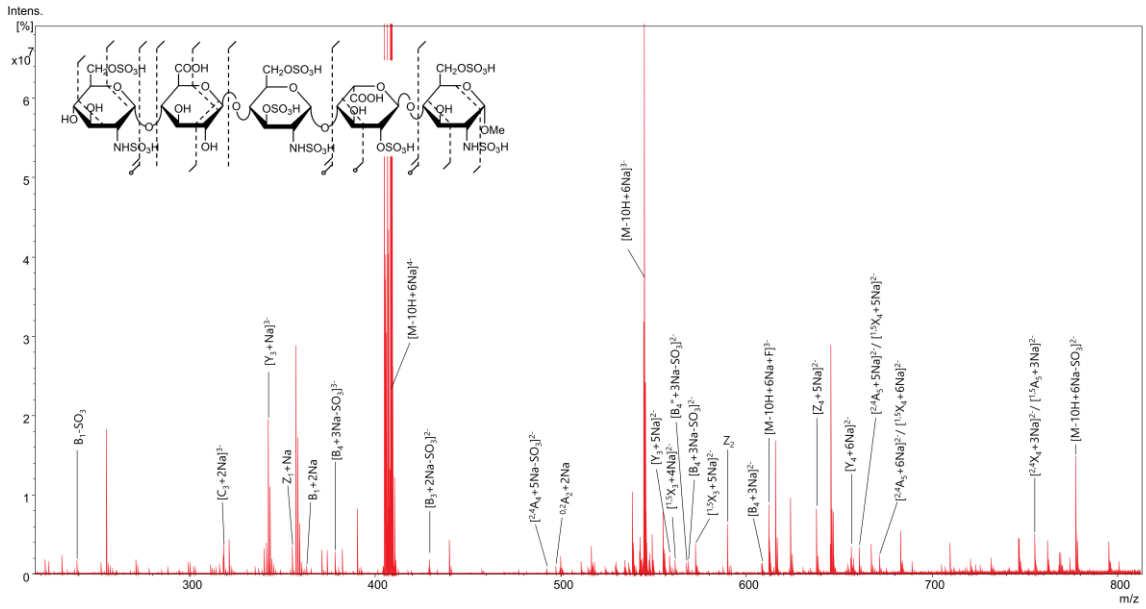

Figure D.6. NETD spectrum of Fondaparinux Sodium precursor ion $[M\text{-}10H+6Na]^{4-}$ (*m/z* 408.7035) with a reaction time of 50 ms and a reagent accumulation time of 800 ms. Inset displays fragment map.

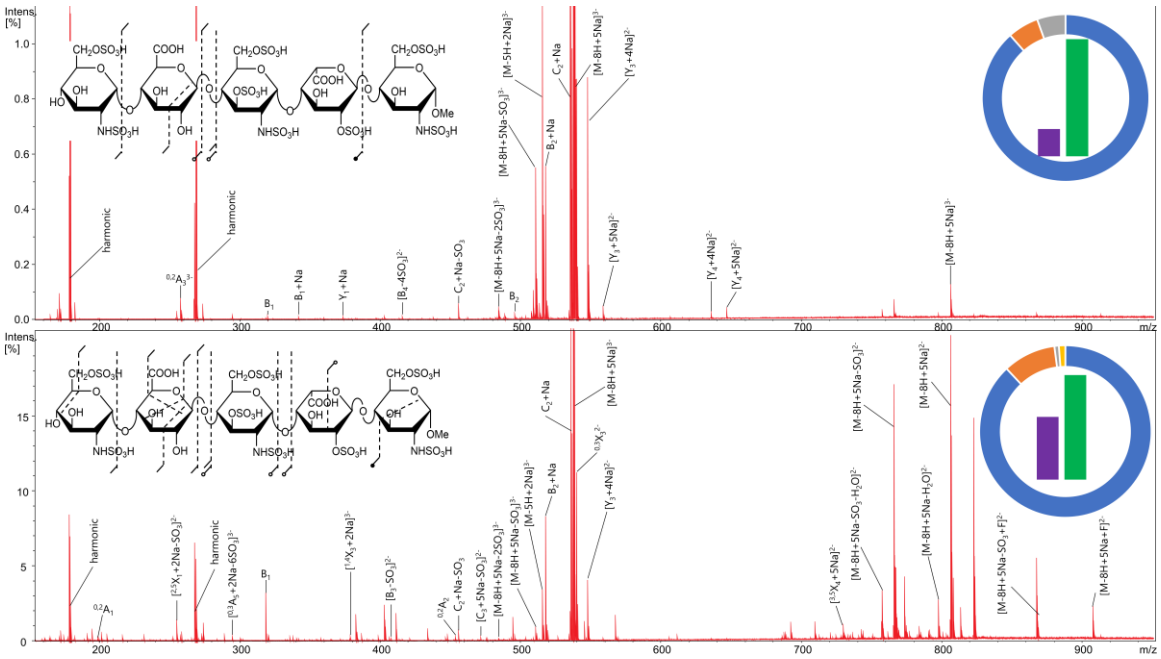

Figure D.7. NETD spectra of the $[M-8H+5Na]^{3-}$ precursor ion with a 50 ms reagent accumulation time (top) and a reagent accumulation time of 950 ms (bottom). Fragment map insets display the fragmentation distribution. Donut plots display the intensity distribution of glycosidic fragments (blue), cross-ring fragments (orange), glycosidic fragments with SO_3 loss (grey) and cross-ring fragments with SO_3 loss (yellow). Bar graphs display the intensity of assigned fragment ions (green) and unassigned fragment ions (purple).

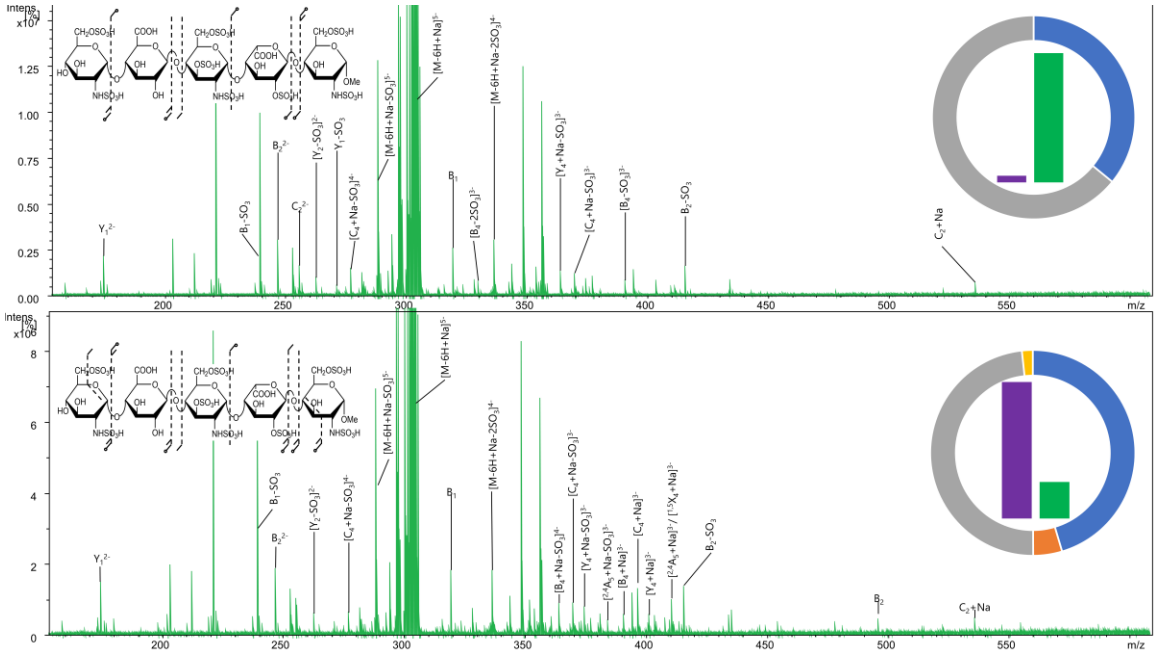

Figure D.8. NETD spectra of the $[M-6H+Na]^{5-}$ precursor ion with a 50 ms reagent accumulation time (top) and a reagent accumulation time of 500 ms (bottom). Fragment map insets display the fragmentation distribution. Donut plots display the intensity distribution of glycosidic fragments (blue), cross-ring fragments (orange), glycosidic fragments with SO_3 loss (grey) and cross-ring fragments with SO_3 loss (yellow). Bar graphs display the intensity of assigned fragment ions (green) and unassigned fragment ions (purple).

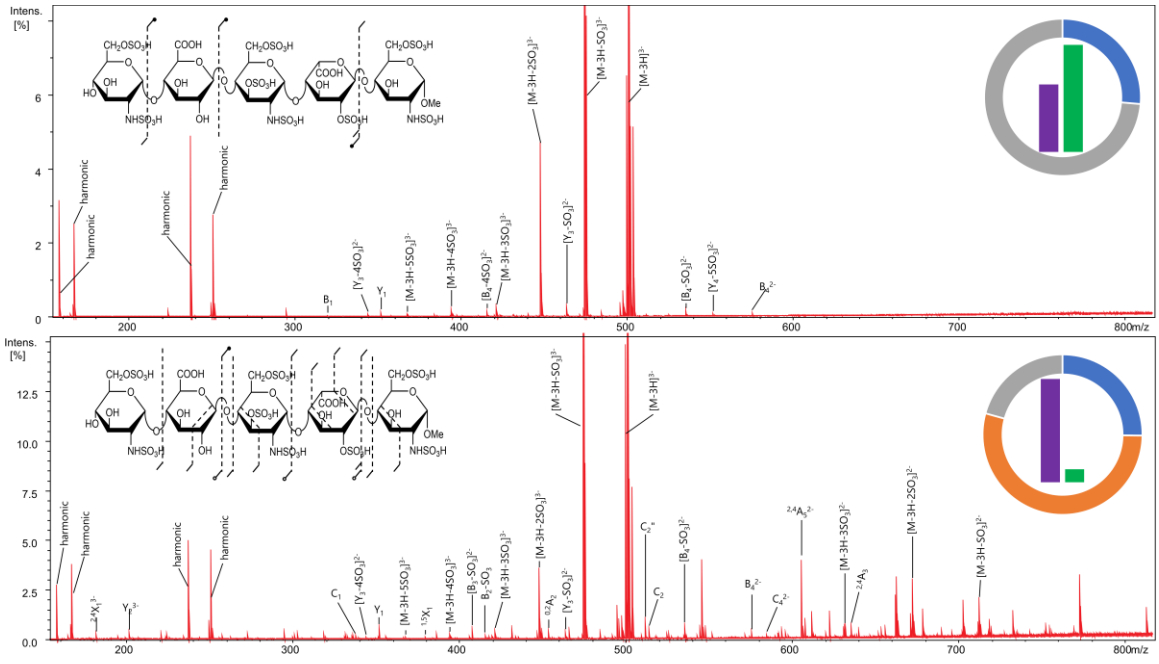

Figure D.9. NETD spectra of the $[M-3H]^{3-}$ precursor ion with a 50 ms reagent accumulation time (top) and a reagent accumulation time of 1200 ms (bottom). Fragment map insets display the fragmentation distribution. Donut plots display the intensity distribution of glycosidic fragments (blue), cross-ring fragments (orange), glycosidic fragments with SO_3 loss (grey) and cross-ring fragments with SO_3 loss (yellow). Bar graphs display the intensity of assigned fragment ions (green) and unassigned fragment ions (purple).

Figure D.10. Comparison of unassigned fragment ion intensity (blue) and assigned fragment ion intensity (orange) produced from NETD of fully ionized precursors at different reagent accumulation times (X-axis).

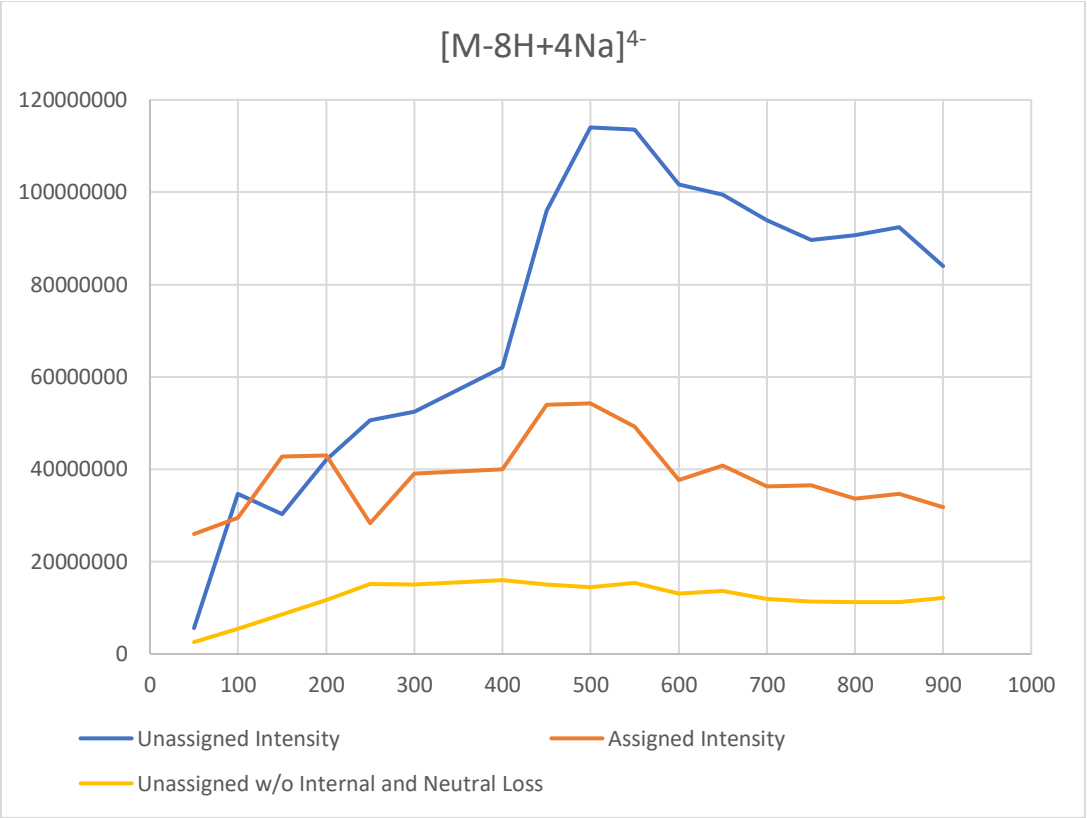

Figure D.11. Comparison of assigned glycosidic and cross-ring fragment ion intensity (orange) with all other unassigned intensity (blue), and unassigned fragment ion intensity without internal fragment ions or neutral loss (yellow), produced from NETD of the $[M-8H+4Na]^{4-}$ precursor ion at different reagent accumulation times (X-axis).